REMOVAL OF PESTICIDES FROM DRINKING WATER BY GRANULAR ACTIVATED CARBON

by

Gökçin Gül

B.Sc. in Chemistry, Boğaziçi University, 2013

M.Sc. in Environmental Sciences, Boğaziçi University, 2016

Submitted to the Institute of Environmental Sciences

in partial fulfillment of the requirements for the degree of

Doctor of Philosophy

in

Environmental Sciences

Boğaziçi University

2025

REMOVAL OF PESTICIDES FROM DRINKING WATER BY GRANULAR ACTIVATED CARBON

APPROVED BY:

Prof. Dr. Ferhan Çeçen Dissertation Advisor	. . . . .
Prof. Dr. Özgür Aktaş	. . . . .
Prof. Dr. Kozet Bakırcı	. . . . .
Prof. Dr. Nadim Copty	. . . . .
Assoc. Prof. Dr. Başak Güven	. . . . .

DATE OF APPROVAL: 18/03/2025

Dedicated to Fulya Taşkın and Kutal İlker, whose light continues to guide my path, though their presence is dearly missed…

ACKNOWLEDGEMENTS

I wish to convey my profound appreciation to everybody who contributed to the completion of my dissertation:

First and foremost, I am deeply grateful to my dissertation advisor, Professor Dr. Ferhan Çeçen. Since the beginning of my academic endeavors, her unflinching support, extraordinary patience, and consistent encouragement have been the foundation of my success. Not only has her direction been instrumental in the development as a researcher and as a person all in one.

I am profoundly grateful to the members of my thesis monitoring committee, Professor Dr. Nadim K. Copty, and Professor Dr. Özgür Aktaş. The quality of this work has been greatly improved as a result of their insightful feedback and constructive criticism. I also extend my sincere gratitude to Professor Dr. Kozet Yapsaklı, and Associate Professor Dr. Başak Güven for serving on my dissertation committee. Their invaluable guidance and expertise have enriched my research journey. I am particularly appreciating their willingness to provide constructive feedback and scholarly insights whenever needed.

In particular, I would like to express my gratitude to Associate Professor Dr. Ulaş Tezel for his kind assistance in providing access to the LC-MS/MS device and for his invaluable guidance. His support has been vital to the accomplishment of my research, as it has made it possible for me to carry out analytical evaluations and arrive at results that are significant. I am also indebted to Associate Professor Dr. Duygu Ağaoğulları, Dr. Sıddıka Mertdinç Ülküseven, İlayda Süzer and Dr. Seyfullah Ceylan all of whom are affiliated with the Department of Metallurgical and Materials Engineering at Istanbul Technical University. Their generous support in granting access to their laboratories and their assistance with the grinding of activated carbon have been instrumental to the success of my research endeavors.

I would like to express my gratitude to my colleague, Başak Kılıç, whose collaboration in the laboratory significantly contributed to my research. Additionally, I am thankful for Filiz Ayılmaz, whose presence in the laboratory consistently provided a sense of comfort and reassurance. Special thanks to my colleagues and friends, Koray Sakarya, Açelya Eren, Aygün Karaçay, Mahir Bozan, Çağlar Akay. Their stimulating discussions mutual support, and collaborative spirit made this journey both enriching and enjoyable.

I want to express my sincere appreciation to Fırat İlker for his support during the difficult stages of this academic journey. His encouragement proved invaluable, especially while dealing with family health issues and frequent hospital visits. I also express my heartfelt gratitude to Elif Irmak Erdem, Sebanur Sarısoy Çukay, Tuna İlker and Dilek İlker Piffaretti for their unwavering belief in my abilities and their continuous support in fostering my independence.

My heartfelt thanks go to my family for their constant love and support. My parents, Tülay Gül and Hasan Basri Gül, and my grandmother Nurten Şenay have been pillars of strength throughout my pursuits. I cherish the memory of Fulya Taşkın and Kutal İlker, who are no longer with us but whose belief in me continues to inspire.

I would also like to acknowledge support from the project titled “Removal of Micropollutants from Drinking Water by Granular Activated Carbon (GAC)” which was funded by Boğaziçi University Research Fund, with Grand Number: 19Y00D5.

ABSTRACT

REMOVAL OF PESTICIDES FROM DRINKING WATER BY GRANULAR ACTIVATED CARBON

This dissertation investigates the adsorption dynamics of micropollutants, particularly pesticides, in drinking water treatment using granular activated carbon. The study examines the physicochemical properties and biotransformation potential of selected pesticides through various databases and analytical tools. Additionally, the likelihood of pesticides for biodegradation during the water treatment processes was investigated. Adsorption characteristics were assessed through batch experiments to determine kinetic and isotherm parameters. The results indicate that the adsorption of selected pesticides follows pseudo-second order kinetics. Isotherm analyses revealed that all pesticides exhibit a strong affinity for GAC, with chlorpyrifos and cyprodinil demonstrating the highest adsorption capacities. However, pesticide affinity decreased in the presence of background natural organic matter (NOM). The breakthrough behavior of pesticides in GAC columns was investigated using Rapid Small-Scale Column Tests (RSSCTs) under continuous-flow conditions. These experiments explored the effects of GAC particle size and empty bed contact time (EBCT), the presence of NOM, and competition on breakthrough behavior under different test conditions. Furthermore, the adsorption design software (AdDesignS) was used to estimate breakthrough curves based on batch isotherm parameters under various conditions. The predicted breakthrough curves demonstrated reliable accuracy in modeling GAC column performance. The findings of this research contribute to the optimization of adsorption-based water treatment processes and provide valuable insights for preliminary system design.

ÖZET

GRANÜLER AKTİF KARBON İLE PESTİSİTLERİN İÇME SUYUNDAN UZAKLAŞTIRILMASI

Bu tezde, granül aktif karbon kullanılarak içme suyu arıtımında mikro kirleticilerin, özellikle pestisitlerin adsorpsiyon dinamikleri araştırılmaktadır. Çalışma, seçilen pestisitlerin fizikokimyasal özelliklerini ve biyotransformasyon potansiyelini çeşitli veri tabanları ve analitik araçlar aracılığıyla incelemektedir. Ayrıca pestisitlerin su arıtma süreçleri sırasında biyobozunma olasılığı da araştırılmıştır. Adsorpsiyon özellikleri, kinetik ve izoterm parametrelerini belirlemek amacıyla yapılan kesikli deneyler yoluyla analiz edilmiştir. Sonuçlar, seçilen pestisitlerin psödo-ikinci derece kinetiği takip ettiğini göstermektedir. İzoterm analizleri, tüm pestisitlerin GAK için güçlü bir afinite gösterdiğini, özellikle klorpirifos ve siprodinilin en güçlü adsorpsiyon kapasitesine sahip olduğunu ortaya çıkarmıştır. Ancak, arka plan doğal organik madde (DOM) varlığında bu afinitenin azaldığı belirlenmiştir. Pestisitlerin GAK kolonlarındaki kırılma davranışı, sürekli akış koşulları altında Hızlı Küçük Ölçekli Kolon Testleri kullanılarak incelenmiştir. Bu deneylerde, GAK partikül boyutu ve boş yatak temas süresi (BYTS), DOM varlığı ve rekabet etkisinin kırılma davranışı üzerindeki etkileri araştırılmıştır. Bunun yanı sıra, farklı koşullarda kesikli deney izoterm parametrelerinden yararlanarak kırılma eğrilerini tahmin etmek için adsorpsiyon tasarım yazılımı (AdDesignS) kullanılmıştır. Tahmin edilen kırılma eğrileri, GAK kolon performansını modellemede yüksek doğruluk göstermiştir. Bu çalışmadan elde edilen veriler, adsorpsiyona dayalı su arıtma süreçlerinin optimizasyonuna katkıda bulunmakta ve sistem tasarımının başlangıç aşamaları için değerli öngörüler sağlamaktadır.

TABLE OF CONTENTS

ACKNOWLEDGEMENTS iv
ABSTRACT vi
ÖZET vii
TABLE OF CONTENTS viii
LIST OF FIGURES xi
LIST OF TABLES xx
LIST OF SYMBOLS/ABBREVIATIONS xxiv
1. INTRODUCTION 1
2. LITERATURE REVIEW 6
2.1. Environmental Fate and Transport Mechanisms of Micropollutants in Aquatic Systems 6
2.2. Limitations of Conventional Water Treatment in Removing Micropollutant Removal 7
2.3. Properties and Mechanisms of Granular Activated Carbon (GAC) 9
2.3.1. Natural Organic Matter (NOM) and Its Effects on Adsorption 10
2.3.2. Biological Activated Carbon (BAC) Filters 11
2.4. Rapid Small-Scale Column Tests (RSSCTs) 12
2.5. Selection of Representative Pesticides 14
3. AIM OF THE STUDY 16
4. MATERIALS AND METHODS 18
4.1. Data-Driven Assessment of Selected Pesticides Physicochemical and Biodegradation Characteristics 18
4.2. Chemicals 19
4.2.1. Selection of Pesticides 19
4.2.2. Selection of Granular Activated Carbon 20
4.3. Grinding of Activated Carbon 21
4.4. Analytical Methods and Measurements 23
4.4.1. LC-MS/MS Analysis 23
4.4.2. Dissolved Organic Carbon (DOC) Analysis 26
4.4.3. Spectrophotometric Measurements 27
4.4.4. pH Measurements 27
4.5. Characterization and Preparation of Synthetic Drinking Water 28
4.6. Evaluation of the Adsorption of Pesticides and Background NOM onto GAC in Batch Reactors 31

4.6.1. Kinetic Experiments 32
4.6.2. Isotherm Experiments 33
4.7. Biodegradation Experiments 36
4.7.1. Initiation and Operation of the Biological Reactor 36
4.7.2. Biodegradation of Natural Organic Matter (NOM) and Pesticides 37
4.7.3. Investigation of the Synergistic Effect between GAC and Biomass in Batch Adsorption Systems 38
4.8. Experiments with Rapid Small-Scale Column Tests (RSSCTs) 39
4.8.1. Evaluation of the Adsorption of Pesticides and Background NOM onto GAC in RSSCTs 39
4.8.2. Tracer Test 42
4.9. Modeling of Pesticides and Background NOM Removal using AdDesignS Software 44
5. RESULTS AND DISCUSSION 49
5.1. Identification and a Data-Driven Analysis of Selected Pesticides: Assessing Physicochemical Properties and Biodegradation Characteristics 49
5.1.1. Pesticides Properties DataBase (PPDB) Profiling 49
5.1.2. Computational Assessment of Pesticides: Estimation Program Interface (EPI) Suite Results 55
5.1.3. MetaCyc Results 57
5.1.4. EAWAG-BBD/ PPS (Biocatalysis/Biodegradation Database Pathway Prediction System) Results 60
5.1.5. EnviPath (The Environmental Contaminant Biotransformation Pathway Resource) Results 64
5.2. Analysis of Adsorption Kinetics and Isotherms 67
5.2.1. Batch Kinetic Experiments with Granular Activated Carbon (GAC) 67
5.2.1.1. Adsorption kinetics of a pesticide mixture in the case of ground GAC 68
5.2.2. Isotherm Experiments with GAC 72
5.2.2.1. Adsorption isotherms of pesticides in a monocomponent system (ground GAC) 73
5.2.2.2. Adsorption isotherms of pesticides in a multicomponent system (ground GAC) 81
5.2.2.3. Adsorption isotherms of pesticides in a multicomponent system (original (non-ground) GAC) 84
5.2.2.4. Adsorption isotherms in the case of background nom (ground GAC). 90

5.2.2.5. Adsorption isotherms in the case of background nom (original (non-ground) GAC) 94
5.2.2.6. Adsorption isotherms in the case of background nom and a pesticide mixture (ground GAC) 98
5.3. Biodegradation Experiments 105
5.3.1. Operation of a Biological Reactor for the Growth of Biomass 105
5.3.2. NOM Biodegradation Experiments 106
5.3.3. Pesticide Biodegradation Experiments 107
5.4. Investigation of the Synergistic Effect between GAC and Biomass in Batch Adsorption Systems 109
5.5. Tests in Continuous-flow Rapid/Small-Scale Columns (RSSCTs) 113
5.5.1. Tracer Test Results 113
5.5.2. Adsorption of Single Pesticides (Cyprodinil and Carbofuran) onto Ground GAC in an RSSCT 115
5.5.3. Adsorption of Background NOM onto Ground GAC in an RSSCT 117
5.5.4. Adsorption of Background NOM onto Non-Ground GAC in an RSSCT 120
5.5.5. Adsorption of a Pesticides Mixture onto Ground GAC in an RSSCT 123
5.5.6. Adsorption of a Pesticides Mixture onto Non-Ground GAC in an RSSCT 125
5.5.7. Simultaneous Adsorption of a Pesticides Mixture and Background NOM onto Ground GAC in an RSSCT 128
5.5.8. Simultaneous Adsorption of Background NOM and a Pesticide Mixture onto Ground GAC Surrounded with Biofilm in an RSSCT 130
6. CONCLUSIONS 133
7. FUTURE WORKS AND RECOMMENDATIONS 135
REFERENCES 137
APPENDIX A: EXPERIMENTS ON ADSORPTION KINETICS 162
APPENDIX B: OPERATIONAL RESULTS OF THE BIOLOGICAL REACTOR 170
APPENDIX C: RESULTS OF NOM BIODEGRADATION EXPERIMENTS 178

LIST OF FIGURES

Figure 1.1. Global pesticide production and import values between 1940-2000.....2

Figure 1.2. Graphical representation of pesticide uses in the world (in tonnes per year).....2

Figure 1.3. Graphical representation of pesticide uses per hectare of cropland in the world.....3

Figure 1.4. Graphical representation of pesticide cycle.....4

Figure 2.1. Main fate and transport mechanisms of micropollutants in the environment.....7

Figure 2.2. Schematic representation of conventional water treatment plants.....8

Figure 2.3. Substrate transport and removal mechanisms in a GAC particle covered by a biofilm.12

Figure 3.1. Schematic representation of the study phases.....17

Figure 4.1. Left: SPEX SamplePrep 8000D Mixer/Mill®, Right: Retch sieve shaker.....22

Figure 4.2. Left: pristine GAC sample (before grinding), Middle: grinding metal balls, Right: GAC sample after grinding.....22

Figure 4.3. LC-MS/MS chromatogram of a sample containing carbofuran, propanil, cyprodinil, malathion, methyl-d3-triphenylphosphonium iodide (IS), and chlorpyrifos.....24

Figure 4.4. Calibration curve of carbofuran (0.1 to 1000 μg/L).....24

Figure 4.5. Calibration curve of chlorpyrifos (0.1 to 1000 μg/L).....25

Figure 4.6. Calibration curve of cyprodinil (0.1 to 1000 μg/L).....25

Figure 4.7. Calibration curve of malathion (0.1 to 1000 μg/L).....25

Figure 4.8. Calibration curve of propanil (0.1 to 1000 μg/L) 26

Figure 4.9. Calibration curve of DOC.....27

Figure 4.10. The batch reactor used for the growth of microorganisms in Ömerli Reservoir water. 37

Figure 4.11. Schematic diagram of RSSCT GAC columns. 42

Figure 4.12. Schematic representation of the AdDesignS software working input parameters.....45

Figure 4.13. Comparison of the best-fit model and experimental results. 47

Figure 4.14. Sensitivity simulations related to K_f and 1/n 48

Figure 5.1. Chlorpyrifos biodegradation pathway obtained from the MetaCyc database.....58

Figure 5.2. Carbofuran biodegradation pathway obtained from the MetaCyc database.....59

Figure 5.3. Possible carbofuran biodegradation pathways obtained from the EAWAG-BBD/PPS. 60

Figure 5.4. Possible chlorpyrifos biodegradation pathways obtained from the EAWAG-BBD/PPS. 61

Figure 5.5. Possible cyprodinil biodegradation pathways obtained from the EAWAG-BBD/PPS..62

Figure 5.6. Possible malathion biodegradation pathways obtained from the EAWAG-BBD/PPS. .63

Figure 5.7. Possible propanil biodegradation pathways obtained from the EAWAG-BBD/PPS 64

Figure 5.8. Possible carbofuran biodegradation pathways obtained from the EnviPath.....65

Figure 5.9. Possible chlorpyrifos biodegradation pathways obtained from the EnviPath 65

Figure 5.10. Possible cyprodinil biodegradation pathways obtained from the EnviPath 66

Figure 5.11. Possible malathion biodegradation pathways obtained from the EnviPath.....66

Figure 5.12. Possible propanil biodegradation pathways obtained from the EnviPath.....67

Figure 5.13. PSO modeling for the adsorption of pesticides onto GAC.....70

Figure 5.14. Adsorption isotherms for carbofuran: (A) Linear, (B) Freundlich, (C) Langmuir, (D) Temkin.....73

Figure 5.15. Adsorption isotherms for chlorpyrifos: (A) Linear, (B) Freundlich, (C) Langmuir, (D) Temkin.....74

Figure 5.16. Adsorption isotherms for cyprodinil: (A) Linear, (B) Freundlich, (C) Langmuir, (D) Temkin.....75

Figure 5.17. Adsorption isotherms for malathion: (A) Linear, (B) Freundlich, (C) Langmuir, (D) Temkin.....76

Figure 5.18. Adsorption isotherms for propanil: (A) Linear, (B) Freundlich, (C) Langmuir, (D) Temkin.....76

Figure 5.19. Isotherms showing the adsorption of carbofuran onto ground GAC in a pesticide mixture: (A) Freundlich, (B) Langmuir.....81

Figure 5.20. Isotherms showing the adsorption of chlorpyrifos onto ground GAC in a pesticide mixture: (A) Freundlich, (B) Langmuir.....81

Figure 5.21. Isotherms showing the adsorption of cyprodinil onto ground GAC in a pesticide mixture: (A) Freundlich, (B) Langmuir.....82

Figure 5.22. Isotherms showing the adsorption of malathion onto ground GAC in a pesticide mixture: (A) Freundlich, (B) Langmuir.....82

Figure 5.23. Isotherms showing the adsorption of propanil onto ground GAC in a pesticide mixture: (A) Freundlich, (B) Langmuir.....82

Figure 5.24. Isotherms showing the adsorption of carbofuran onto non-ground GAC in a pesticide mixture: (A) Linear, (B) Freundlich, (C) Langmuir, (D) Temkin.....85

Figure 5.25. Isotherms showing the adsorption of chlorpyrifos onto non-ground GAC in a pesticide mixture: (A) Linear, (B) Freundlich, (C) Langmuir, (D) Temkin.....86

Figure 5.26. Isotherms showing the adsorption of cyprodinil onto non-ground GAC in a pesticide mixture: (A) Linear, (B) Freundlich, (C) Langmuir, (D) Temkin.....87

Figure 5.27. Isotherms showing the adsorption of malathion onto non-ground GAC in a pesticide mixture: (A) Linear, (B) Freundlich, (C) Langmuir, (D) Temkin.....88

Figure 5.28. Isotherms showing the adsorption of propanil onto non-ground GAC in a pesticide mixture: (A) Linear, (B) Freundlich, (C) Langmuir, (D) Temkin.....88

Figure 5.29. Adsorption isotherms of background NOM onto ground GAC: (A) Freundlich, (B) Langmuir (In terms of DOC).....91

Figure 5.30. Adsorption isotherms of background NOM onto ground GAC: (A) Freundlich, (B) Langmuir (In terms of UV absorbance).....91

Figure 5.31. Adsorption isotherms of background NOM onto ground GAC: (A) Freundlich, (B) Langmuir (In terms of color absorbance).....92

Figure 5.32. Adsorption isotherms of background NOM onto non-ground GAC: (A) Freundlich, (B) Langmuir (In terms of DOC).....94

Figure 5.33. Adsorption isotherms of background NOM onto non-ground GAC: (A) Freundlich, (B) Langmuir (In terms of UV absorbance).....95

Figure 5.34. Adsorption isotherms of background NOM onto non-ground GAC: (A) Freundlich, (B) Langmuir (In terms of color absorbance).....96

Figure 5.35. Isotherms showing the adsorption of carbofuran onto ground GAC in the case of background NOM and a pesticide mixture: (A) Freundlich, (B) Langmuir.....99

Figure 5.36. Isotherms showing the adsorption of cyprodinil onto ground GAC in the case of background NOM and a pesticide mixture: (A) Freundlich, (B) Langmuir.....99

Figure 5.37. Isotherms showing the adsorption of malathion onto ground GAC in the case of background NOM and a pesticide mixture: (A) Freundlich, (B) Langmuir.....99

Figure 5.38. Isotherms showing the adsorption of propanil onto ground GAC in the case of background NOM and a pesticide mixture: (A) Freundlich, (B) Langmuir.....100

Figure 5.39. Isotherms showing the adsorption of background NOM onto ground GAC in the case of background NOM and a pesticide mixture: (A) Freundlich, (B) Langmuir (In terms of DOC) 102

Figure 5.40. Isotherms showing the adsorption of background NOM onto ground GAC in the case of background NOM and a pesticide mixture: (A) Freundlich, (B) Langmuir (In terms of UV_{254}).....103

Figure 5.41. Isotherms showing the adsorption of background NOM onto ground GAC in the case of background NOM and a pesticide mixture: (A) Freundlich, (B) Langmuir (In terms of UV_{280}).....103

Figure 5.42. Isotherms showing the adsorption of background NOM onto ground GAC in the case of background NOM and a pesticide mixture: (A) Freundlich, (B) Langmuir (In terms of $Color_{400}$). 103

Figure 5.43. Isotherms showing the adsorption of background NOM onto ground GAC in the case of background NOM and a pesticide mixture: (A) Freundlich, (B) Langmuir (In terms of $Color_{436}$). 104

Figure 5.44. Background NOM removal profile in a batch reactor: normalized DOC concentrations versus time (C_0 = 3.5 mg DOC/L) 106

Figure 5.45. Pesticide removal profile in a batch reactor: normalized pesticide concentrations versus time (C_0 = 200 µg/L for each pesticide).....108

Figure 5.46. Removal of cyprodinil over time under five experimental conditions: Control (I), GAC (II), Biomass (III), Combined GAC + biomass (IV), and Biomass with NaN_3 inhibitor (V).....110

Figure 5.47. Final cyprodinil removal efficiency (%) across all treatment conditions.....110

Figure 5.48. Removal of carbofuran over time under five experimental conditions: Control (I), GAC (II), Biomass (III), Combined GAC + biomass (IV), and Biomass with NaN_3 inhibitor (V).....111

Figure 5.49. Final carbofuran removal efficiency (%) across all treatment conditions.....112

Figure 5.50. Tracer test results for both experiment and model 114

Figure 5.51. Comparison of experimental and AdDesignS-predicted breakthrough curves in the case of carbofuran onto ground GAC in an RSSCT (C_0 = 1000 µg/L). 115

Figure 5.52. Comparison of experimental and AdDesignS-predicted breakthrough curves in the case of cyprodinil onto ground GAC in an RSSCT (C_0 = 1000 µg/L) 116

Figure 5.53. AdDesignS-predicted complete breakthrough curves for cyprodinil and carbofuran. 117

Figure 5.54. Experimental breakthrough curve of background NOM (in terms of absorbances and DOC) onto ground GAC in an RSSCT ($C_{0\text{-}DOC}$ = 3.5 mg DOC/L, $C_{0\text{-}254}$ = 0.105 cm^{-1}, $C_{0\text{-}280}$= 0.099 cm^{-1}).....118

Figure 5.55. Comparison of experimental and AdDesignS-predicted breakthrough curves based on DOC measurements in the case of adsorption onto ground GAC in an RSSCT.....119

Figure 5.56. Experimental breakthrough curve of background NOM (in terms of absorbances and DOC) onto non-ground GAC in an RSSCT ($C_{0\text{-}DOC}$ = 3.5 mg DOC/L, $C_{0\text{-}254}$ = 0.105 cm^{-1}, $C_{0\text{-}280}$= 0.099 cm^{-1}) 120

Figure 5.57. Breakthrough curves generated using AdDesign software and the experimental breakthrough curve measured in terms of DOC measurements onto non-ground GAC in an RSSCT 122

Figure 5.58. Experimental breakthrough curves in the case of a pesticide mixture onto ground GAC in an RSSCT (C_0 = 200 μg/L for each pesticide). 124

Figure 5.59. AdDesignS-predicted complete breakthrough curves for a pesticide mixture in the case of ground GAC 125

Figure 5.60. Experimental breakthrough curves in the case of a pesticide mixture onto non-ground GAC in an RSSCT (C_0 = 200 μg/L for each pesticide) 126

Figure 5.61. AdDesignS-predicted complete breakthrough curves for background NOM and pesticide mixture in the case of non-ground GAC. 127

Figure 5.62. Experimental breakthrough curves in the case of simultaneous adsorption of a pesticide mixture and background NOM (in terms of absorbances and DOC) onto ground GAC in an RSSCT. 128

Figure 5.63. AdDesignS-predicted complete breakthrough curves for background NOM and pesticides in the case of ground-GAC 129

Figure 5.64. Experimental breakthrough curves of background NOM (in terms of absorbances and DOC) in the case of ground BAC in an RSSCT 131

Figure 5.65. Experimental breakthrough curves of pesticides in case of ground BAC in an RSSCT (C_0 = 200 μg/L for each pesticide) 131

Figure A.1. Adsorption kinetics of carbofuran in pesticide mixture + ground GAC experiments. 162

Figure A.2. Adsorption kinetics of chlorpyrifos in pesticide mixture + ground GAC experiments. 162

Figure A.3. Adsorption kinetics of cyprodinil in pesticide mixture + ground GAC experiments. .162

Figure A.4. Adsorption kinetics of malathion in pesticide mixture + ground GAC experiments. .163

Figure A.5. Adsorption kinetics of propanil in pesticide mixture + ground GAC experiments. 163

Figure A.6. Adsorption kinetics of DOC in background NOM + ground GAC experiments. 163

Figure A.7. Kinetics of organic substance removal: UV_{254} absorbance decay in background NOM + ground GAC experiments.....164

Figure A.8. Kinetics of organic substance removal: UV_{280} absorbance decay in background NOM + ground GAC experiments.....164

Figure A.9. Kinetics of organic substance removal: $Color_{400}$ absorbance decay in background NOM + ground GAC experiments 165

Figure A.10. Kinetics of organic substance removal: $Color_{436}$ absorbance decay in background NOM + ground GAC experiments 165

Figure A.11. Kinetics of organic substance removal: UV_{254} absorbance decay in background NOM 166

Figure A.12. Kinetics of organic substance removal: UV_{280} absorbance decay in background NOM 166

Figure A.13. Kinetics of organic substance removal: $Color_{400}$ absorbance decay in background NOM + non-ground GAC experiments.....167

Figure A.14. Kinetics of organic substance removal: $Color_{436}$ absorbance decay in background NOM + non-ground GAC experiments. 167

Figure A.15. Kinetics of organic substance removal: UV_{254} absorbance decay in background NOM + pesticide mixture + ground GAC experiments.....168

Figure A.16. Kinetics of organic substance removal: UV_{280} absorbance decay in background NOM + pesticide mixture + ground GAC experiments.....168

Figure A.17. Kinetics of organic substance removal: $Color_{400}$ absorbance decay in background NOM + pesticide mixture + ground GAC experiments 168

Figure A.18. Kinetics of organic substance removal: $Color_{436}$ absorbance decay in background NOM + pesticide mixture + ground GAC experiments. 169

Figure C.1. Background NOM removal profile in a batch reactor: normalized UV_{254} absorbance measurements versus time.....178

Figure C.2. Background NOM removal profile in a batch reactor: normalized UV_{280} absorbance measurements versus time.....178

Figure C.3. Background NOM removal profile in a batch reactor: normalized $Color_{400}$ absorbance measurements versus time.....179

Figure C.4. Background NOM removal profile in a batch reactor: normalized $Color_{436}$ absorbance measurements versus time.....179

LIST OF TABLES

Table 2.1. Important parameters in RSSCT 13

Table 4.1. Molecular structures and physicochemical properties of the selected pesticides. 20

Table 4.2. Properties of the chosen activated carbon 21

Table 4.3. The operation conditions of the liquid chromatography-tandem mass spectrometry (LC-MS/MS) 24

Table 4.4. Recipe for synthetic soft freshwaters 29

Table 4.5. Synthetic Ömerli Reservoir water preparation formulation 30

Table 4.6. Water quality parameters of a laboratory-prepared synthetic drinking water and the real water obtained from the Ömerli Reservoir 31

Table 4.7. Composition of stock feed 36

Table 4.8. Basic mathematical connections used for RSSCT design 40

Table 4.9. Full list of parameters entered to AdDesignS software 46

Table 5.1. Relevant parameters from Pesticide Properties Database (PPDB) 49

Table 5.2. Output of BIOWIN models indicating the probability of biodegradation or biodegradation time 56

Table 5.3. Summary of the kinetic models 69

Table 5.4. R^2 values for three kinetic models 69

Table 5.5. Pseudo-second order kinetic model parameters for a pesticide mixture adsorbing on ground GAC....71

Table 5.6. Summary of adsorption isotherm models, their respective equations and associated parameters....72

Table 5.7. Isotherm parameters describing the sorption of individual pesticides onto ground GAC 79

Table 5.8. Comparative analysis of pesticide adsorption: literature values and own experimental results. 80

Table 5.9. Isotherm parameters describing the sorption of a pesticide from a pesticide mixture onto ground GAC....84

Table 5.10. Isotherm parameters describing the sorption of a pesticide from a pesticide mixture onto non-ground GAC 90

Table 5.11. Isotherm parameters of the isotherm models describing the sorption of background NOM onto ground GAC (in terms of mg DOC/L and absorbance measurements).....94

Table 5.12. Isotherm parameters describing the sorption of background NOM onto non-ground GAC (in terms of mg DOC/L and absorbance measurements) 97

Table 5.13. Comparative analysis of background NOM adsorption: literature values and own experimental results 98

Table 5.14. Isotherm parameters describing the sorption of a pesticide from a mixture composed of background NOM and pesticides onto ground GAC....100

Table 5.15. Isotherm parameters describing the sorption of a pesticide from a mixture composed of background NOM and pesticides onto ground GAC (pesticide concentrations were expressed in terms of DOC)....100

Table 5.16. Isotherm parameters describing the sorption of background NOM from a mixture composed of background NOM and pesticides onto ground GAC (in terms of mg DOC/L and absorbance measurements).....104

Table 5.17. Operational Results of the Biological Reactor – April 2023. 105

Table 5.18. Parameters determined from the tracer test.....114

Table B.1. Operational Results of the Biological Reactor – January 2023.....170

Table B.2. Operational Results of the Biological Reactor – February 2023.....170

Table B.3. Operational Results of the Biological Reactor – March 2023.....171

Table B.4. Operational Results of the Biological Reactor – April 2023.....171

Table B.5. Operational Results of the Biological Reactor – May 2023.....172

Table B.6. Operational Results of the Biological Reactor – June 2023.....172

Table B.7. Operational Results of the Biological Reactor – July 2023 173

Table B.8. Operational Results of the Biological Reactor – October 2023 173

Table B.9. Operational Results of the Biological Reactor – November 2023 174

Table B.10. Operational Results of the Biological Reactor – December 2023.....174

Table B.11. Operational Results of the Biological Reactor – January 2024.....175

Table B.12. Operational Results of the Biological Reactor – February 2024.....175

Table B.13. Operational Results of the Biological Reactor – March 2024.....176

Table B.14. Operational Results of the Biological Reactor – April 2024.....176

Table B.15. Operational Results of the Biological Reactor – June & September 2024.....177

Table B.16. Operational Results of the Biological Reactor – October & January 2024-2025 177

LIST OF SYMBOLS/ABBREVIATIONS

Symbol	Explanation	Unit
1/n	Freundlich Adsorption Intensity	
α_x	Longitudinal Dispersivity	cm
A	Cross-sectional Area	cm^2
b_T	Temkin Constant	J/mole
C_e	Equilibrium Concentration	mg/L
D_x	Dispersion Coefficient	cm^2/min
D_m	Molecular Diffusion Coefficient	cm^2/min
k_1	Pseudo-First Order Rate Constant	h^{-1}
k_2	Pseudo-Second Order Rate Constant	g/mg.h
K_d	Equilibrium Dissociation Constant	mL/day
K_f	Freundlich Equilibrium Coefficient	
K_L	Langmuir Equilibrium Coefficient	L/mg
k_i	Intraparticle Diffusion Rate Constant	$mg/g.h^{1/2}$
K_T	Temkin Equilibrium Coefficient	L/mg
K_{oc}	Organic Carbon-Water Partition Coefficient	
K_{ow}	Octanol-Water Partition Coefficient	
n	Porosity	
pH_{PZC}	Point of Zero Charge	
Q	Flow Rate	mL/min
q	Adsorption Capacity	mg/g
q_e	Adsorption Capacity at equilibrium	mg/g
q_{max}	Maximum Adsorption Capacity	mg/g
q_t	Adsorption Capacity at time t	mg/g
v	Flow Velocity	cm/min

Abbreviation	Explanation
2,4-D	2,4-Dichlorophenoxyacetic Acid
AdDesignS	The Adsorption Design Software
AERU	Agriculture and Environment Research Unit
AOPs	Advanced Oxidation Processes

BAC	Biological Activated Carbon
BBD	Biodegradation/Biocatalysis Database
BCF	Bio-concentration Factor
CAS	Chemical Abstracts Service
CBF	Carbofuran
CPF	Chlorpyrifos
CYP	Cyprodinil
DDT	Dichlorodiphenyltrichloroethane
DOC	Dissolved Organic Carbon
DOM	Dissolved Organic Matter
EBCT	Empty Bed Contact Time
EnviPath	Environmental Contaminant Biotransformation Pathway Resource
EPA	Environmental Protection Agency
EPI	Estimation Programs Interface
ESI	Electrospray Ionization
FAST	Fixed-bed Adsorption Simulation Tool
FAO	Food and Agriculture Organization
GAC	Granular Activated Carbon
D	Diffusion Coefficients
DF	Design Factor
HPLC	High Performance Liquid Chromatography
ICP	Inductively Coupled Plasma
IS	Internal Standard
KHP	Potassium Hydrogen Phthalate
LC-MS/MS	Liquid Chromatography- Tandem Mass Spectrometry
MLT	Malathion
MLSS	Mixed-Liquor Suspended Solid
MLVSS	Mixed-Liquor Volatile Suspended Solid
MITI	Japanese Ministry of International Trade and Industry
MRM	Multiple Reaction Monitoring
NOM	Natural Organic Matter
RMSE	Root Mean Square Error
PFAS	per- and Polyfluoroalkyl Substances
PFO	Pseudo-First Order
PPCP	Pharmaceuticals and Personal Care Products

PPDB	Pesticide Properties Database
PPS	Pathway Prediction System
PRP	Propanil
PSDM	Pore and Surface Diffusion Model
PSO	Pseudo-Second Order
PTFE	Polytetrafluoroethylene
RSSCT	Rapid Small-Scale Column Test
SF	Scaling Factor
SCFB	Semi-Continuously Fed Batch
SMILES	Simplified Molecular Input Entry Specification
SUVA	Specific Ultraviolet Absorbance
TOC	Total Organic Carbon
OECD	Organization for Economic Co-operation and Development
QSAR	Quantitative Structure Activity Relationship
WHO	World Health Organization

1. INTRODUCTION

Dating back to the beginning of the 18th century and escalating during the Industrial Revolution, anthropogenic activities have significantly affected the environment and the biotic community within it. These human activities have become so pervasive that humankind has emerged as a global geological force. The extensive and devastating effects of these activities have placed the resilience of the Earth System in danger. According to the Earth System Science approach, which recently identified nine planetary boundaries critical for maintaining the stability of the Earth System, humanity has already passed six of these boundaries (Steffen et al., 2015). These include climate change, biogeochemical flow, novel entities, freshwater change, biosphere integrity, land system change. Of particular relevance to the scope of this research are the boundaries concerning novel entities (formerly named: chemical pollution) and freshwater change.

Annually, human activities result in the production of over 350,000 chemicals, amounting to over 250 billion tonnes (Chemical Pollution, 2024; Wang et al., 2020). Regardless of their original application sites, many of these chemicals ultimately disseminate into aquatic environments at the end of their life cycle. Even at trace concentrations, measured in nanograms or micrograms per liter, certain chemicals exhibit detrimental effects on the environment and various life forms, including humans. These trace-level contaminant chemicals are classified as micropollutants. The presence of a xenobiotic chemical, even at trace-levels, in freshwater systems poses a significant threat to global drinking water resources, as many conventional drinking water treatment plants are not equipped to effectively remove these xenobiotic micropollutants (Schwarzenbach et al., 2006).

The most prevalent micropollutants in aquatic environments include hormones, pharmaceuticals and personal care products (PPCPs), pesticides, brominated flame retardants, dyes, fragrances, disinfectants, antiseptic agents, microplastics, drugs, per and polyfluoroalkyl substances (PFAS), and various other industrial chemicals. Due to their extensive global application in agriculture, pesticides have emerged as one of the most frequently detected categories of environmental micropollutants. The post-World War II period, especially the 1950s and 1960s, witnessed a significant proliferation of novel synthetic pesticides (Vig, 1988). As illustrated in Figure 1.1 there was a significant and unprecedented increase in global pesticide production and import values during the period from 1940 to 2000. Ecobichon (2001) reports that global pesticide usage has experienced a fifty-fold increase since 1950. In the current context, it is estimated that the European Union alone accounts for the annual sale of approximately 350,000 tonnes of pesticides (Statistics | Eurostat, 2024). The extensive

use of pesticides in contemporary agricultural and industrial practices is evidenced by the substantial volumes reported in recent data, as shown in Figure 1.2, which illustrates pesticide usage by country measured in tonnes per annum (Pesticides - Our World in Data, 2022). Global annual pesticide utilization is estimated at approximately 2 million tonnes (Sharma, Kumar, Shahzad, Tanveer, Preet Singh Sidhu, et al., 2019). To fully comprehend the magnitude of pesticide application, examining the usage rates per unit area is instructive. Figure 1.3 provides a comparative analysis of pesticide usage across countries, expressed in terms of application per hectare, offering a more nuanced perspective on the intensity of pesticide use in various regions (Pesticide Use per Hectare of Cropland, 2021).

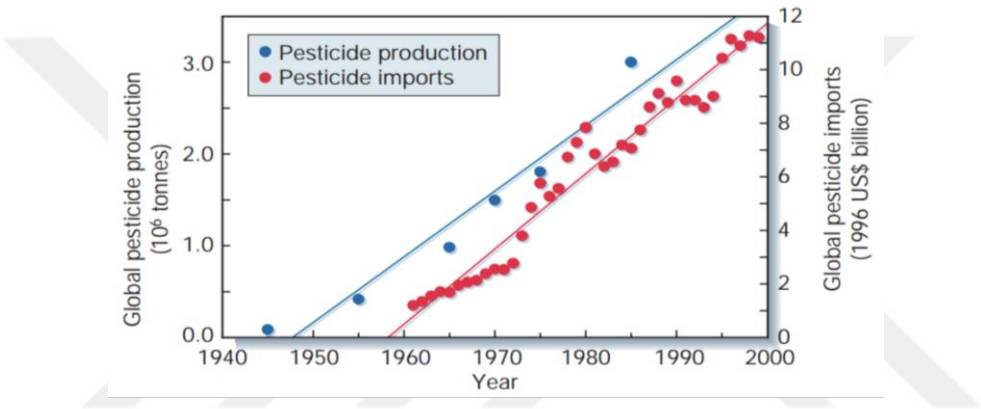


Figure 1.1. Global pesticide production and import values between 1940-2000 (Pesticide Production vs Time Graph, 2017).

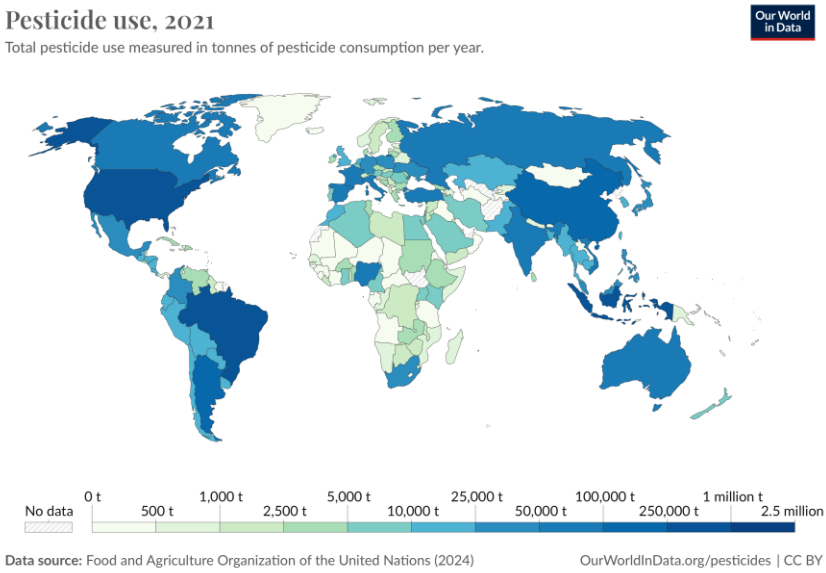


Figure 1.2. Graphical representation of pesticide uses in the world (in tonnes per year) (Pesticides - Our World in Data, 2022)

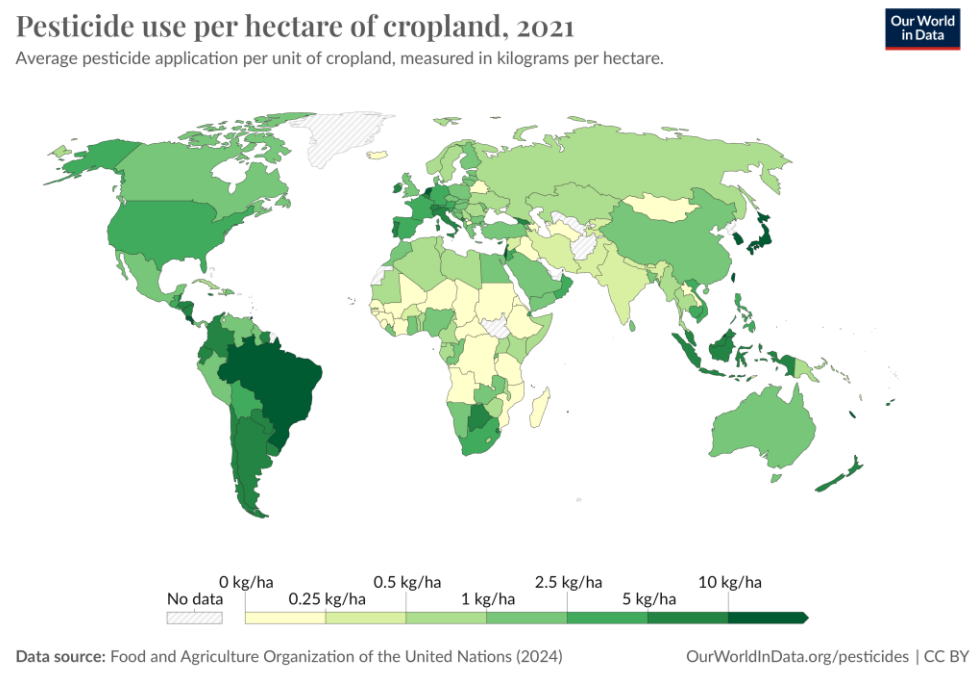


Figure 1.3. Graphical representation of pesticide uses per hectare of cropland in the world (Pesticide Use per Hectare of Cropland, 2021)

While potentially beneficial for crop protection and yield enhancement, the application of such agrochemicals has raised serious concerns among researchers, environmentalists, and public health experts. The widespread application of pesticides has undeniably resulted in various unintended consequences. Growing evidence suggests widespread pesticide usage poses significant challenges across multiple environmental and health domains. Research demonstrates their substantial impact on ecosystem diversity, degradation of soil conditions, contamination of water resources, and potential risks to public health and well-being (Beaumelle et al., 2023; Pathak et al., 2022; Sharma et al., 2019).

The pervasive contamination of water resources by pesticides can be primarily attributed to three main pathways: agricultural runoff, leaching from contaminated soils, and atmospheric deposition of pesticide particles, as illustrated in Figure 1.4. Agricultural runoff, a major contributor, occurs when excess water from irrigation or precipitation transports pesticides from treated fields into adjacent water bodies. Moreover, leaching from contaminated soils enables these chemical compounds to percolate through soil layers, eventually reaching groundwater reservoirs. Additionally, atmospheric deposition plays a crucial role in the widespread distribution of pesticide particles, as these substances can be transported over considerable distances via air currents before settling onto various surfaces, including aquatic ecosystems.

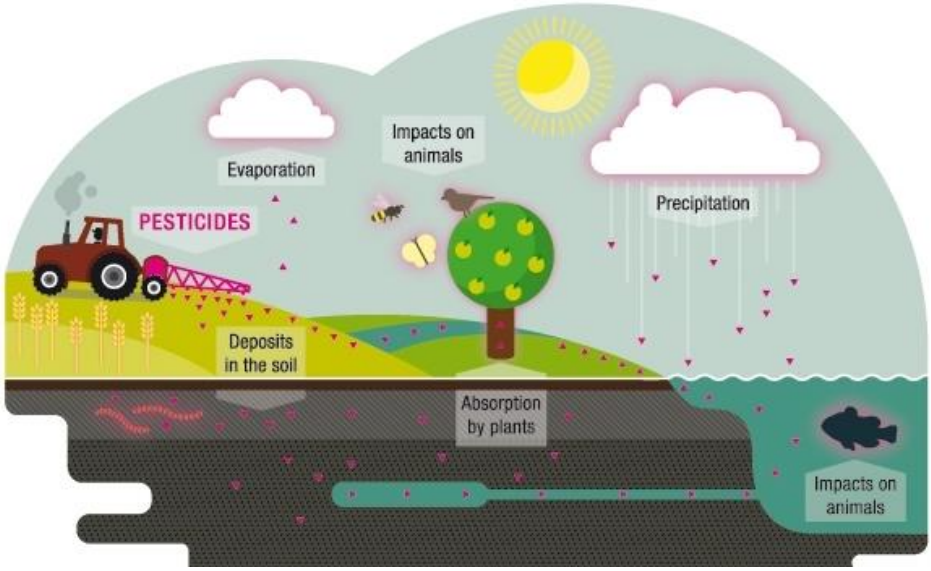


Figure 1.4. Graphical representation of pesticide cycle.

Regulatory bodies have implemented stringent guidelines in reaction to these environmental and health issues. For instance, the European Union's Drinking Water Directive (80/778/EEC) stipulates that individual pesticide concentrations should not exceed 0.1 μg/L, with the total concentration of all pesticides not surpassing 0.5 μg/L in treated drinking water. The "Regulation on Water Intended for Human Consumption" in Turkey also contains the pesticide standards implied in EU Drinking Water Directive (80/778/EEC).

Despite these regulatory efforts, the contamination of water resources with pesticides remains a pressing issue. Research indicates widespread contamination of water resources with agricultural chemicals, with many samples showing pesticide levels that surpass established safety limits (Sishu et al, 2022; Stehle & Schulz, 2015).

The potential for bioaccumulation and biomagnification of pesticides within food chains is particularly concerning, as it may lead to chronic illnesses over extended periods, even at low exposure levels (Fenner et al., 2013; Katagi, 2010). A significant proportion of pesticides currently in use have been recognized as Endocrine Disrupting Chemicals (EDCs), with 127 confirmed and numerous others under suspicion (McKinlay et al, 2008). EDCs are known to interfere with hormonal functions by mimicking or blocking natural hormones (Gibert et al, 2019; Guarnotta et al., 2022). Notably, EDCs can elicit biological responses even at very low concentrations (Guarnotta et al., 2022). These compounds have been associated with a range of adverse health outcomes, including but not limited to obesity, diabetes, thyroid dysfunction, reproductive disorders, and certain types of cancer (Gibert et al., 2019; Guarnotta et al., 2022; Predieri et al., 2022).

Given these concerns, pesticides must be eliminated urgently from all water bodies, especially drinking water sources. However, conventional water treatment processes often demonstrate inadequate efficiency in completely removing pesticides (Jatoi et al., 2021). To safeguard public health, novel, effective methods for pesticide removal from drinking water must be developed and implemented.

Implementing Granular Activated Carbon (GAC) filtration systems is a highly effective approach to eliminating trace chemical compounds from drinking water sources. Despite extensive research demonstrating the efficacy of GAC in addressing a wide range of micropollutants, there exists a considerable deficiency of research explicitly investigating the utilization of GAC for pesticide elimination in water treatment processes. The deficiency in the literature provides an opportunity for further investigation into the potential of GAC as a targeted solution for pesticide contamination in drinking water sources.

In light of these considerations, this study aims to investigate the efficacy of GAC filtration in removing micropollutants, specifically pesticides, from drinking water. The research focuses on five representative pesticides: carbofuran, chlorpyrifos, cyprodinil, malathion, and propanil. Through a series of laboratory-scale experiments, the study examines the adsorption of the target pesticides and the influence of background Natural Organic Matter (NOM) on the adsorption process. Through the analysis of adsorption kinetics and isotherms, coupled with the employment of Rapid/Small-Scale Column Tests (RSSCTs) in continuous-flow experiments, this research aims to elucidate the underlying adsorption mechanisms and the overall effectiveness of GAC in pesticide removal during water treatment processes. The findings of this study are expected to contribute valuable insights to the water treatment field, potentially informing strategies to enhance drinking water quality and public health.

2. LITERATURE REVIEW

2.1. Environmental Fate and Transport Mechanisms of Micropollutants in Aquatic Systems

Micropollutants, which encompass a diverse group of organic and inorganic substances present in water at trace concentrations (typically in the range of nanograms to micrograms per liter), pose unique challenges to the health of humans and all other living forms. These compounds include pharmaceuticals and personal care products (PPCPs), endocrine-disrupting compounds (EDCs), pesticides, industrial chemicals, trace metals, microplastics, and various other synthetic organic compounds (Galindo-Miranda et al., 2019; Tijani et al., 2015). The presence of these micropollutants in water resources has generated considerable apprehension due to their potentially harmful impacts on human health and aquatic ecosystems, even at very low concentrations (Arman et al., 2021).

Micropollutants enter the environment through various human activities. Once released, they spread widely and can be transported to different environmental compartments. Those pollutants infiltrate the environment through diverse pathways, predominantly via effluents from wastewater treatment plants (WWTPs) and terrestrial runoff, as presented in Figure 2.1 (Farré et al., 2008). Pesticides can migrate from their initial application sites to neighboring aquatic ecosystems, including rivers, lakes, streams, and groundwater reserves, through a process where precipitation or irrigation washes them away from their applied areas and carries them into adjacent water resources (Capel et al., 2001; Dabrowski et al., 2002). Furthermore, the application of manure or sewage sludge as fertilizers to agricultural fields can facilitate the leaching of various pharmaceuticals and antibiotics through similar mechanisms (Christian et al., 2003; Lyu et al., 2020; Peyton et al., 2016; Tagg et al., 2022). Human pharmaceuticals and microplastics enter aquatic environments through excretion and insufficient removal during WWTP processes.

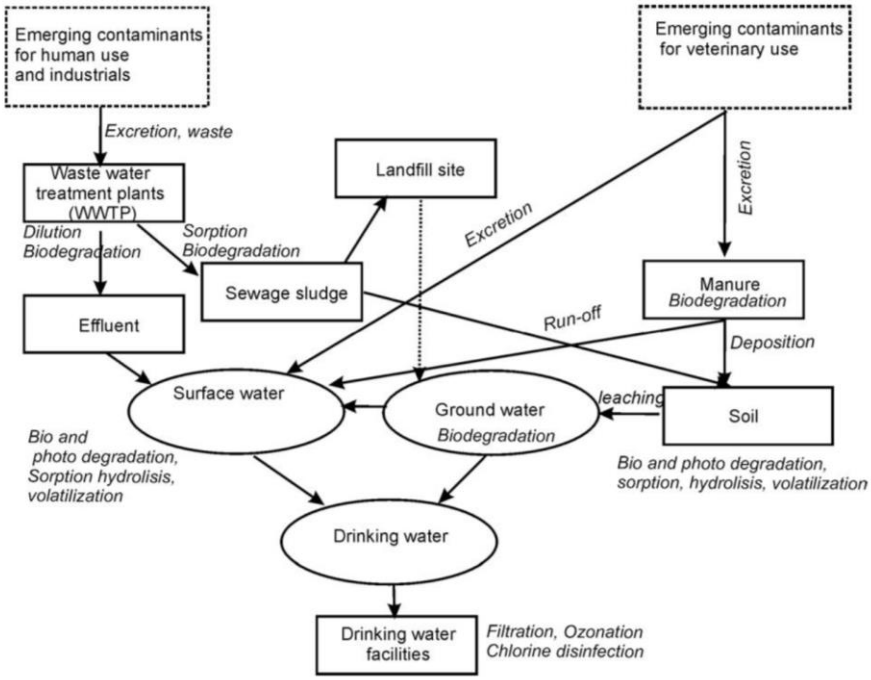


Figure 2.1. Main fate and transport mechanisms of micropollutants in the environment (Farré et al., 2008).

The aforementioned contamination pathways are of particular concern due to their potential to facilitate the accumulation of micropollutants in diverse aquatic environments, thereby posing potential risks to both aquatic biota and human health. The persistence and bioaccumulation of these micropollutants in the environment pose significant challenges for water quality management (Schwarzenbach et al., 2006). As a result, there is a growing need for advanced drinking water treatment technologies. The persistent nature and bioaccumulative properties of these pollutants within environmental matrices present substantial obstacles for effective water quality management (Aljerf & AlMasri, 2018). The escalating number and concentrations of micropollutants in water resources pose significant challenges for conventional drinking water treatment facilities, which are not primarily designed to eliminate these contaminants (Rodriguez-Narvaez et al., 2017; Schwarzenbach et al., 2006).

2.2. Limitations of Conventional Water Treatment in Removing Micropollutant Removal

Conventional water treatment systems are designed to eliminate several types of contaminants from water. These include colloidal particles (fine particles suspended in the water), dissolved salts, and harmful microorganisms (Rodriguez-Narvaez et al., 2017). Their capacity to eliminate micropollutants is, nevertheless, quite variable and restricted (Teodosiu et al., 2018). The difficulty in developing tailored treatment technologies stems from the extremely low quantities of these

pollutants, which frequently go below detection criteria (Saravanan et al., 2021). The unique chemical characteristics of the compounds, the treatment methods employed, and the system's operating settings all significantly impact how well micropollutants are removed from the environment. Important elements affecting removal effectiveness are the micropollutants' molecular structure, polarity, solubility, and persistence (Luo et al., 2014).

Conventional water treatment typically involves a series of physical and chemical processes, including coagulation, flocculation, sedimentation, filtration, and disinfection, as shown in Figure 2.2. While these processes have proven effective for many common contaminants, their capacity to eliminate micropollutants is inconsistent and often limited (Borrull et al., 2021; Luo et al., 2014).

While some micropollutants can be partially removed through processes like coagulation and flocculation, which can adsorb certain compounds onto particulate matter, the success of these methods largely depends on the specific characteristics of the micropollutants (Ballard & MacKay, 2005). Unfortunately, many micropollutants resist these traditional treatment processes (Teodosiu et al., 2018). As a result, these micropollutants can pass through conventional water treatment systems largely unaffected, posing potential risks to water quality and environmental health (Cantoni et al., 2020).

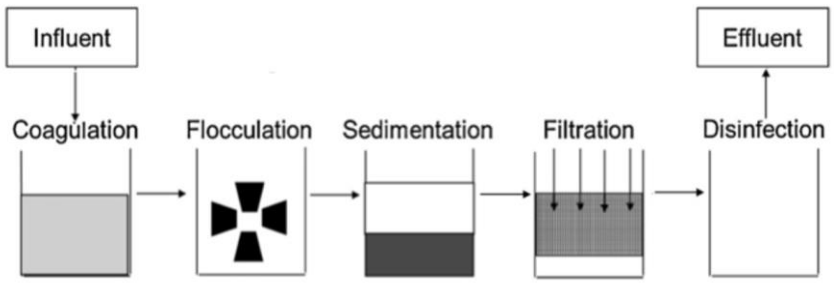


Figure 2.2. Schematic representation of conventional water treatment plants.

Advanced treatment technologies, including advanced oxidation processes (AOPs), membrane filtration, and activated carbon adsorption, have demonstrated significant potential in enhancing the removal of micropollutants (Borrull et al., 2021; Saravanan et al., 2021; Tröger et al., 2017). However, implementing these technologies in large-scale water treatment facilities presents several challenges, primarily related to cost-effectiveness, energy consumption, and operational complexity (Ibrahim et al., 2023).

AOPs, while effective, necessitate precise control of operating conditions and are characterized by high energy requirements (Miklos et al., 2018). Furthermore, there is a critical need for continuous monitoring to detect the potential formation of byproducts (Ike et al., 2019). Although highly efficient, membrane filtration technologies require substantial energy input due to the high pressure involved in their operation (Ibrahim et al., 2023). Additionally, membrane systems are susceptible to fouling, necessitating regular maintenance and cleaning protocols (Guo et al., 2012; Peiris et al., 2013).

Among the various advanced treatment processes, adsorption is considered the most commonly used method because of its cost-effectiveness, operational simplicity, and ease of regeneration (Saravanan et al., 2021; Teodosiu et al., 2018). Numerous studies have highlighted that among various adsorbent materials, activated carbon stands out as the most widely utilized and efficient adsorbent for micropollutant removal in water treatment (Rodriguez-Narvaez et al., 2017; Sangkarak et al., 2020; Sophia & Lima, 2018; Teodosiu et al., 2018; Zhao et al., 2022). This technology has shown promise in effectively removing a wide range of micropollutants without the associated high operational costs of other advanced treatment methods. However, further research is required to optimize its application in large-scale water treatment facilities and to assess its long-term efficiency in micropollutant removal (Tröger et al., 2020).

2.3. Properties and Mechanisms of Granular Activated Carbon (GAC)

Adsorption by activated carbon is a popular treatment technique that can effectively remove micropollutants and several pesticides (Teodosiu et al., 2018). Since activated carbon has a large surface area due to its high porosity, it provides adsorption sites for removing water contaminants (Çeçen & Aktaş, 2011). In drinking water treatment plants, powdered activated carbon (PAC) and granular activated carbon (GAC) are widely used as physical processes to eliminate a wide range of contaminants including various pesticides (Rodriguez-Narvaez et al., 2017). In general, PAC is used as a temporary treatment for transient contaminants, and GAC is used to reduce NOM, synthetic organic compounds, taste and odor compounds in fixed-beds (Çeçen & Aktaş, 2011). In many cases, GAC filtration is more advantageous than PAC (Meinel et al., 2015).

When a dissolved substance comes into contact with a solid surface, two primary mechanisms drive its attachment: electrostatic and hydrophobic interactions (Nam et al., 2014). The first type of interaction is linked to the hydrophobicity of solute. Electrostatic interactions significantly influence

the solute's affinity for the solid adsorbent. Chemical attractions and van der Waals forces primarily establish the solute's affinity towards an adsorbent (Beck, 1973).

Numerous other factors influence the efficacy of activated carbon in micropollutant removal. These include the type of carbon, physicochemical properties of carbon, the particle size of carbon, density, external and internal surface area, pore size distribution, and surface chemistry (Çeçen, 2024; Mailler et al., 2016; Teodosiu et al., 2018). Additionally, the effectiveness is impacted by operational parameters such as contact time, initial concentration of pollutants, pH, temperature, and water content of the system (Kennedy et al., 2015; Mailler et al., 2016; Çeçen, 2024).

Furthermore, the adsorption process is significantly influenced by the morphological properties of the adsorbate, including its size and molecular geometry (Takam et al., 2020). These characteristics play a crucial role in determining the efficiency and effectiveness of the adsorption mechanism. In the literature, it is widely acknowledged that the adsorption capacity of a chemical compound exhibits a positive correlation with both its molecular mass and the number of functional groups present in its structure (Çeçen & Aktaş, 2011). This relationship implies that as the compound's propensity for adsorption is generally enhanced as the molecular complexity increases, either through a higher molecular weight or a greater number of functional moieties. To illustrate, certain functional groups impact a molecule's ability to be adsorbed. Specifically, hydroxyl, sulfonic, and amino groups typically decrease adsorbability. In contrast, the presence of nitro groups tends to increase a molecule's adsorbability (Hassler, 1963). Adsorption of aromatic compounds provides another example. π-π stacking interactions with graphene-based adsorbents and aromatic compound compounds enhance the adsorption process since the planar structures of benzene rings in aromatic compounds allow these interactions (Björk et al., 2010).

2.3.1. Natural Organic Matter (NOM) and Its Effects on Adsorption

Water composition is another factor that strongly affects the removal of micropollutants by activated carbon; for example, both the concentration and the characteristics of NOM strongly influence the success of activated carbon (Mailler et al., 2016). NOM is a diverse mixture of organic compounds present in all natural water sources. It is primarily composed of humic and fulvic acid substances and humin, which are byproducts of the decomposition of living organisms (Stevenson, 1994). The presence of NOM can substantially impact water quality and treatment processes, particularly in the context of eliminating micropollutants.

Since there is a competition between micropollutants and NOM and the concentration of NOM is higher than concentrations of micropollutants, NOM can interfere with the removal of micropollutants by activated carbon (Kilduff & Karanfil, 2002). When NOM and micropollutants are adsorbed simultaneously, NOM components with molecular sizes comparable to that of the micropollutants can significantly reduce adsorption capacity by directly competing for the adsorption sites (Snoeyink et al., 2003; Newcombe et al., 1997). In addition, due to their relatively slow adsorption rates, micropollutants move more slowly than NOM through the GAC columns, leading to NOM preloading the GAC before r micropollutants can be effectively adsorbed (Li et al., 2003; Speth, 1991). This results in pore blockage in continuous-flow systems.

2.3.2. Biological Activated Carbon (BAC) Filters

On GAC a biofilm layer can develop a biofilm layer over time in certain drinking water treatment applications, transforming it into Biological Activated Carbon (BAC) (Yuan et al., 2022). This innovative treatment process combines two powerful mechanisms: activated carbon's physical adsorption properties and microorganisms' natural biodegradation capabilities. This dual-action approach has demonstrated remarkable effectiveness in removing a broad spectrum of water pollutants (Jin et al., 2013; Levine et al., 2000).

The performance of BAC filters can be attributed to their sophisticated operational mechanisms. As contaminants adhere to the activated carbon surface, they create an optimal environment for microbial colonization. These microorganisms subsequently utilize the trapped contaminants and convert them into byproducts. This synergistic relationship between physical adsorption and biological degradation helps maintain the carbon’s effectiveness, thereby extending its operational lifespan (Levine et al., 2000; Rattier et al., 2012; Scharf et al., 2010).

In BAC filters, the following mechanisms are active, as shown in Figure 2.3 (Çeçen & Aktaş, 2011; Liang et al., 2007).

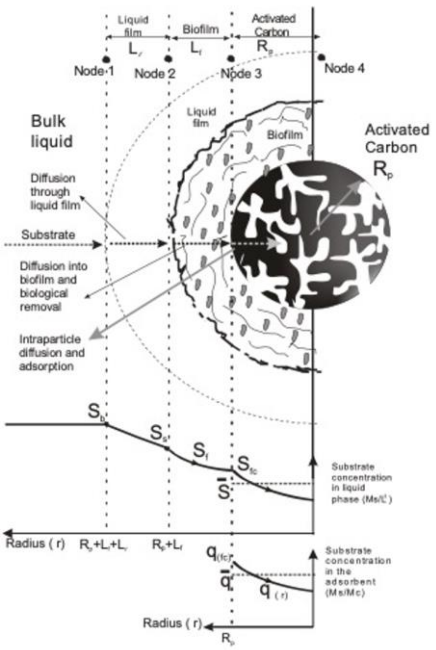


Figure 2.3. Substrate transport and removal mechanisms in a GAC particle covered by a biofilm (Çeçen & Aktaş, 2011).

2.4. Rapid Small-Scale Column Tests (RSSCTs)

The Rapid Small-Scale Column Test methodology helps researchers evaluate how well adsorption materials like granular activated carbon can remove contaminants from water samples in a short period of time. Scientists developed this approach in the 1980s to provide a smaller alternative to full-scale testing of GAC systems (Crittenden et al., 1991a; Poddar et al., 2013). RSSCTs are employed to generate comparable breakthrough curves for predicting full-scale adsorber performance (Çeçen & Aktaş, 2011). Findings indicate that RSSCTs can offer more accurate results than batch tests (Merle et al., 2020; Poddar et al., 2013).

RSSCTs are experimental procedures designed to study how a chosen adsorbent adsorbs micropollutants in a continuous-flow system. This method involves passing water at a specific flow rate through a small column filled with adsorbent. RSSCTs are very advantageous since they decrease the amount of water and adsorbent used while also reducing operation time and material requirements compared to full or pilot-scale studies (Salih et al., 2013). Moreover, these tests enable researchers to assess various treatment scenarios, refining design parameters prior to the deployment of full-scale systems. Studies have shown that RSSCTs provide a method for evaluating how different operating conditions affect the overall removal performance of contaminants (Chowdhury, 2013; Westerhoff et al., 2008).

RSSCTs operate by maintaining dynamic similarity between the small-scale and full-scale systems. This is achieved through careful scaling of specific parameters during the test design. The methodology ensures that the results obtained from laboratory testing can reliably predict the performance of larger treatment systems. In order to do that, several parameters, including empty bed contact time (EBCT), flow rate (Q), and hydraulic loading rate (HLR), carbon usage rate (CUR), and adsorbent particle size (represented in Table 2.1.), are essential for interpreting results accurately and comparing with the existing literature.

Table 2.1. Important parameters in RSSCT.

Parameters	Definition	Equation	Units
Empty Bed Contact Time (EBCT)	The EBCT is a hypothetical measure that calculates the expected duration a liquid would remain in a filter if no packing material were present.	$EBCT = \frac{V_B}{Q}$	min or s
Flow Rate (Q)	The flow rate refers to the quantity of water that passes through a column during a specific time interval.	$Q = \frac{V}{t}$	m^3/d, m^3/s or mL/min
Hydraulic Loading Rate (HLR)	The hydraulic loading rate is a measure that indicates how much the flow rate is per surface area of a column. This rate is typically expressed in units of volume per unit area per unit time.	$HLR = \frac{Q}{A}$	m/h or cm/min
Bed Volume (BV)	This dimensionless parameter represents a standardized ratio between the volume of water flow and the volume of the activated carbon bed.	$BV = \frac{t}{EBCT} = \frac{V_L}{V_B}$	unitless
Carbon Usage Rate (CUR)	The lifespan of GAC in water treatment is measured by this metric. It shows how much activated carbon is needed to reach the breakthrough level.	$CUR = \frac{M_{GAC}}{Q * t_{breakthrough}}$	mg/L

When designing RSSCTs, researchers must consider various factors, including the scaling equations, appropriate particle size reduction ratios, and maintenance of similar flow conditions to ensure an accurate representation of full-scale performance. This systematic approach enables the development of more effective water treatment solutions while minimizing resource expenditure.

2.5. Selection of Representative Pesticides

Most of the studies about the removal of pesticides by activated carbon focus on pesticides that were banned decades ago, such as DDT, HCH, and dieldrin (Ninkovic et al., 2010; Ormad et al., 2008; Tomaszewski et al., 2007). Therefore, there are a limited number of studies with granular activated carbon (GAC) and biological activated carbon (BAC) for the removal of currently used pesticides. It is thought that this study may fill this gap in the scientific literature about the removal of pesticides from drinking water using activated carbon.

As representatives of problematic pesticides, 5 pesticides were selected in this study:

- **Carbofuran** (carbamate insecticide, nematicide),
- **Chlorpyrifos** (organophosphate insecticide),
- **Cyprodinil** (pyrimidine fungicide),
- **Malathion** (organophosphate insecticide), and
- **Propanil** (anilide herbicide).

These pesticides were selected based on their prevalence in water sources and diverse physicochemical properties, allowing a broad assessment of GAC performance under varying conditions.

Propanil is a post-emergence herbicide extensively utilized within the agricultural sector, with a particular emphasis on its application in rice cultivation (Zahan et al., 2017). Propanil, with 12,000 tonnes of annual production by local firms, is among Türkiye's most produced pesticides (Başpinar et al., 2010).

Chlorpyrifos is an organophosphorus insecticide commonly employed to manage pests. It functions as an acetylcholinesterase inhibitor and poses toxicity risks to non-target species, including mammals (Qiao et al., 2021). In addition, chlorpyrifos is on the list of priority substances (PSs) in Directive 2013/39/EU (European Commission, 2013).

Cyprodinil is a fungicide widely utilized in agriculture to manage various diseases in crops like grapes, apples, and strawberries (Knauf-Beiter et al., 1995). It is part of the anilinopyrimidine chemical pesticide group. It was found that exposure to cyprodinil led to increased DNA damage to the gills of zebrafish (Toğay et al., 2021). According to a recent report, cyprodinil consumption in 2008 was 20,890 kg (Başpınar et al., 2010). It may not be considered a huge consumption. However, today, cyprodinil and chlorpyrifos are the pesticides most detected in food analyses in Türkiye (Tiryaki, 2016).

Carbofuran, sold as Furadan, is a highly toxic N-methyl carbamate pesticide widely used as an insecticide and nematicide. This compound poses significant toxicity risks to mammals, birds, and honeybees, and exhibits moderate to high toxicity to most aquatic life forms (Mishra et al., 2020).

Malathion is a synthetic organophosphate broad-spectrum insecticide that is genotoxic (Guyton et al., 2015).

In addition, chlorpyrifos, carbofuran, and malathion pesticides are known to have endocrine disrupting properties which pose a public health threat (Sethi and Ghosh, 2011; Ventura et al., 2016; Goad et al., 2004). Carbofuran, chlorpyrifos, cyprodinil, malathion, and propanil are the commonly encountered pesticides in Türkiye. According to the NORMAN Association (Network of Reference Laboratories for Monitoring of Emerging Environmental Pollutants), which provides the most frequently detecting emerging pollutant list, malathion, cyprodinil, and propanil are also considered emerging micropollutants (NORMAN Network et al., 2022).

3. AIM OF THE STUDY

Numerous studies have identified micropollutants as emerging contaminants present in the drinking water resources of many urban areas (Arman et al., 2021; Borrull et al., 2021). Conventional drinking water treatment processes and operations have often proven insufficient in effectively removing micropollutants, necessitating the exploration of advanced treatment methods (Arman et al., 2021; Borrull et al., 2021). While Granular Activated Carbon (GAC) has shown promise in micropollutant removal, a comprehensive evaluation of its capabilities, especially concerning pesticides, remains lacking in the scientific literature (Golovko et al., 2020; Sperlich et al., 2017; Zietzschmann et al., 2016). Consequently, there is a need for a systematic examination of the efficacy of GAC filters in removing pesticides in drinking water treatment systems.

The main objective of this thesis is to evaluate the effectiveness of GAC filters in removing micropollutants, with a specific focus on pesticides, from drinking water treatment systems. Through a systematic, multi-phase investigation, this research aims to thoroughly understand GAC's adsorption mechanisms and removal efficiency for five representative pesticides.

To achieve these objectives, the study is structured into four distinct phases (Figure 3.1):

Phase 1: Information was gathered from various databases and tools to enhance the understanding of the physicochemical adsorption, and biodegradation properties of selected pesticides. Specifically, the properties of the pesticides were investigated using the PPDB, MetaCyc, EPI Suite, EAWAG-BBD/PPS, and EnviPath programs and databases.

Phase 2: This phase examined the adsorption behavior of selected micropollutants onto GAC through comprehensive kinetic and isotherm studies. This phase aimed explicitly to (1) evaluate the adsorption kinetics, determine the equilibrium time for adsorption processes, (3) analyze the adsorption isotherms using various models, and (4) assess the influence of Natural Organic Matter (NOM) on micropollutant removal efficiency. Kinetic and isotherm modeling were used to understand the underlying mechanisms of the adsorption process.

Phase 3: This phase investigated the biodegradation of micropollutants using batch reactor systems. The experimental approach used an inoculum developed through the enrichment and acclimation of bacterial communities obtained from the Ömerli reservoir in suspended-growth systems.

Additionally, this part of the study examined the potential synergistic effects of combined GAC adsorption and biodegradation processes on micropollutant removal in batch reactor systems.

Phase 4: The phase aimed to evaluate the efficacy of GAC on micropollutant removal through continuous-flow experiments utilizing Rapid/Small-Scale Column Tests (RSSCTs). This methodology was selected to address the practical limitations associated with pilot/laboratory-scale GAC columns, including excessive water consumption and economic constraints. RSSCTs provided an efficient method for evaluating GAC performance in continuous-flow systems in a shorter experimental period than pilot or laboratory-scale columns. Multiple RSSCT experiments were designed and conducted to comprehensively evaluate GAC's capacity for micropollutant removal in continuous-flow systems. The results were compared with the Adsorption Design Software (AdDesignS), along with column parameters, to simulate breakthrough curves and forecast treatment system performance.

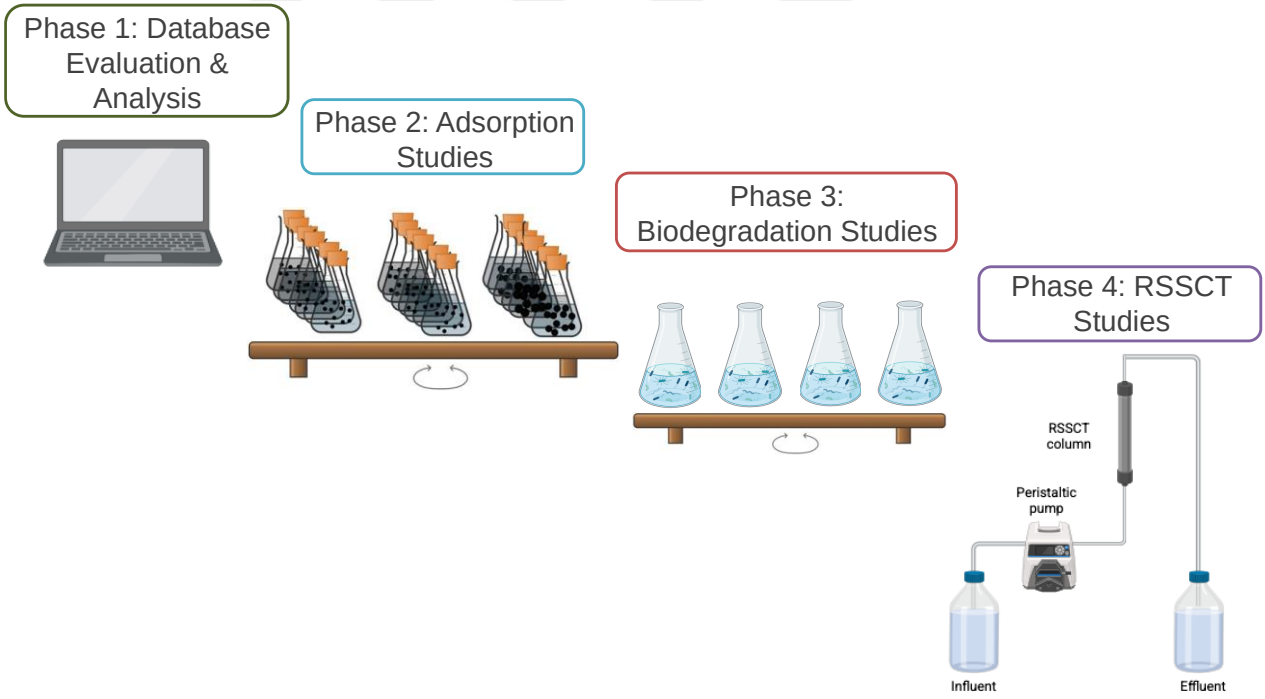


Figure 3.1. Schematic representation of the study phases.

4. MATERIALS AND METHODS

4.1. Data-Driven Assessment of Selected Pesticides Physicochemical and Biodegradation Characteristics

In contemporary environmental technology research, it is crucial to obtain initial data about chemicals before designing experimental setups. Various databases and tools provide essential information about chemical properties, including their toxicity levels, ability to biodegrade, and solubility characteristics. By leveraging this information, researchers can better assess risks and create more efficient and safer experimental protocols. Additionally, understanding the physicochemical properties can aid in selecting appropriate materials and methods for handling, storing, and disposing chemicals, ensuring compliance with environmental regulations and standards.

The Pesticide Properties DataBase (PPDB) serves as an extensive repository of information detailing the chemical, physical, and biological characteristics of pesticides (Lewis et al., 2016). It is an indispensable resource for researchers and professionals engaged in pesticide research. The PPDB offers extensive information on various pesticides, encompassing their chemical composition, physical characteristics, environmental behavior, toxicological effects, and ecological impacts.

BIOWIN is a part of the comprehensive EPI Suite software package created by the US Environmental Protection Agency (EPA). The biodegradation potential of a substance can be estimated using the BIOWIN module (Çeçen & Gül, 2021). BIOWIN includes seven discrete models that assess aerobic or anaerobic biodegradation potential, some of which provide qualitative biodegradation data and rapid biodegradation potential based on Japanese Ministry of International Trade and Industry (MITI) data (Boethling & Costanza, 2010). Additional models within the EPI Suite BIOWIN module estimate both primary and terminal biological degradation.

MetaCyc, a comprehensive metabolic pathway database, is a significant resource for identifying whether a substance can undergo biotransformation by microorganisms (Caspi et al., 2016). The database contains comprehensive information on biodegradation processes, featuring detailed records of metabolic pathways from thousands of organisms (Caspi et al., 2020). It incorporates molecular-level data, including genetic information, enzymatic processes, regulatory factors like cofactors and modulators, and, where applicable, quantitative measurements of reaction kinetics for specific compound degradation (Caspi et al., 2020). Furthermore, MetaCyc offers information on potential

biotransformation metabolites, enzymes, test conditions, and metabolite structures in related literature (Çeçen & Tezel, 2017). A substance of interest can be easily searched by its name within this database; its presence suggests its potential for biotransformation by environmental microorganisms. The data within MetaCyc is derived from experimental studies reported in scientific literature. Conversely, the absence of a substance in this database suggests either non-biodegradability or a lack of biodegradation studies.

Additionally, the EAWAG Biodegradation/Biocatalysis Database (BBD) offers further insights into biodegradation possibilities and stages. The EAWAG BBD provides detailed information on biocatalytic reactions and the biological degradation of xenobiotic compounds, including enzymes, microorganisms, reactions, and biotransformation products (Gao et al., 2010). The database also features a Pathway Prediction System (PPS) that identifies organic functional groups in a compound and predicts possible transformation based on established biotransformation rules. Furthermore, the EnviPath (Environmental Contaminant Biotransformation Pathway Resource) tool builds upon this functionality to predict microbial biotransformation of previously unstudied organic pollutants.

The utilization of these tools and databases to gather preliminary information about physicochemical properties and biodegradation potential provides crucial guidance for experimental design, helping researchers determine appropriate methodologies and parameters for their studies.

4.2. Chemicals

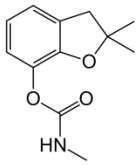
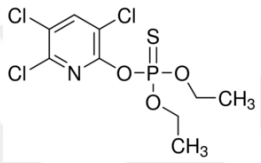
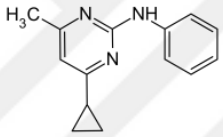
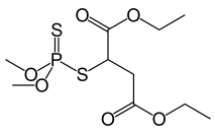
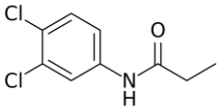
4.2.1. Selection of Pesticides

The research examines five key pesticides: carbofuran, chlorpyrifos, cyprodinil, propanil, and malathion. These pesticides were selected based on their usage in Türkiye and the findings presented in Section 5.1. According to established guidelines, substances can be categorized into three groups based on their sorption potential: those with log K_{ow} below 2.5 exhibit low sorption potential, those between 2.5 and 4.0 show medium sorption potential, and those exceeding 4.0 demonstrate high sorption potential, as documented in the scientific literature (Rogers, 1996).

Cyprodinil and chlorpyrifos were selected as pesticides with a high sorption potential, with log K_{ow} values of 4 and 4.96, respectively. Propanil, with a log K_{ow} of 3.07, was selected as a moderately adsorbable pesticide. Malathion and carbofuran, with log K_{ow} values of 2.36 and 2.32, respectively, are pesticides that are less likely to adsorb.

The pesticides were obtained in high purity (analytical standards) from Sigma Aldrich Chemicals Company. The properties of these pesticides were described in Table 4.1.

Table 4.1. Molecular structures and physicochemical properties of the selected pesticides.

Pesticides	Molecular Structure	CAS #	SMILES*	log K_{ow}
Carbofuran $C_{12}H_{15}NO_3$ 221.25 g/mole		1563-66-2	CC1(CC2=C(O1)C(=CC=C2)OC(=O)NC)C	2.32
Chlorpyrifos $C_9H_{11}Cl_3NO_3PS$ 350.59 g/mole		2921-88-2	CCOP(=S)(OCC)OC1=NC(=C(C=C1Cl)Cl)Cl	4.96
Cyprodinil $C_{14}H_{15}N_3$ 225.29 g/mole		121552-61-2	CC1=NC(=NC(=C1)C2CC2)NC3=CC=CC=C3	4
Malathion $C_{10}H_{19}O_6PS_2$ 330.36 g/mole		121-75-5	CCOC(=O)CC(C(=O)OCC)SP(=S)(OC)OC	2.36
Propanil $C_9H_9Cl_2NO$ 218.08 g/mole		709-98-8	CCC(=O)NC1=CC(=C(C=C1)Cl)Cl	3.07

**SMILES: Simplified Molecular Input Line Entry Specification*

4.2.2. Selection of Granular Activated Carbon

For this research, granular activated carbon (GAC) was sourced from the Cabot Company. After consulting regarding the research objectives, the company recommended their specific product, Norit® GAC 1240AF, as the most suitable variant for the experimental procedures. The physicochemical properties of the selected Norit® GAC 1240AF are presented in Table 4.2.

Table 4.2. Properties of the chosen activated carbon.

Properties	Norit® GAC 1240AF
Activation Type	Steam Activation
Iodine Number (mg/g)	1000 (min)
Methylene Blue Adsorption (mg/g)	22
Particle size > 12 mesh (1.70 mm)	5% (max)
Particle size < 40 mesh (0.425 mm)	5% (max)
Apparent Density	470 (kg/m^3)
Moisture	5% (max)
Total Surface Area (B.E.T.)	1100 (m^2/g)
Mesopore Surface Area (S_{meso})	170 (m^2/g)*
Micropore Volume (V_{micro})	0.36 (cm^3/g)*
Specific Pore Volume (V_p)	0.34 (cm^3/g)*
pH	Alkaline
pHpzc	7.6*

* *(Sampaio et al., 2022)*

4.3. Grinding of Activated Carbon

To accurately simulate full-scale adsorption in a laboratory setting, it is necessary to reduce the particle size of granular activated carbon (GAC) in Rapid Small-Scale Column Tests (RSSCTs). Decreasing the GAC size ensures that mass transfer and adsorption kinetics remain comparable to those in larger systems, despite the significantly reduced contact time. By reducing the particle size, the test can maintain similarity, allowing for reliable performance predictions.

This process involved reducing the size of Norit® GAC 1240AF from its original particle size of approximately 1 mm. The GAC particles were reduced to achieve a target size of 100 μm through grinding and sieving procedures. This ten-fold reduction in particle size enables a hundred times decrease in the EBCT, as detailed in Section 4.8.

In the laboratories of Istanbul Technical University's Chemical and Metallurgical Engineering Faculty, these GAC particles were downsized utilizing a ball mill (SPEX SamplePrep 80000D Mixer/Mill) and a sieve shaker (Retch) with varying size sieves (Figure 4.1). The optimal operational conditions were ascertained by exploring diverse GAC and grinding ball ratios. The most optimum

ratio was found by putting 15 g of GAC and 20 g of grinding balls into the metal grinding container to yield the desired GAC particle size of 100 µm (Figure 4.2). After two identical metal grinding containers were prepared, they were placed in a ball mill and operated for 5 min at a speed of 1200 rpm. This procedure was repeated multiple times to achieve a sufficient quantity of GAC of the desired size. The ground GAC was then inserted into a sieve shaker with four different sieve sizes (70 µm, 100 µm, 125 µm, and 150 µm, respectively). After a 10-minute sieving operation, the GAC that remained within the 100 µm sieve was gathered and stored for subsequent experiments.



Figure 4.1. Left: SPEX SamplePrep 8000D Mixer/Mill®, Right: Retch sieve shaker.



Figure 4.2. Left: pristine GAC sample (before grinding), Middle: grinding metal balls, Right: GAC sample after grinding

Before each experiment with GAC, a specified amount of the grounded or pristine GAC underwent a washing procedure using ultrapure water. This was implemented with the intent to eliminate any fine particles that may be present in GAC. Subsequently, the GAC samples were subjected to a drying phase in an oven at a temperature of 105 °C for a period of two days. After

drying, the GAC samples were carefully preserved in a desiccator till the experiment to ensure their integrity.

4.4. Analytical Methods and Measurements

4.4.1. LC-MS/MS Analysis

The qualitative and quantitative pesticides analysis was carried out by using LC-MS/MS (API Q-Trap 4500 triple quadrupole linear ion trap mass spectrometry). An accucore aQ C18 column from Thermo Fisher Scientific was employed. During the analysis, Methyl-d3-triphenylphosphonium iodide was used as an internal standard (IS). A binary solvent system was used as mobile phase, consisting of liquid chromatography grade methanol buffered with 0.1% formic acid (Pump A) and liquid chromatography grade water buffered with 0.1% formic acid (Pump B).

Detection of pesticides based on non-scheduled multiple reaction monitoring (MRM) was performed using electrospray ionization (ESI) probe positive ionization modes. The source parameters for ESI positive mode were as follows: curtain gas, 30; ion spray voltage, 5500 V/4500 V; temperature 550 °C; ion source gas1; 50 and ion source gas 2, 60. The percentage of the mobile phases during the analysis was given in Table 4.3. For instrument control and data acquisition, Analyst Software 1.6.2 (AB Sciex) and the peak integration, MultiQuant 3.0.1 (AB Sciex) were used.

In the procedure for the liquid chromatography-tandem mass spectrometry (LC-MS/MS) analysis, a volume of 1 mL of the specimen was mixed with 0.8 mL of methanol of liquid chromatography grade. Following this, the resulting mixture was filtered using a hydrophilic Polytetrafluoroethylene (PTFE) filter with a pore size of 0.22 μm. Consequently, a portion of 0.9 mL of filtered sample was introduced into an HPLC vial in conjunction with 0.1 mL of the Internal Standard (IS) solution, which had been prepared to a concentration of 100 μg/L. Determination of pesticides in the prepared samples was carried out at the μg/L level using unscheduled MRM parameters for each pesticide.

Figure 4.3 presents an indicative liquid chromatography-tandem mass spectrometry (LC-MS/MS) chromatogram of pesticides. Subsequently, Figures 4.4 through 4.8 depict the calibration curves for these pesticides.

Table 4.3. The operation conditions of the liquid chromatography-tandem mass spectrometry (LC-MS/MS).

Time Intervals	Percentage of Mobile Phases
0 min	60% Methanol + 40% Water
4 min	60% Methanol + 40% Water
4.1 min	95% Methanol + 5% Water
14 min	95% Methanol + 5% Water
14.1 min	60% Methanol + 40% Water
18 min	60% Methanol + 40% Water

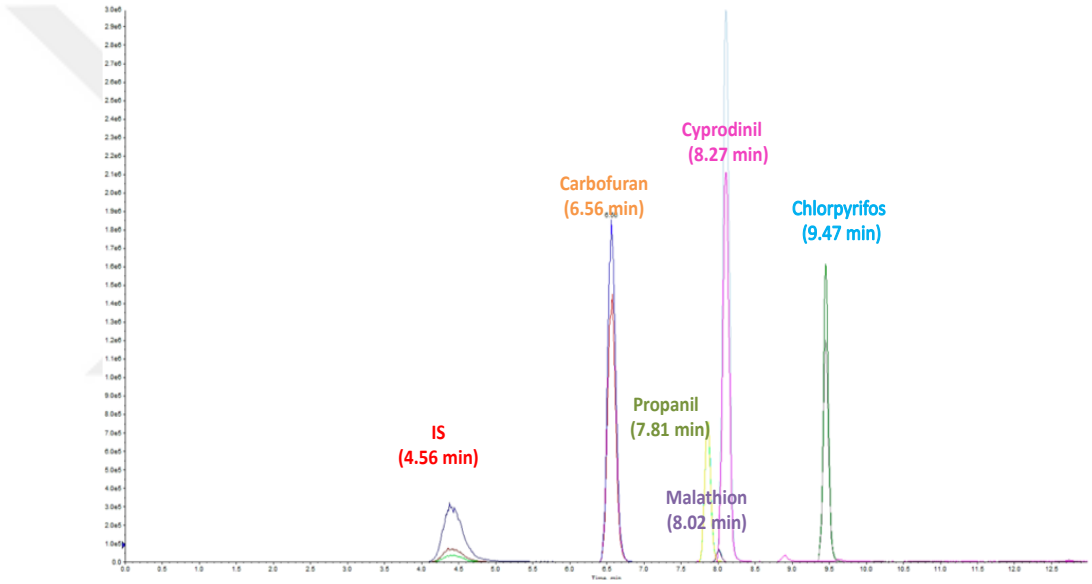


Figure 4.3. LC-MS/MS chromatogram of a sample containing carbofuran, propanil, cyprodinil, malathion, methyl-d3-triphenylphosphonium iodide (IS), and chlorpyrifos.

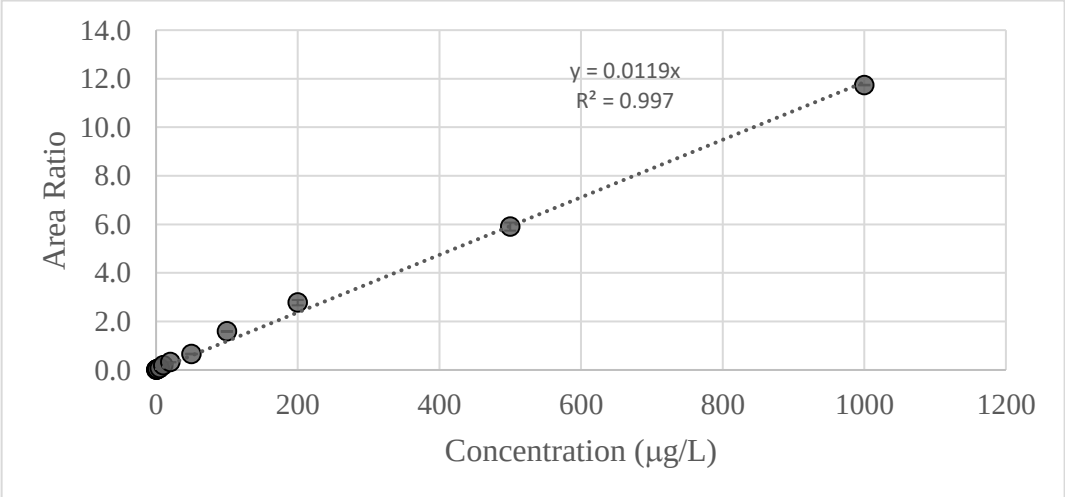


Figure 4.4. Calibration curve of carbofuran (0.1 to 1000 µg/L).

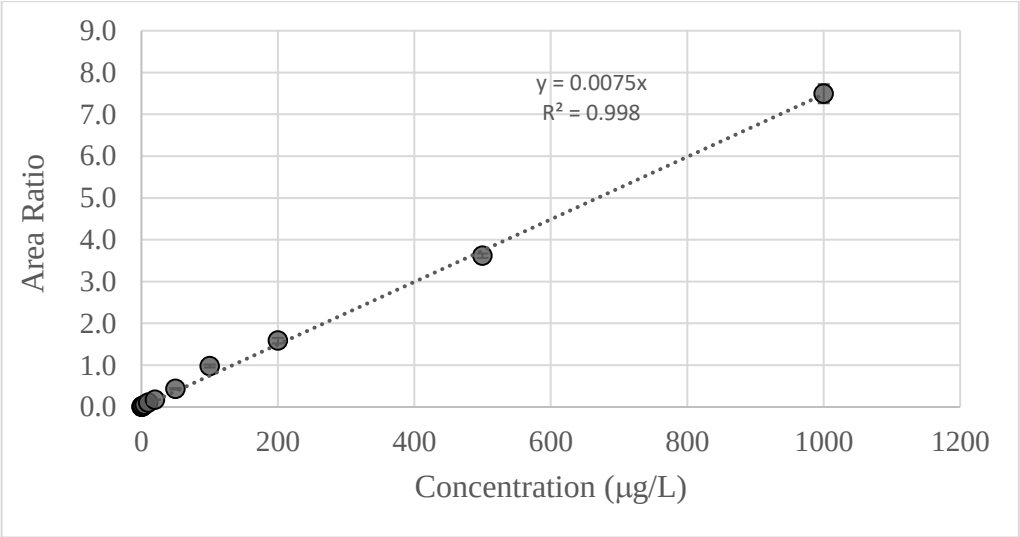


Figure 4.5. Calibration curve of chlorpyrifos (0.1 to 1000 µg/L).

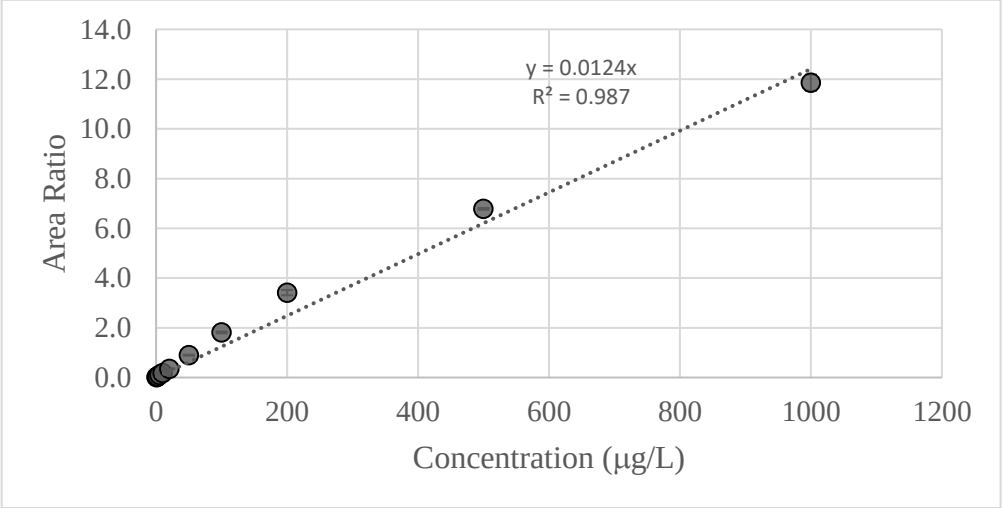


Figure 4.6. Calibration curve of cyprodinil (0.1 to 1000 µg/L).

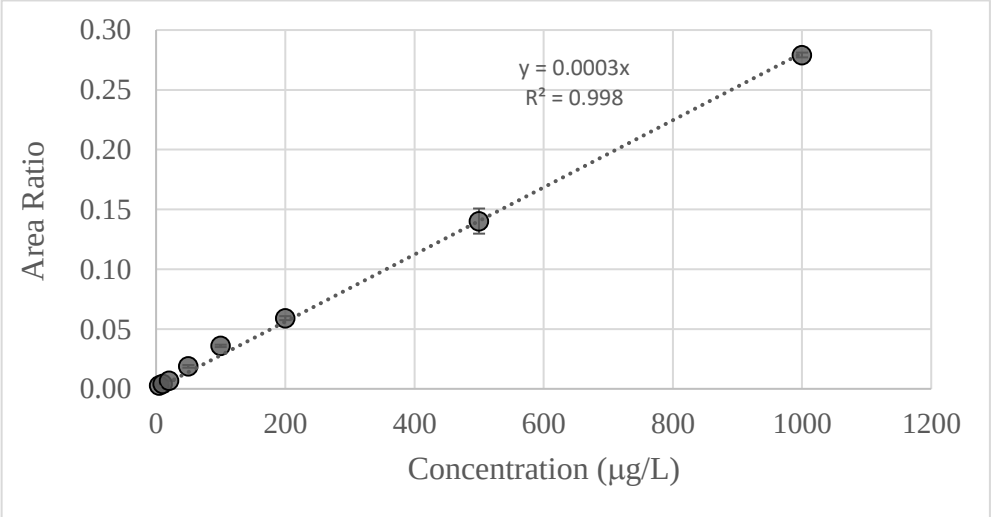


Figure 4.7. Calibration curve of malathion (0.1 to 1000 µg/L).

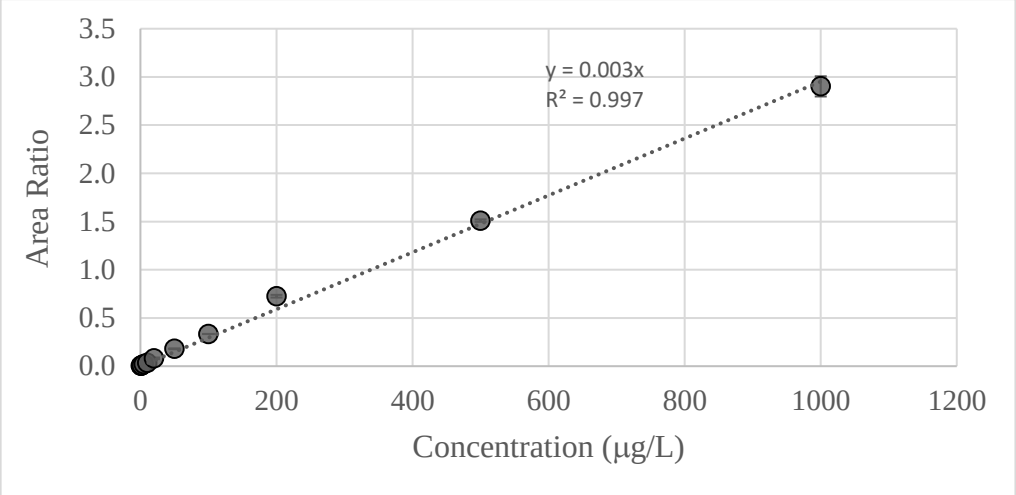


Figure 4.8. Calibration curve of propanil (0.1 to 1000 µg/L).

4.4.2. Dissolved Organic Carbon (DOC) Analysis

DOC analysis was performed to measure the background NOM, which consists of various chemicals, including humic acid, in drinking water. These compounds are measured collectively in water studies due to their non-uniform molecular weights.

The Shimadzu TOC-V analyzer was employed to quantify the background organic carbon content. The analyzer was calibrated using potassium hydrogen phthalate (KHP) solutions at different concentrations. Before DOC measurement, samples were subjected to a 0.45 µm Hydrophobic Polytetrafluoroethylene (PTFE) filter. The calibration curve, which covers a range of 0-5 mg/L DOC, is depicted in Figure 4.9.

To preclude the introduction of any extraneous organic matter potentially originating from water, ultrapure water was used in all experiments and dilutions. Ultrapure water was obtained from the Milipore Mili-Q gradient A10 device.

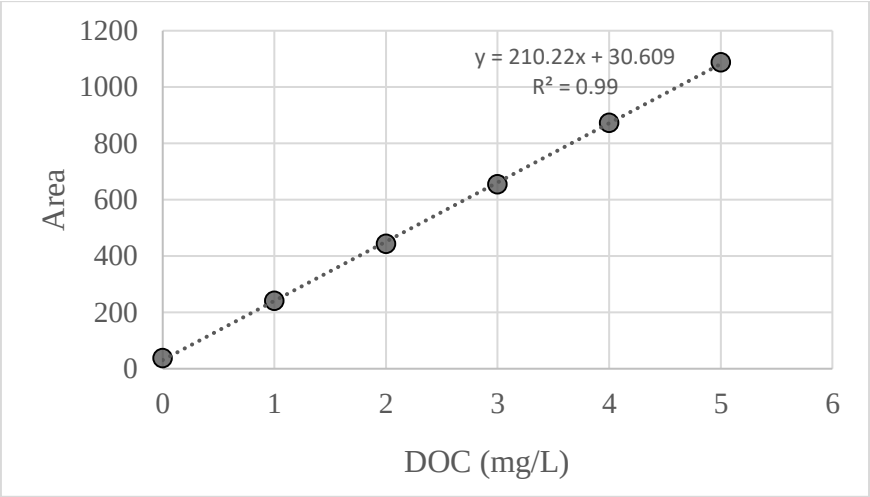


Figure 4.9. Calibration curve of DOC.

4.4.3. Spectrophotometric Measurements

Spectrophotometric measurements were performed using a Shimadzu UV-160A UV-VIS double-beam spectrophotometer and a VWR UV-1600PC spectrophotometer. The selected wavelengths for UV-VIS absorbance measurements encompassed 254 nm, 280 nm, 400 nm, 436 nm because UV and color absorbance at these wavelengths can effectively characterize NOM (Dorota, 2018). These absorbance measurements aid in identifying various chromophores of humic acid and following their concentration. Absorbance at 254 nm correlates with the presence of aromatic groups, while absorbance at 280 nm indicates aromatic amino groups (Korshin et al., 2009; Sambo et al., 2020).The absorbance at 400 and 436 nm indicates the existence of functional groups responsible for water coloration, ranging from yellow to brown, which are structures containing conjugated double bonds (Dorota, 2018).

To ensure the removal of granular activated carbon or any undissolved particles, all samples were subjected to filtering through a 0.45 μm hydrophilic PTFE filter. Quartz cells with a path length of 1 cm were employed for all spectrophotometric measurements. Each absorbance was measured twice, and the reported values represent the average of these two readings.

4.4.4. pH Measurements

WTW Inolab-1 and VWR pHenomenal pH meters were used for pH measurements. The calibration of the pH probe was done every 2 or 3 weeks by using standard buffer solutions having pH values of 4 and 7.

4.5. Characterization and Preparation of Synthetic Drinking Water

This study aims to investigate the adsorption of selected pesticides onto GAC from drinking water, specifically focusing on emulating the water quality of Ömerli Dam, Istanbul's largest water source.

The Ömerli Dam, constructed between 1968 and 1972 in Istanbul, is a critical infrastructure for providing potable water to the city. It is Istanbul's largest dam, with a substantial annual water capacity of 220 million cubic meters. The water from this reservoir undergoes purification at the Ömerli Drinking Water Treatment Facilities before being distributed to the urban population (İSKİ, 2024).

This dam supplies water to almost the entire Anatolian Side of Istanbul. Ömerli Drinking Water Treatment Facilities are composed of four central plants: Orhaniye, Muradiye, Osmaniye and Emirli (Yavuz Sultan Selim). Additionally, the facility can supply 500,000 cubic meters of potable water daily to the European Side of Istanbul via transmission lines connecting Sarayburnu and Salacak. The dam has a basin area of 621 square kilometers (İSKİ, 2024).

A comprehensive year-long study by Yapsaklı (2008) provided extensive data on the Ömerli Dam's water quality parameters. This study encompassed 60 measurements, from which minimum, maximum, and average values, along with standard deviations, were derived. These extensive data, presented in Table 4.7, provide a robust foundation for the synthetic water prepared in this study.

A synthetic water formulation was developed to address the variable composition of the Ömerli Reservoir's water, which experiences variations due to seasonal patterns, thermal changes, and weather conditions. This laboratory-prepared artificial formulation was specifically designed to simulate the essential physicochemical characteristics of the reservoir water, enabling consistent and reproducible experimental conditions for analytical procedures.

A meticulous process is needed to make synthetic drinking water that has the same qualities as the source water, which in this case is water from the Ömerli Reservoir. The existing protocol for soft fresh water preparation, as described by Smith et al. (2002), and represented in Table 4.4., was adopted and modified to align with the specific compositional characteristics of the Ömerli raw. This

adaptation process necessitated various adjustments to the original protocol to ensure its relevance to the Ömerli water.

Table 4.4. Recipe for synthetic soft freshwaters (Smith et al., 2002).

# of stock solution	Ingredients	Mass (g) of salt per volume of MilliQ water	Concentration factor
S1		***1L***	x 1000
	$MgCl_2 .6H_2O$	12.168 g	
	$CaCl_2 .6H_2O$	17.500 g	
	$Ca(NO_3)_2 .4H_2O$	3.542 g	
S2		***5L***	x 1.1
	$CaCO_3$	0.0936 g	
S3		***1L***	x 1000
	Na_2SO_4	16.334 g	
	$KHCO_3$	2.502 g	
	$NaHCO_3$	1.678 g	

The experimental methodology involved a systematic approach to address the compositional disparities between Ömerli reservoir water and the synthetic soft freshwater recipe proposed by Smith et al. (2002). In order to address the deficiencies identified in the recipe compared to Ömerli water composition, quantitative calculations were conducted to determine the precise concentrations of ferrous (Fe^{2+}) and manganese (Mn^{2+}) ions. Based on reference measurements, the target concentrations were established at 0.02 mg/L and 0.07 mg/L for Fe^{2+} and Mn^{2+}, respectively. Stock solutions were prepared accordingly, and the concentrations of ferrous and manganese were verified using Inductively Coupled Plasma (ICP) spectroscopy. Subsequently, the requisite levels of NO_3^--N and NH_4^+-N were established by dissolving $NaNO_3$ and $(NH_4)_2SO_4$ salts. The resulting concentrations were validated using the Cadmium Reduction Method (Hach Method 8192) and the Nesslerization Method (Method 4500-NH_3) as described in Standard Methods.

The final phase of optimization focused on achieving target values for TOC, DOC, and Specific Ultraviolet Absorbance at 254 nm ($SUVA_{254}$) by incorporating humic acid sodium salts as natural organic matter. $SUVA_{254}$ is highly correlated with the aromaticity of dissolved organic matter in water samples (Sambo et al., 2020). Multiple iterations were required to optimize these parameters due to the inherent variability of humic acid. Following the adjustment of primary parameters, secondary parameters such as alkalinity and hardness were adjusted. Since the initial measurements revealed that the values for alkalinity and hardness were below the desired range, the quantities of S1 and S3 stock solutions in the Smith et al. (2002) recipe were increased threefold to achieve the target levels. The optimized recipe resulting from these methodological refinements is presented in Table 4.5.

Table 4.5. Synthetic Ömerli Reservoir water preparation formulation.

# of stock solution	Ingredients	Mass (g) of salt per volume of MilliQ water	Concentration factor	Concentration (mL /L)
S1		***1L***	x 333	3
	$MgCl_2 .6H_2O$	12.168 g		
	$CaCl_2 .6H_2O$	17.500 g		
	$Ca(NO_3)_2 .4H_2O$	3.542 g		
S2		***5L***	x 1.1	909
	$CaCO_3$	0.0936 g		
S3		***1L***	x 333	3
	Na_2SO_4	16.334 g		
	$KHCO_3$	2.502 g		
	$NaHCO_3$	1.678 g		
S4		***1L***	x 100	10
	$FeSO_4 .7H_2O$	0.100 g		
	$MnSO_4.4H_2O$	0.248 g		
S5		***1L***	x 100	10
	$(NH_4)_2SO_4$	0.165 g		
S6		***1L***	x 100	10
	$NaNO_3$	0.400 g		
S7		***1L***	x 100	10
	Humic acid sodium salt	0.800 g		

A comparative analysis of the parameters between the synthetic drinking water and Ömerli water, represented in Table 4.6, demonstrated a high degree of concordance, validating the efficacy of the developed methodology. The stepwise optimization process, including the adjustment of primary and secondary parameters, ensured accurate replication of the target water composition, thus providing a foundation for subsequent experiments utilizing synthetic drinking water.

Table 4.6. Water quality parameters of a laboratory-prepared synthetic drinking water and the real water obtained from the Ömerli Reservoir.

Parameter	Synthetic Water	Average Ömerli reservoir values (standard deviation) (Yapsaklı, 2008)	Min. value measured in Ömerli reservoir (Yapsaklı, 2008)	Max. value measured in Ömerli reservoir (Yapsaklı, 2008)
TOC, mg/L	4.67	4.06 (0.63)	2.95	5.12
DOC, mg/L	3.54	3.65 (0.53)	2.85	4.89
NH_4^+-N, mg/L	0.6	0.34 (0.29)	0.15	0.98
NO_3^--N, mg/L	1	0.66 (0.39)	0.16	1.45
pH	7.9	7.85 (0.49)		
Alkalinity, mg/L as $CaCO_3$	52	58.28 (5.70)	47.5	68.77
Hardness, mg/L as $CaCO_3$	74	78 (6.30)	54	90
Conductivity, µS/cm	270	255 (35)	200	395
Fe^{2+}, mg/L	0.02	0.02 (0.01)	0.01	0.125
Mn^{2+}, mg/L	0.07	0.07 (0.04)	0.03	0.354
UV_{254}, cm^{-1}	0.095	0.093 (0.02)	0.067	0.211
UV_{280}, cm^{-1}	0.079	0.073 (0.02)	0.052	0.175
$SUVA_{254}$, L $mg^{-1}.m^{-1}$	2.68	2.54 (0.56)	1.99	5.26

4.6. Evaluation of the Adsorption of Pesticides and Background NOM onto GAC in Batch Reactors

All adsorption experiments were carried out in a 250 mL Erlenmeyer flask placed on an orbital shaker at 120 rpm. The experiments were done at 25 °C in duplicate measurements. Adsorption capacity (q) was calculated using mg/g or mg DOC/g. The q is expressed in Eq. 4.1.

$$q = \frac{V(C_{initial} - C_{final})}{m_{gac}} \quad (4.1)$$

In Eq. 4.1, V (L) is the volume of the experiment, $C_{initial}$ (mg/L) is the initial adsorbate concentration, C_{final} (mg/L) is the final adsorbate concentration, m_{gac} (g) is the mass of the GAC adsorbent.

Removal efficiency (%) is given by Eq. 4.2.

$$Removal\ efficiency\ (\%) = \frac{\left(C_{initial} - C_{final}\right)}{C_{final}} x\ 100 \quad (4.2)$$

4.6.1. Kinetic Experiments

The duration necessary for adsorption to reach equilibrium was determined through kinetic experiments conducted in completely-mixed batch reactors at different concentrations of GAC.

Each experimental set was conducted in an Erlenmeyer flask on an orbital shaker operating at 120 rpm and maintained at a constant temperature of 25 °C. Each experimental setup comprised a total volume of 200 mL with varying GAC concentrations ranging from 50 mg/L to 1500 mg/L. No buffering agents were introduced during the kinetic experiments, and the samples were preserved at their intrinsic pH levels.

Throughout the experimental process, regular sample collection was performed to analyze various parameters. The changes in pesticide and dissolved organic matter (DOM) concentrations, and absorbance characteristics were measured. The pesticide concentration monitoring utilized LC-MS/MS analytical techniques, with specific details outlined in Section 4.4.1. DOM variations were tracked through dissolved organic carbon (DOC) measurements. To evaluate equilibrium timing instantly, absorbance readings were taken at specific wavelengths (254, 280, 400, and 436 nm) concurrent with the experimental procedures. The justification for selecting these wavelengths was previously detailed in Section 4.4.3.

After conducting experiments and measuring results, two commonly utilized kinetic models for describing adsorption kinetics, pseudo-first order and the pseudo-second order model, were employed. Additionally, the intra-particle diffusion model was also applied.

The pseudo-first order kinetic model posits that the adsorption rate is directly proportional to the number of available adsorption sites on the adsorbent (Rudzinski & Plazinski, 2006). The pseudo-first order rate equation is expressed as follows (Eq. 4.3):

$$\ln(\ q_{e,exp}\ - q_t) = \ln q_{e,cal} - \ k_1\ t \quad (4.3)$$

In Eq. 4.3, $q_{e,\,exp}$ (mg/g activated carbon) is the experimental equilibrium adsorption capacity, $q_{e,cal}$ (mg/g activated carbon) is the calculated equilibrium adsorption capacity, q_t (mg/g activated carbon) is the adsorption capacity of time t, and k_1 (1/h) is the pseudo-first order rate constant.

The pseudo-second order kinetic model postulated that the adsorption rate is a function of both the number of available sites and the adsorbate concentration (Liu, 2008). The linearized form of the pseudo-second order rate equation can be expressed as follows (Eq. 4.4):

$$\frac{t}{q_t} = \frac{1}{k_2\, q_e^2} + \frac{1}{q_e}\, t \tag{4.4}$$

In Eq. 4.4, q_e (mg/g activated carbon) is the experimental equilibrium adsorption capacity, q_t (mg/g activated carbon) is the adsorption capacity of time t, and k_2 (g/mg.h) is the pseudo-second order rate constant.

The intra-particle diffusion model incorporates the diffusion of the adsorbate within the pores of the adsorbent as well as its adsorption on the internal surfaces (Saleh, 2022). This model is instrumental in elucidating the role of diffusion in the overall adsorption kinetics. The intra-particle diffusion rate equation is expressed as follows (Eq. 4.5):

$$k_i = \frac{q_t}{t^{1/2}} + B \tag{4.5}$$

In Eq. 4.5, q_t (mg/g activated carbon) is the adsorption capacity of time t, k_i (mg/g.h$^{1/2}$) is the intra-particle diffusion rate constant, and B (mg/g.h$^{1/2}$) is the intercept related to boundary layer thickness.

4.6.2. Isotherm Experiments

The experimental setups were conducted in an Erlenmeyer flask positioned on an orbital shaker operating at 120 rpm and maintained at a constant temperature of 25 °C. Each experimental setup comprised a total volume of 200 mL with GAC concentrations ranging from 50 mg/L to 1500 mg/L. No buffering agents were introduced during the isotherm experiments, and the samples were preserved at their intrinsic pH levels.

During the isotherm experiments, sample collection was performed at two points: at the start and upon reaching equilibrium. The experiment duration was selected based on findings from related kinetic experiments. Changes in pesticide and background NOM concentrations were measured as explained in Section 4.6.1. The initial and final concentrations were evaluated to calculate adsorption capacity (q) and removal efficiency, as expressed in Equations 4.1 and 4.2.

The experimental equilibrium adsorption capacity, denoted as q_e (mg/g GAC), was employed throughout the equilibrium studies. To analyze the results of the isotherm experiments, various isotherm models, including Linear, Freundlich, Langmuir, and Temkin were examined. The coefficients for each model were derived from the linearized forms of their respective equations. Comprehensive analysis of these models allows for a deeper understanding of the adsorption process, thereby facilitating the optimization of adsorption systems in continuous-flow systems.

The Freundlich isotherm is an equation that describes heterogeneous adsorption onto surfaces with non-uniform energies (Halsey, 1948). The Freundlich isotherm equation is articulated as follows (Eq. 4.6):

$$q_e = K_F \, C_e^{\,1/n} \tag{4.6}$$

In Eq. 4.6, q_e (mg/g activated carbon) is the adsorption capacity of activated carbon, C_e (mg/g activated carbon) is the equilibrium concentration of the adsorbate, 1/n (unitless) is the Freundlich equilibrium constant and K_f ((mg/g). $(L/mg)^{1/n}$) is the Freundlich equilibrium coefficient which is primarily related to the adsorbent's capacity for the adsorbate.

The linearized representation of the Freundlich isotherm equation can be articulated as follows (Eq. 4.7):

$$ln\, q_e = \ln\, K_f + \frac{1}{n}\, ln\, C_e \tag{4.7}$$

The linear isotherm represents a specific instance of the Freundlich isotherm in which the Freundlich equilibrium constant (1/n) is precisely 1, where k_d (L/g) is the distribution coefficient (Eq. 4.8)

$$q_e = C_e \, k_d \tag{4.8}$$

The Langmuir isotherm is a model that assumes that adsorption occurs on a surface with a fixed number of identical sites (Koresh, 1982). It describes a monolayer adsorption process, where the adsorbate molecules occupy the available sites on the surface without any interaction between the adsorbed molecules (Koresh, 1982). The Langmuir isotherm equation is expressed as follows (Eq. 4.9):

$$q_e = \frac{q_{max}\ K_L\ C_e}{1 + K_L\ C_e} \tag{4.9}$$

The linearized representation of the Langmuir isotherm equation can be expressed as follows (Eq. 4.10):

$$\frac{1}{q_e} = \frac{1}{q_{max}\ K_L\ C_e} + \frac{1}{q_{max}} \tag{4.10}$$

In Eq. 4.10, q_e (mg/g activated carbon) represents the adsorption capacity of activated carbon (mg/g activated carbon), C_e (mg/L) denotes the equilibrium concentration of the adsorbate, q_{max} (mg/g) indicates the maximum adsorption capacity, and K_L (L/mg) denotes the Langmuir equilibrium constant.

The Temkin isotherm introduces the concept of decreasing binding energy as the surface becomes increasingly occupied by adsorbate molecules (Yang, 1993). The Temkin isotherm equation is expressed as follows (Eq. 4.11):

$$q_e = \frac{RT}{b_T}\ \ln\ K_T\ C_e \tag{4.11}$$

The linearized form of the Temkin isotherm equation can be expressed as follows (Eq. 4.12):

$$q_e = \frac{RT}{b_T}\ \ln\ K_T + \frac{RT}{b_T}\ ln\ C_e \tag{4.12}$$

In Eq. 4.12, q_e carbon (mg/g activated carbon) is the adsorption capacity of activated carbon, R (8.314 J/mol K) is the gas constant, T (K) is the temperature, b_T (J/mol) is the Temkin constant, K_T (L/g) is the Temkin equilibrium constant, C_e is the equilibrium concentration of the adsorbate.

4.7. Biodegradation Experiments

4.7.1. Initiation and Operation of the Biological Reactor

One of the key aims of this study is to explore the biodegradation of pesticides and NOM. To accomplish this objective, batch experiments were conducted to enrich microorganisms in Ömerli Reservoir water so that this biomass could further be used in biodegradation experiments.

For this study, the bacteria in the water collected from the Ömerli Reservoir were enriched in a 2-liter reactor. The reactor was supplied with a biogenic feed consisting of readily biodegradable organic carbon (glucose) and essential minerals. The composition of the stock feed can be found in Table 4.7.

Table 4.7. Composition of stock feed.

Feed	Compound Name	Molecular Formula	Molecular Weight (g/mol)	Concentration (mg/L)
Organics	D (+) glucose monohydrate	$C_6H_{12}O_6.H_2O$	198.20	3750
Inorganics	Ammonium sulphate	$(NH_4)_2SO_4$	132.14	314
	Sodium bicarbonate	$NaHCO_3$	84.01	300
	Di-potassium hydrogen phosphate	K_2HPO_4	174.18	67
	Potassium dihydrogen phosphate	KH_2PO_4	136.08	67
	Magnesium sulphate heptahydrate	$MgSO_4.7H_2O$	246.37	67
	Manganese (II) sulphate monohydrate	$MnSO_4.H_2O$	169.02	2
	Calcium sulphate dihydrate	$CaSO_4.2H_2O$	172.17	33
	Iron sulphate heptahydrate	$FeSO_4.7H_2O$	278.01	23

The prepared feed was added to the reactor twice a week. The feed contains the necessary nutrients to supply the growth of the bacteria as well as to enable bacteria to produce specific enzymes

for biodegradation. Figure 4.10 shows the batch reactor. The daily loading rate was 30 mg DOC/L. day and 1.2 mg NH_4^+-N/L. day.



Figure 4.10. The batch reactor used for the growth of microorganisms in Ömerli Reservoir water.

4.7.2. Biodegradation of Natural Organic Matter (NOM) and Pesticides

This part systematically investigated the biodegradation kinetics of background NOM and pesticides. The inoculum utilized for the experiments was sourced from a batch reactor, as detailed in 4.7. The kinetic experiments were conducted in Erlenmeyer flasks, positioned on an orbital shaker operating at 120 rpm and maintained at a constant temperature of 25 °C, with air supplied to support biomass growth. Each experimental setup comprised a total volume of 200 mL, with varying bacterial concentrations ranging from 10 mg/L to 500 mg/L. No buffering agents were introduced during the kinetic experiments, and the samples were maintained at their intrinsic pH levels.

In the initial experiment the inoculum's biodegradation efficacy was assessed using synthetic water, wherein humic acid served as the sole carbon source available for microbial utilization. Different bacterial concentrations were employed to evaluate biodegradation's the effectiveness and kinetic parameters. Throughout the experiments, samples were collected regularly for subsequent analysis of dissolved organic matter (DOC).

In a subsequent experiment, the biodegradation efficacy of the inoculum was examined in the presence of individual pesticides, with each pesticide present at a concentration of 200 μg/L. 500mg/L bacterial concentration was employed to assess their effectiveness and kinetic parameters in biodegradation. Samples were periodically collected for analysis, and the change in pesticide concentration was monitored using liquid chromatography-tandem mass spectrometry (LC-MS/MS).

Various kinetic models describe the biodegradation of chemicals, including Monod kinetics, zero-order kinetics, and first-order kinetics. When the initial concentration of the substrate is low, first-order kinetics, which follows an exponential decay pattern, often provide a more accurate representation of the biodegradation process (Nelson et al., 2018). The equation for first-order kinetic is given in Eq. 4.13.

$$(\frac{dC}{dt}) = -k_{biol} C_t VSS_{active} \tag{4.13}$$

By incorporating these variables, Eq. 4.14 allows for calculating the biodegradation rate constant (k_{biol}), providing insight into the rate at which DOC is broken down in the experimental system.

$$\ln(\frac{C_i}{C_t}) = k_{biol} VSSt \tag{4.14}$$

Where C_i is the initial concentration (mg/L), C_t is the concentration at time t (mg/L), k_{biol} (L/(g VSS day) is the first-order biodegradation rate constant, VSS is the mixed liquor volatile suspended solid (MLVSS) concentration (mg/L) and t is the elapsed time in the batch reactor (day), respectively.

4.7.3. Investigation of the Synergistic Effect between GAC and Biomass in Batch Adsorption Systems

In this part, the combined impact of GAC adsorption and biodegradation was evaluated for two pesticides: cyprodinil and carbofuran. The combined GAC + biomass treatment consists of two main phases: first, the adsorption of pesticides onto the carbon surface, and second, the breakdown of these pollutants by microbial communities, with the effectiveness depending on how well the microorganisms can break down the specific compound present (Quintelas et al., 2010). We selected these pesticides based on their distinct characteristics. Cyprodinil exhibits low biodegradation but better adsorption than other pesticides, while carbofuran exhibits moderate biodegradation and moderate sorption properties.

The experiments were performed at a constant temperature of 25 °C with continuous agitation at 120 rpm. The biomass samples used in these experiments were obtained from the semi-continuously fed batch (SCFB) reactor as explained in detail in Section 4.7.1. Throughout the

experimental period, samples were periodically collected to monitor and analyze changes in cyprodinil/carbofuran concentration.

To comprehensively evaluate the removal mechanisms, five experimental conditions were established for each pesticide:

I. The single pesticide (1000 μg/L),
II. The pesticide (1000 μg/L) + ground GAC (500 mg/L),
III. The pesticide (1000 μg/L) + biomass (500 mg/L VSS),
IV. The pesticide (1000 μg/L) + ground GAC (500 mg/L) + biomass (500 mg/L VSS),
V. The pesticide (1000 μg/L) + biomass (500 mg/L VSS) + NaN_3 (300 mg/L).

These conditions were designed to isolate and analyze individual removal mechanisms. The first (I) experimental condition provided reference data. Under the second and third conditions (II and III), adsorption and biodegradation were separately examined, while under the fourth condition (IV), the combined effect was investigated. Incorporating sodium azide (NaN_3) as a microbial inhibitor (Hamed et al., 2021) in the final condition (V) provided insights into the relative contributions of adsorption versus biodegradation mechanisms in the biomass-mediated removal process. By inhibiting the biological activity of bacteria by adding 300 mg/L NaN_3, this approach enabled differentiation between biodegradation and physical/chemical adsorption processes within biomass systems (Rattier et al., 2012).

4.8. Experiments with Rapid Small-Scale Column Tests (RSSCTs)

4.8.1. Evaluation of the Adsorption of Pesticides and Background NOM onto GAC in RSSCTs

The removal of pesticides and background NOM was assessed in a continuous-flow GAC filter. In the RSSCT (Rapid Small-Scale Column Test) design, the objective is to scale down a large-scale activated carbon column to a smaller scale. This objective is realized through applying mathematical correlations, as detailed in Table 4.8, following the methodology described by Reinert (2013). The critical focus is to achieve similitude between the large-scale and small-scale columns via dimensional analysis. Upon achieving such similarity, the breakthrough behavior observed in both scales can be comparable. Breakthrough time reduction in RSSCT enables the simulation of large-scale column performance under multiple conditions in a shorter time.

Table 4.8. Basic mathematical connections used for RSSCT design (Reinert, 2013).

Parameter	Equation	Relationship
Scaling factor (SF)	$SF = \left[\frac{d_{p.LC}}{d_{p.SC}}\right]$	Provides initial basis for bench scale design dependence on GAC particle diameters
Diffusion Coefficients (D)	$D_{SC} = \left[\frac{d_{p.SC}}{d_{p.LC}}\right]^{x} D_{LC} = [SF]^{-x} D_{LC}$	Dependence of intraparticle diffusivity on particle size
Empty Bed Contact Time (EBCT)	$\frac{EBCT_{SC}}{EBCT_{LC}} = \left[\frac{d_{p.SC}}{d_{p.LC}}\right]^{2} x \left[\frac{D_{LC}}{D_{SC}}\right]$	Empty Bed Contact Time (EBCT) is related to the size of GAC in each adsorber and the dependence of intraparticle diffusivity on particle size
Design Factor (DF)	$\frac{EBCT_{SC}}{EBCT_{LC}} = \left[\frac{d_{p.SC}}{d_{p.LC}}\right]^{2-x} = \left[\frac{t_{SC}}{t_{LC}}\right] = [SF]^{x-2} = DF$	Provides relationship between scaling factor, empty bed contact time, intraparticle diffusivity, and times to run the large column and small column

The appropriate selection of hydraulic loading rates and Empty Bed Contact Time (EBCT) in RSSCTs is of paramount importance, as emphasized by Crittenden et al. (1991). Increasing the hydraulic load in rapid small-scale columns enhances the mass transfer process. Assuming equivalent diffusion coefficients for both GACs, this results in a substantial reduction in breakthrough time.

In rapid small-scale columns, the diameters of the original granular activated carbon (GAC) particles are significantly reduced through grinding. As illustrated in Table 4.8, when the particle GAC particle size is reduced to one-tenth of the laboratory scale, and x equals zero, the EBCT is reduced to one-hundredth of its original value. This reduction allows the filters to operate with extremely low EBCT times, sometimes as brief as a few seconds (Crittenden et al., 2012). Additionally, the RSSCT method employs very small columns.

The EBCT for drinking water treatment plants can vary depending on the treatment process and design factors. In GAC, typical EBCT values may range from 5 to 30 minutes or even more, depending on the specific contaminants being targeted and the desired treatment level (Çeçen & Aktaş, 2011; Crittenden et al., 2012; Kennedy et al., 2015; Servais et al., 1994).

The investigations utilized both original and ground granular activated carbon (GAC) to facilitate a comparative analysis using constant diffusivity rapid small-scale columns (CD-RSSCT). As previously mentioned, reducing the GAC particle size to one-tenth of its original size resulted in a corresponding reduction in EBCT and flow rate by a factor of one hundredth, as shown by the equations in Table 4.8. This modification resulted in a significant decrease in breakthrough time, reducing it by a factor of 100.

In the light of the information provided above, the specifications used for RSSCT employing **original GAC** with a particle size of approximately 1 mm are outlined as follows:

- Column diameter: 1 cm
- Column height: 2 cm
- EBCT: 20 minutes
- Flow rate: 0.078 mL/min.

The specifications used for RSSCT utilizing **ground GAC** with a particle size of approximately 100 μm are outlined as follows:

- Column diameter: 1 cm
- Column height: 2 cm
- EBCT: 0.20 minutes
- Flow rate: 7.85 mL/min.

To achieve the objective, Bio-Rad Econo-Column®, which had an inner diameter of 1 cm and a length of 10 cm, was utilized. While the columns had a total length of 10 cm, with 2 cm of them were filled with granular activated carbon. The remaining portion of the column was packed with glass beads. Figure 4.11 presents a detailed illustration of the experiment.

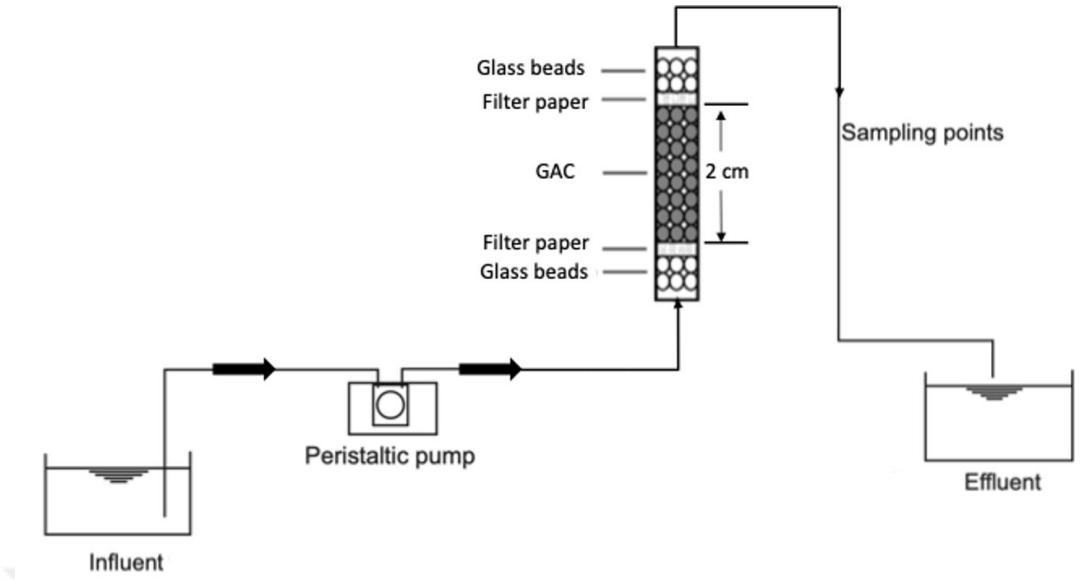


Figure 4.11. Schematic diagram of RSSCT GAC columns.

The experimental methodology encompassed maintaining continuous-flow through the column for specified durations during each experimental run. Sample collection from the effluent was conducted at predetermined intervals to enable thorough analytical assessment. Pesticides and DOM were measured as explained in 4.6.2. The dynamic behavior of adsorbate concentrations in the effluent was characterized through breakthrough curve evaluation, which provided valuable experimental data for subsequent analysis.

4.8.2. Tracer Test

Before the RSSCT experiments, a tracer test was conducted in an RSSCT column to evaluate the hydrodynamic characteristics of the system. A 1 g/L NaCl solution was used as a conservative tracer, and conductivity measurements were taken to monitor changes in NaCl concentration. The column was filled with **ground GAC** and operated at a constant flow rate of 7.85 mL/min. Prior to tracer injection, the system was flushed with deionized water until baseline conductivity stabilized. Effluent samples were systematically collected at designated time intervals to analyze tracer breakthrough.

The velocity (v) was determined using the Eq 4.15:

$$v = \frac{Q}{n\,A} \tag{4.15}$$

where v (cm/min) is the velocity, Q (mL/min) is the flow rate, A (cm^2) is the cross-sectional area, and n is the column porosity.

To model tracer transport, one-dimensional advection-dispersion equation (Eq. 4.16) was applied.

$$C(x,t) = \frac{C_0}{2}\left[erfc\left(\frac{x - vt}{2\sqrt{D_x t}}\right) + \exp\left(\frac{vx}{D_x}\right) + \text{erfc}\left(\frac{x + vt}{2\sqrt{D_x t}}\right)\right] \quad (4.16)$$

where C (x, t) is the tracer concentration at position x and time t, C_0 is the initial tracer concentration (g/L), x is the distance along the column, v is flow velocity (cm/min), D_x is the dispersion coefficient (cm^2/min), t is time (min) and erfc is the complementary error function.

The optimal dispersion coefficient was determined by minimizing the root mean square error (RMSE) between experimentally measured and model-predicted effluent concentrations. This was accomplished by iteratively adjusting D_x to minimize the sum of squared differences between observed and simulated concentration data.

The longitudinal dispersivity (α_x) is calculated using the Eq. 4.17:

$$D_x = v\,\alpha_x + D_m \quad (4.17)$$

where D_m is molecular diffusion coefficient (cm^2/min) of tracer at studied temperature in water and α_x is longitudinal dispersivity (cm).

After finding the dispersion coefficient, the relationship between advection and dispersion can be described using a dimensionless parameter called the Péclet number. This helps us understand which transport mechanism dominates in a given flow situation by comparing the relative rates of advection and dispersion. The mathematical expression for this relationship is given in the Eq. 4.18:

$$\text{Péclet number} = \frac{v\,L}{D_x} \quad (4.15)$$

4.9. Modeling of Pesticides and Background NOM Removal using AdDesignS Software

The Adsorption Design Software (AdDesignS^{TM}), which was introduced in 1994, was engineered by researchers at Michigan Technological University to facilitate adsorption system design and analysis (Mertz et al., 1994). This software has been widely utilized by both academic and industry professionals for the design and optimization of adsorption-based treatment systems (Scharf et al., 2010).

The software's primary function is to model and forecast how substances will behave in adsorption columns. When designing these systems, researchers must consider numerous variables, from the physical and chemical properties of the materials involved to the specific operational parameters of the system. The software uses statistical techniques to analyze these multiple variables simultaneously, helping users determine the most effective configuration for their application.

In the software, users can input various parameters, including:

- Compound information (adsorbate's physicochemical properties, initial concentration, Freundlich isotherm parameters, diffusion kinetics),
- Column information (bed length, bed diameter, flow rate, EBCT, amount of adsorbate in the column),
- Adsorbent information (apparent density, particle radius, porosity),
- Simulation parameters (collocational point selection and experimental duration settings).

By entering these parameters, the model enables the prediction of adsorption system performance under various conditions.

As illustrated in Figure 4.12, AdDesignS integrates various input parameters to generate predictive models for adsorption behavior. Table 4.9 provides a detailed overview of all parameters entered into the AdDesignS software. The table demonstrates our systematic approach, where experimental data from batch isotherms are combined with column parameters to simulate breakthrough curves and forecast treatment system performance. To analyze the breakthrough behavior of pesticides and/or background NOM under different conditions, the pore surface diffusion model (PSDM), a component of the AdDesignS package was employed.

For diffusion parameters, relevant correlations were used. The Gnielinski correlation was applied for film diffusion, while the Sontheimer correlation was used for surface diffusion. Pore diffusion

was set at 9.71 x 10^{-6} cm^2/s. Film diffusion coefficients were determined using the Gnielinski correlation, yielding values of 14.58 x 10^{-2} cm/s for ground GAC and 1.19 x 10^{-3} cm/s for non-ground GAC. Surface diffusion was determined using the Sontheimer correlation and varied for each adsorbate.

This approach enables the modeling and prediction of adsorption behavior in dynamic column systems, offering insights into the continuous-flow process. By combining the Freundlich isotherm parameters with the adsorption design software, system performance can be evaluated under various operating conditions. This model was used for two purposes: first, to simulate actual RSSCT performance, and second, to forecast long-term pesticide/NOM removal patterns in actual water treatment systems.

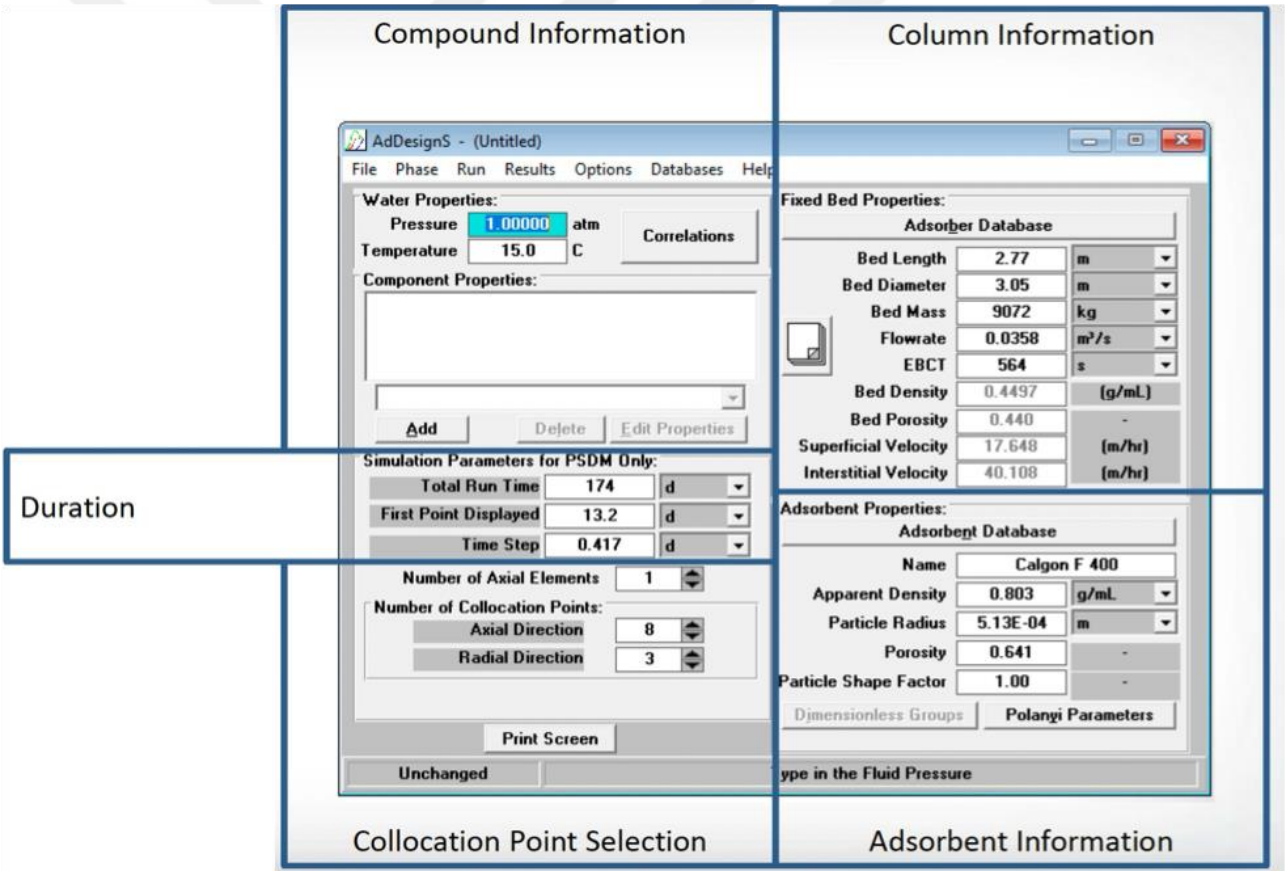


Figure 4.12. Schematic representation of the AdDesignS software working input parameters.

Table 4.9. Full list of parameters entered to AdDesignS software.

Type	Parameter	Source	Notes
Water Properties	Pressure	Experimental Setup/ This Study	Entered manually or keep default values
	Temperature		
Adsorbate Properties	Name	This Study	Entered manually or imported through StEPP Export File
	Molecular Weight	Pesticides Properties DataBase (PPDB)	
	Molar Volume at Normal Boiling Point		
	Boiling Point		
	Initial Concentration	Experimental Setup/ This Study	
	Liquid Density	Pesticides Properties DataBase (PPDB)	
	Solubility		
	Vapor Pressure		
	Refractive Index		
Equilibrium Parameters	Freundlich K_f	Batch Isotherm Experiments/ This Study	Entered manually or estimated within AdDesisngS
	Freundlich 1/n		
Kinetic Parameters	Tortuosity	Estimated within AdDesignS	Entered manually or estimated within AdDesisngS
	Surface-to-Pore-Diffusion Flux Ratio (SPDFR)		
	Film Mass Transfer Coefficient		
Column Properties	Bed Length	Experimental Setup/ This Study	Entered manually or chosen from an adsorber database
	Bed Mass		
	Flow Rate		
	EBCT		
	Apparent Bed Density		
	Bed Porosity		
	Superficial Velocity		
	Interstitial Velocity		
Adsorbent Properties	Name	This Study	Entered manually or chosen from an adsorber database
	Apparent Particle Density	Experimental Measurement / This Study	
	Particle Radius		
	Particle Porosity		
	Particle Shape Factor		
Simulation Parameters	Total Run Time	Model Fitting / This Study	Entered manually or keep default values
	First Point Displayed		
	Time Step		
	Number of Axial Elements		
Number of Collection Points	Axial Direction	Model Fitting / This Study	Entered manually or keep default values
	Radial Direction		

**Adopted from Reinert (2013).*

For the calibration and validation of the model's predictive accuracy, experimental carbofuran data obtained from isotherm and RSSCT experiments were used. The RSSCT experiment with carbofuran was divided into two distinct time-based segments. The first segment, comprising the initial 48 hours, was used for model calibration, during which key parameters were adjusted to achieve the best fit between experimental and simulated results. The second segment (48 to 80 hours)

was then used for validation, providing an independent assessment of the model's ability to predict effluent concentration over time.

Figure 4.13 present a comparison between the experimental breakthrough curve and the model-generated breakthrough curve corresponding to the second segment of the carbofuran experiment. This comparison demonstrates the model's effectiveness in accurately simulating carbofuran's transport and adsorption behavior. The agreement between these curves confirms the model's reliability and reinforcer its suitability for predicting time-dependent effluent concentrations under similar conditions.

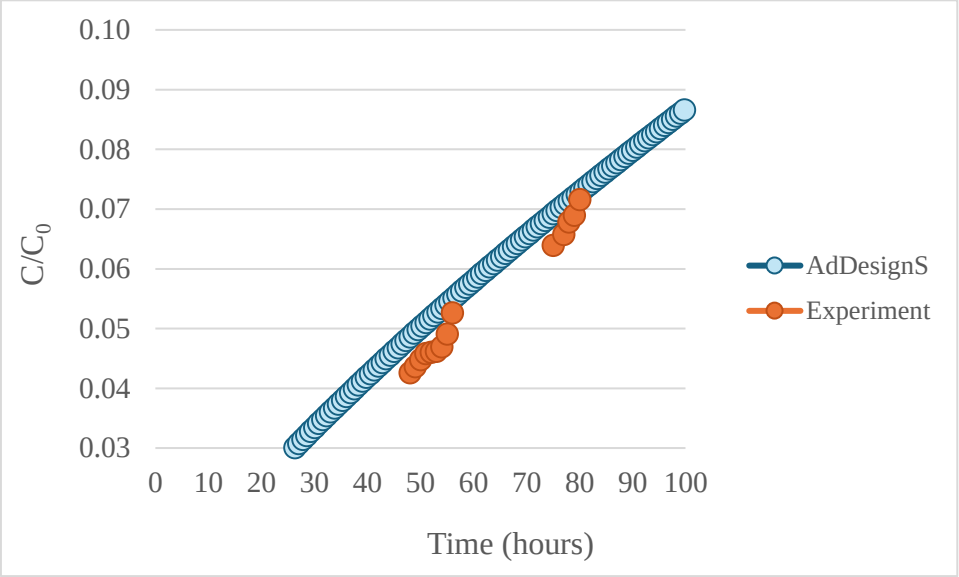


Figure 4.13. Comparison of the best-fit model and experimental results.

The sensitivity analysis conducted using the PSDM model provided valuable insights into the influence of the Freundlich isotherm parameters on breakthrough curves. This analysis focused solely on the Freundlich parameters, as all other input parameters were fixed values derived either from the experimental setup or estimated within the model or the physicochemical properties of the compound. To assess their individual effects the K_f and 1/n parameters systematically varied by ± 50%, adjusting them one at a time. The resulting changes in the breakthrough curves, illustrated in Figure 4.14.

Consistent with established literature, K_f was found to be directly proportional to breakthrough time, whereas 1/n exhibited an inverse relationship (Crittenden et al.1986; Cantoni et al., 2021; Velten et al., 2011). Additionally, the findings reveal that ± 50% change in 1/n has a more significant influence on the breakthrough curve compared to an equivalent variation in K_f. This highlights the

greater sensitivity of the model to changes in 1/n, suggesting that even small deviations in this parameter can lead to notable shifts in predicted effluent concentrations.

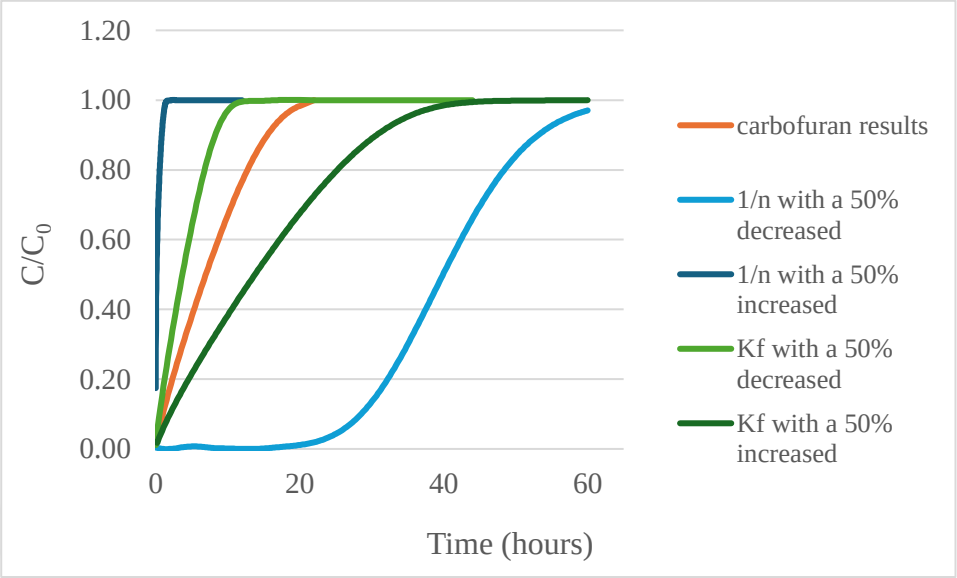


Figure 4.14. Sensitivity simulations related to K_f and 1/n.

5. RESULTS AND DISCUSSION

5.1. Identification and a Data-Driven Analysis of Selected Pesticides: Assessing Physicochemical Properties and Biodegradation Characteristics

5.1.1. Pesticides Properties DataBase (PPDB) Profiling

The Pesticide Properties DataBase (PPDB) is a centralized repository that collects and organizes detailed data about pesticides. This database encompasses characteristics, potential impacts on human health, and effects on environmental systems. Created and maintained by researchers at the University of Hertfordshire's AERU (Agriculture and Environment Research Unit), this tool enables professionals to conduct thorough evaluations and implement effective control measures regarding pesticide usage. Table 5.1 presents a summary of relevant parameters for five pesticides: carbofuran (CBF), chlorpyrifos (CPF), cyprodinil (CYP), malathion (MLT), and propanil (PRP). These parameters offer valuable insights into the environmental behavior and potential risks associated with each pesticide.

Table 5.1. Relevant parameters from Pesticide Properties Database (PPDB).

Selected Parameters from PPDB/ Pesticides	**Carbofuran (CBF)**	**Chlorpyrifos (CPF)**	**Cyprodinil (CYP)**	**Malathion (MLT)**	**Propanil (PRP)**
Type of pesticide	Insecticide, nematicide	Organophosphate insecticide	Fungicide	Organophosphate insecticide	Herbicide
Water Solubility	Moderately soluble	Low solubility	Low solubility	Moderately soluble	Moderately soluble
Volatility	Non-volatile	Moderately volatile	Non-volatile	Non-volatile	Non-volatile
Henry's Constant ($Pa.m^3 mol^{-1}$)	5.0×10^{-05}	0.478	6.60×10^{-03}	1.00×10^{-3}	4.4×10^{-4}
Dissociation constant pK_a at 25 °C	No dissociation	No dissociation	Weak base 4.44	No dissociation	No dissociation 19.1

Table 5.1. Continued.

Selected Parameters from PPDB/ Pesticides	Carbofuran (CBF)	Chlorpyrifos (CPF)	Cyprodinil (CYP)	Malathion (MLT)	Propanil (PRP)
Persistency	High potential for leaching to groundwater, it may be persistent in water	Moderately persistent in soil, not persistent in water systems	Moderately persistent in water systems	Not persistent	Not persistent
Toxicity	Highly toxic to mammals, birds, most aquatic organisms, moderately toxic to earthworms	Highly toxic to mammals, birds, fish, aquatic invertebrates, honeybees.	Moderately toxic to mammals, birds, most aquatic organisms and earthworms	Moderately toxic to mammals, honeybees, aquatic species, birds, earthworms	Moderately toxic to mammals and most fauna and flora
Threshold of Toxicological concern (Cramer class)	High (class 3) *	High (class 3) *	High (class 3) *	High (class 3) *	High (class 3) *
Toxicity	Endocrine disruptor, Reproduction/ development effects	Reproduction/ development effects, cholinesterase inhibitor, neurotoxicant	Respiratory tract irritant, skin irritant, skin sensitizer, eye irritant	Cholinesterase inhibitor, neurotoxicant	Eye irritant, possible human carcinogen
BCF (Bio-concentration Factor) (L/kg)	12	1374	393	103	111

** High (class 3): Substances with chemical structures that permit no strong initial presumption of safety or may even suggest significant toxicity or have reactive functional groups.*

Table 5.1. Continued.

Selected Parameters from PPDB/ Pesticides	Carbofuran (CBF)	Chlorpyrifos (CPF)	Cyprodinil (CYP)	Malathion (MLT)	Propanil (PRP)
Known metabolites	3-hydroxycarbofuran	3,5,6-trichloro-2-pyridinol (persistent pollutant),	4-cyclopropyl-6-methyl-pyrimidine-2-ylamine	Malathion monocarboxylic acid	3,4-dichloroaniline (toxic)
	3-ketocarbofuran	2,3,5-trichloro-6-methoxypyridine	3-(4-cyclopropyl-6-methylpyrimidin-2-ylamino)phenol (pollutant)	Malathion dicarboxylic acid	3,4-dichloronitrobenzene
	2,3.dihydro-2,2-diemethyl-7-benzofuranol	O-ethyl-O-(3,5,6-trichloro-2-pyridyl)phosphorothioic acid	6-cyclopropyl-2-phenylamino-pyrimidin-4-yl)-methanol	Isomalathion	(Z)-1-(3,4-dichlorophenyl)-2-hydroxydiazene
			4-(4-cyclopropyl-6-methyl-pyrimidin-2-yl-amino)-phenol	Desmethyl malathion	3,3,4,4-tetrachloroazobenzene
			4-cyclopropyl-6-methyl-2-phenylamino-pyrimidin-5-ol	diethyl (2RS)-2-[(dimethoxyphosphoryl)sulfanyl]butanedioate (More toxic than malathion)	3,3,4,4-tetrachloroazoxybenzene
			4-cyclopropyl-6-methyl-pyrimidin-2-ol		n-hydroxy-3,4-dichloroaniline
			(2-amino-6-cyclopropyl-pyrimidin-4-yl)-methanol		3,4-dichloroacetanilide
					3,4-dichlorogucosylamine

Table 5.1. Continued.

Selected Parameters from PPDB/ Pesticides	Carbofuran (CBF)	Chlorpyrifos (CPF)	Cyprodinil (CYP)	Malathion (MLT)	Propanil (PRP)
Drinking water standards	Non-statutory WHO drinking water guideline 0.007 mg/L	Non-statutory WHO drinking water guideline 0.03 mg/L	-	-	-
K_d (Linear)(mL/g)	-	126.6	-	-	-
K_{oc} (Linear) (mL/g)	-	5509	-	1800	149
K_f (Freundlich) (mL/g)	1.14	91.6	21.27	1.58	6.95
K_{foc} (Freundlich) (mL/g)	86.5	3954	2277	217	535
1/n (Freundlich)	0.89	0.92	0.88	0.94	0.92
Log P	1.8	4.7	4	2.75	2.29

Examining the data, significant variations can be observed among the pesticides under consideration, particularly with respect to their physicochemical characteristics and environmental impacts:

Type of pesticide: The selected compounds represent a diverse range of pesticide types, including insecticides (carbofuran, chlorpyrifos, malathion), a fungicide (cyprodinil), and an herbicide (propanil).

Water Solubility: The pesticides exhibit varying degrees of water solubility, ranging from low (chlorpyrifos and cyprodinil) to moderate (carbofuran, malathion, and propanil). The solubility of a compound in water is a fundamental physicochemical property that plays a critical role in elucidating its potential for transport and distribution within aquatic environments. This characteristic is of particular importance in environmental chemistry and toxicology, as it directly influences the bioavailability, persistence, and potential environmental impact of various substances. Understanding the water solubility of compounds is essential for predicting their fate in water bodies, assessing their

potential for bioaccumulation, risk assessment, and developing effective strategies for drinking water removal.

Volatility: The Henry's Constant values provide information on the pesticides' tendency to volatilize from water to air. Most of the pesticides analyzed are categorized as non-volatile chemicals. The sole exception is chlorpyrifos, which exhibits a comparatively elevated Henry's Constant (0.478 Pa m^3/mol), placing it in the moderately volatile category. The volatility plays a crucial role in determining the pesticides' tendency for atmospheric transport and subsequent deposition. The volatility of a pesticide significantly influences its environmental fate and potential for long-range transport, which are important factors in assessing their environmental impact and persistence in various environmental compartments.

Persistence: The environmental persistence of selected pesticides varies significantly. Carbofuran has a high potential for leaching into groundwater and may persist in water. In contrast, chlorpyrifos and cyprodinil exhibit moderate persistence in soil and aquatic environments. Malathion and propanil, however, are categorized as non-persistent compounds.

Toxicity: All five pesticides exhibit varying degrees of toxicity to different organisms. Carbofuran and chlorpyrifos are highly toxic to a wide range of species, while cyprodinil, malathion, and propanil are generally moderately toxic. Notably, all these pesticides are classified as having a high threshold of toxicological concern (Cramer class 3). Cramer class 3 chemicals pose the highest risk for oral toxicity in the Cramer classification system (Roberts et al., 2015).

Bio-concentration Factor (BCF): The phenomenon of bioaccumulation is quantitatively characterized by the BCF, defined as the ratio between the concentration of a specific chemical compound in an organism or biological tissue and its concentration in the surrounding aqueous environment. BCF values provide insight into the bioaccumulation potential of a substance. Among the pesticides under consideration, chlorpyrifos has the highest BCF (1374 L/kg), indicating a significant potential for bioaccumulation in aquatic organisms. In contrast, carbofuran has the lowest BCF (12 L/kg), suggesting a lower tendency to accumulate in living tissues.

Adsorption Parameters (log P, K_d, K_{oc}, K_f, K_{foc}, 1/n, log P): How pesticides move and behave in the environment, mainly how they stick to different surfaces, can be understood through various measurement parameters. These include the distribution coefficient (K_d), octanol-water partition coefficient (Log P or Log K_{ow}), organic carbon partition coefficient (K_{oc}), and Freundlich constants

(K_f and 1/n). These parameters are essential for scientists to predict and analyze how pesticides interact with soil, water, and other environmental components. The distribution coefficient (K_d) denotes the ratio of the pesticide concentration in the soil solid phase to that in the aqueous phase at equilibrium. Log K_{ow}, the logarithm of the octanol-water partition coefficient, is a measure of the pesticide's affinity for solid particles. The Freundlich isotherm, characterized by the constants K_f and 1/n, describes the non-linear relationship between the amount of pesticide adsorbed and its concentration in solution. K_f represents the adsorption capacity, whereas 1/n indicates the intensity of adsorption. A higher K_f value suggests stronger adsorption, while 1/n values closer to 1 indicate more linear adsorption behavior.

Chlorpyrifos shows the highest adsorption potential among all pesticides, with the highest values for K_d (126.6 mL/g), K_{oc} (5509 mL/g), K_f (91.6 mL/g), and K_{foc} (3954 mL/g). Its high log K_{ow} value of 4.7 indicates strong hydrophobicity, suggesting it tends to bind strongly to soil organic matter rather than remain in water.

Cyprodinil demonstrates the second-highest adsorption tendency, with relatively high K_f (21.27 mL/g) and K_{foc} (2277 mL/g) values. Its log K_{ow} value of 4.0 indicates significant hydrophobicity, though less than chlorpyrifos.

Malathion shows moderate adsorption characteristics with a K_{oc} value of 1800 mL/g but relatively low K_f (1.58 mL/g) values. Its log K_{ow} value of 2.75 suggests moderate hydrophobicity.

Propanil exhibits lower adsorption potential than chlorpyrifos and cyprodinil, with a relatively low K_{oc} value (149 mL/g) but moderate K_f value (6.95 mL/g). Its log K_{ow} value of 2.29 indicates moderate hydrophobicity.

Carbofuran shows the lowest adsorption tendency among all pesticides, with the lowest K_f value (1.14 mL/g) and log K_{ow} value (1.8), suggesting it has the highest potential for mobility in soil and water systems.

The Freundlich exponent (1/n) values for all pesticides are relatively similar (ranging from 0.88 to 0.94) and close to 1, indicating that the adsorption behavior is somewhat linear for all pesticides. This suggests that adsorption capacity increases proportionally with increasing pesticide concentration in solution.

5.1.2. Computational Assessment of Pesticides: Estimation Program Interface (EPI) Suite Results

The EPI Suite's BIOWIN models, integral components of both the EPI Suite and the OECD QSAR Toolbox, are designed to predict the biodegradation of substances in aquatic and terrestrial environments. These models employ regression equations utilizing molecular substructures (fragments) to calculate endpoint values for chemical structures (Boethling & Costanza, 2010). The BIOWIN approach involves deconstructing molecules into their constituent fragments and evaluating each fragment's contribution to overall biodegradability. This methodology in BIOWIN enables the generation of numerical values that serve as indicators of a compound's likelihood to undergo biodegradation (Pavan & Worth, 2008). These numerical outputs serve as valuable predictors of a substance's environmental persistence and potential ecological impact. The BIOWIN module comprises seven models, with models 1 through 6 specifically designed to predict aerobic biodegradation processes. In contrast, BIOWIN7 is tailored for anaerobic biodegradation prediction. However, given that the current study focuses on aerobic biodegradation mechanisms, only the six initial models are employed.

BIOWIN1, linear probability model, and BIOWIN2, nonlinear probability model, are computational models designed to estimate the likelihood of rapid biodegradation based on qualitative biodegradation data (Boethling & Costanza, 2010). These models employ a probabilistic approach, where a value exceeding 0.5 is indicative of "rapid biodegradation", while a value below 0.5 suggests a slower degradation. This binary classification system provides a simplified framework for assessing the biodegradation potential of various compounds.

Table 5.2. Output of BIOWIN models indicating the probability of biodegradation or biodegradation time.

	BIOWIN1 (Linear Probability Model)	**BIOWIN2** (Non-linear Probability Model)	**BIOWIN3** (Ultimate Biodegradation Model)	**BIOWIN4** (Primary biodegradation Model)	**BIOWIN5** (MITI linear model prediction)	**BIOWIN6** (MITI non-linear model prediction)	**Readily Biodegradability Prediction**
	> 0.5: fast biodegradation < 0.5: not to degrade fast		5-4.75: hours 4.75-4.25: hours to days 4.25-3.75: days 3.75-3.25: days to weeks 3.25-2.75: weeks 2.75-2.25: weeks to months 2.25-1.75: months < 1.75: refractory		> 0.5: rapidly biodegradable < 0.5: not to rapidly biodegradable		Yes or No
Carbofuran	0.7244	0.8785	2.3184	3.5773	0.2435	0.1936	No
Chlorpyrifos	0.1928	1.0000	1.7442	3.2925	-0.0832	0.0014	No
Cyprodinil	0.6440	0.7018	2.4387	3.2821	0.0047	0.0310	No
Malathion	1.2526	1.0000	2.9033	4.2944	0.6707	0.5691	Yes
Propanil	0.4890	0.1934	2.2498	3.4078	0.2768	0.0749	No

According to the results shown in Table 5.2, the BIOWIN1 and BIOWIN2 models predict rapid degradation for carbofuran, cyprodinil, and malathion. Conversely, propanil is anticipated to exhibit limited biodegradability according to both models, although its BIOWIN1 value approaches the threshold of 0.5. Chlorpyrifos presents an interesting case, with the BIOWIN1 model predicting slow degradation while the BIOWIN2 model suggests rapid degradation.

BIOWIN3 and BIOWIN4 models utilize expert survey data to generate probabilistic estimates of a chemical's susceptibility to biodegradation processes. BIOWIN3, Expert Survey Ultimate Biodegradation Model, focuses on the complete mineralization of a substance. It provides a quantitative assessment of the likelihood that a given chemical will undergo ultimate biodegradation, resulting in the formation of harmless, and the simplest end products. This model is particularly valuable for evaluating the potential long-term environmental persistence of any xenobiotic compound. In contrast to BIOWIN3, BIOWIN4 (Expert Survey Primary Biodegradation Model) focuses on the initial stages of biodegradation. This model estimates the probability of a chemical undergoing primary biodegradation, which involves the initial transformation of the parent compound into simpler molecular structures. While these intermediate transformation products may still have

some environmental impact, primary biodegradation represents a crucial first step in the overall degradation process. Both models employ a scoring system that correlates probability scores with estimated biodegradation timeframes. Higher scores, typically in the range of 5.00 to 4.75, indicate rapid biodegradation occurring within hours. Conversely, lower scores suggest extended biodegradation periods, ranging from days to months. Scores below 1.75 are interpreted as indicative of a recalcitrant compound that persists in the environment. The complementary nature of BIOWIN3 and BIOWIN4 allows for a more comprehensive evaluation of a chemical's environmental fate. By considering both ultimate and primary biodegradation probabilities, one can acquire significant information regarding the potential persistence of a substance.

The results derived from the BIOWIN3 model, as represented in Table 5.2, indicate that all five pesticides exhibit the potential for complete biodegradation within a relatively short timeframe, spanning from weeks to months. Within this context, malathion demonstrates the highest tendency for rapid biodegradation, whereas chlorpyrifos exhibits the lowest biodegradation among the pesticides studied. According to the outputs of the BIOWIN4 model, as represented in Table 5.2, all five pesticides have the potential to undergo primary biodegradation within a relatively short period of time, ranging from days to weeks. However, among all the pesticides analyzed, malathion is the most likely to biodegrade at the fastest rate.

The BIOWIN5 and BIOWIN6 models were created by MITI to evaluate rapid biodegradation potential. These models utilize different regression methods – linear and nonlinear, respectively – similar to their BIOWIN1 and BIOWIN2 counterparts, but with distinct coefficient values (Boethling & Costanza, 2010). Both models produce numerical outputs that predict rapid biodegradation probability, with values of 0.5 or higher indicating likely rapid biodegradation. When these models were applied to evaluate five pesticides, the analysis revealed that only malathion showed strong potential for quick biodegradation among the all-tested compounds, as detailed in Table 5.2.

5.1.3. MetaCyc Results

MetaCyc is an extensive database that includes enzymes and metabolic pathways from various organisms. It offers in-depth details on chemical compounds, reactions, and metabolism processes, with its content being verified from scientific publications.

The MetaCyc database lacked information on the biodegradation of malathion, cyprodinil, and propanil. Nevertheless, it contained data about chlorpyrifos and carbofuran. Figure 5.1 illustrates the details about to the degradation of chlorpyrifos.

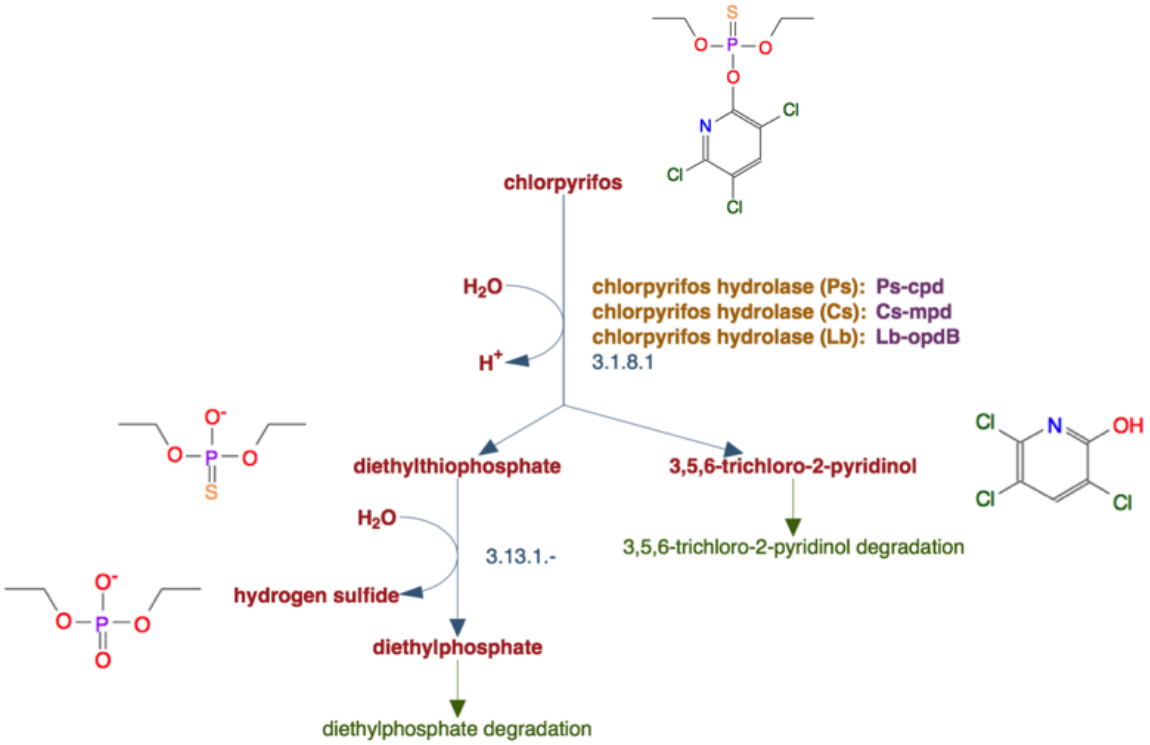


Figure 5.1. Chlorpyrifos biodegradation pathway obtained from the MetaCyc database (Caspi and SRI International, 2019).

The MetaCyc database has identified a diverse array of microbial species capable of participating in the degradation processes of chlorpyrifos. These organisms represent a wide range, encompassing various genera, including *Bacillus cereus, Bacillus licheniformis*, *Bacillus pumilus*, *Cupriavidus nantongensis, Cupriavidus sp. DT-1*, *Hypocreales sp. DSP*, *Levilactobacillus brevis*, *Ochrobactrum sp. JAS2*, *Paracoccus sp. TRP*, *Pseudomonas aeruginosa*, *Stenotrophomonas sp. G1*, *Streptomyces sp. AC7* (Chen et al., 2012; Dubey & Fulekar, 2012; Islam et al., 2010; Li et al., 2007; Lu et al., 2013; Yadav et al., 2016; Yang, et al., 2006). Notably, some of these microorganisms, particularly *Bacillus* species and *Pseudomonas aeruginosa*, are more likely to be encountered in drinking water supplies (WHO, 2017)

The initial step in the biodegradation of chlorpyrifos involves hydrolysis, catalyzed by specific enzymes in certain bacteria and fungi. These enzymes include esterase (oppdB), methyl parathion hydrolase (MPH), and chlorpyrifos-hydrolyzing enzyme (CPH)(Islam et al., 2010; Yadav et al.,

2016). These enzymatic actions transform chlorpyrifos into two primary metabolites: diethylthiophosphate and 3,5,6-triochloro-2-pyridinol (TCP) (Caspi, 2019).

TCP exhibits significant antimicrobial properties that can interfere with further degradation processes. Moreover, it has been classified as a persistent pollutant and considered potentially carcinogenic to humans by the United States Environmental Protection Agency (EPA, 2014). Despite these challenges, certain microorganisms have demonstrated the capacity to degrade TCP (S. Chen et al., 2012; Lu et al., 2013).

Diethylthiophosphate, another metabolite of chlorpyrifos, undergoes further transformation through a phosphor dethio reaction, yielding diethylphosphate. Subsequently, as evidenced in the MetaCyc database, various microorganisms can biotransform diethylphosphate into phosphate, completing the degradation pathway (Caspi, 2019).

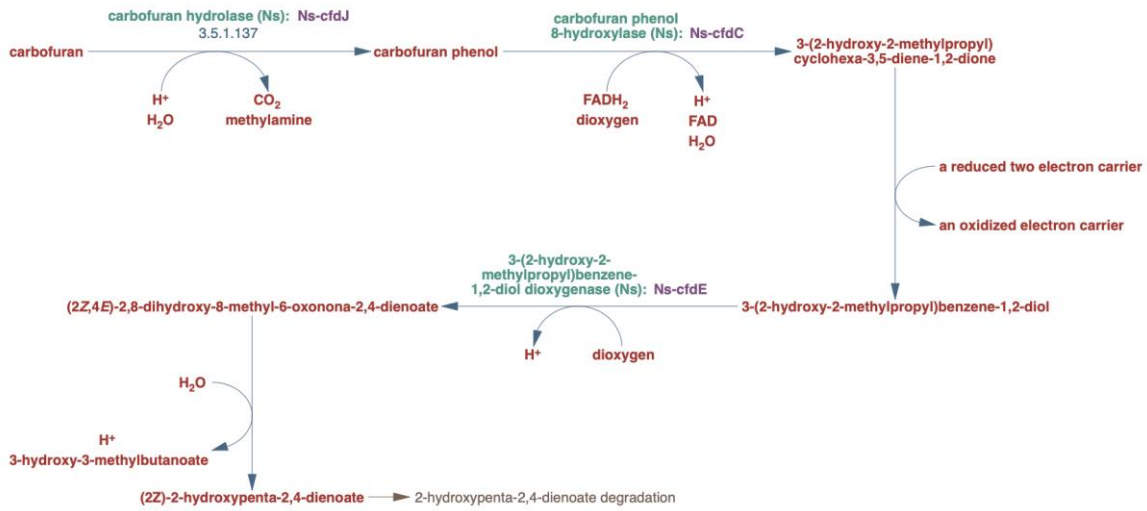


Figure 5.2. Carbofuran biodegradation pathway obtained from the MetaCyc database (Caspi, 2021).

The MetaCyc database delineates the biodegradation pathway for carbofuran, as illustrated in Figure 5.2. Genera such as *Pseudomonas*, *Flavobacterium*, *Achromobacter*, *Sphingomonas*, *Novosphingobium*, *Paracoccus* all identified as carbofuran degrading bacteria, are likely to be found in drinking water resources (Kremer et al., 1992; Nguyen et al., 2015; Peng et al., 2008; Tomasek & Karns, 1989; Yan et al., 2018). However, most these microorganisms are limited in their metabolic capabilities, being able to perform only the initial hydrolysis of carbofuran-to-carbofuran phenol.

The carbofuran degradation pathway is illustrated in Figure 5.2. It involves two distinct carbofuran hydrolases, Mcd and CfdJ, isolated from *Achromobacter sp. WN111*, *Sphingomonas sp. SB5*, and *Novosphingobium sp. KN65.2*, respectively (Kim et al., 2004; Nguyen et al., 2015; Tomasek & Karns, 1989). Key enzymes in the pathway include CfdC (a monooxygenase) and CfdE (a dioxygenase), which are part of the cfd operon (Nguyen et al., 2015). The degradation process produces several intermediates, including 3-(2-hydroxy-2-methylpropyl) benzene-1,2-diol and carbofuran phenol (Kim et al., 2004). Some strains generate red metabolites as shunt products during degradation (Park et al., 2006). While significant progress has been made in understanding this pathway, some enzymatic steps remain unidentified.

5.1.4. EAWAG-BBD/ PPS (Biocatalysis/Biodegradation Database Pathway Prediction System) Results

The potential biodegradation pathways for the pesticides under investigation were identified using their CAS registration number. Figures 5.3 to 5.7 illustrate the probable decomposition routes for chosen pesticides through biological processes. Within these figures, arrows represent the probability of specific reactions occurring in aerobic environments. The color coding of the arrows provides additional information: green arrows signify a high likelihood of the aerobic reaction taking place, while orange arrows indicate a moderate or neutral probability.

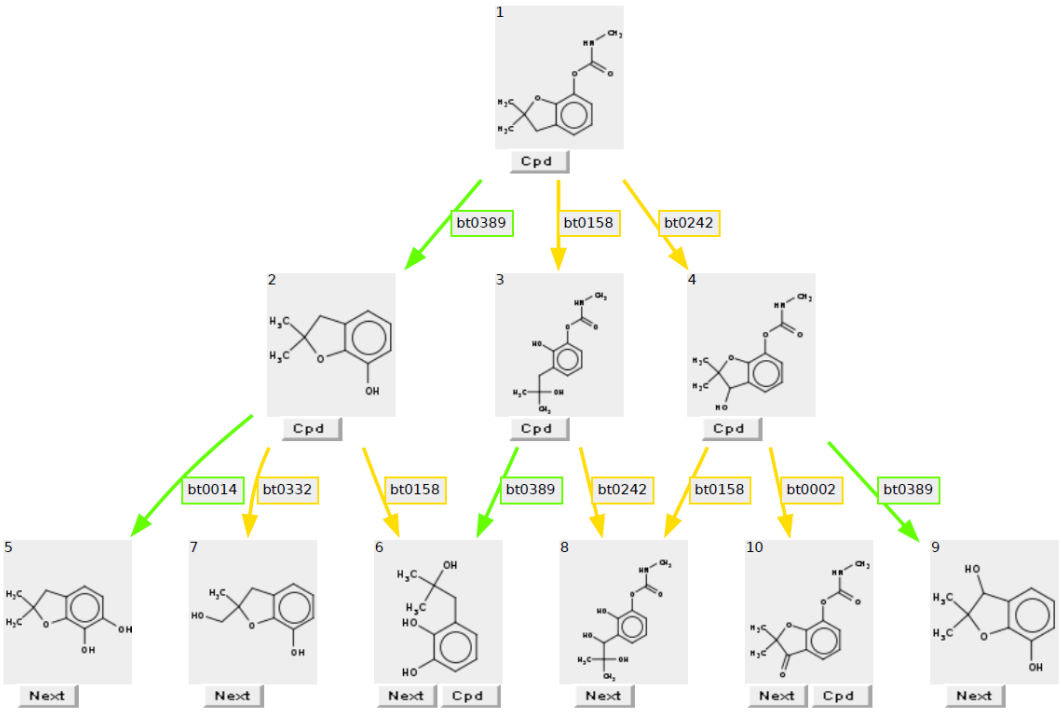


Figure 5.3. Possible carbofuran biodegradation pathways obtained from the EAWAG-BBD/PPS.

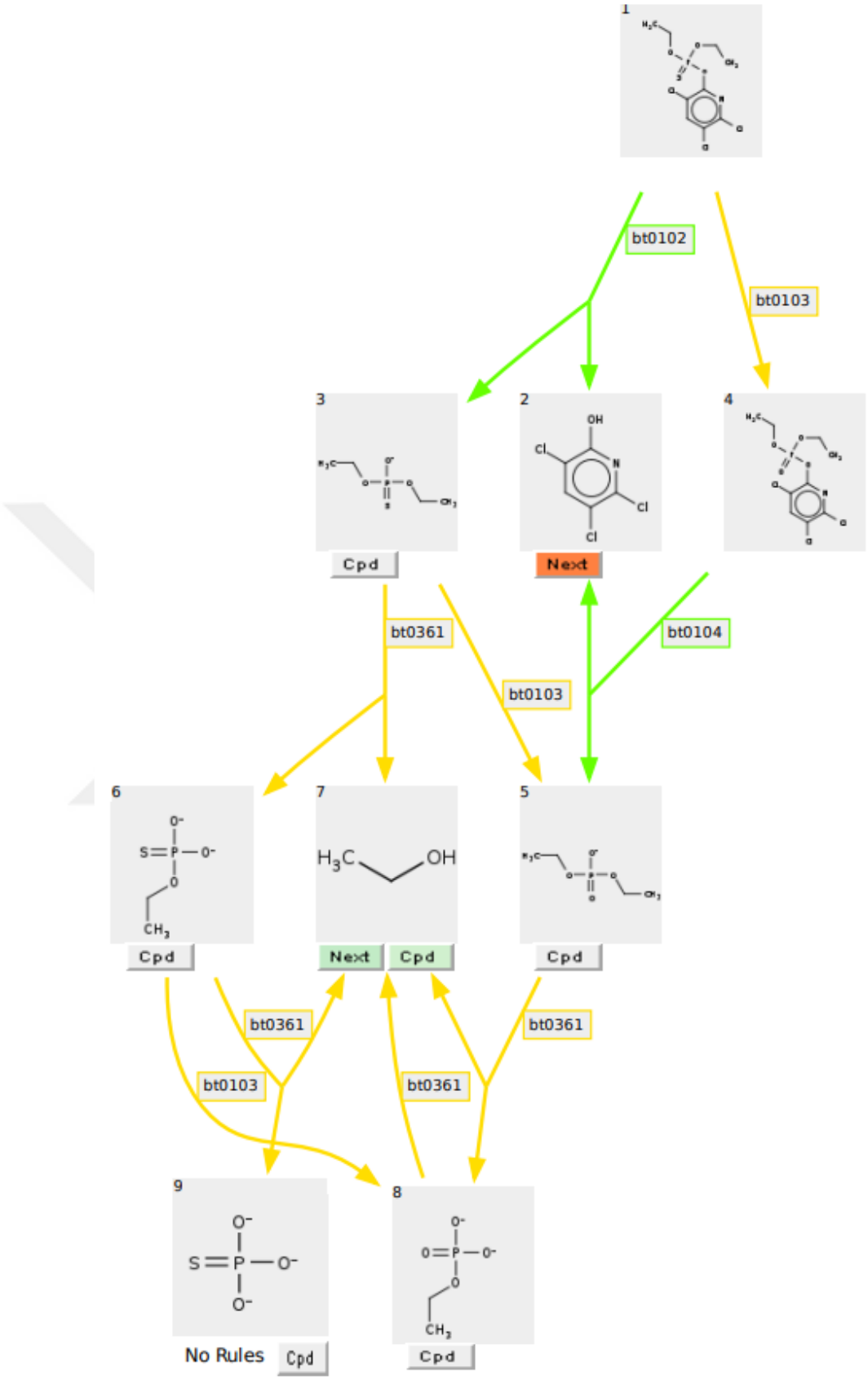


Figure 5.4. Possible chlorpyrifos biodegradation pathways obtained from the EAWAG-BBD/PPS.

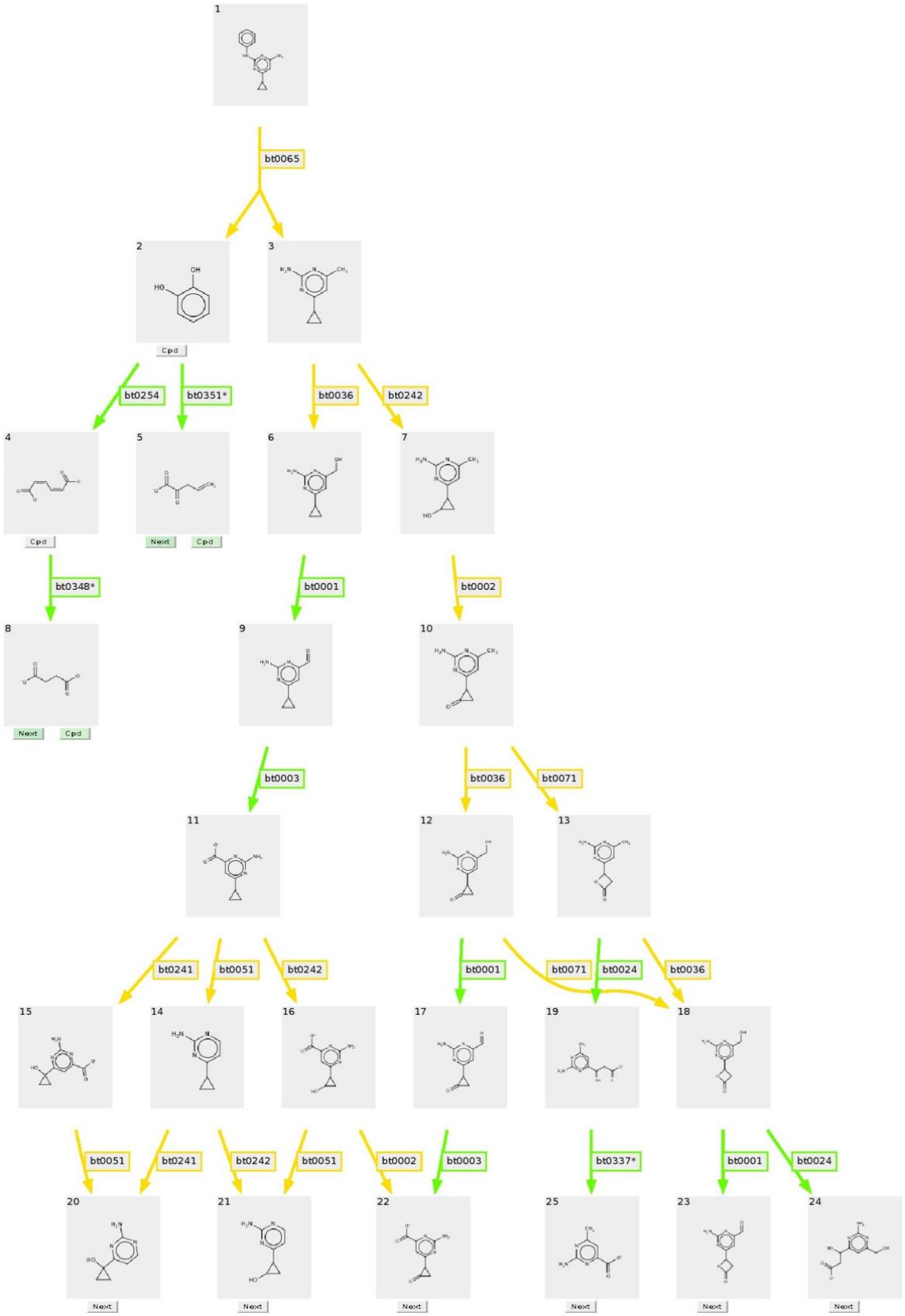


Figure 5.5. Possible cyprodinil biodegradation pathways obtained from the EAWAG-BBD/PPS.

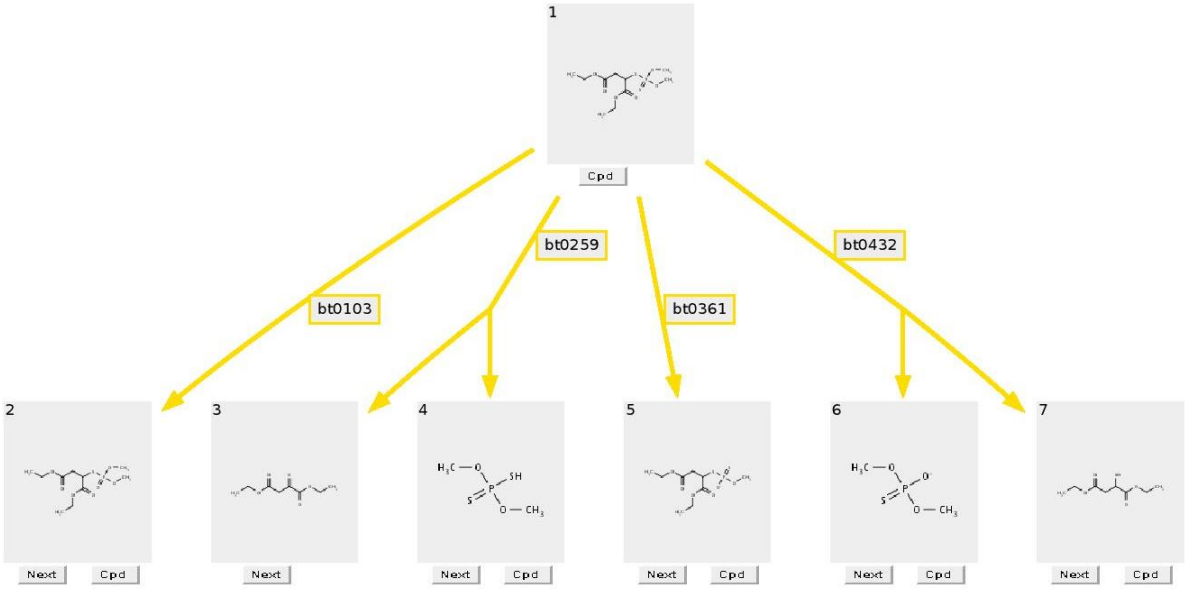


Figure 5.6. Possible malathion biodegradation pathways obtained from the EAWAG-BBD/PPS.

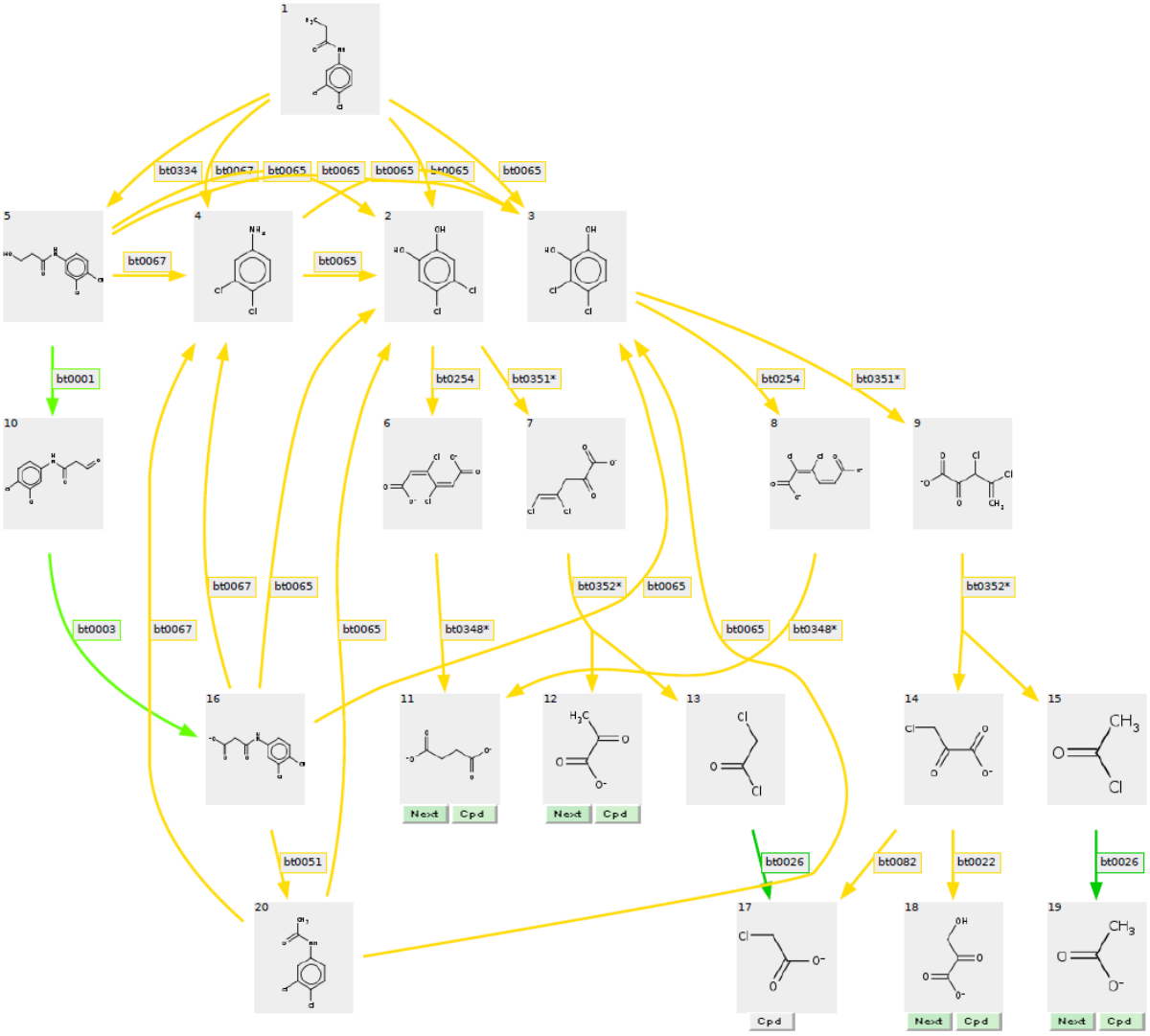


Figure 5.7. Possible propanil biodegradation pathways obtained from the EAWAG-BBD/PPS.

5.1.5. EnviPath (The Environmental Contaminant Biotransformation Pathway Resource) Results

An online tool called EnviPath, designed to extend the functionality of EAWAG-BBD/PPS, was used to predict possible biodegradation pathways of selected pesticides. EnviPath is a database and estimation system designed to predict microbial biotransformation of organic environmental pollutants that have not been studied to date. It displays visually the biological decomposition steps of a substance based on experimental data. Possible biodegradation pathways for selected pesticides were predicted and shown in Figures 5.8 to 5.12.

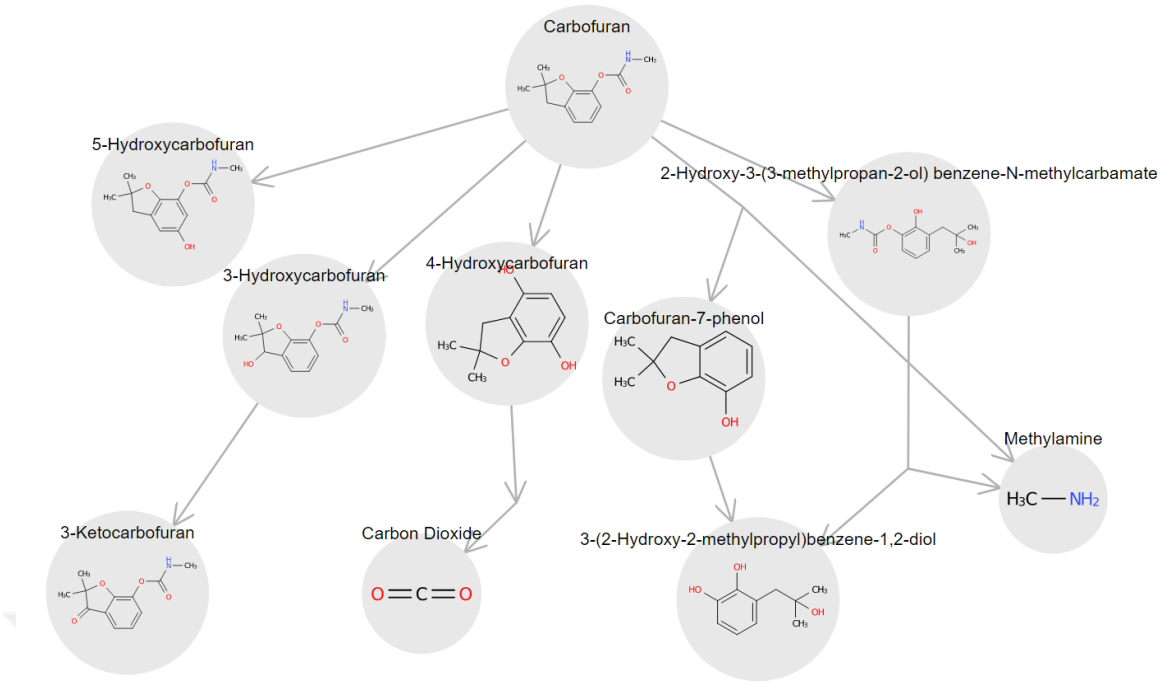


Figure 5.8. Possible carbofuran biodegradation pathways obtained from the EnviPath.

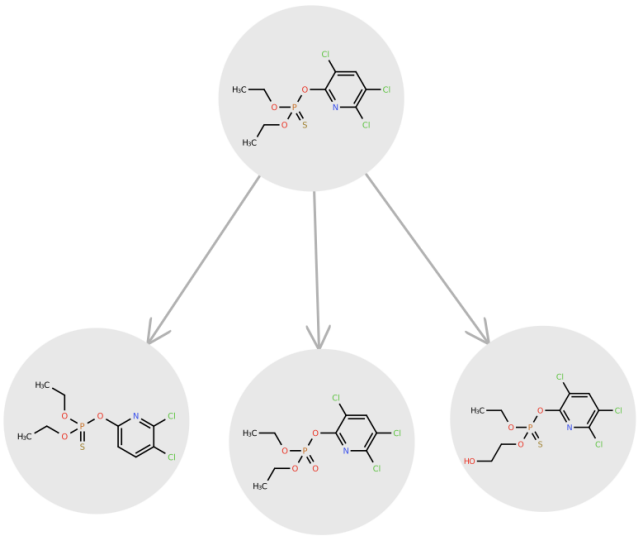


Figure 5.9. Possible chlorpyrifos biodegradation pathways obtained from the EnviPath.

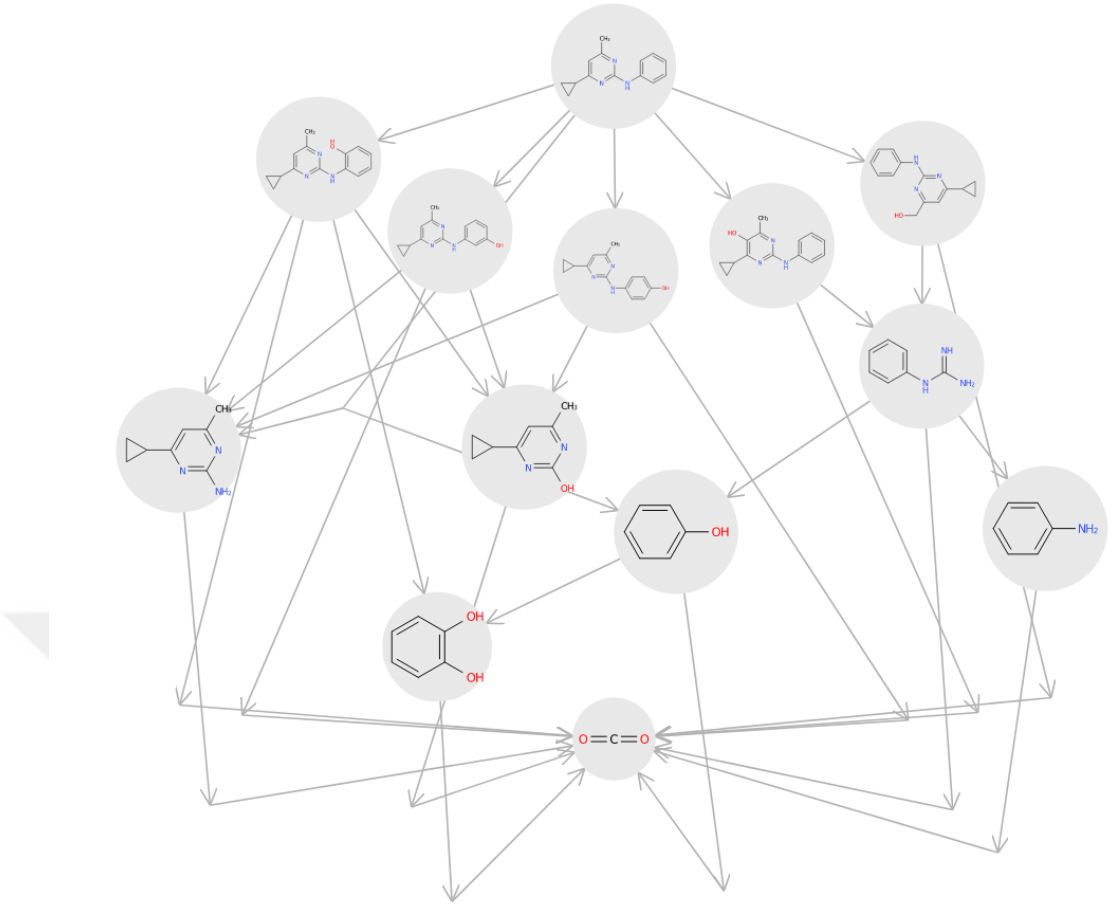


Figure 5.10. Possible cyprodinil biodegradation pathways obtained from the EnviPath.

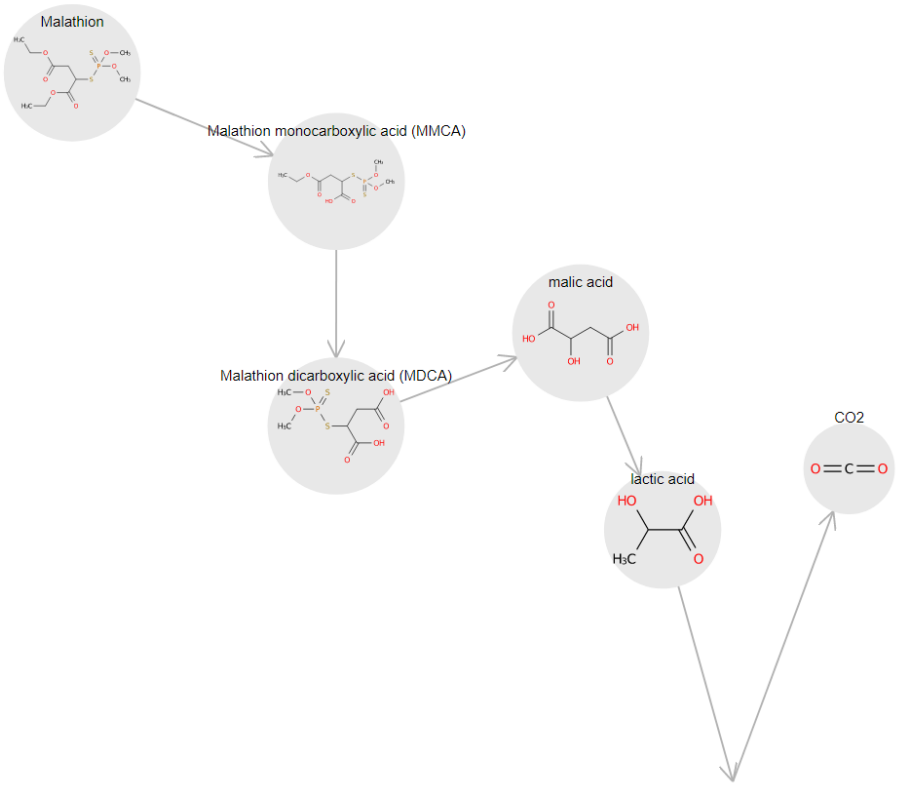


Figure 5.11. Possible malathion biodegradation pathways obtained from the EnviPath.

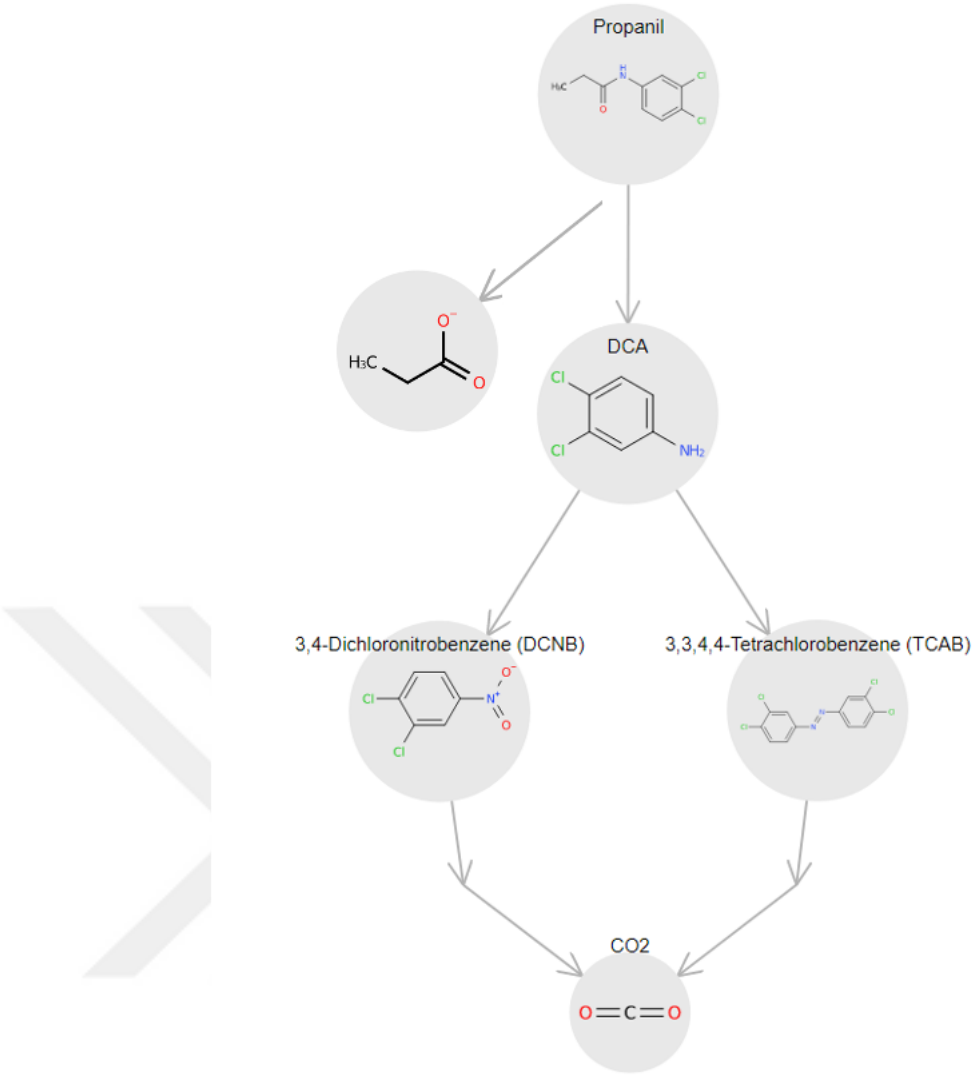


Figure 5.12. Possible propanil biodegradation pathways obtained from the EnviPath.

5.2. Analysis of Adsorption Kinetics and Isotherms

5.2.1. Batch Kinetic Experiments with Granular Activated Carbon (GAC)

Kinetic experiments were carried out in five different sets, namely:

i. Pesticide mixture + ground GAC,
ii. Pesticide mixture + non-ground (original) GAC,
iii. Background NOM + ground GAC,
iv. Background NOM + non-ground (original) GAC,
v. Background NOM + pesticide mixture + ground GAC.

Absorbance measurements were utilized for experiments involving background NOM to establish the equilibrium time. This method was chosen because it provides results concurrently with the experimental data. In other words, the absorbance readings let us determine when the system reached equilibrium in real time.

Results have shown that the size of GAC particles used in kinetic studies significantly affects the equilibrium time. Ground GAC particles, ranging from 100-125 μm, and non-ground (original) GAC particles, approximately 1 mm in size, exhibit markedly different equilibrium times. Experiments using ground GAC reached equilibrium within hours, while those with original GAC required days to achieve equilibrium.

Appendix B graphically presented the results of five distinct experiments, showing concentration changes over time. Experiments conducted with ground GAC reached equilibrium within 24 hours. In contrast, when using non-ground, original size GAC, the time to achieve equilibrium extended to about 120-174 hours. These findings highlight the advantages of employing ground GAC in such experiments, as it substantially decreases the time required to reach equilibrium.

The reduced particle size of ground GAC facilitates improved diffusion of substances into the material. The equilibrium time for the original GAC being more than six times longer than ground GAC aligns with the study's objective of conducting experiments in RSSCT, as this ensures faster data acquisition. The shorter time requirement for equilibrium in ground GAC demonstrates the effectiveness of using ground GAC for accelerated experimental results.

5.2.1.1. *Adsorption kinetics of a pesticide mixture in the case of ground GAC.* Our analysis employed the most utilized kinetic models to better understand the dynamics of adsorption. Table 5.3 presents a comprehensive summary of various adsorption kinetic models, including their respective equations and associated parameters. The kinetic data were fitted to three kinetic models: pseudo-first order (PFO), pseudo-second order (PSO), and intraparticle diffusion. Table 5.4 shows the corresponding coefficient of determination (R2) values for the studied pesticides across these three distinct kinetic models.

Table 5.3. Summary of the kinetic models.

Kinetic Model	Equations	Plot	Rate Constants
Pseudo-First Order	$\ln(q_{e,exp} - q_t) = \ln q_{e,cal} - k_1 t$	ln (q_e-q_t) vs t	k_1 (1/h)
Pseudo-Second Order	$\frac{t}{q_t} = \frac{1}{k_2 q_e^2} + \frac{1}{q_e} t$	t/q_t vs t	k_2 (g/mg.h)
Intraparticle diffusion	$k_i = \frac{q_t}{t^{1/2}} + B$	q_t vs $t^{1/2}$	B (mg/g) k_i (mg/g.$h^{1/2}$)

Table 5.4. R^2 values for three kinetic models.

Initial GAC con. (mg/L)	Pseudo-first order kinetic model					Pseudo-second order kinetic model					Intraparticle Diffusion model				
	CBF	CPF	CYP	MLT	PRP	CBF	CPF	CYP	MLT	PRP	CBF	CPF	CYP	MLT	PRP
100	0.62	0.64	0.58	0.77	0.64	0.99	0.99	0.99	0.98	0.99	0.72	0.75	0.61	0.68	0.58
200	0.63	0.64	0.60	0.73	0.56	0.99	0.99	0.99	0.89	0.99	0.80	0.79	0.78	0.69	0.59
500	0.85	0.60	0.62	0.87	0.65	1	1	1	0.93	1	0.61	0.72	0.65	0.76	0.85
750	0.84	0.65	0.75	0.64	0.66	1	1	1	0.99	1	0.74	0.73	0.73	0.78	0.81
1000	0.79	0.59	0.72	0.80	0.78	1	1	1	0.99	1	0.79	0.78	0.69	0.65	0.64
1500	0.84	0.73	0.84	0.91	0.77	1	1	1	0.99	1	0.82	0.68	0.75	0.76	0.67

**CBF: carbofuran, CPF: chlorpyrifos, CYP: cyprodinil, MLT: malathion, PRP: propanil.*

Applying these models allow for a deeper understanding of the adsorption mechanisms and rates. By comparing the R^2 values, we can determine which model best describes the adsorption kinetics for each pesticide. The R^2 analysis reveals that the pseudo-second order (PSO) kinetics provides the most accurate description of the adsorption process for all investigated pesticides. This conclusion is drawn from the PSO model's adjusted R^2 values being nearest to unity. The superior fit of the PSO model implies that the adsorption rate is predominantly determined by the number of available adsorption sites on the GAC surface rather than the pesticide concentration in the solution (Liu, 2008). Previous studies support the observation that the removal of micropollutants and pesticides using GAC generally follows the PSO kinetic model (Ayranci & Hoda, 2005; Daneshvar et al., 2007; Mansour et al., 2017; Salman & Hameed, 2010; Habila et al., 2015).

The graphical depiction of the pseudo-second order kinetic model's fit for the adsorption kinetics of pesticides is presented in Figure 5.13. Analysis of the PSO kinetic model involved calculating the key parameters k_2 and q_e by examining the linear relationship between t/q_t and time, specifically using the gradients and y-intercepts of these plots. These calculations were based on Eq.4. 5, which represents the linearized form of the PSO model. The resulting values for all studied pesticides are represented in Table 5.5. The calculated equilibrium values ($q_{e,cal}$) for pesticides closely align with experimental results ($q_{e,exp}$). This correlation suggests a high degree of accuracy in the theoretical model used to predict pesticide adsorption behavior.

The observed similarity between calculated and experimental q_e values not only validates the selected model but also enhances our confidence in utilizing this model for future predictions and analyses in our study.

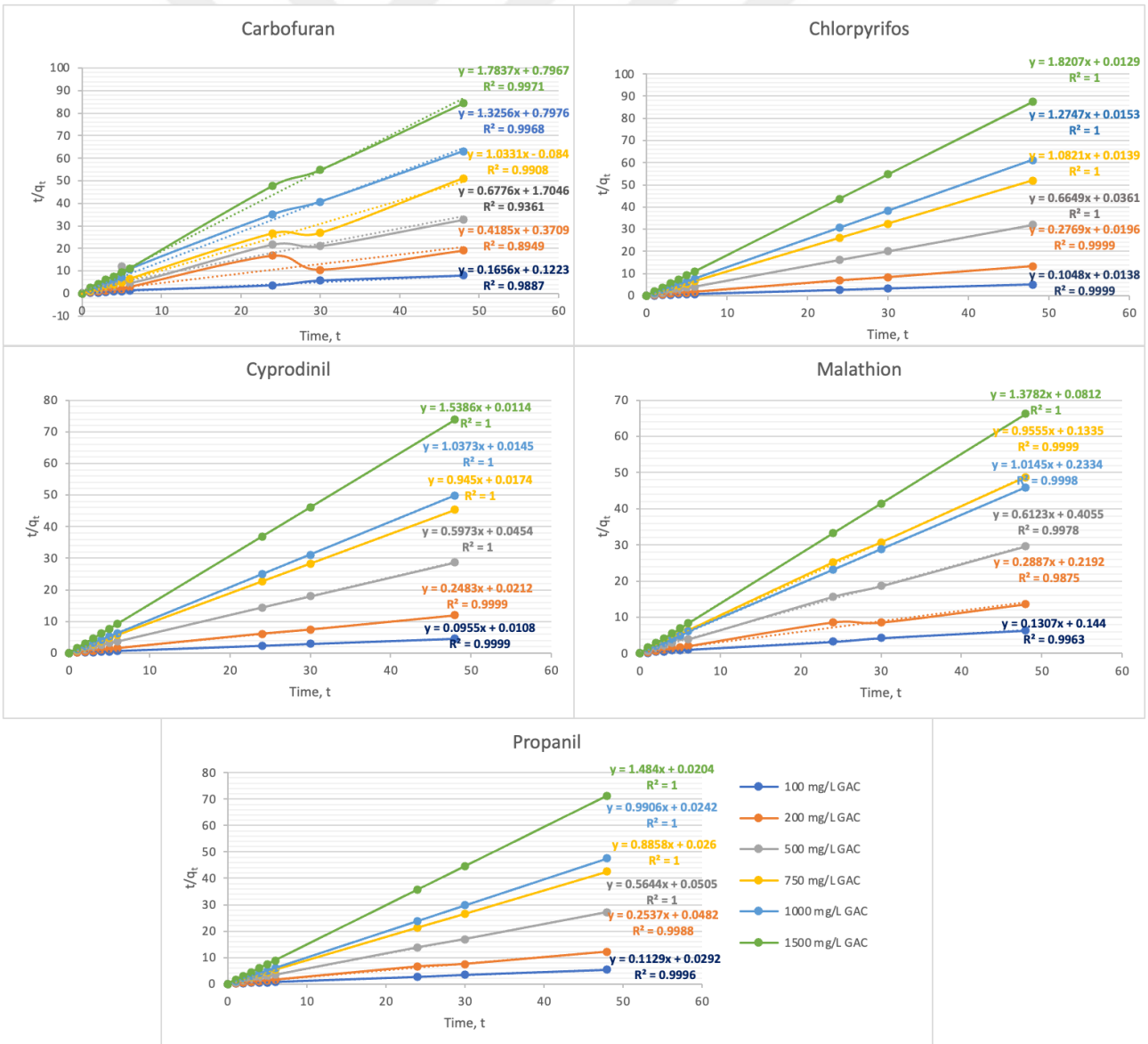


Figure 5.13. PSO modeling for the adsorption of pesticides onto GAC

Table 5.5. Pseudo-second order kinetic model parameters for a pesticide mixture adsorbing on ground GAC.

Initial GAC con. (mg/L)	Carbofuran				Chlorpyrifos				Cyprodinil				Malathion				Propanil			
	$q_{e.exp}$ (mg/g)	K_2 (g/mg.h)	$q_{e.cal}$ (mg/g)	R_2	$q_{e.exp}$ (mg/g)	K_2 (g/mg.h)	$q_{e.cal}$ (mg/g)	R_2	$q_{e.exp}$ (mg/g)	K_2 (g/mg.h)	$q_{e.cal}$ (mg/g)	R_2	$q_{e.exp}$ (mg/g)	K_2 (g/mg.h)	$q_{e.cal}$ (mg/g)	R_2	$q_{e.exp}$ (mg/g)	K_2 (g/mg.h)	$q_{e.cal}$ (mg/g)	R_2
100	7.60	0.12	7.65	0.99	9.54	0.80	9.54	0.99	10.6	0.84	10.4	0.99	7.93	0.22	6.04	0.99	8.95	0.44	8.86	1
200	3.54	0.38	3.46	0.99	3.61	3.91	3.61	0.99	4.05	2.91	4.03	0.99	2.87	0.47	2.39	0.90	3.99	1.34	3.94	1
500	1.63	0.92	1.63	0.99	1.50	12.25	1.50	1	1.68	7.86	1.67	1	1.47	0.27	1.48	0.94	1.78	6.31	1.77	1
750	0.99	4.41	0.99	0.99	0.92	84.24	0.92	1	1.06	51.32	1.06	1	1.12	1.71	0.97	0.99	1.12	30.18	1.13	1
1000	1.05	6.84	1.05	0.99	0.78	106.2	0.78	1	0.97	74.21	0.96	1	7.93	0.22	6.04	0.99	1.01	40.55	1.01	1
1500	0.73	23.39	0.73	1.00	0.54	256.9	0.55	1	0.65	207.6	0.65	1	2.87	0.47	2.39	0.90	0.68	107.9	0.67	1

5.2.2. Isotherm Experiments with GAC

After conducting kinetic experiments, the equilibration time for each experimental set was determined. An experimental set similar to kinetic experiments was prepared for isotherm experiments by considering the equilibration time. During the experimental procedures, specimens were collected at two distinct time points – one at the start and another at the end of the trials – which aligned with the established equilibrium period.

For the data analysis, four well-established adsorption models were employed: linear, Freundlich, Langmuir, and Temkin. These models are commonly employed to describe the adsorption of molecules onto activated carbon. The mathematical expressions and key parameters of each model can be found in Table 5.6.

Table 5.6. Summary of adsorption isotherm models, their respective equations and associated parameters.

Isotherm	Equations (Nonlinear Forms)	Equations (Linear Forms)	Plot	Parameters
Linear	$q_e = C_e k_d$	$ln\ q_e = \ln\ k_d + ln\ C_e$	q_e vs C_e	K_d (L/g)
Freundlich	$q_e = K_f\ {C_e}^{1/n}$	$ln\ q_e = \ln\ K_f + \frac{1}{n}\ ln\ C_e$	ln q_e vs ln C_e	1/n (unitless) K_f $(mg/g)(L/mg)^{1/n}$
Langmuir	$q_e = \frac{q_{max}\ K_L\ C_e}{1 + K_L\ C_e}$	$\frac{1}{q_e} = \frac{1}{q_{max} K_L C_e} + \frac{1}{q_{max}}$	1/ q_e vs 1/ C_e	q_{max} (mg/g) K_L (L/mg)
Temkin	$q_e = \frac{RT}{b_T} \ln K_T C_e$	$q_e = \frac{RT}{b_T} \ln\ K_T + \frac{RT}{b_T}\ ln\ C_e$	q_e vs ln C_e	b_T (J/mol) K_T (L/g)

5.2.2.1. *Adsorption isotherms of pesticides in a monocomponent system (ground GAC).* In this part of the study, adsorption isotherm experiments were conducted separately for each pesticide. The initial concentration of each pesticide was set at 1 mg/L. Adsorption isotherms were established using ground GAC doses from 50 to 1500 mg/L. Preliminary kinetic experiments demonstrated that a 24-hour period was sufficient to achieve equilibrium for all ground GAC doses. Samples were taken at the beginning of the experiment to determine qe and Ce and again after 24 hours.

The resultant data were utilized to construct isotherm graphs for four commonly used adsorption models: Linear, Freundlich, Langmuir, and Temkin. Analysis of the coefficients of determination (R^2) for these isotherm models revealed that the Freundlich model exhibited superior fit to the experimental data (Figures 5.14-5.18). The Langmuir model was found to be the second model that showed a relatively better fit to the observed data, after the Freundlich isotherm. Consequently, the parameters of these two adsorption models were calculated for each pesticide and are presented in Table 5.7.

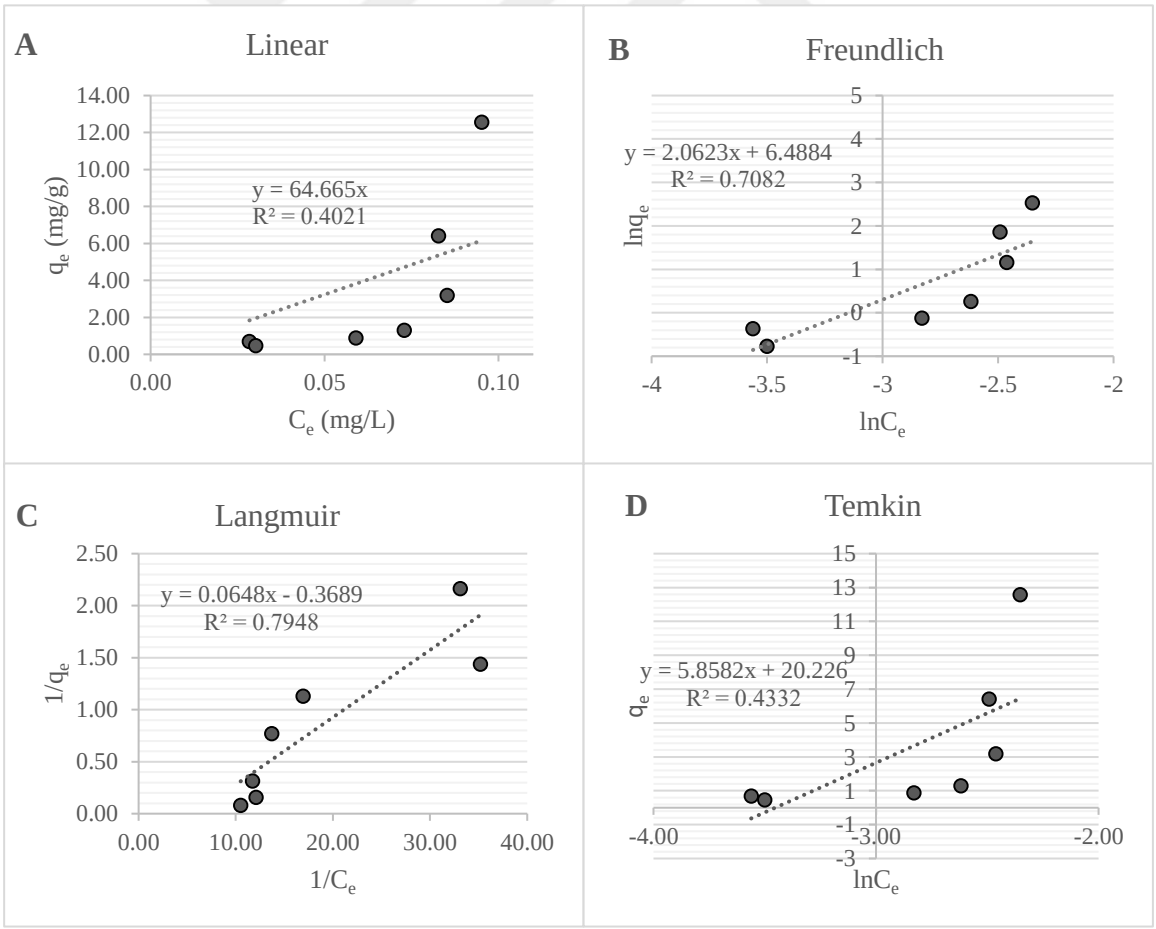


Figure 5.14. Adsorption isotherms for carbofuran: (A) Linear, (B) Freundlich, (C) Langmuir, (D) Temkin.

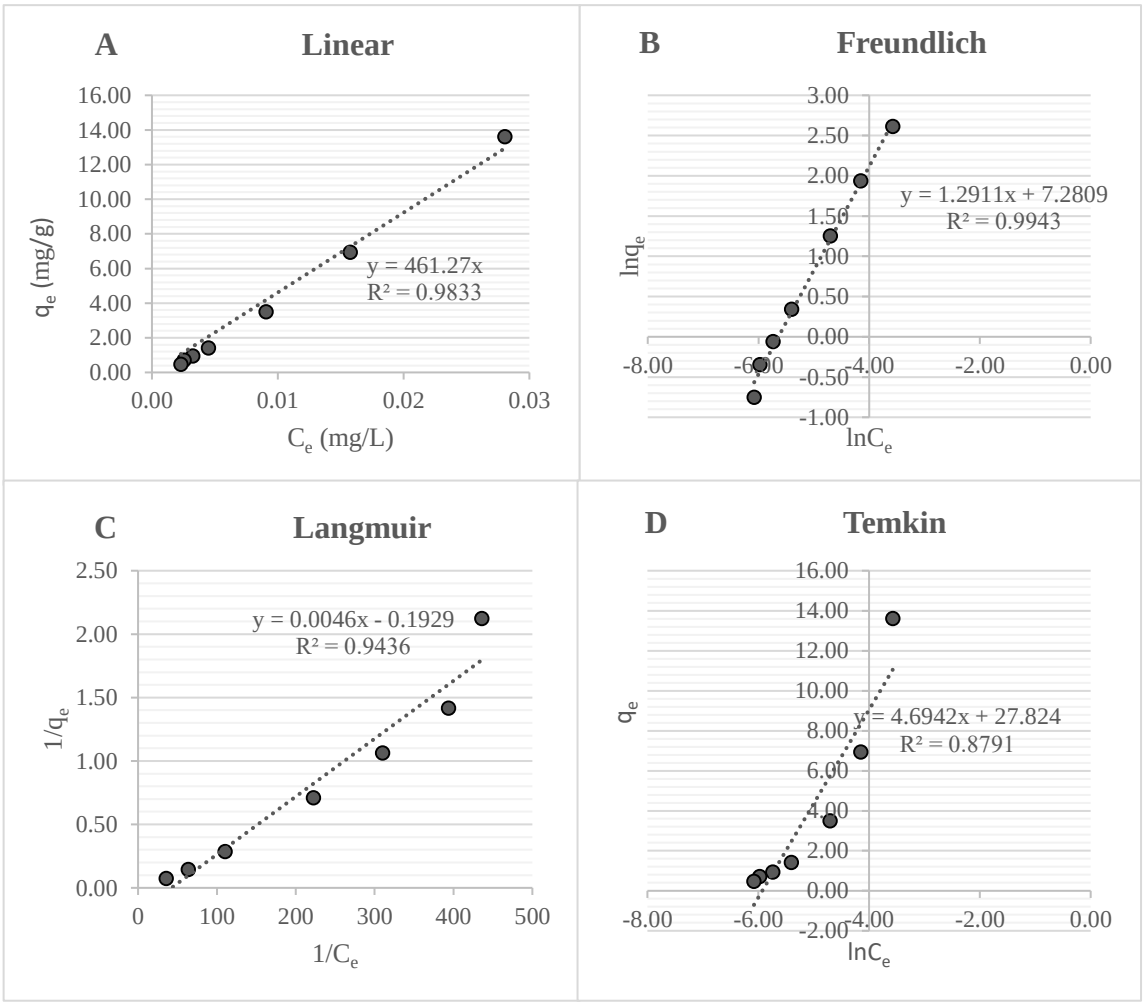


Figure 5.15. Adsorption isotherms for chlorpyrifos: (A) Linear, (B) Freundlich, (C) Langmuir, (D) Temkin.

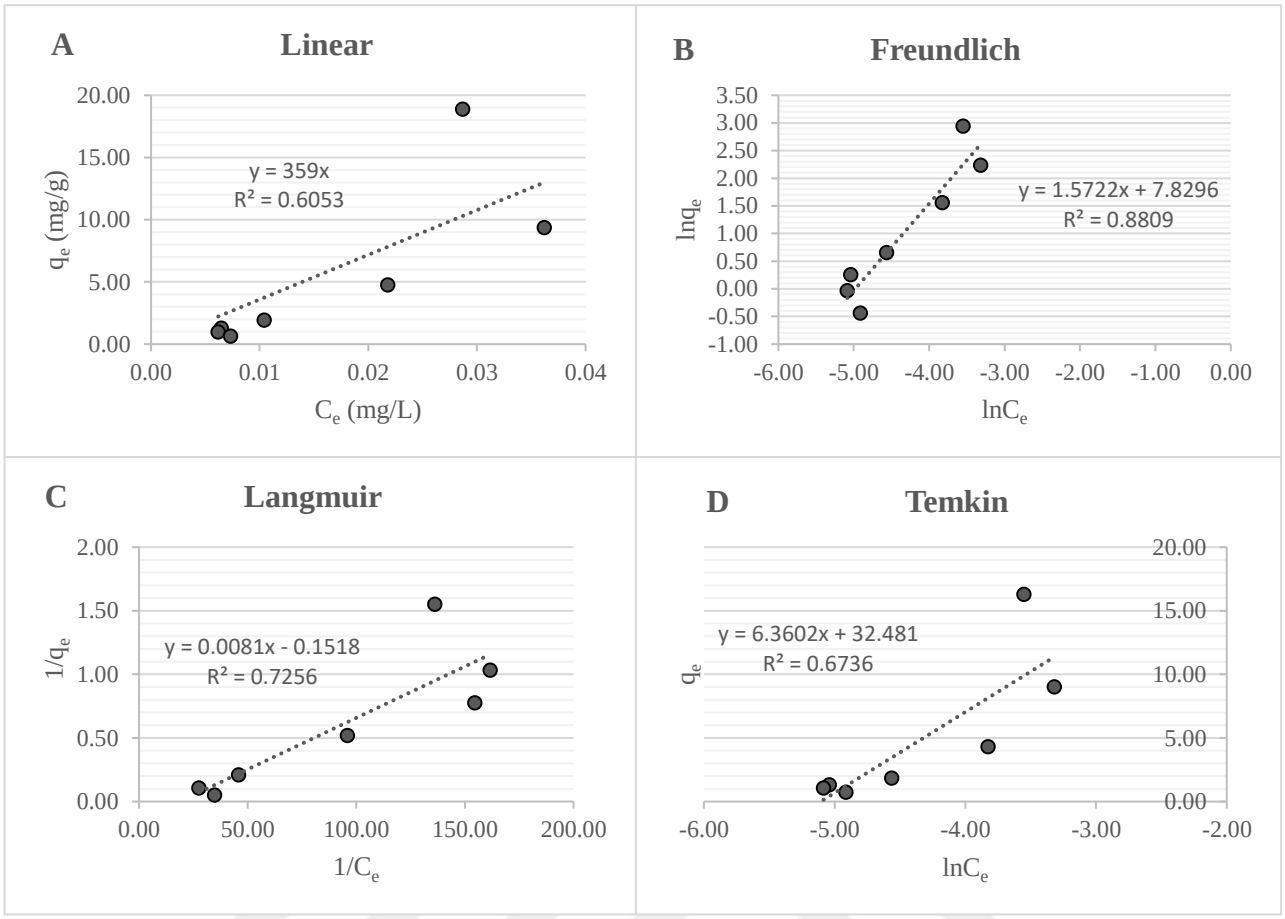


Figure 5.16. Adsorption isotherms for cyprodinil: (A) Linear, (B) Freundlich, (C) Langmuir, (D) Temkin.

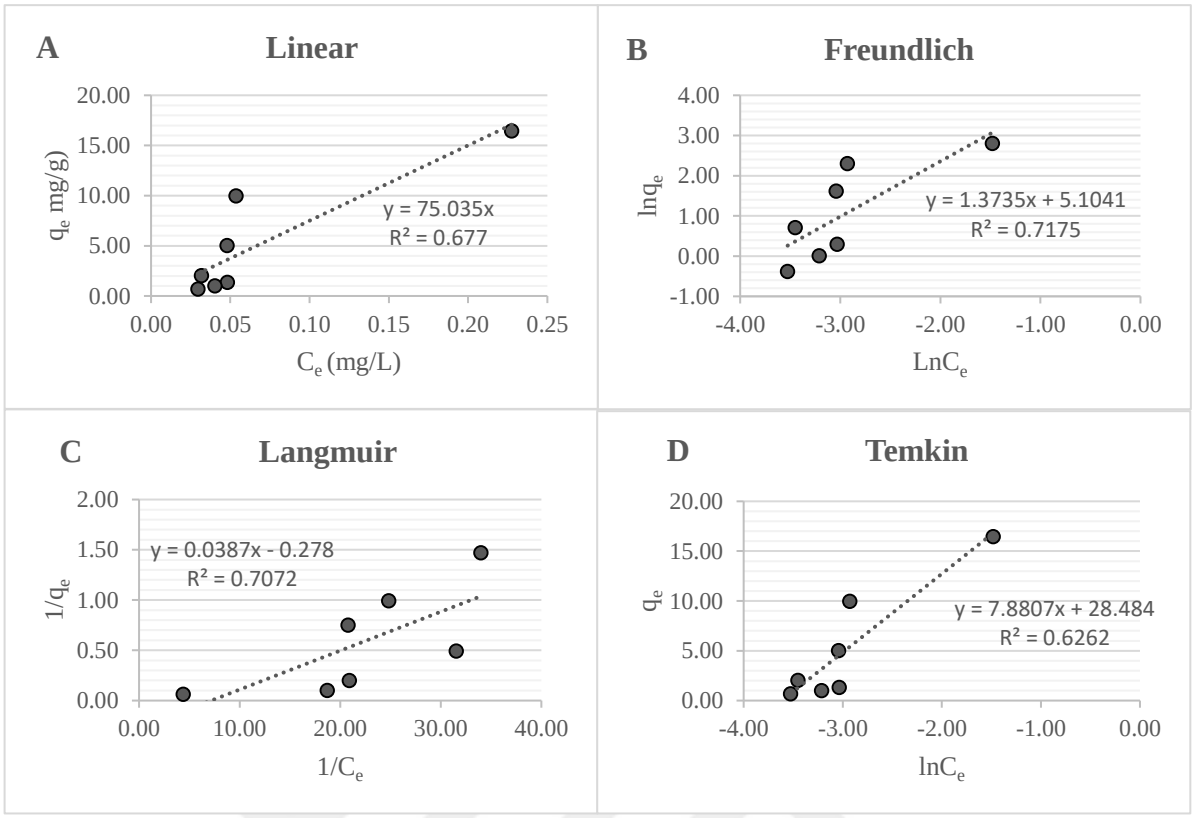


Figure 5.17. Adsorption isotherms for malathion: (A) Linear, (B) Freundlich, (C) Langmuir, (D) Temkin.

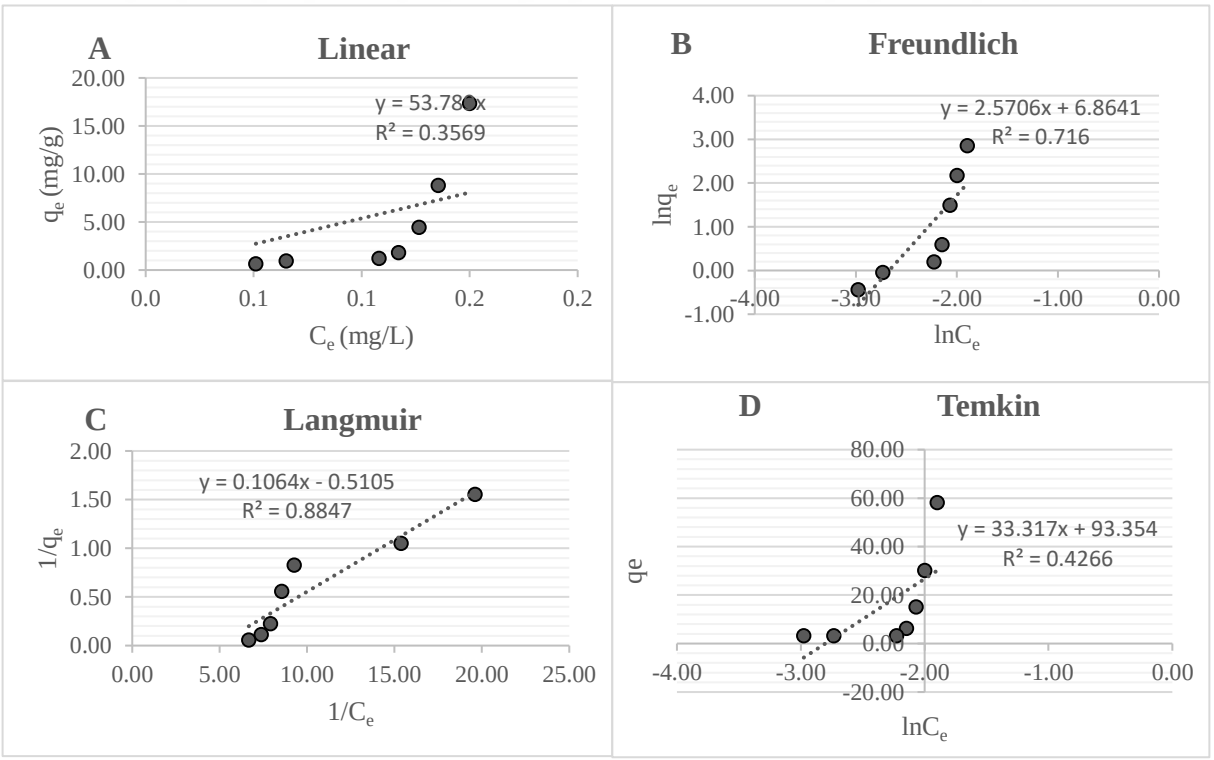


Figure 5.18. Adsorption isotherms for propanil: (A) Linear, (B) Freundlich, (C) Langmuir, (D) Temkin.

The results showed removal efficiencies for chlorpyrifos (CPF) and cyprodinil (CYP) after 24 hours were between 90% and 98% for different GAC doses. For propanil (PRP) and carbofuran (CBF), removal efficiencies were between 70% and 90%. Malathion (MLT) showed the lowest removal efficiency, ranging between 50% and 90% across various GAC doses from 50 mg/L to 1500 mg/L.

The results demonstrate varying adsorption efficiencies among different pesticides when treated with GAC. CHF and CYP showed the highest removal, while MLT exhibited the lowest. The varying removal efficiencies between pesticides can be attributed to the specific physicochemical characteristics of each pesticide. The primary physicochemical factors influencing micropollutant adsorption onto GAC include molecular weight, size, hydrophobicity, functional groups, charge, and ionic strength of a pesticide. The relationship between the pesticide's chemical structures and their adsorption behavior becomes apparent. More complex molecular structures with multiple aromatic rings and chlorine substituents (such as chlorpyrifos) generally exhibit stronger adsorption characteristics compared to simpler structures (as in carbofuran) (Blachnio et al., 2020). Among the physicochemical properties, the octanol-water partition coefficient tends to have a higher impact on the adsorbability of a substance (Koyama et al., 2024).

The Langmuir equilibrium coefficients (K_L) are a quantitative measure of adsorption strength. A higher K_L value correlates with an increased capacity for adsorbent loading, indicating a more efficient adsorption process. A significant relationship exists between the Langmuir equilibrium coefficients (K_L) and the octanol-water partition coefficient (Log K_{ow}) of pesticides. The log K_{ow} values of the studied pesticides were 4.96, 4, 3.07, 2.36, and 2.32 for CPF, CYP, PRP, MLT, and CBF, respectively. When comparing the K_L values of pesticides, it was observed that pesticides with higher log K_{ow} values also exhibited higher K_L values. The K_L values were 41.93, 18.74, 4.80, 7.18, and 5.69 L/mg for CPF, CYP, PRP, MLT, and CBF, respectively.

The log K_{ow} value is a quantitative measure of a compound’s hydrophilicity, indicating its propensity to partition between a nonpolar and a polar phase. A higher log K_{ow} value suggests a greater affinity for nonpolar chemicals. The correlation between K_L and log K_{ow} can be attributed to the predominantly nonpolar nature of activated carbon (Li et al., 2002). Compounds exhibiting higher log K_{ow} values, indicative of increased hydrophobicity, are more likely to engage in stronger interactions with hydrophobic adsorbers. Numerous studies in the literature have also demonstrated this correlation (Kaur et al., 2018; Nemeth-Konda et al., 2002; Koyama et al., 2024).

Despite its theoretical foundation, the Langmuir isotherm often exhibits limitations in accurately describing experimental isotherm data, particularly for activated carbon adsorbents (Worch, 2021). This inadequacy primarily stems from its underlying assumptions, notably monolayer coverage and energetic homogeneity of adsorption sites, which are frequently violated in real-world adsorption scenarios. Conversely, the Freundlich isotherm better represents adsorption phenomena within the medium concentration range, even if it has limitations at extreme concentrations. It has emerged as a standard model for characterizing adsorption processes in water treatment applications, especially those involving activated carbon (Worch, 2021). The Freundlich isotherm has gained widespread recognition and application, particularly in its integration into equilibrium relationships for breakthrough curve models. Notable examples of its implementation can be found in advanced predictive modeling software, including Adsorption Design Software (AdDesignS) and Fixed-bed Adsorption Simulation Tool (FAST).

Moreover, the Freundlich model provides a relatively better fit to our results compared to the other models investigated. In the Freundlich isotherm model, while the Freundlich equilibrium coefficient (K_f) is associated with the adsorbent's capacity for the adsorbate, the Freundlich equilibrium constant (1/n) is connected to the intensity of the adsorption process (Worch, 2021). The 1/n and the K_f of studied pesticides onto GAC vary, as demonstrated by the findings presented in Table 5.7.

According to our results, 1/n values for all tested pesticides are higher than 1. The Freundlich isotherm constant (1/n) values exceeding 1, typically indicate S-type isotherms. These isotherms are less typical but are frequently observed when examining low concentration ranges of substances with polar functional groups (ECETOC, 2024). Some research indicates that the fraction of the compound adsorbed on the solid phase may increase substantially at extremely low concentrations (ECETOC, 2024). When we compare 1/n values of tested pesticides, we show that CPF, CYP, and MLT have 1/n values between 1 and 2, while PRP and CBF have 1/n values greater than 2. As we know from the literature, adsorption intensity is inversely proportional to 1/n values; adsorption intensity is higher for CPF, CYP, and MLT pesticides than others (Worch, 2021).

In addition, the Freundlich equilibrium coefficients (K_f) of the tested pesticides were also compared. As mentioned, K_f is directly proportional to the adsorbent's capacity for the adsorbate. Results indicate that CPF and CYP exhibit superior adsorption capabilities compared to the rest of the pesticides. These two pesticides also have log K_{ow} values exceeding 4. In contrast, MLT, with a

log K_{ow} of 2.3, shows comparatively weaker adsorption characteristics than the other pesticides in the study.

Table 5.7. Isotherm parameters describing the sorption of individual pesticides onto ground GAC.

Isotherm	Parameters	Carbofuran (CBF)	Chlorpyrifos (CPF)	Cyprodinil (CYP)	Malathion (MLT)	Propanil (PRP)
Freundlich	1/n	2.06	1.29	1.57	1.37	2.57
	K_f (mg/g) $(L/mg)^{1/n}$	657.47	1452.29	2513.92	164.70	957.28
	R^2	0.71	0.99	0.88	0.71	0.72
Langmuir	q_{max} (mg/g)	2.71	5.18	6.59	3.60	1.96
	K_L (L/mg)	5.69	41.93	18.74	7.18	4.80
	R^2	0.80	0.94	0.73	0.70	0.89

We compared our experimental findings with previously published research on pesticide adsorption and compiled the comparative data in Table 5.8, explicitly focusing on activated carbon-based adsorbents. The results demonstrate varying levels of effectiveness, with our adsorbent Norit GAC 1240AF showing both advantages and limitations compared to existing studies. However, it is essential to acknowledge that direct comparisons between different studies are challenging due to variations in experimental parameters, particularly in terms of initial pesticide concentrations and adsorbent quantities used. The absence of standardized protocols for adsorption experiments further complicates meaningful comparisons across different research works.

Table 5.8. Comparative analysis of pesticide adsorption: literature values and own experimental results.

Pesticide	Adsorbent	q_e (mg/g)	1/n	q_{max} (mg/g)	Reference
Carbofuran (CBF)	Activated carbon-F200	20	1.57		(Salman et al., 2011)
	Coal fly ash	0.2 to 1.6			(Kumari, Singh, & Saxena, 1988)
	Chestnut shell		0.54	2.39	(Memon et al., 2007)
	GAC F400		0.41		(Speth & Miltner, 1990)
	Ground Norit® GAC 1240AF	0.46 to 12.57	2.06	2.71	This study
Chlorpyrifos (CPF)	Activated Biochar from tobacco			0.68 to 1.60	(Gonçalves et al., 2022)
	AC from cinnamon waste	11.1	4.09	12.4	(Ettish et al., 2021)
	AC fiber			175	(Jocić et al., 2022)
	Cellulose based-carbon fiber	180	1.45	73	(Bedia et al., 2024)
	Spent coffee grounds	2.1 to 12	1.36 to 2.07	3.4 to 19.4	(Milanković et al., 2024)
	Ground Norit® GAC 1240AF	0.47 to 13.61	1.29	5.18	This study
Cyprodinil (CYP)	Lignocellulosic biosorbent	5.03	9.82	21.27	(Velinov et al., 2019)
	Ground Norit® GAC 1240AF	0.64 to 18.89	1.57	6.59	This study
Malathion (MLT)	AC from waste			32.1	(Habila et al., 2015)
	GAC			909	(Jusoh et al., 2011)
	PAC	0.41		22	(Kumar et al., 2014)
	AC fiber			165	(Jocić et al., 2022)
	Spent coffee grounds	1.3 to 13.2	1.72 to 2.08	7.15 to 11.2	(Milanković et al., 2024)
	Ground Norit® GAC 1240AF	0.68 to 16.45	1.37	3.60	This study
Propanil (PRP)	AC-cloth	40 to 118	0.30	114	(Ayranci & Hoda, 2004)
	Black carbon	75 to 225			(Xiao et al., 2012)
	Ground Norit® GAC 1240AF	0.64 to 17.32	2.57	1.96	This study

5.2.2.2. *Adsorption isotherms of pesticides in a multicomponent system (ground GAC).* In this part of the research, adsorption isotherms were constructed using a mixture of pesticides, in contrast to the previous section, where isotherms of pesticides were studied separately. By studying pesticide adsorption in both isolated and mixed conditions, we seek to understand how multiple solutes interact and influence each other during adsorption.

The initial concentration of each pesticide was set at 1 mg/L, resulting in a combined pesticide concentration of 5 mg/L. Adsorption isotherms were established using ground GAC doses from 100 to 1500 mg/L. Preliminary kinetic experiments demonstrated that a 24-hour period was sufficient to achieve equilibrium for all ground GAC doses. To determine q_e and C_e, samples were taken at the beginning of the experiment and again after a 24-hour period.

Figures 5.19 to 5.23 illustrate the Freundlich, and the Langmuir isotherm graphs for each pesticide under investigation. Based on these analyses, the parameters for both adsorption models were determined for each pesticide and summarized in Table 5.9.

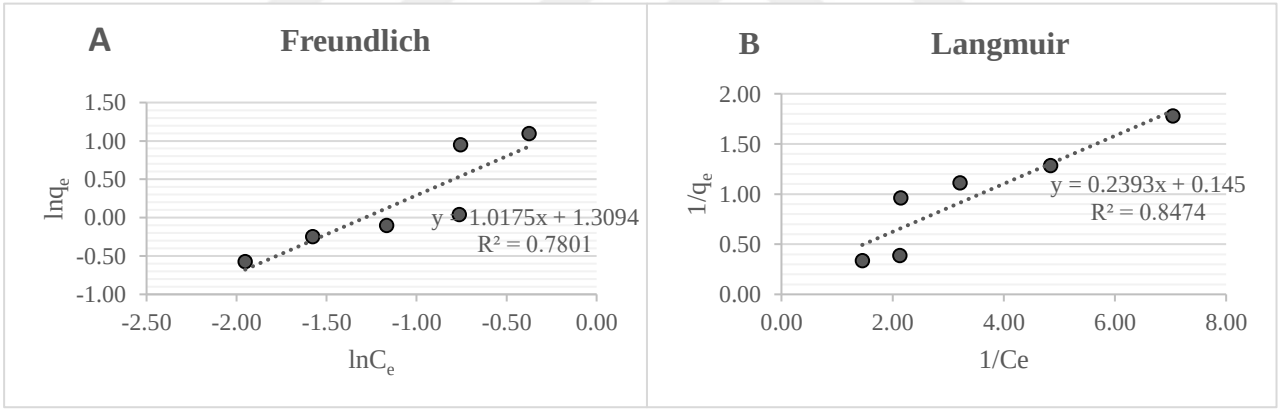


Figure 5.19. Isotherms showing the adsorption of carbofuran onto ground GAC in a pesticide mixture: (A) Freundlich, (B) Langmuir.

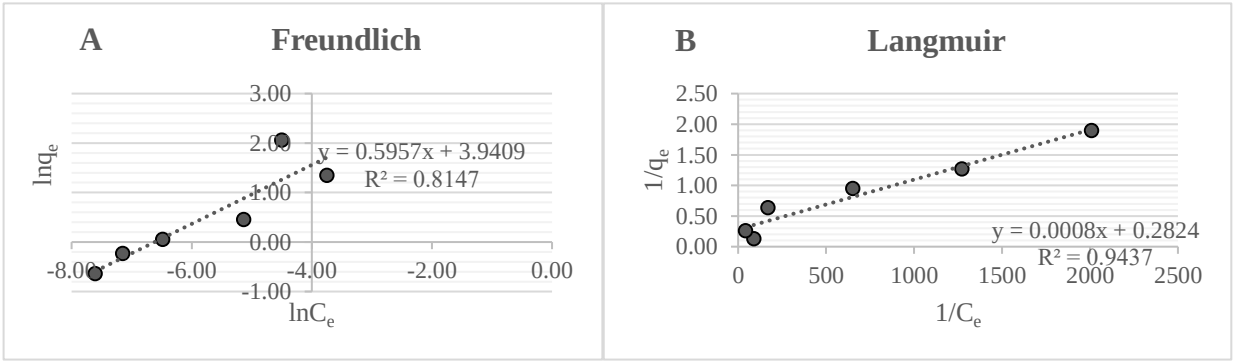


Figure 5.20. Isotherms showing the adsorption of chlorpyrifos onto ground GAC in a pesticide mixture: (A) Freundlich, (B) Langmuir.

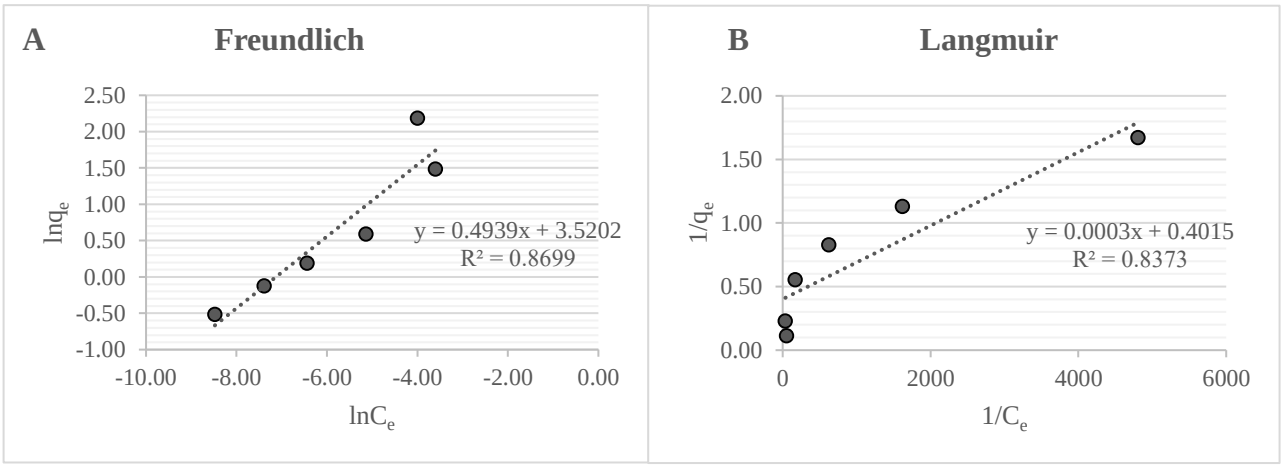


Figure 5.21. Isotherms showing the adsorption of cyprodinil onto ground GAC in a pesticide mixture: (A) Freundlich, (B) Langmuir.

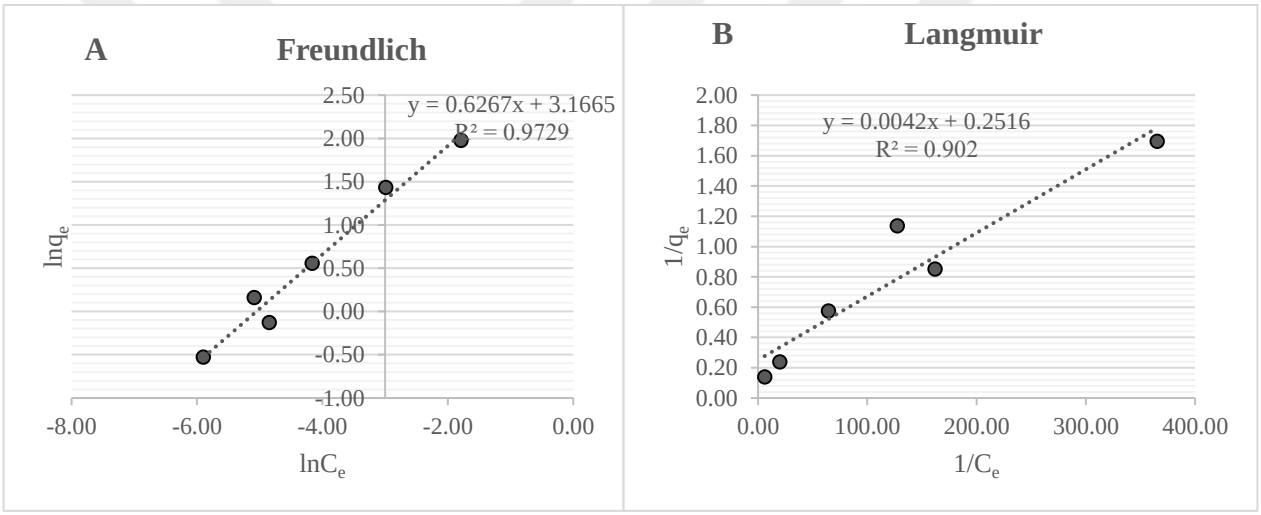


Figure 5.22. Isotherms showing the adsorption of malathion onto ground GAC in a pesticide mixture: (A) Freundlich, (B) Langmuir.

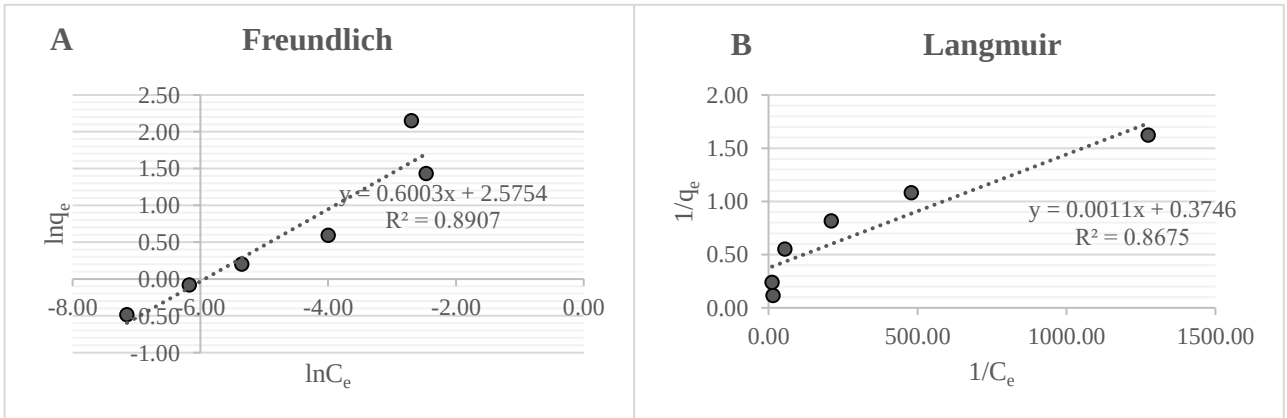


Figure 5.23. Isotherms showing the adsorption of propanil onto ground GAC in a pesticide mixture: (A) Freundlich, (B) Langmuir.

When comparing the isotherm parameters of pesticides in mono- and multicomponent experiments, it was observed that the adsorption capacity of ground GAC for all pesticides decreased when the tested pesticides were present together rather than separately (as seen in Table 5.7 and Table 5.9).

This decrease is evidenced by the reduction in K_f and q_{max} values for all pesticides when they were adsorbed from a mixed solution compared to their individual adsorption. It has been observed in the literature that the adsorption capacity of activated carbon for pesticides is lower when pesticides are in the same solution than when they are alone (Faur et al., 2005). This observation suggests competition between different pesticide molecules for adsorption sites on the GAC surface, resulting in a lower overall adsorption capacity for each pesticide in a mixture than in single-solute conditions.

Despite the overall decrease in adsorption capacity, the relative adsorption capabilities of the pesticides remained consistent whether they were present individually or in a mixture. The K_f values indicated that CPF and CYP demonstrated superior adsorption capabilities than other pesticides. Conversely, CBF and MLT exhibited relatively weaker adsorption among the pesticides examined.

When comparing the Freundlich equilibrium constants (1/n), which are inversely proportional to adsorption intensity, we observe lower 1/n values for pesticides in the mixture compared to single pesticide experiments. This decrease indicates higher adsorption intensity in the mix, which may be attributed to pH differences. The pH of the pesticide mixture is higher than that of individual pesticide experiments, approaching the pH_{pzc} of the studied GAC (7.6). At this pH_{pzc}, the GAC surface is predominantly neutral, whereas it becomes negatively charged above pH_{pzc} and positively charged below it (Bernal et al., 2017). While single pesticide solutions have pH values below 7.6, the pesticide mixture solution is close to 7.6. According to PPDB, the studied pesticides remain neutral without dissociation (as seen in Table 5.1). Consequently, the neutral GAC surface interacts more strongly with the pesticides, leading to increased adsorption intensity and decreased 1/n values.

Table 5.9. Isotherm parameters describing the sorption of a pesticide from a pesticide mixture onto ground GAC.

Isotherm	Parameters	Carbofuran (CBF)	Chlorpyrifos (CPF)	Cyprodinil (CYP)	Malathion (MLT)	Propanil (PRP)
Freundlich	1/n	1.01	0.59	0.49	0.60	0.49
	K_f (mg/g)(L/mg)$^{1/n}$	3.70	51.46	33.79	13.07	18.35
	R^2	0.78	0.81	0.87	0.97	0.89
Langmuir	q_{max} (mg/g)	1.90	3.54	3.49	2.85	2.97
	K_L (L/mg)	0.61	353.00	1338.33	51.66	340.55
	R^2	0.85	0.94	0.84	0.89	0.87

5.2.2.3. *Adsorption isotherms of pesticides in a multicomponent system (original (non-ground) GAC).* In this part of the study, the adsorption characteristics of the pesticide mixture on original, non-ground GAC were examined through an adsorption isotherm experiment. Adsorption isotherms of non-ground GAC doses from 50 to 1500 mg/L were established. Preliminary kinetic experiments demonstrated that a 120-hour period was sufficient to achieve equilibrium for all non-ground GAC doses. To determine qe and Ce, samples were taken at the beginning of the experiment and again after a 120-hour period.

The isotherm graphs for each pesticide under investigation are presented in Figures 5.24 to 5.28. Based on these analyses, the parameters for both adsorption models were determined for each pesticide separately and summarized in Table 5.10.

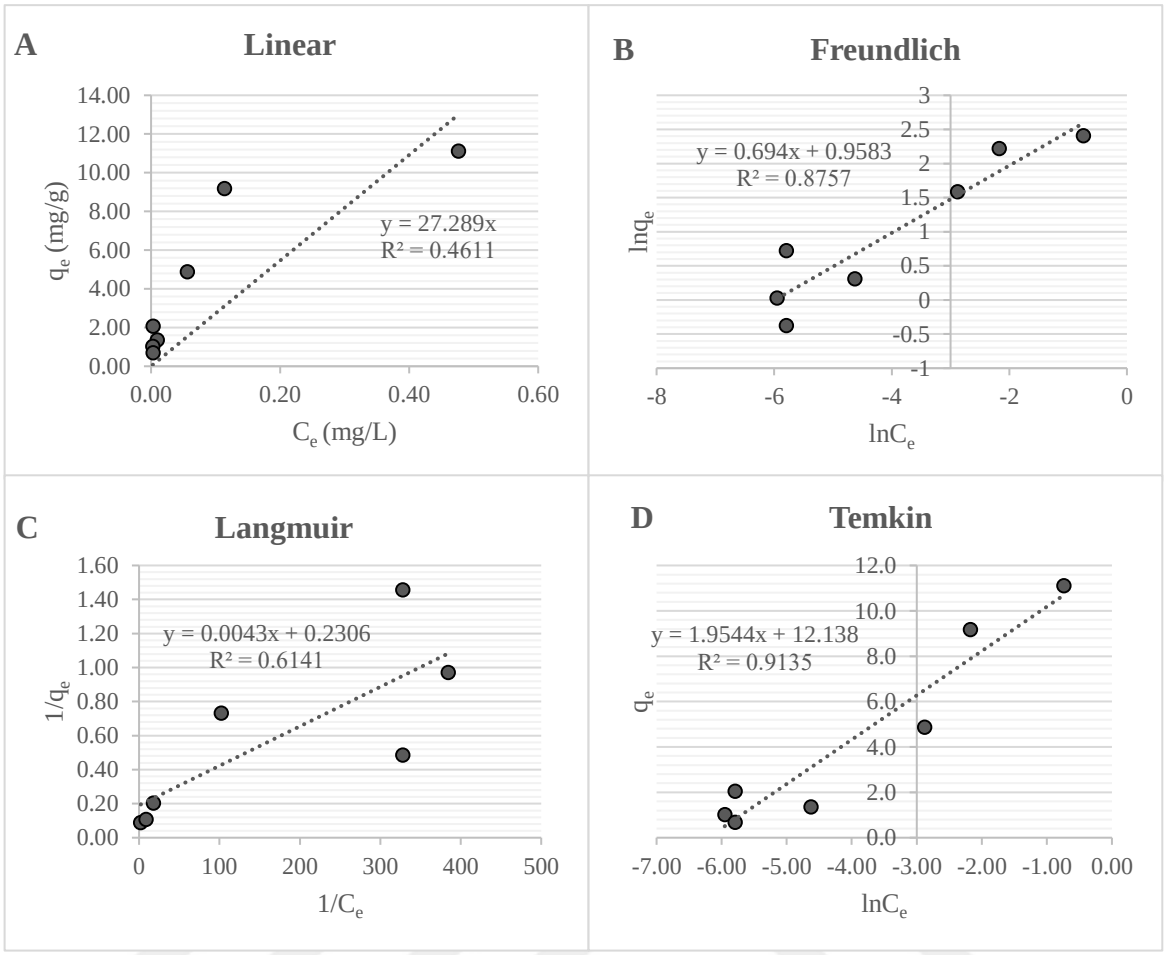


Figure 5.24. Isotherms showing the adsorption of carbofuran onto non-ground GAC in a pesticide mixture: (A) Linear, (B) Freundlich, (C) Langmuir, (D) Temkin.

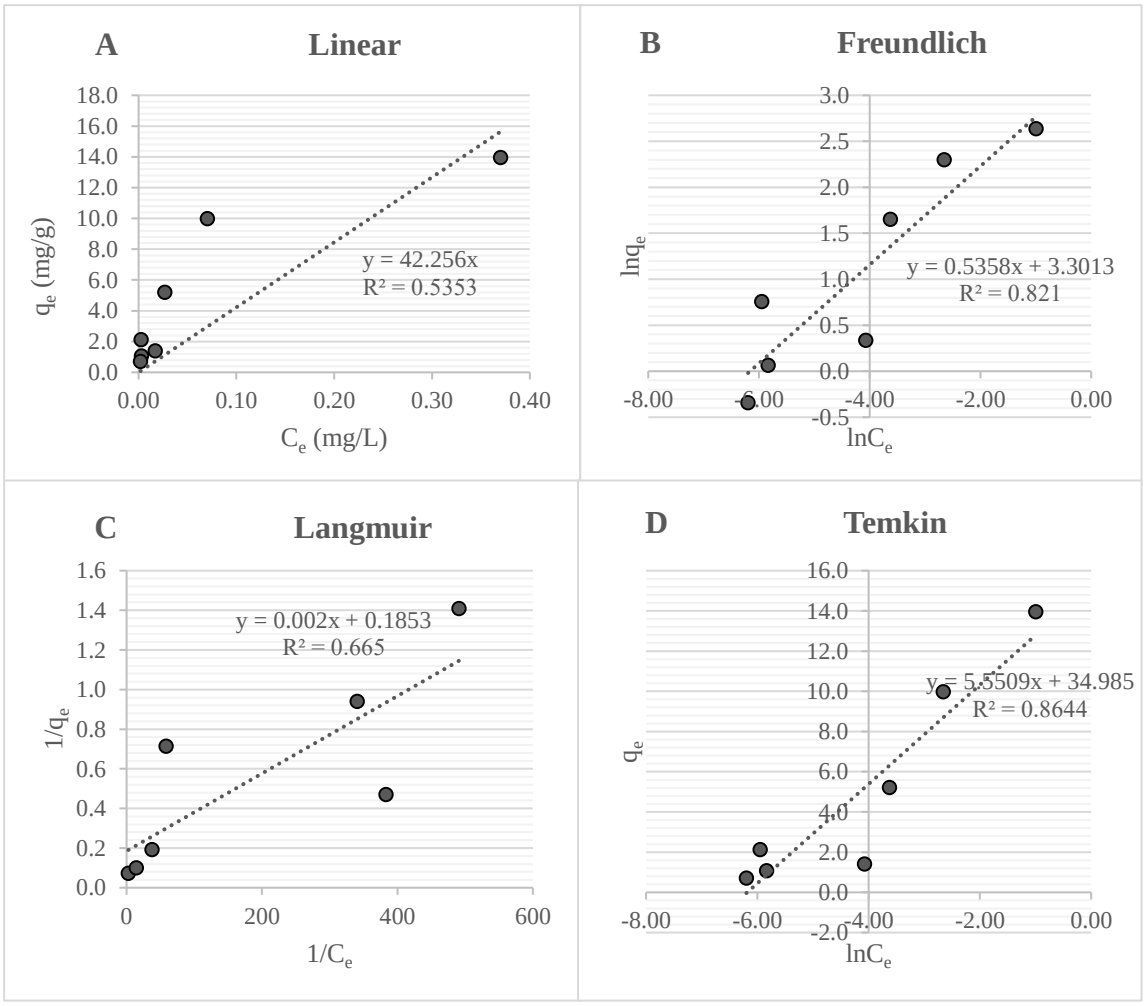


Figure 5.25. Isotherms showing the adsorption of chlorpyrifos onto non-ground GAC in a pesticide mixture: (A) Linear, (B) Freundlich, (C) Langmuir, (D) Temkin.

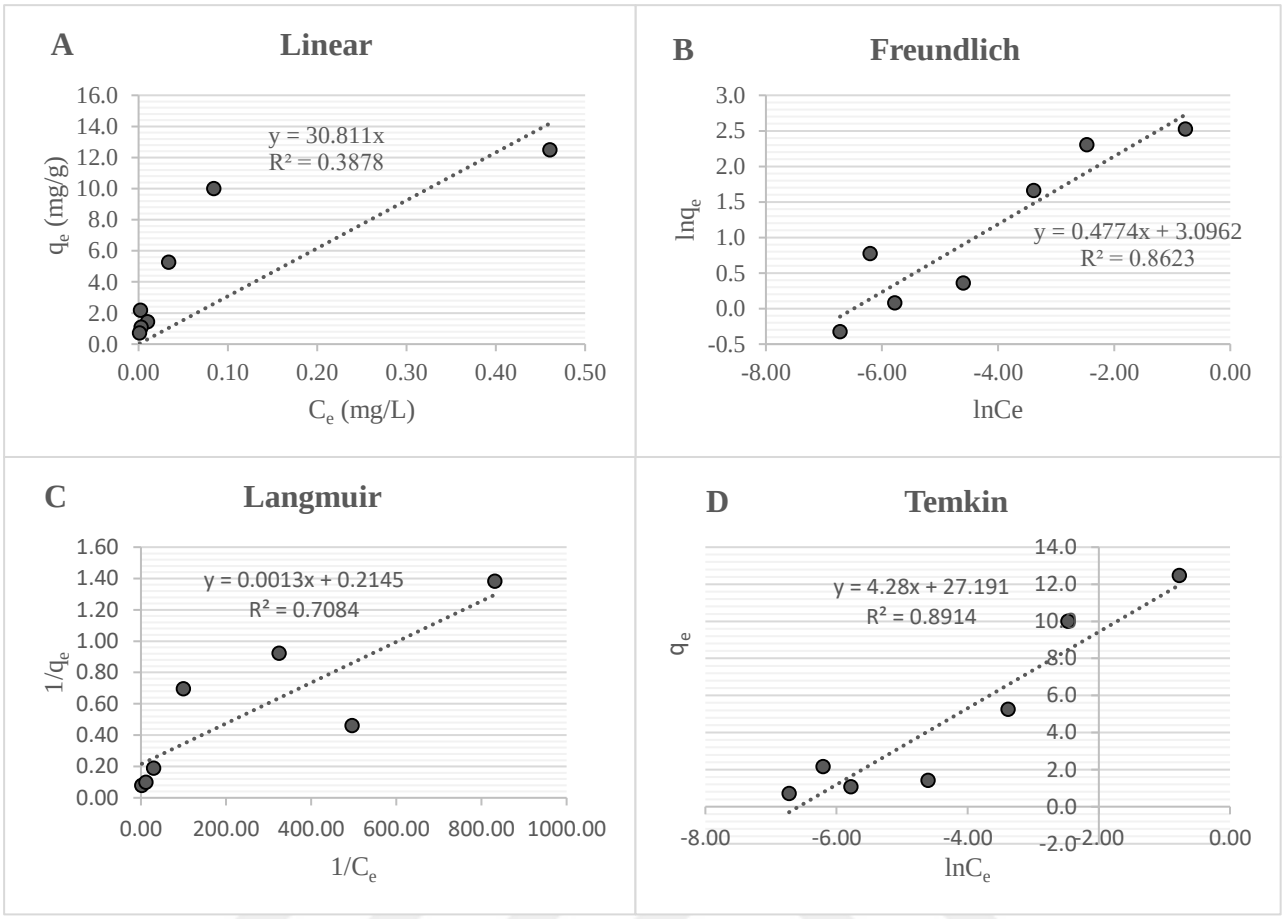


Figure 5.26. Isotherms showing the adsorption of cyprodinil onto non-ground GAC in a pesticide mixture: (A) Linear, (B) Freundlich, (C) Langmuir, (D) Temkin.

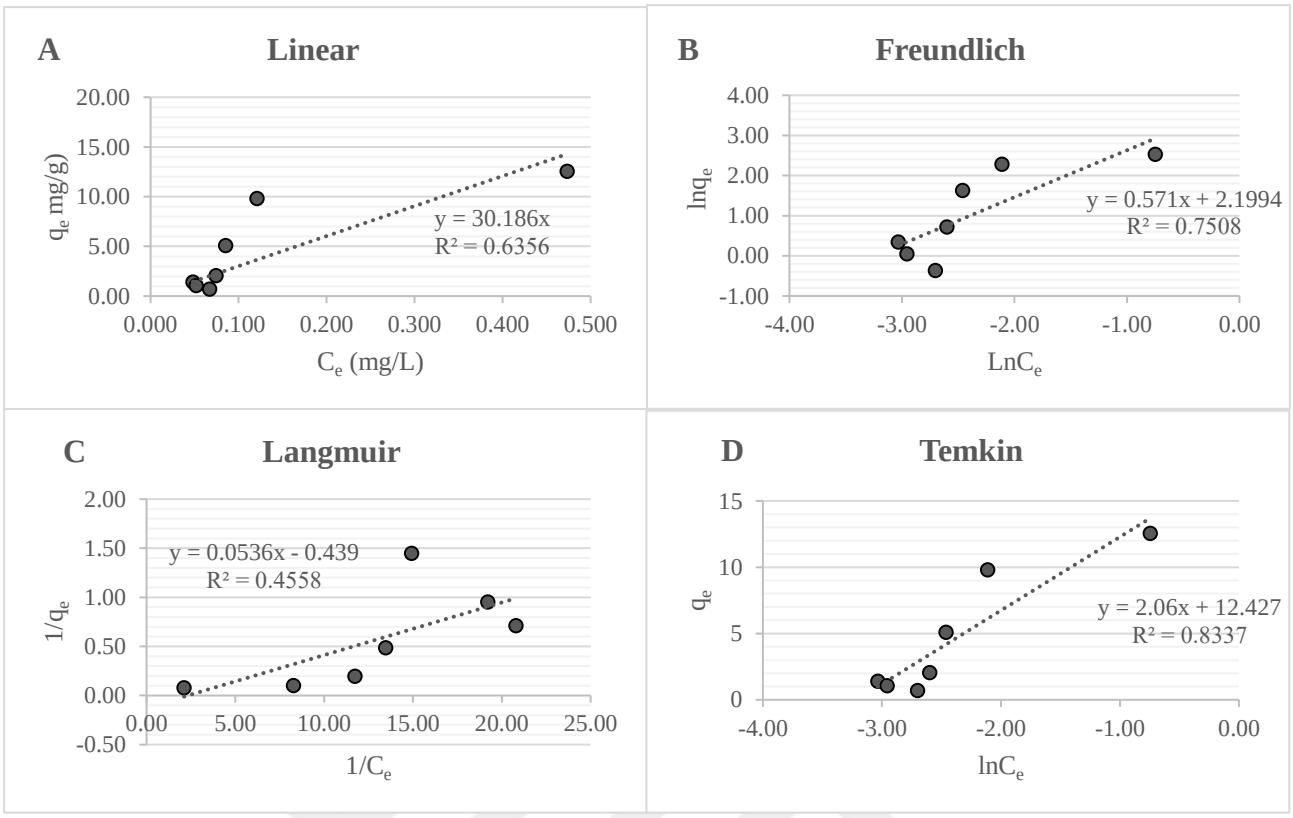


Figure 5.27. Isotherms showing the adsorption of malathion onto non-ground GAC in a pesticide mixture: (A) Linear, (B) Freundlich, (C) Langmuir, (D) Temkin.

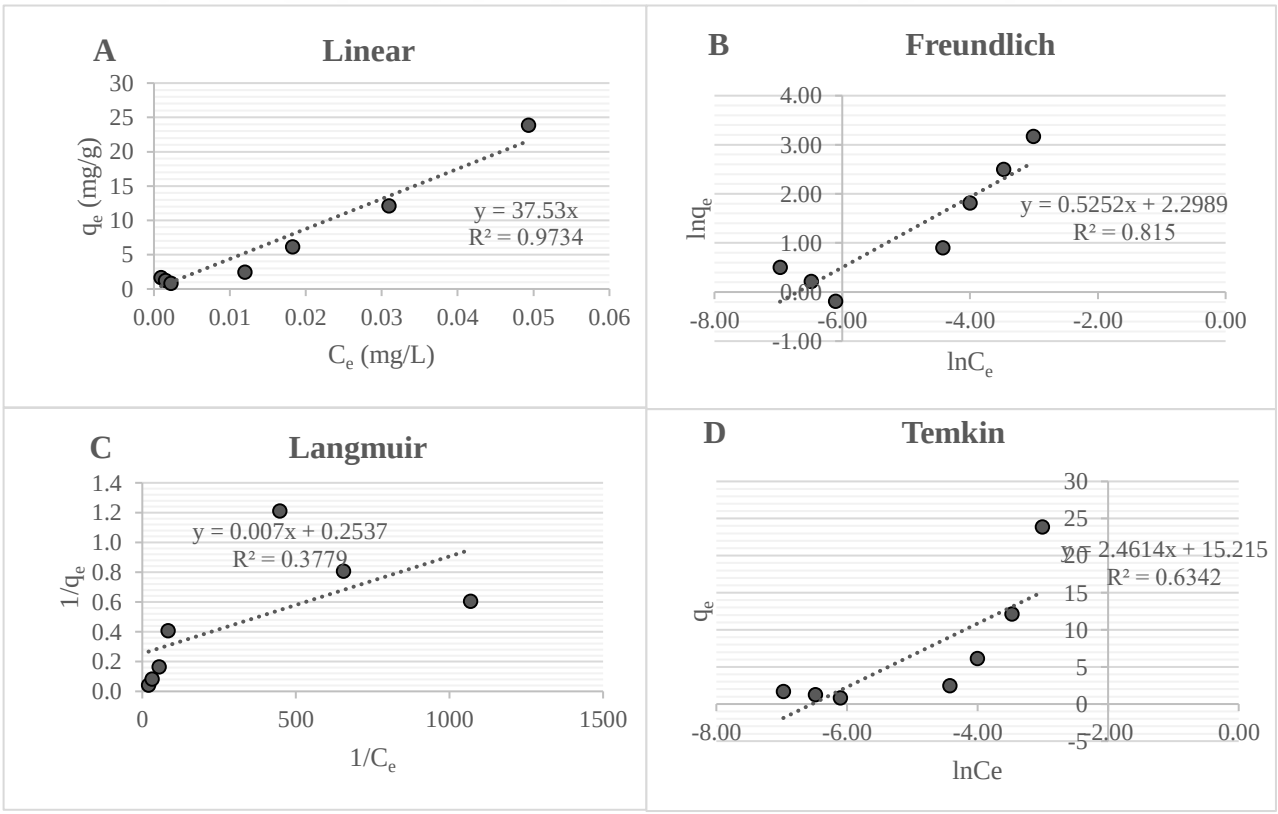


Figure 5.28. Isotherms showing the adsorption of propanil onto non-ground GAC in a pesticide mixture: (A) Linear, (B) Freundlich, (C) Langmuir, (D) Temkin.

According to these isotherm experiments, the Temkin isotherm showed a better fit, unlike in pesticides with ground GAC experiments. The Freundlich isotherm model was found to be the second model that showed a relatively better fit to the observed data, after the Temkin isotherm, based on the resulting R^2 values.

Smaller particles provide a larger surface area and more accessible micropores, creating a more heterogeneous surface for micropollutants (Lee et al., 2023). The Freundlich model describes this heterogeneity well (Halsey, 1948). The Freundlich model effectively captures this heterogeneity, as it accounts for variations in adsorption energies across multiple active sites (Halsey, 1948). The dominance of the Freundlich isotherm for ground GAC indicates that adsorption is primarily influenced by surface heterogeneity and multilayer formation across diverse energy sites.

In contrast, larger particles exhibit reduced heterogeneity in surface energy, leading to a more uniform distribution of adsorption energies (Yang, 1993). These particles often have more flat, accessible surfaces, which increase lateral interactions between adsorbed molecules (Yang, 1993). The dominance of the Temkin isotherm for pesticide mixture and non-ground GAC suggests that adsorption is more influenced by uniform surface energies rather than heterogeneous adsorption sites.

The particle size of non-ground GAC is about a hundred times larger (1 mm) than ground GAC (100 μm). Literature indicates that as carbon particle size decreases, the material's adsorption capacity and equilibrium retention ability increase (Matsui et al., 2015; Musthofa et al., 2023). Our experimental results support this finding, demonstrating higher pesticide removal percentages and greater K_f values when using ground GAC compared to non-ground GAC (as seen in Table 5.9 and Table 5.10).

The findings revealed that regardless of whether the GAC was in ground or non-ground form, the comparative adsorption patterns of different pesticides remained consistent. Analysis of the Freundlich constants showed that CPF and CYP achieved the highest adsorption levels among the studied pesticides. In contrast, CBF and MLT showed the lowest adsorption effectiveness.

Table 5.10. Isotherm parameters describing the sorption of a pesticide from a pesticide mixture onto non-ground GAC.

Isotherm	Parameters	Carbofuran (CBF)	Chlorpyrifos (CPF)	Cyprodinil (CYP)	Malathion (MLT)	Propanil (PRP)
Freundlich	1/n	0.69	0.54	0.47	0.57	0.52
	K_f (mg/g)(L/mg)$^{1/n}$	2.61	27.11	21.98	8.94	9.87
	R^2	0.88	0.82	0.86	0.75	0.81
Temkin	b_T (J/mol)	1267.38	446.23	578.54	1202.41	1003.88
	K_T (L/g)	498.00	688.20	719.21	424.86	484.26
	R^2	0.91	0.86	0.89	0.83	0.63

5.2.2.4. *Adsorption isotherms in the case of background nom (ground GAC).* In this part of the study, an adsorption isotherm was conducted to investigate the adsorption behavior of background NOM. The synthetic Ömerli water, resembling the water taken from the Ömerli Dam (explained in detail in Section 4.5.), served as the source of background natural organic matter. Adsorption isotherms were established using ground GAC doses from 50 to 1500 mg/L. Preliminary kinetic experiments demonstrated that a 24-hour period was sufficient to achieve equilibrium for all ground GAC doses. To determine qe and Ce, samples were taken at the beginning of the experiment and again after a 24-hour period.

Absorbance measurements were also taken to investigate potential variations in NOM adsorption behavior based on the presence of different chromophores. Two isotherms, Freundlich and the Langmuir, showing a relatively better fit for DOC and absorbance at specific wavelengths, are presented in Figures 5.29 to 5.31. Based on these analyses, the parameters for both adsorption models were determined and summarized in Table 5.11. Table 5.16

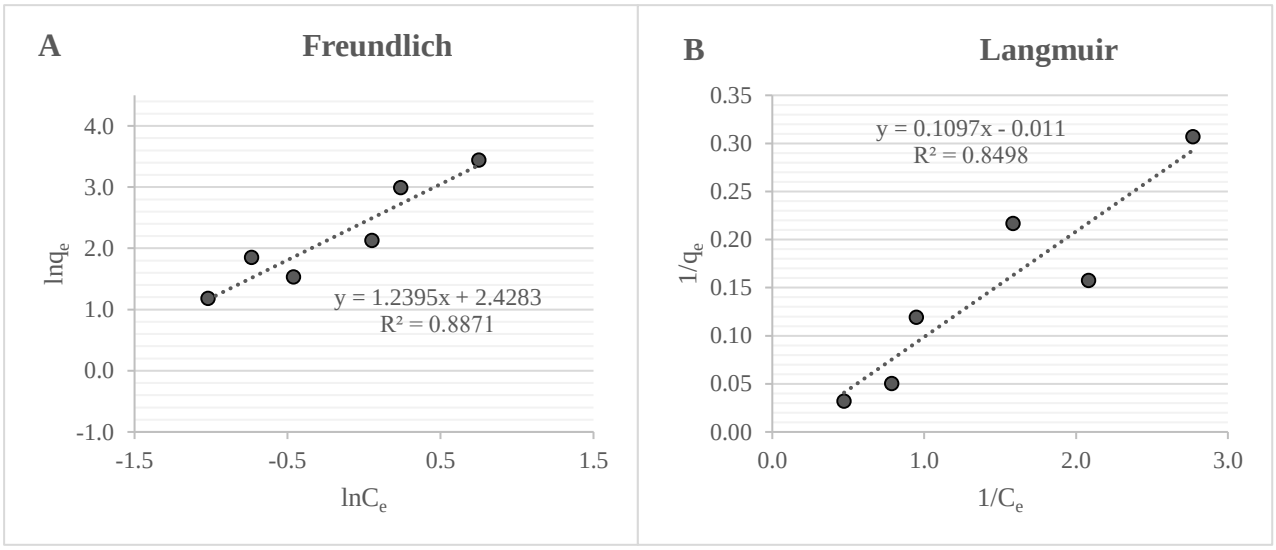


Figure 5.29. Adsorption isotherms of background NOM onto ground GAC: (A) Freundlich, (B) Langmuir (In terms of DOC).

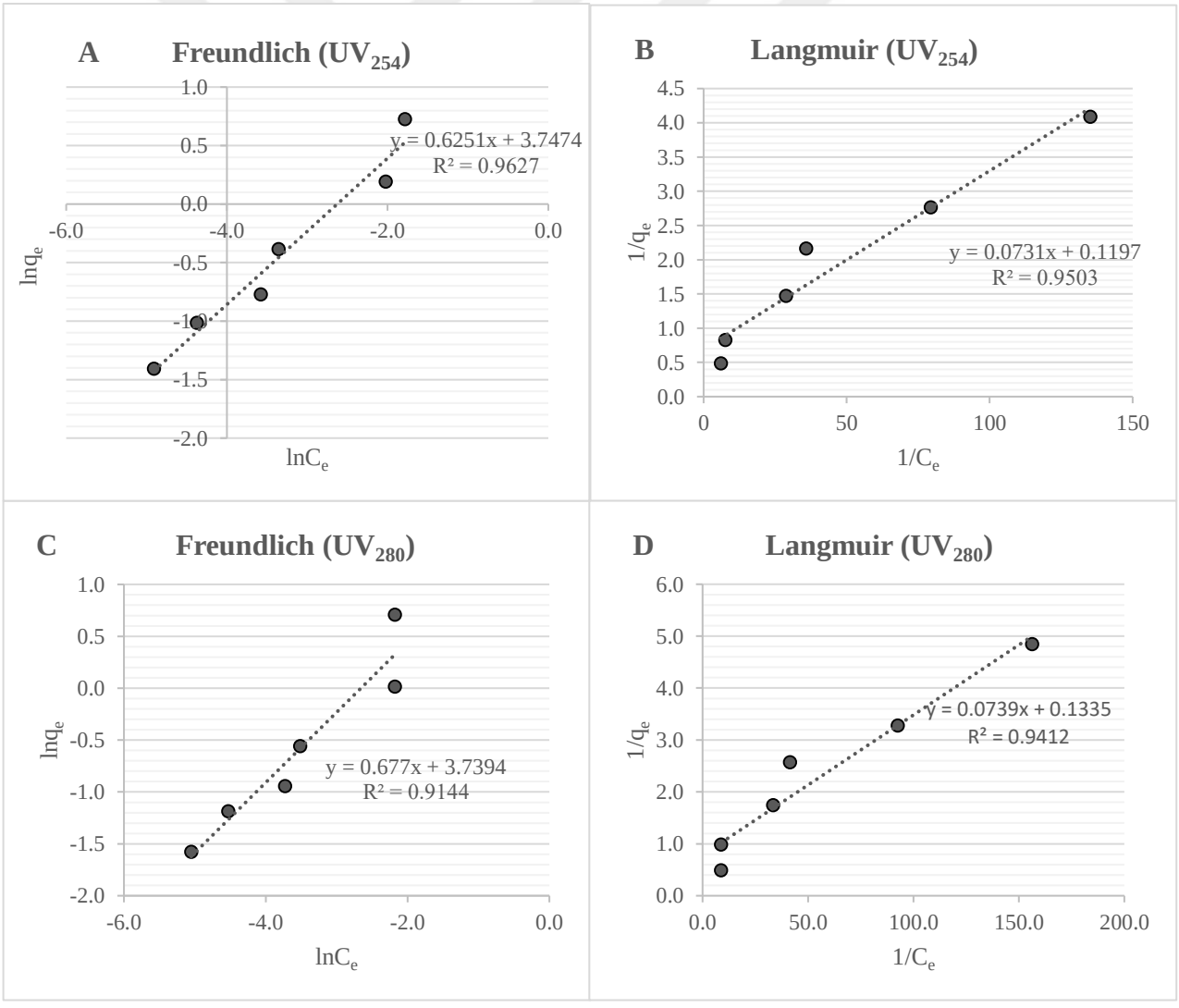


Figure 5.30. Adsorption isotherms of background NOM onto ground GAC: (A) Freundlich, (B) Langmuir (In terms of UV absorbance).

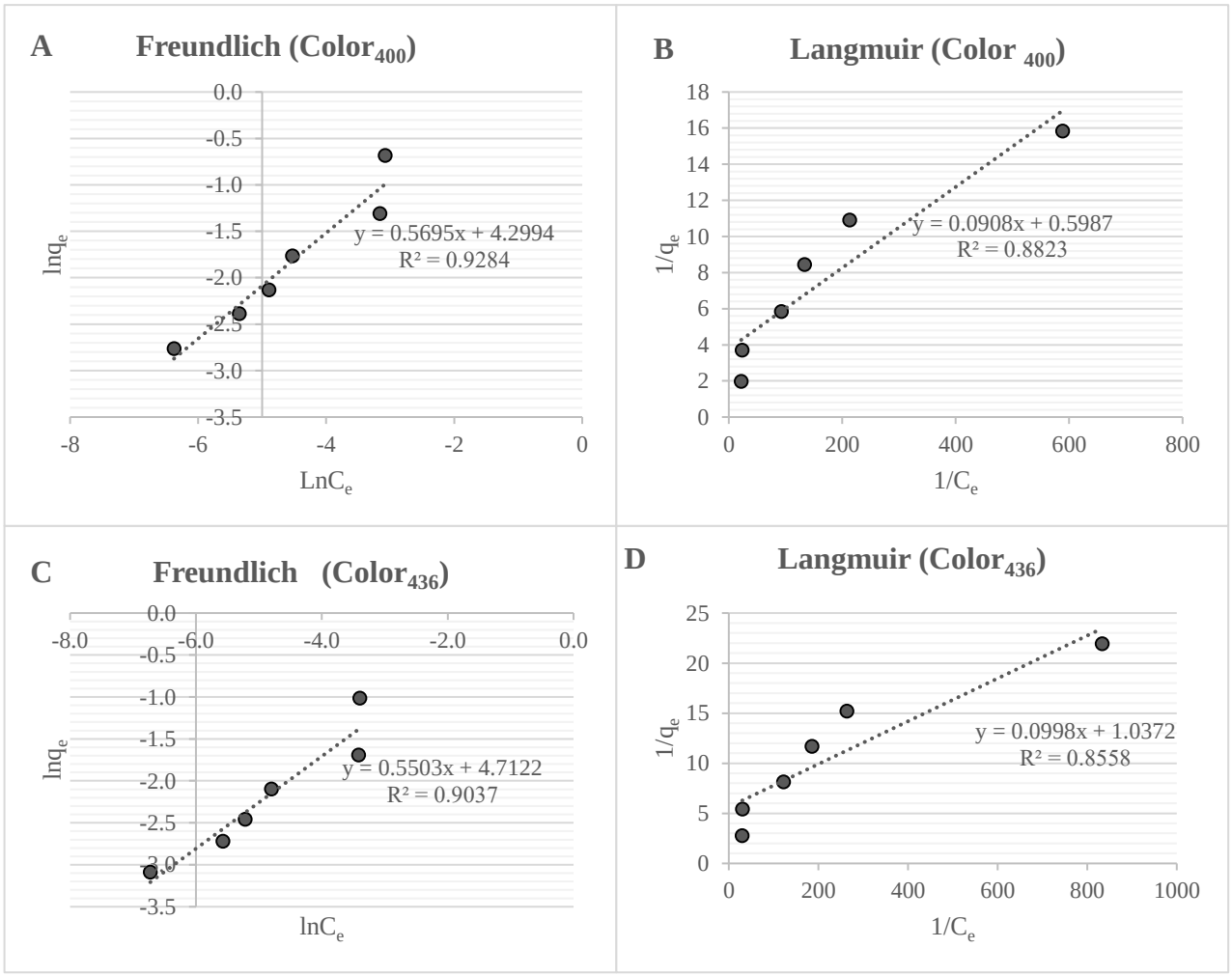


Figure 5.31. Adsorption isotherms of background NOM onto ground GAC: (A) Freundlich, (B) Langmuir (In terms of color absorbance).

According to the results, removal efficiencies of background NOM by ground GAC were between 50% and 98% for different GAC doses. The removal efficiency for UV and color-absorbing moieties was slightly higher than total DOC removal.

The analysis of the coefficients of determination, R^2, for various isotherm models indicated that the Freundlich model provides a better fit to NOM behavior onto ground GAC. The Freundlich isotherm parameters obtained from DOC measurements revealed values of 1.2 and 11.24 (mg DOC/g)(L/mg DOC)$^{1/n}$ for 1/n and K_f, respectively. In a comparative study, researchers investigated the adsorption behavior of NOM onto two distinct types of GACs (Iriarte-Velasco et al., 2008). Their findings demonstrated varying adsorption characteristics, with 1/n values of 0.42 and 1.59, and corresponding K_f values of 1.67 and 5.85 (mg DOC/g)(L/mg DOC)$^{1/n}$. Another study investigated the adsorption parameters of humic acid by GAC (Yang & Fox, 2018). This study is more relevant to our results since humic acid is the only organic carbon source in our synthetic drinking water recipe (as

explained in Section 4.5. Their study indicated values of 0.92 and 0.131 (mg DOC/g)(L/mg DOC)$^{1/n}$ for 1/n and K_f, respectively (Yang & Fox, 2018). They also investigated Langmuir parameters, reporting values of 16.66 mg DOC/g and 0.004 L/mg DOC for q_{max} and K_L, respectively (Yang & Fox, 2018). These differences in isotherm parameters suggest that the adsorption mechanisms and capacities vary significantly between different types of GACs.

The Freundlich isotherms parameters differ significantly for DOC and absorbance measurements (as seen in Table 5.11). Specifically, the Freundlich isotherm for DOC showed a steeper slope with a higher 1/n value than the absorbance measurements, indicating a lower adsorption intensity. This observation aligns with literature (Iriarte-Velasco et al., 2008). While DOC measurements capture the entire range of organic matter fractions, absorbance measurements selectively detect specific components of organic matter present in background NOM. The differences observed between DOC and absorbance measurements can be attributed to the complex nature of humic acid. Humic acid consists of various molecular weight fractions and functional groups, some of which may have limited or no affinity for adsorption onto the surface of GAC. This heterogeneity in molecular composition directly influences overall adsorption behavior and accounts for the variations in the parameters.

The Freundlich equilibrium constant (1/n) values of 0.63 and 0.68, along with their corresponding K_f values of 5.17 and 6.04 (1/g cm)(cm)$^{1/n}$, were calculated using UV spectroscopy at wavelengths of 254 nm and 280 nm, respectively. Additionally, 1/n values of 0.6 and 0.55, with their corresponding K_f values of 2.14 and 1.64 (1/g cm)(cm)$^{1/n}$, were obtained through color spectroscopy at 400 nm and 436 nm, respectively.

Generally, aromatic chromophores in NOM are associated with absorbance at 254 nm and 280 nm, while the color forming components in humic acid primarily absorb at 400 nm and 436 nm wavelengths (Dorota H, 2018; Korshin et al., 2009). The Freundlich equilibrium coefficient (K_f) analyses derived from UV and color absorbance measurements revealed that the K_f expressed by UV absorbance were slightly higher than those related to color absorbance. This observation suggests that the aromatic components within the NOM exhibited a greater tendency to adsorb onto ground GAC compared to the components responsible for color formation. The enhanced adsorption behavior of UV absorbing moieties is also supported by previous literature findings (Ando et al., 2011). The higher adsorption affinity of aromatic components can be attributed to their molecular structure and electronic properties. Aromatic rings in NOM molecules facilitate stronger π-π interactions with the activated carbon surface, leading to enhanced adsorption compared to aliphatic or color forming moieties.

Table 5.11. Isotherm parameters of the isotherm models describing the sorption of background NOM onto ground GAC (in terms of mg DOC/L and absorbance measurements).

Isotherm	Parameters	DOC	UV_{254}	UV_{280}	$Color_{400}$	$Color_{436}$
Freundlich	1/n	1.24	0.63	0.68	0.6	0.55
	K_f (mg DOC/g)(L/mg DOC)$^{1/n}$ or (1/g cm)(cm)$^{1/n}$	11.34	42.41	42.07	73.66	111.30
	R^2	89.00	0.96	0.92	0.88	0.90
Langmuir	q_{max} (mg DOC/g) or (1/g cm)	90.91	8.35	7.49	1.67	0.96
	K_L (L/mg DOC) or (cm)	0.10	1.64	1.81	6.57	10.39
	R^2	0.85	0.95	0.84	0.88	0.86

5.2.2.5. *Adsorption isotherms in the case of background nom (original (non-ground) GAC).* In this part of the study, the adsorption characteristics of background NOM onto original, non-ground GAC were examined through an adsorption isotherm experiment. Adsorption isotherms were established using non-ground GAC doses from 50 to 1500 mg/L. Preliminary kinetic experiments demonstrated that a 174-hour period was sufficient to achieve equilibrium for all non-ground GAC doses. To determine qe and Ce, samples were taken at the beginning of the experiment and again after a 174-hour period.

Figures 5.32 to 5.34. present the Freundlich and the Langmuir isotherm graphs for DOC and absorbance at specific wavelengths. Based on these analyses, the parameters for both adsorption models were determined and summarized in Table 5.12.

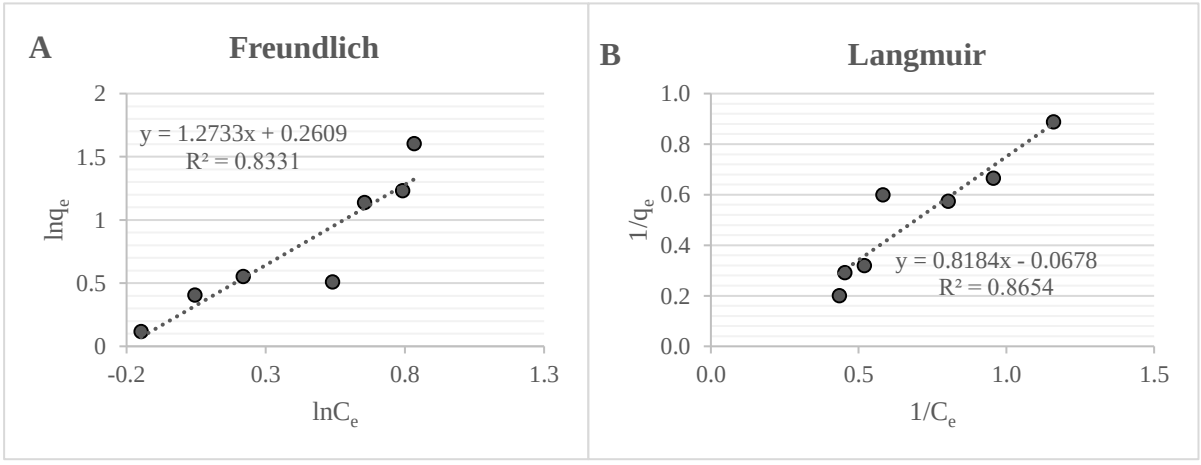


Figure 5.32. Adsorption isotherms of background NOM onto non-ground GAC: (A) Freundlich, (B) Langmuir (In terms of DOC).

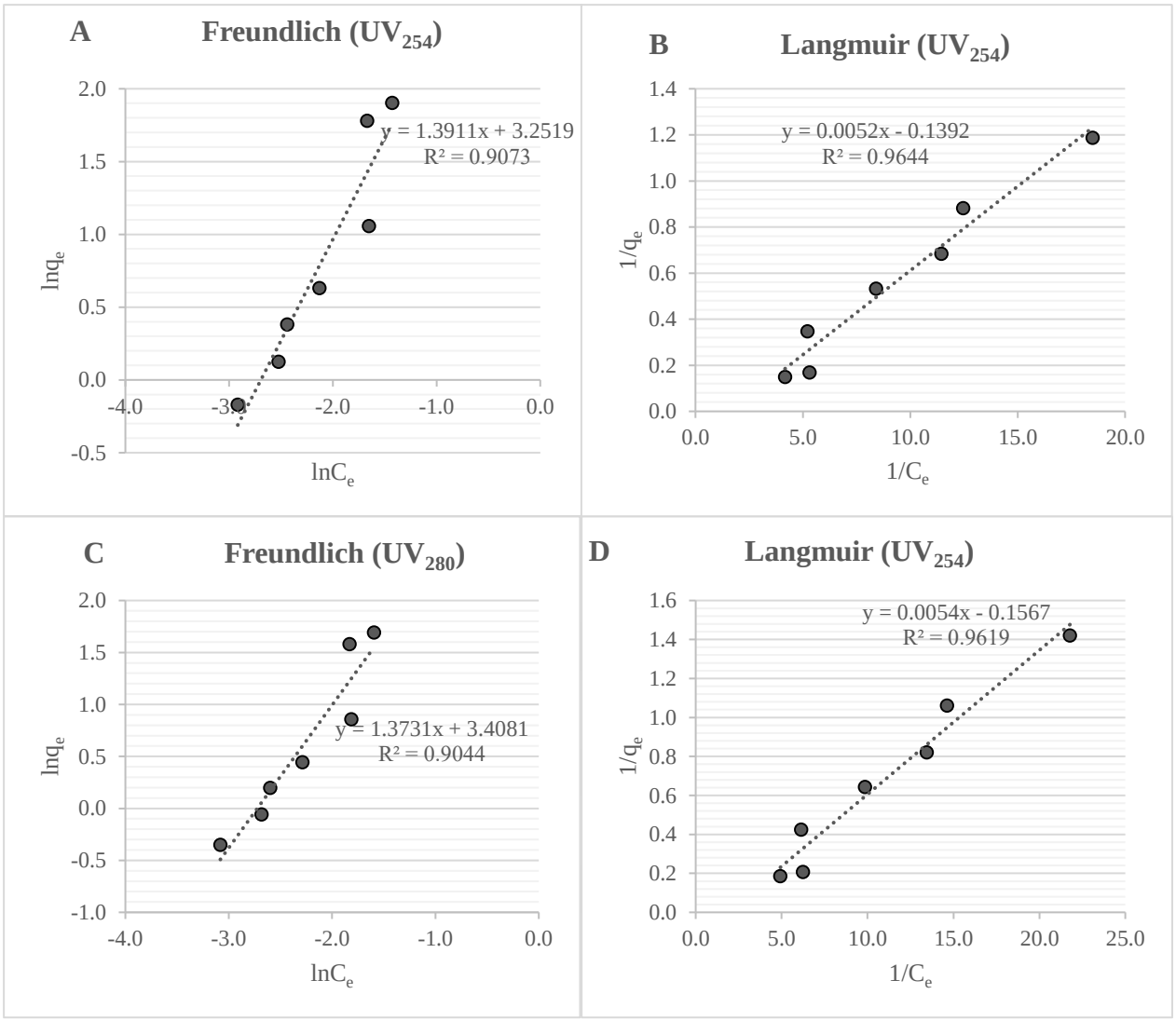


Figure 5.33. Adsorption isotherms of background NOM onto non-ground GAC: (A) Freundlich, (B) Langmuir (In terms of UV absorbance).

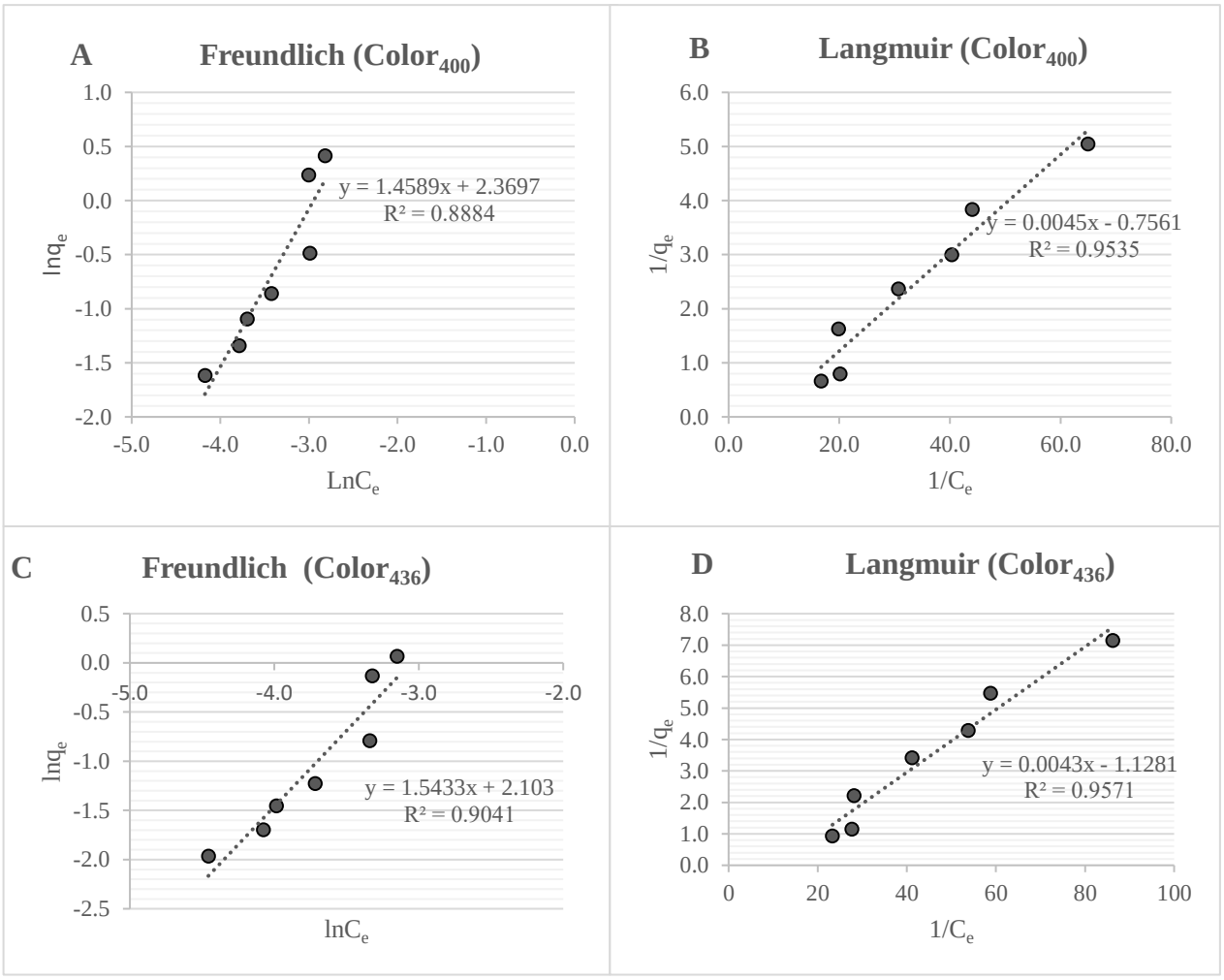


Figure 5.34. Adsorption isotherms of background NOM onto non-ground GAC: (A) Freundlich, (B) Langmuir (In terms of color absorbance).

Analysis of the coefficients of determination (R^2) for various isotherm models revealed different results based on the size of the GAC used. For the adsorption of NOM by non-ground GAC particles, the Langmuir model demonstrated the better fit to the experimental data (Table 5.12). In contrast, for NOM adsorbed by ground GAC particles, the Freundlich isotherm model provided a superior fit to the observed results (Table 5.11).

When we analyze the effect of GAC size on adsorption, similar to the pesticide adsorption results, the removal of background NOM is more significant with higher K_f and q_{max} values when using ground GAC compared to non-ground GAC. In other words, the ground GAC demonstrated a higher adsorption capacity for NOM adsorption than its non-ground counterpart, as indicated by the variations in their respective Freundlich and Langmuir isotherm parameters (as seen in Table 5.11 and Table 5.12). Another research finding also suggested that the adsorption capacity for large

molecular weight substances increased as the size of activated carbon particles decreased (Ando et al., 2011; Pan et al., 2017).

The findings also revealed that regardless of whether the GAC was in ground or non-ground from, the comparative adsorption patterns of UV and color-absorbing moieties in NOM were the same. Comparison of the Freundlich and Langmuir constants showed that the UV-absorbing fraction in NOM achieved higher adsorption levels than its color-absorbing counterparts (as seen in Table 5.11 and Table 5.12).

Table 5.12. Isotherm parameters describing the sorption of background NOM onto non-ground GAC (in terms of mg DOC/L and absorbance measurements).

Isotherm	Parameters	DOC	UV_{254}	UV_{280}	$Color_{400}$	$Color_{436}$
Freundlich	1/n	1.27	1.39	1.37	1.46	1.54
	K_f (mg DOC/g)(L/mg DOC)$^{1/n}$ or (1/g cm)(cm)$^{1/n}$	1.30	25.84	30.21	10.69	8.18
	R^2	83.00	0.91	0.90	0.89	0.90
Langmuir	q_{max} (mg DOC/g) or (1/g cm)	14.75	1.45	1.28	0.26	0.18
	K_L (L/mg DOC) or (cm)	0.08	26.58	29.01	168.76	263.58
	R^2	0.86	0.96	0.96	0.95	0.96

The results of the background NOM adsorption were compared with existing literature and shown in Table 5.13. Using ground Norit GAC 1240AF as our adsorbent material, we observed several advantages compared to previous studies. Our ground GAC demonstrated higher adsorption capacity with higher K_f and q_{max} values than its non-ground counterpart and all other tested adsorbents reported in the literature. The improved performance can be attributed to properties of selected GAC and the increased surface area and accessibility of adsorption sites achieved through grinding.

Table 5.13. Comparative analysis of background NOM adsorption: literature values and own experimental results.

Adsorbate	Adsorbent	1/n	K_f (mg TOC/g)(L/mg TOC)$^{1/n}$	q_{max} (mg TOC/g)	K_L (L/mg TOC)	Reference
NOM	GAC-A	0.42	1.67	1.17	0.53	(Iriarte-Velasco et al., 2008)
NOM	GAC-F	1.59	5.85	7.34	0.27	(Iriarte-Velasco et al., 2008)
Humic Acid	GAC 1230C	0.92	0.13	16.66	0.004	(Yang & Fox, 2018)
Humic Acid	PAC 1230C	0.90	0.08	20.83	0.004	(Yang & Fox, 2018)
Humic Acid	GAC 1240CAT	4.35	0.96	3.62	0.08	(Yang & Fox, 2018)
Humic Acid	PAC 1240CAT	1.11	11.22	8.47	0.007	(Yang & Fox, 2018)
Humic Acid	Acid-activated Greek bentonite	0.79	0.11	10.75	0.007	(Doulia et al., 2009)
Humic Acid	Ground Norit® GAC 1240AF	1.24	11.34	90.91	0.10	This study
Humic Acid	Non-ground Norit® GAC 1240AF	1.27	1.30	14.75	0.08	This study

5.2.2.6. *Adsorption isotherms in the case of background nom and a pesticide mixture (ground GAC).*
This section examines the competitive nature of adsorption between background NOM and pesticides onto GAC surfaces. Adsorption isotherms were established using non-ground GAC doses from 50 to 1500 mg/L.

Figures 5.35 to 5.38 illustrate the Freundlich, and the Langmuir isotherm graphs for each pesticide under investigation. Based on these analyses, the parameters for both adsorption models were determined for each pesticide and summarized in Table 5.14. To facilitate comparison with the isotherm experiment results obtained using background NOM, isotherm parameters for pesticide were also calculated in terms of DOC parameter and displayed in Table 5.15.

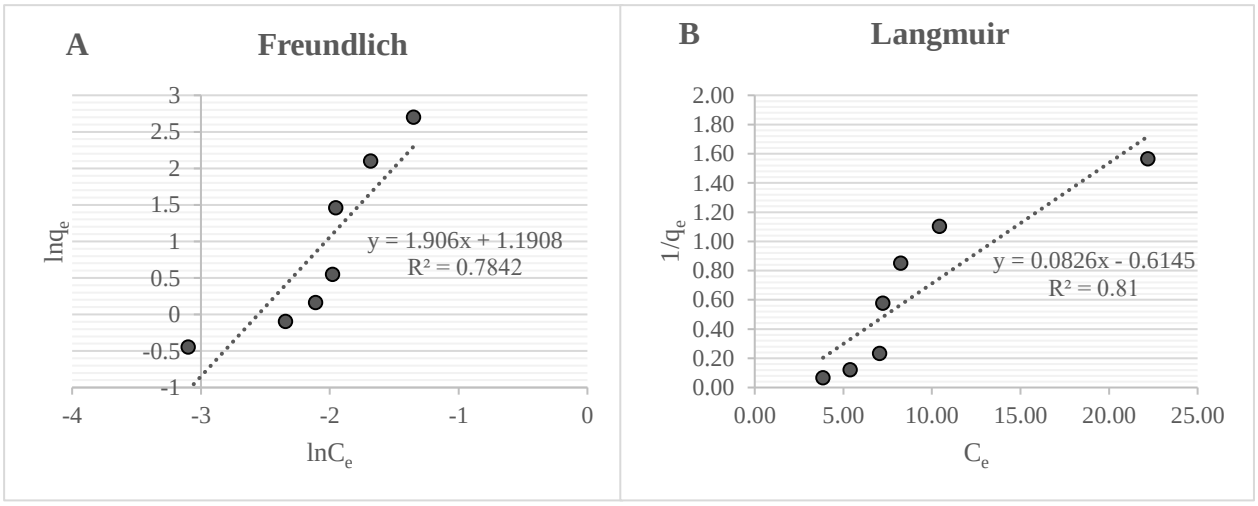


Figure 5.35. Isotherms showing the adsorption of carbofuran onto ground GAC in the case of background NOM and a pesticide mixture: (A) Freundlich, (B) Langmuir.

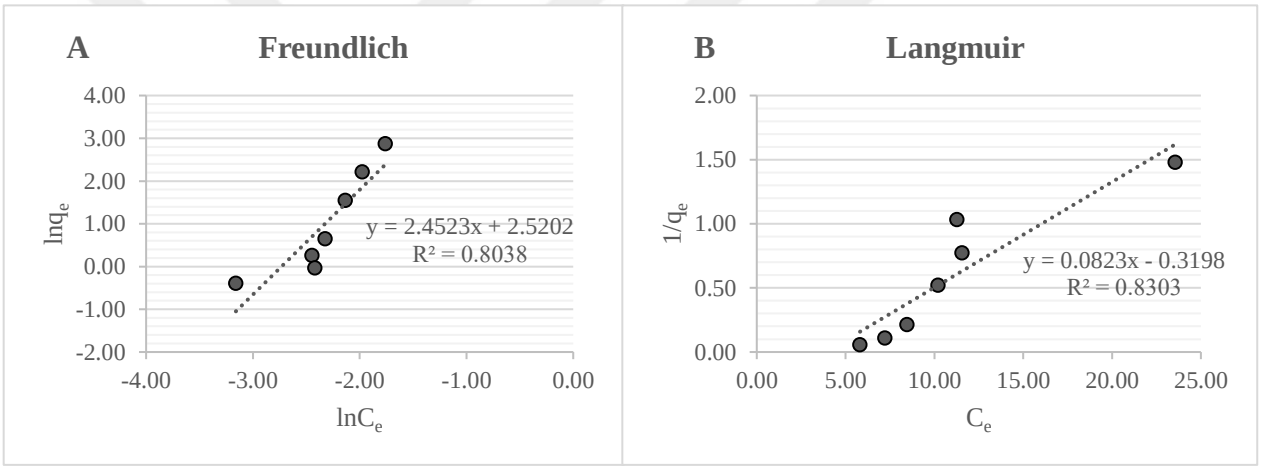


Figure 5.36. Isotherms showing the adsorption of cyprodinil onto ground GAC in the case of background NOM and a pesticide mixture: (A) Freundlich, (B) Langmuir.

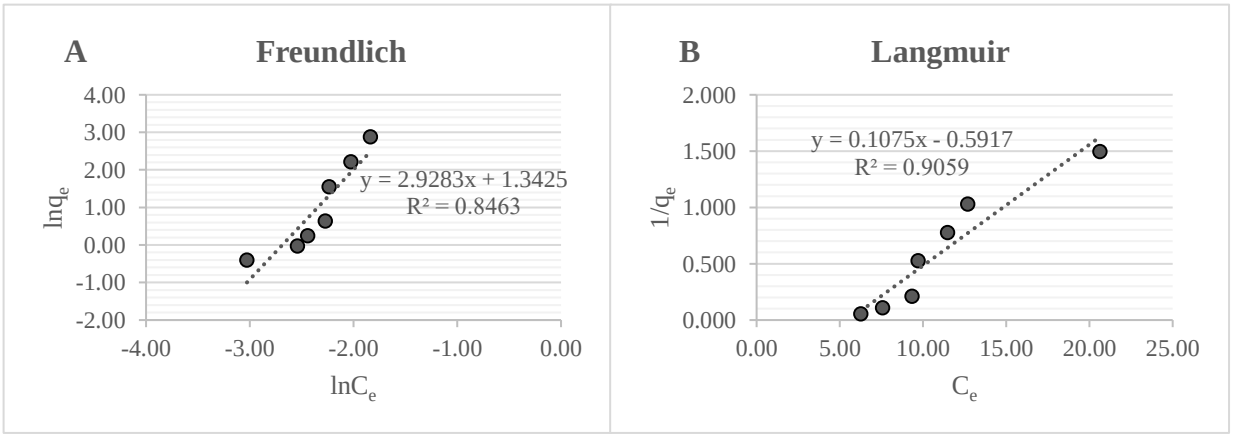


Figure 5.37. Isotherms showing the adsorption of malathion onto ground GAC in the case of background NOM and a pesticide mixture: (A) Freundlich, (B) Langmuir.

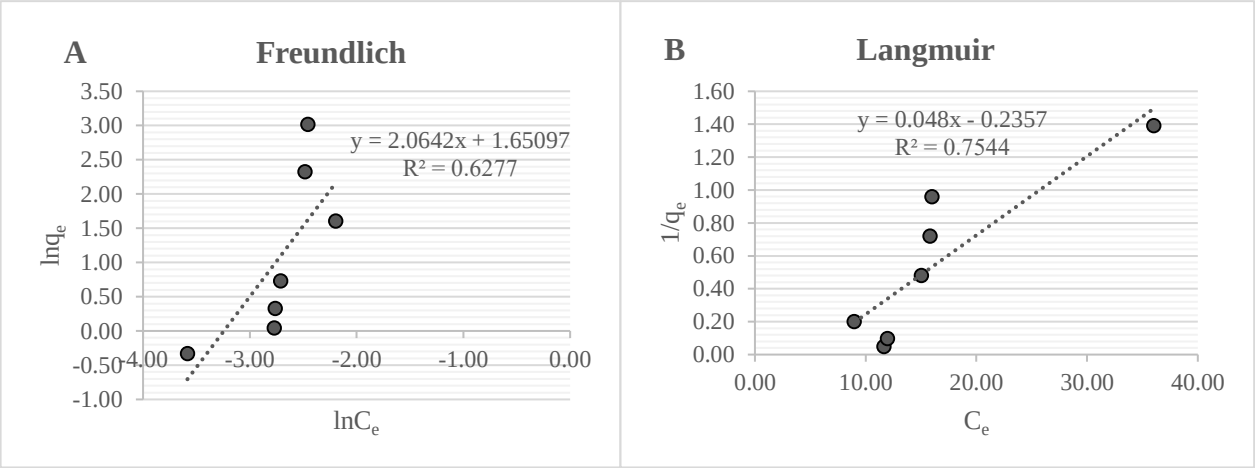


Figure 5.38. Isotherms showing the adsorption of propanil onto ground GAC in the case of background NOM and a pesticide mixture: (A) Freundlich, (B) Langmuir.

Table 5.14. Isotherm parameters describing the sorption of a pesticide from a mixture composed of background NOM and pesticides onto ground GAC.

Isotherm	Parameters	Carbofuran (CBF)	Cyprodinil (CYP)	Malathion (MLT)	Propanil (PRP)
Freundlich	1/n	1.90	2.45	2.92	2.06
	K_f (mg/g)(L/mg)$^{1/n}$	1.19	12.43	3.83	4.53
	R^2	0.78	0.80	0.85	0.62
Langmuir	q_{max} (mg/g)	1.63	3.13	1.60	4.24
	K_L (L/mg)	7.44	3.89	5.50	4.91
	R^2	0.81	0.83	0.91	0.75

Table 5.15. Isotherm parameters describing the sorption of a pesticide from a mixture composed of background NOM and pesticides onto ground GAC (pesticide concentrations were expressed in terms of DOC).

Isotherm	Parameters	Carbofuran (CBF)	Cyprodinil (CYP)	Malathion (MLT)	Propanil (PRP)
Freundlich	1/n	1.90	2.45	2.92	2.06
	K_f (mg DOC/g)(L/mg DOC)$^{1/n}$	9.19	36.34	9.12	24.86
	R^2	0.78	0.80	0.85	0.62
Langmuir	q_{max} (mg DOC/g)	1.24	2.56	1.78	5.76
	K_L (L/mg DOC)	1.13	14.73	14.84	8.95
	R^2	0.81	0.83	0.91	0.75

The analysis of Freundlich isotherm parameters revealed significant differences when pesticides were present alone (as seen in Table 5.10) and when they were in the presence of background NOM (as seen in Table 5.14). The presence of NOM in the solution substantially altered the adsorption characteristics of pesticides, as evidenced by changes in the isotherm parameters.

Notably, the 1/n values associated with pesticides increased, exceeding 1, suggesting a reduction in the adsorption strength of pesticides when NOM was present. Scientific studies indicate that competing solutes during adsorption can lead to higher 1/n values in adsorption isotherms (Attia et al., 2003; Wu et al., 2002). Additionally, the pesticides have higher K_f values when there is no background NOM, indicating that ground GAC has a reduced adsorption capacity towards pesticides in the presence of NOM.

Further evidence from literature supports this phenomenon. The presence of NOM influences micropollutant adsorption onto GAC through two mechanisms: adsorption competition and pore blocking (Matsui et al., 2002; G. Newcombe & Drikas, 1997; Pelekani & Snoeyink, 1999; Quinlivan et al., 2005; Shimabuku et al., 2017). Newcombe (1994) stated that when NOM attaches to activated carbon, it imparts a negative charge to the carbon. This effect can enhance electrostatic repulsion, leading to decreased adsorption of anionic micropollutants (De Ridder et al., 2011). Research also shows that there is a decrease in propanil adsorption in the presence of DOM (Xiao et al., 2012).

To accurately determine the change in the amount of background NOM during the experiment, a two-step process is used. First, the total organic carbon (TOC) equivalent of all pesticides measured in the samples is calculated. Next, the sum of the TOC equivalent of pesticides is subtracted from the overall DOC measurement. This method allows for a more precise estimation of the background NOM content by accounting for the contribution of pesticides, which are also considered part of the dissolved organic matter. Initially, pesticides contributed 40% of the DOC; however, this percentage decreased to an average of 7% (ranging from 3% to 15% for different GAC doses) when equilibrium was reached. This decrease indicates that pesticides have a higher affinity for GAC than background NOM. This can be seen when comparing the K_f of pesticides and background NOM (Table 5.15 and Table 5.16).

Moreover, absorbance measurements were taken to investigate the potential variations in NOM adsorption behavior based on the different chromophores present. The resultant data were utilized to construct isotherm graphs for Freundlich, and Langmuir models. The Freundlich and the Langmuir isotherm graphs for DOC and absorbance at specific wavelengths are presented in Figures 5.39 to

5.43. Based on these analyses, the parameters for both adsorption models were determined and summarized in Table 5.16.

Control experiments conducted with absorbance measurements revealed that pesticides also exhibited absorbance at UV_{254} and UV_{280} wavelengths. This observation is expected because all pesticides, excluding malathion, contain aromatic rings in their molecular structure. It is known that aromatic functional groups give absorption at those wavelengths (Korshin et al., 2009). However, it is important to note that the impact of pesticides on the UV absorbances was minimal when compared to background NOM alone. This suggests that while pesticides do contribute to UV absorption, their interference is relatively insignificant in the context of the overall experimental results.

Significant variations were observed when comparing the Freundlich and Langmuir isotherm parameters of background NOM (Table 5.11) alone and the addition of a pesticide mixture to the background NOM (Table 5.16). The presence of pesticides resulted in notable changes in the adsorption behavior of background NOM, as evidenced by the altered isotherm parameters. Specifically, the 1/n related to background NOM increased in the presence of pesticides and approached or exceeded 1, which indicates decrease in the strength of adsorption of NOM. Also, the K_f and q_{max} parameters were decreased in the presence of pesticides which indicated a lowered adsorption capacity.

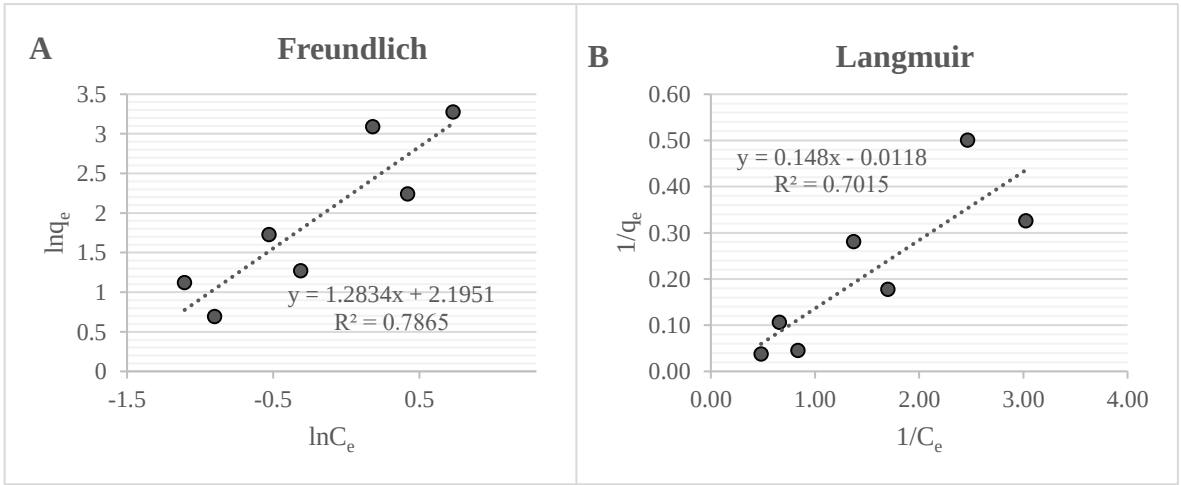


Figure 5.39. Isotherms showing the adsorption of background NOM onto ground GAC in the case of background NOM and a pesticide mixture: (A) Freundlich, (B) Langmuir (In terms of DOC).

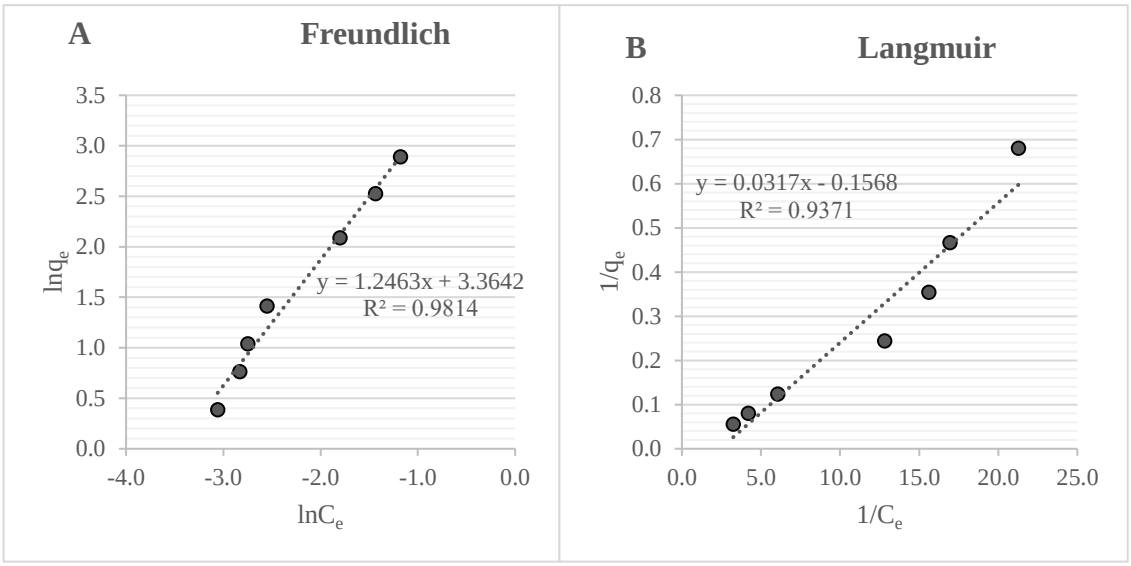


Figure 5.40. Isotherms showing the adsorption of background NOM onto ground GAC in the case of background NOM and a pesticide mixture: (A) Freundlich, (B) Langmuir (In terms of UV_{254}).

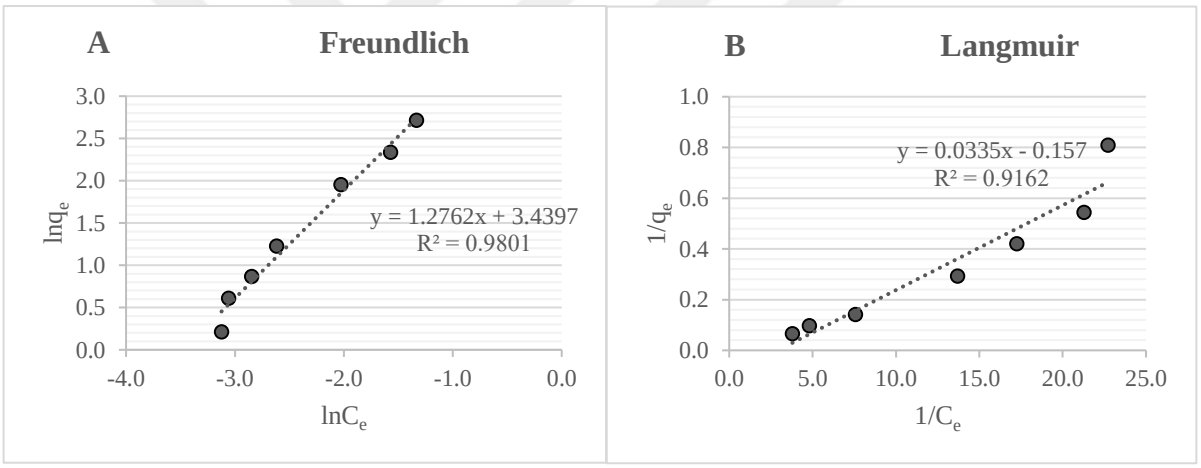


Figure 5.41. Isotherms showing the adsorption of background NOM onto ground GAC in the case of background NOM and a pesticide mixture: (A) Freundlich, (B) Langmuir (In terms of UV_{280}).

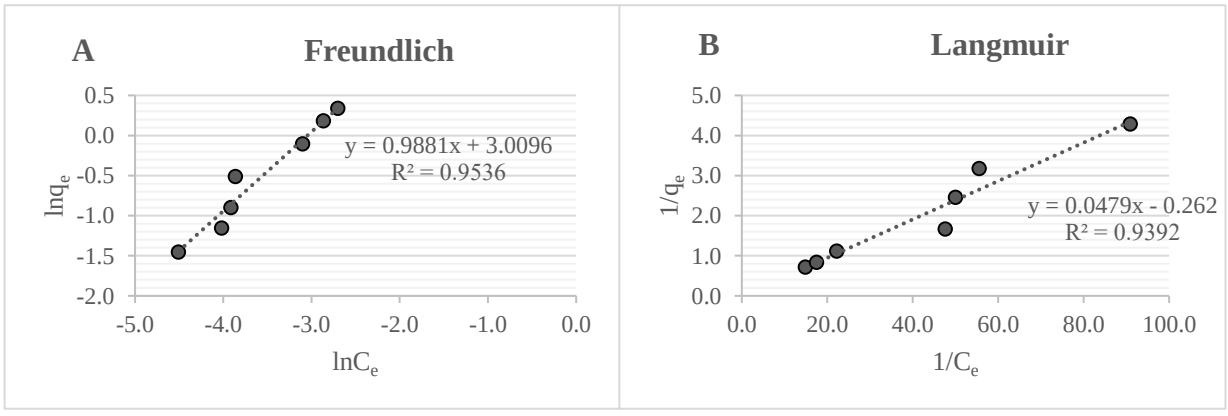


Figure 5.42. Isotherms showing the adsorption of background NOM onto ground GAC in the case of background NOM and a pesticide mixture: (A) Freundlich, (B) Langmuir (In terms of $Color_{400}$).

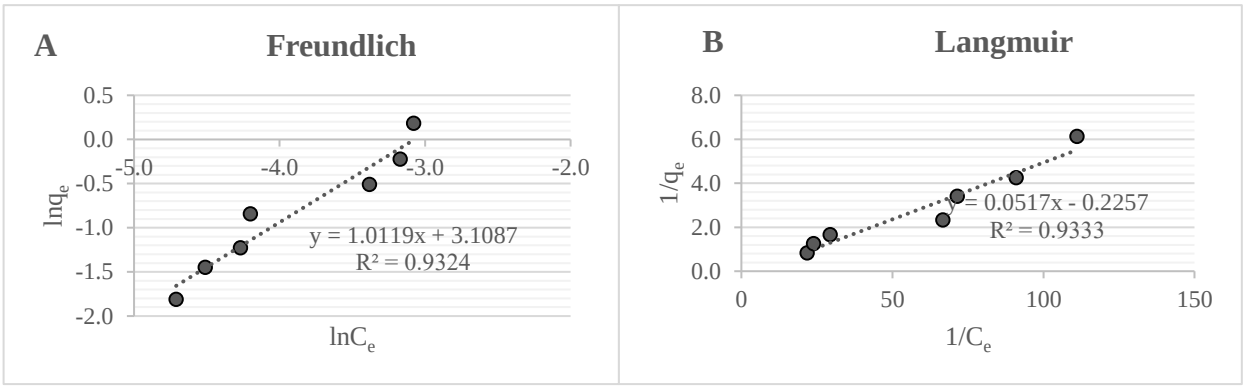


Figure 5.43. Isotherms showing the adsorption of background NOM onto ground GAC in the case of background NOM and a pesticide mixture: (A) Freundlich, (B) Langmuir (In terms of $Color_{436}$).

Table 5.16. Isotherm parameters describing the sorption of background NOM from a mixture composed of background NOM and pesticides onto ground GAC (in terms of mg DOC/L and absorbance measurements).

Isotherm	Parameters	DOC	UV_{254}	UV_{280}	$Color_{400}$	$Color_{436}$
Freundlich	1/n	1.28	1.24	1.27	0.98	1.01
	K_f (mg DOC/g)(L/mg DOC)$^{1/n}$ or (1/g cm)(cm)$^{1/n}$	8.98	28.91	31.18	20.28	22.39
	R^2	0.79	0.98	0.98	0.95	0.92
Langmuir	q_{max} (mg/g) or (1/g cm)	0.98	6.38	6.37	3.82	4.43
	K_L (L/mg DOC) or (cm)	0.08	4.95	4.48	5.43	4.37
	R^2	0.70	0.93	0.92	0.93	0.93

When we consider all isotherm experiments, the Freundlich isotherm model can be selected as the most suitable isotherm for this research, based on its demonstrated capacity to represent the adsorption characteristics of the systems under study accurately.

In the subsequent phases of our research, the Adsorption Design Software (AdDesignS) was used to simulate breakthrough curves in continuous-flow column experiments. These simulations were based on parameters derived from the Freundlich isotherm model. To analyze the breakthrough behavior of pesticides and/or background NOM, the pore surface diffusion model (PSDM), which is a component of the AdDesignS software package was employed.

This approach allows us to model and predict adsorption behavior in dynamic column systems, providing insights into the continuous-flow process. By combining the Freundlich isotherm

parameters with the AdDesign software, we can predict system's performance under various operating conditions.

5.3. Biodegradation Experiments

5.3.1. Operation of a Biological Reactor for the Growth of Biomass

One of the key aims of this study is to elucidate the biodegradation of pesticides and natural organic matter (NOM) and evaluate the efficacy of biological activated carbon (BAC) filtration systems. Using a batch reactor, indigenous microorganisms in the Ömerli water were grown under controlled conditions.

The operation of batch reactors started in December 2022. Several semi-continuous runs were done. The reactor was fed using the recipe represented in Table 4.7. The reactor was fed on Mondays and Thursdays. The daily loading rate was 30 g DOC/L day and 1.2 mg NH_4^+-N /L day. The reactor was regularly monitored by measuring temperature, Dissolved Organic Carbon (DOC), Mixed-Liquor Suspended Solids (MLSS), Mixed-Liquor Volatile Suspended Solids (MLVSS), NH_4^+-N, and pH parameters. The aim was to reach a steady MLVSS concentration so that a sufficient inoculum was obtained for further experiments. An example of the one-month operational details of this reactor is illustrated in Table 5.17. Operational details of this reactor are shown in Appendix B.

Table 5.17. Operational Results of the Biological Reactor – April 2023.

Run	**1**		**2**		**3**		**4**	
Date	3.04	7.04	10.04	14.04	17.04	20.04	24.04	28.04
pH	7.21	7.15	6.89	7.02	7.13	6.88	6.73	6.33
Temperature (°C)	22.9	23.1	23.4	22.8	22.4	22.6	22.8	23.4
DOC (mg/L)	85	9.7	101.2	11.1	96.4	10.4	80.2	14.7
DOC Removal (%)	88.6		89.0		89.2		81.9	
NH_4^+-N (mg/L)	2.2	0.03	2.45	0.02	2.85	0.05	1.05	0.03
NH_4^+-N Removal (%)	98.6		99.2		98.2		97.1	
MLSS (mg/L)	980		1305		1235		1240	
MLVSS (mg/L)	935		1105		1070		1195	
Run Period (day)	3.86		3.86		2.87		3.87	
F:M Ratio (mg DOC/mg MLVSS.day)	0.024		0.024		0.031		0.023	
S_0/X_0 (mg DOC/mg MLVSS)	0.091		0.092		0.090		0.066	

According to the results, the reactor has a DOC removal efficiency of approximately 80-90%. pH measurements were done at the start and the end of each semi-continuous feeding period in order to control the reactor. The pH values were changing in the range 6.0-7.4.

5.3.2. NOM Biodegradation Experiments

In this part of the study, the biodegradation of background NOM was investigated. The experiments were conducted in a system with a total volume of 200 mL, utilizing different biomass concentrations: 10 mg/L, 20 mg/L, 50 mg/L, 100 mg/L and 200 mg/L. The biomass samples used in these experiments were obtained from the semi-continuously fed batch (SCFB) reactor, as explained in Section 5.3.1. Biodegradation experiments were performed using continuous aeration while maintaining a steady temperature at 25 °C. Over the course of 48 hours, samples were collected to evaluate the decrease in DOC.

The first-order biodegradation rate constants (k_{biol}) were calculated using DOC measurements from the graphs presented in Figure 5.44. According to calculated k_{biol} values, moderate removal in DOC can be achieved at both biomass concentrations. The experimental results in Figure 5.44 illustrate that increased biomass concentrations correlate with enhanced NOM removal efficiency, characterized by quicker and more thorough elimination. Conversely at low biomass levels, the biodegradation process decreases, resulting in slower removal rates.

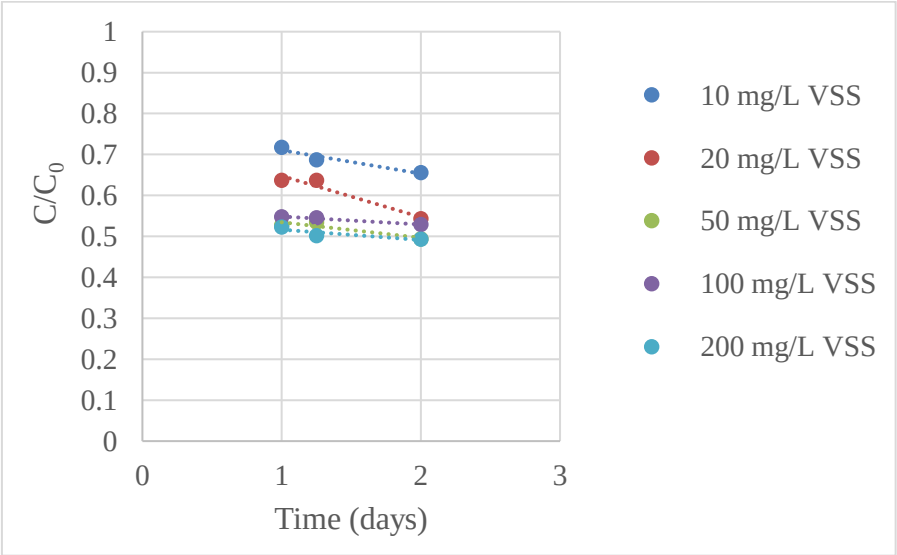


Figure 5.44. Background NOM removal profile in a batch reactor: normalized DOC concentrations versus time (C_0 = 3.5 mg DOC/L).

Background NOM removal profiles in the batch reactor were also analyzed through absorbance measurements at different wavelengths to understand the biodegradability of different NOM components. The results of absorbance measurements at 254, 280, 400, and 436 nm are shown in Appendix C, Figures C.1 to C.4. The results revealed that NOM components in the color region underwent more significant biodegradation than those in the UV region. This finding indicates that the aromatic substances present in NOM, which show absorbance in the UV region, are less biodegradable than NOM fractions that show absorbance in the color region, which are mainly functional groups composed of conjugated double bonds (Dorota H, 2018; Korshin et al., 2009; Sambo et al., 2020).

The higher biodegradability of color-absorbing NOM components could be attributed to their simpler molecular structure and the presence of more easily metabolizable functional groups. This observation aligns with previous studies demonstrating the recalcitrant nature of aromatic compound in natural organic matter (Crapart et al., 2021; Toosi et al., 2012; Zhou et al., 2021).

5.3.3. Pesticide Biodegradation Experiments

In this part of the study, the biodegradation of pesticides was investigated. The experiments were conducted in a system with a total volume of 200 mL, employing a biomass concentration of 500 g/L MLVSS. The biomass samples used in these experiments were obtained from the semi-continuously fed batch (SCFB) reactor, as explained in Section 5.3.1. Biodegradation experiments were performed using continuous aeration while maintaining a steady temperature at 25 °C. Over the course of 48 hours, samples were collected to evaluate the decrease in pesticides.

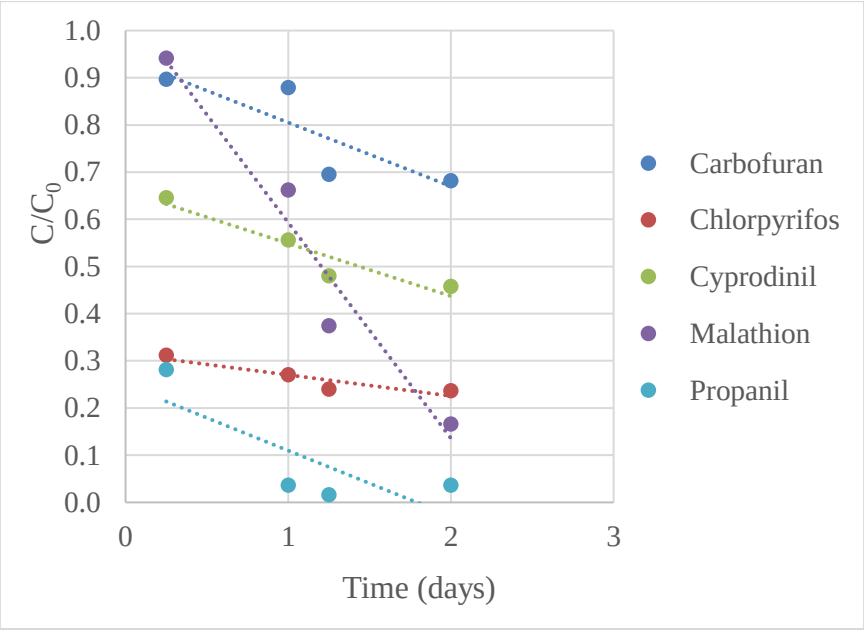


Figure 5.45. Pesticide removal profile in a batch reactor: normalized pesticide concentrations versus time (C_0 = 200 µg/L for each pesticide).

Using pesticide measurements, the first-order biodegradation rate constants (k_{biol}) were calculated from graphs presented in Figure 5.45. The biodegradation rate constants were calculated using Eq. 4.13. The results showed varying k_{biol} values for different pesticides: carbofuran had a k_{biol} of 0.345, chlorpyrifos 0.329, cyprodinil 0.149, malathion 2.127, and propanil 3.786 $g_{MLVSS}^{-1}.d^{-1}$.

According to Ternes and Joss (2006), who proposed a classification system for micropollutants, k_{biol} values in the range of 0.1 to 10 $g_{MLVSS}^{-1}.d^{-1}$ indicate a moderate removal level. Below this value, the biodegradability is low, and above it there is a high biodegradability (Ternes & Joss, 2006). For all studied pesticides, k_{biol} values were greater than 0.1, which suggested moderate removal. These findings align with the BIOWIN 1 & 2 results presented in Table 5.2, which indicate that all pesticides, except propanil, are prone to fast biodegradation.

On the other hand, experimental results indicate that propanil exhibits the highest biodegradation rate among the pesticides studied, almost with complete removal occurring in a very short timeframe. Interestingly, this finding contradicts the BIOWIN predictions, which suggested that propanil had the lowest potential for rapid biodegradation. This discrepancy between experimental biodegradation rates and BIOWIN predictions warrants further investigation. Several factors could contribute to this inconsistency, including the limitations of predictive models in capturing complex environmental interactions and the specific experimental conditions employed in this study. The observed rapid

biodegradation of propanil in experimental conditions might be attributed to the presence of specific microbial communities adapted to metabolize this compound.

According to the MetaCyc results (shown in Section 5.1.3. several bacterial genera commonly found in drinking water systems are capable of biodegrading pesticides such as carbofuran and chlorpyrifos. These include species from genera like *Pseudomonas*, *Sphingomonas*, and *Achromobacter*, which possess specific enzymatic pathways for breaking down these compounds. Probably these bacterial communities were present in the seed used in experiments and contributed to observed biodegradation.

The semi-continuously fed batch reactor may have facilitated the growth of unique bacterial strains capable of degrading propanil. These results present promising opportunities for investigating novel microorganisms and their pathways for propanil degradation. EnviPath (Environmental Contaminant Biotransformation Pathway Resource) and EAWAG-BBD/PPS (Biodegradation/Biocatalysis Database/Pathway Prediction System) predict that hydrolysis is likely to occur at the carbon-nitrogen bond in the amide group via an amidase-type enzyme, as shown in Figure 5.7 and Figure 5.12. This reaction produces propionic acid and the toxic 3,4-dichloroaniline (3,4-DCA), both of which have been previously reported as degradation products of propanil (Chen & Schäffer, 2016; Kanawi et al., 2016; Zhang et al., 2011). Further research on the bacterial strain responsible for propanil biodegradation may provide deeper insights into the mechanisms.

This finding highlights the importance of combining both experimental data and predictive modeling approaches when assessing the environmental fate of pesticides. Even though predictive tools are helpful for making initial assessments, experimental validation is still needed to accurately determine biodegradation rates. Also, a comprehensive examination of the proposed biodegradation pathways for these pesticides is provided in Section 5.1.

5.4. Investigation of the Synergistic Effect between GAC and Biomass in Batch Adsorption Systems

This section aims to investigate the synergistic effects between GAC and biomass in batch systems. The study focused on two pesticides, carbofuran and cyprodinil, chosen for their distinct biodegradation and adsorption properties. Five experimental conditions were established to evaluate different removal mechanisms, including the individual and combined effects of GAC adsorption and biodegradation. Condition I served as a control baseline, while conditions II and III examined

adsorption and biodegradation independently. Condition IV investigated their combined effect. The addition of sodium azide as a microbial inhibitor in condition V helped distinguish between adsorption and biodegradation mechanisms by suppressing bacterial activity. The details of the experimental procedure are described in detail in Section 4.7.3.

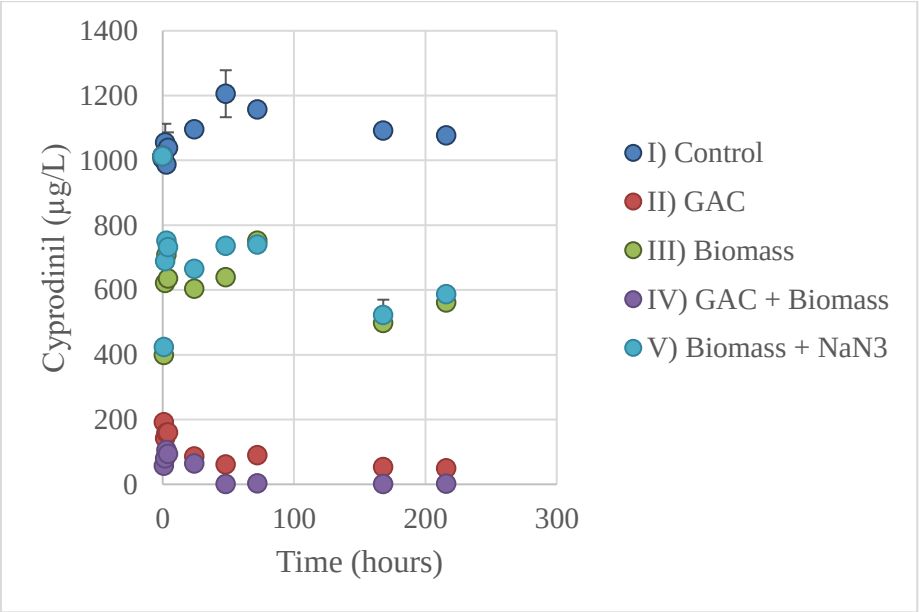


Figure 5.46. Removal of cyprodinil over time under five experimental conditions: Control (I), GAC (II), Biomass (III), Combined GAC + biomass (IV), and Biomass with NaN_3 inhibitor (V).

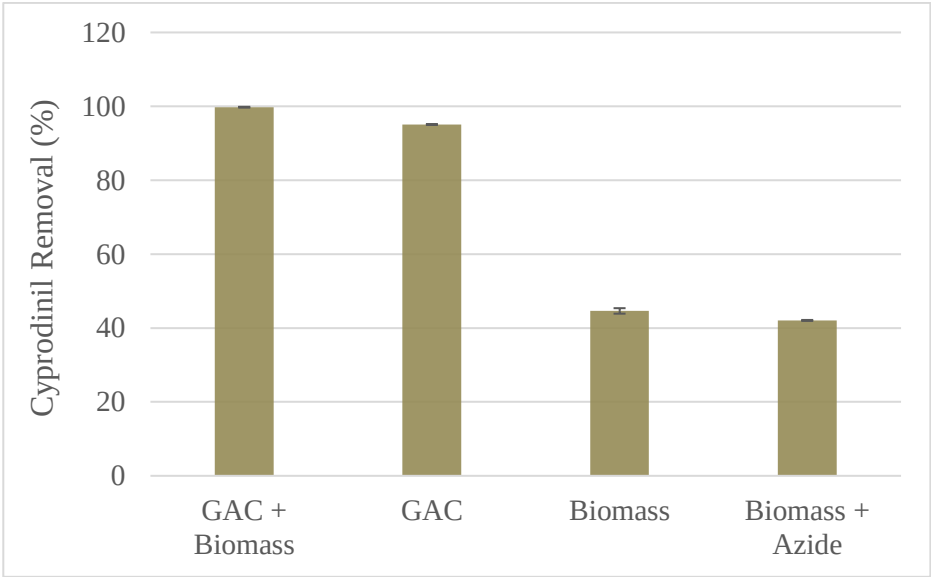


Figure 5.47. Final cyprodinil removal efficiency (%) across all treatment conditions.

The experimental results for cyprodinil removal are represented in Figures 5.46-47. In the control condition (Condition I), minimal removal was observed, confirming that natural degradation or volatilization effects were negligible. The GAC-only system (Condition II) demonstrated strong

removal performance (~95%), with a sharp initial decline in concentration due to rapid adsorption onto the activated carbon surface. The combined GAC + biomass system (Condition IV) exhibited the highest removal efficiency (99%). Since the difference in the adsorption between these two conditions is not substantial, a t-test was conducted to assess statistical significance. The t-test yielded a p-value of 0.00062, which is much smaller than 0.05, confirming a statistically significant difference. This indicates that the removal of the GAC + biomass system is significantly higher than that of the GAC-only system, suggesting a synergistic effect between the GAC and biomass mechanisms.

The biomass-only system (Condition III) showed moderate removal efficiency (45%). The addition of sodium azide to the biomass (Condition V) resulted in slightly lower removal (42%) than the biomass-only system, prompting a t-test to determine whether sodium azide inhibited bacterial activity or not. The test produced a p-value of 0.0058, confirming a statistically significant difference between these two conditions. This suggests that NaN_3 inhibits at least some of the bacteria present in the biomass. The results reveal that both degradation and adsorption mechanisms play roles in cyprodinil removal in biomass systems, with biosorption being the dominant process.

The minimal difference in removal efficiency between the biomass-only system and the biomass with sodium azide system suggests that biological degradation plays only a minor role in the overall removal process. If biodegradation were the primary mechanism, a more substantial decline in removal efficiency would have been observed upon microbial inhibition.

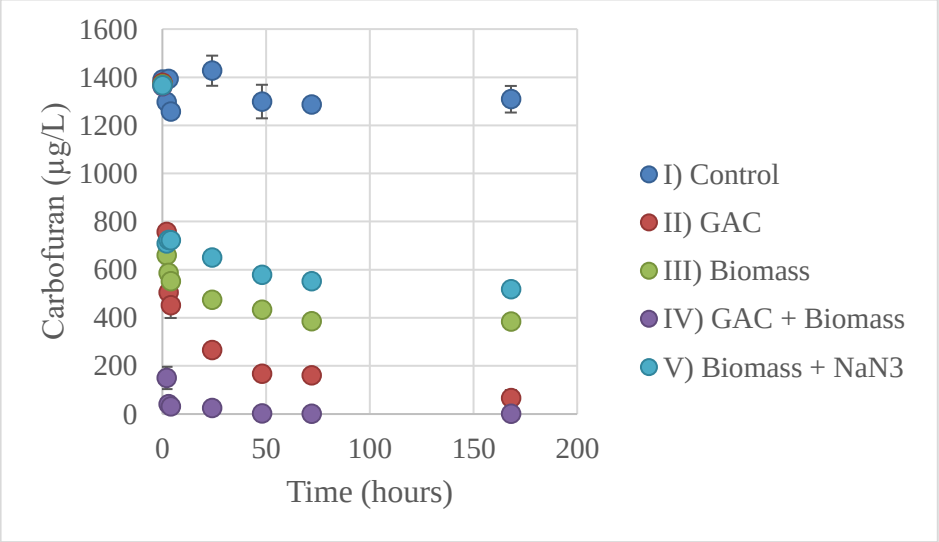


Figure 5.48. Removal of carbofuran over time under five experimental conditions: Control (I), GAC (II), Biomass (III), Combined GAC + biomass (IV), and Biomass with NaN_3 inhibitor (V).

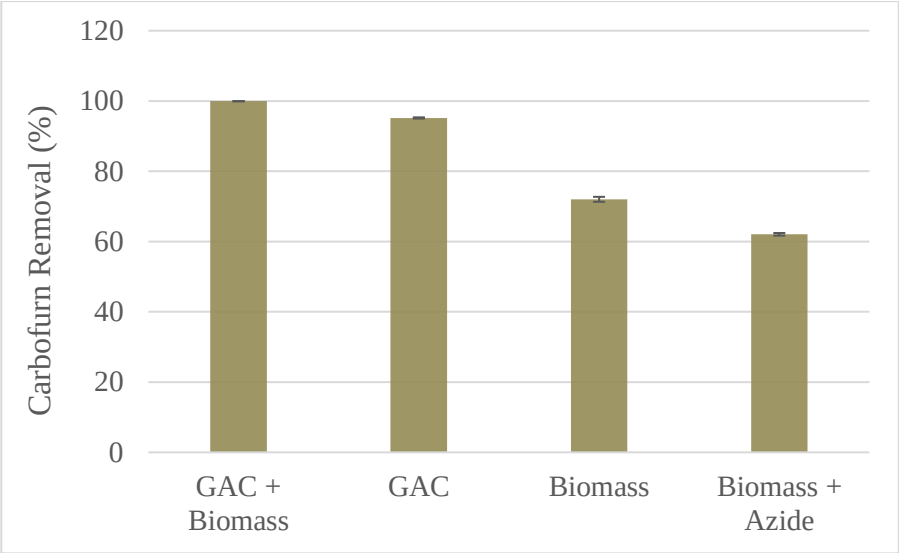


Figure 5.49. Final carbofuran removal efficiency (%) across all treatment conditions.

Similarly, the experimental results for carbofuran are shown in Figure 5.48 and Figure 5.49. The control condition (Condition I) exhibited minimal removal, confirming that natural degradation or volatilization was negligible for carbofuran. The GAC-only system (Condition II) displayed strong removal efficiency (95%), while the combined GAC + biomass system (Condition IV) achieved the highest removal efficiency (99%). A t-test comparing these two conditions yielded a p-value of 0.0084, indicating a statistically significant difference and reinforcing the synergistic effect of combining GAC and biomass for carbofuran removal as well.

The biomass-only system (Condition III) exhibited higher removal efficiency (72%), compared to cyprodinil (45%). The sodium azide-treated biomass (condition V) exhibited lower removal (62%). These results confirm that both degradation and adsorption mechanisms contribute to carbofuran removal in biomass systems. Although biodegradation plays a greater role compared to cyprodinil, adsorption remains the dominant removal mechanism in biomass-containing systems.

Furthermore, it was observed that the removal of carbofuran in biomass-only condition (72%) is higher than the removal of cyprodinil (45%). This is in line with our previous findings (Section 5.5.2.) regarding k_{biol} values for these pesticides. Carbofuran has a higher k_{biol} value (0.345 $g_{MLVSS}^{-1}.d^{-1}$) compared to cyprodinil (0.149 $g_{MLVSS}^{-1}.d^{-1}$), indicating greater biodegradability. BIOWIN results further support these findings. As shown in Table 5.2, carbofuran has higher numeric values for all BIOWIN models than cyprodinil, reinforcing its higher biodegradation potential.

Overall, experimental results demonstrated that the combined effect of adsorption and biodegradation mechanisms enhanced the removal efficiency of both pesticides, which aligns with findings reported in the literature (Rattier et al., 2012). Combining GAC and biomass improved the overall pesticide removal performance compared to applying each method separately. This synergistic interaction suggests that we can effectively exploit the complementary nature of these two removal mechanisms for enhanced pesticide remediation.

5.5. Tests in Continuous-flow Rapid/Small-Scale Columns (RSSCTs)

Rapid/Small-Scale Column Tests (RSSCT) were conducted using both original and ground granular activated carbon (GAC). All experiments are conducted at 25 °C. As previously mentioned, based on the equations presented in Table 4.8, reducing the particle size of GAC to one-tenth results in a proportional reduction of both Empty Bed Contact Time (EBCT) and flow rate to one-hundredth of their original values. Therefore, for the **original GAC** (size 1 mm), the 2 cm column was operated at a flow rate of 0.078 mL/min with an EBCT of 20 minutes. On the other hand, for the **ground GAC** (100-125 μm), the flow rate was increased to 7.85 mL/min while the EBCT was reduced to 0.20 minutes.

The number of Bed Volumes (BV) required to reach the specified breakthrough time was calculated for RSSCT experiments. Additionally, the Carbon Usage Rate (CUR) was determined for various RSSCT experiments. CUR serves as an essential metric in continuous-flow adsorption studies, indicating the efficiency of activated carbon consumption when treating a given fluid volume under specific operational conditions. Both the BV and CUR calculations were performed using the formulas outlined in Table 2.1.

Additionally, the AdDesignS software was employed to predict the breakthrough behavior of the studied cases. The simulation was performed using the relevant parameters outlined in Section 4.9.

5.5.1. Tracer Test Results

The tracer test was done to elucidate the **ground GAC** column's hydrodynamic characteristics at a flow rate of 7.85 mL/min. At time zero, the tracer was introduced into the system when the pump was started. For the tracer breakthrough calculations, the lengths and internal diameters of the tubing entering and exiting the column were recorded. A time correction was applied to account for the delay between the tracer entering the system and reaching the column, as well as the delay between the

tracer exiting the column and leaving the tubing. The resulting breakthrough curve for a tracer test is shown in Figure 5.50. Tracer test results for both experiment and model. , along with the corresponding best-fit analytical solution. The experimental breakthrough curve from the tracer test is shown along with the best-fit analytical model. Sodium chloride was used as a conservative tracer, and the measured breakthrough closely aligned with the analytical model derived from the Eq. 4. 16. This agreement suggests homogeneous packing within the column and the absence of preferential flow paths.

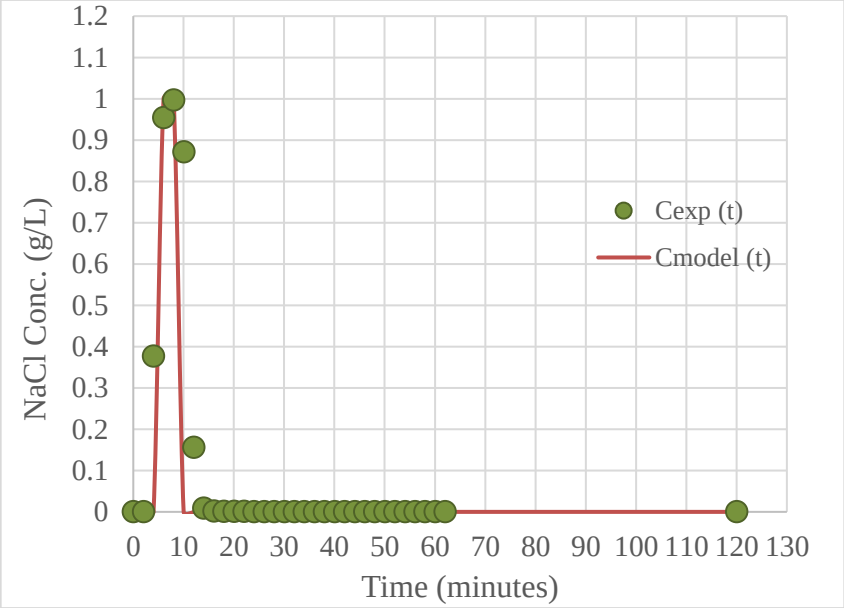


Figure 5.50. Tracer test results for both experiment and model.

To determine the optimal dispersion coefficient, the root mean square error (RMSE) between the observed and modeled data was minimized. The porosity of the column was found to be 0.5. The molecular diffusion coefficient (D_m) of NaCl in water at 25 °C was reported in the literature as 1.05 10^{-5} cm^2/min (Miller et al., 2007). The calculated parameters are summarized in Table 5.18. The results indicate that the transport process in the column is advection-dominated while there is a small dispersion, as evidenced by the Péclet number of 80, which exceeds the threshold of 50 for advection-dominated systems (Taigbenu & Liggett, 1986).

Table 5.18. Parameters determined from the tracer test.

Porosity (n)	0.5
Velocity (v)	10 cm/min
Dispersion coefficient (D_x)	0.50 cm^2/min
Longitudinal dispersivity (α_x)	0.03 cm
Péclet number (vL/D_x)	80

5.5.2. Adsorption of Single Pesticides (Cyprodinil and Carbofuran) onto Ground GAC in an RSSCT

In this experimental investigation, the rapid small-scale column was packed with ground granular activated carbon (GAC, 100-125 μm). In separate experiments, a solution containing cyprodinil or carbofuran pesticides (1000 μg/L) was continuously fed to the column. Effluent samples were obtained hourly and subsequently subjected to LC-MS/MS analysis for pesticide quantification. The results of these experiments are shown in Figure 5.51 and Figure 5.52.

The graphs represent the adsorption breakthrough curve for the studied pesticide, comparing experimental data (orange markers) with model predictions (blue markers) generated using AdDesignS software. The model predictions were based on the Freundlich isotherm parameters obtained from monocomponent pesticide isotherm experiments explained in Section 5.2.2.1. . As shown in Table 5.7, carbofuran has Freundlich parameters of 1/n = 2.06 and K_f = 657.47 $(mg/g)(L/mg)^{1/n}$, while cyprodinil has values of 1/n = 1.57 and K_f = 1452.29 $(mg/g)(L/mg)^{1/n}$.

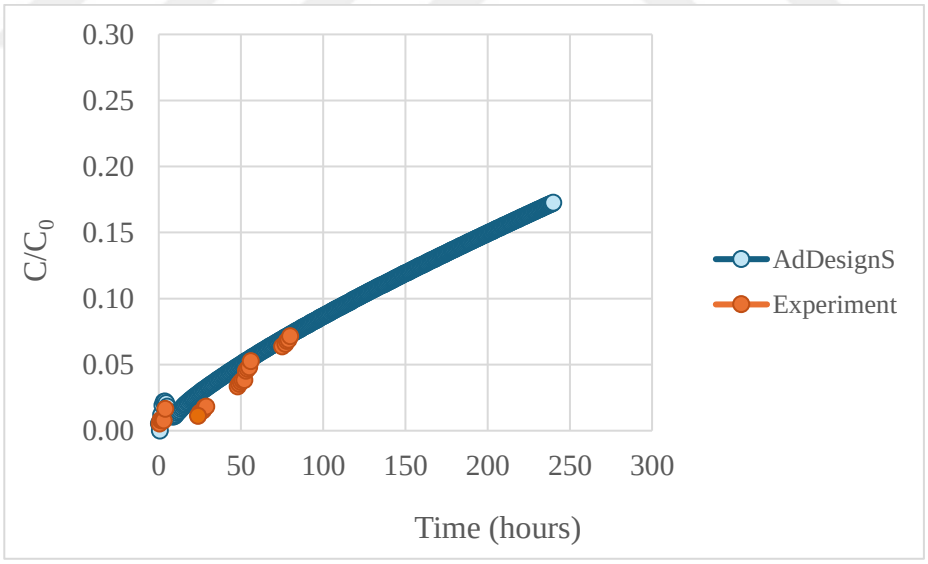


Figure 5.51. Comparison of experimental and AdDesignS-predicted breakthrough curves in the case of carbofuran onto ground GAC in an RSSCT (C_0 = 1000 μg/L).

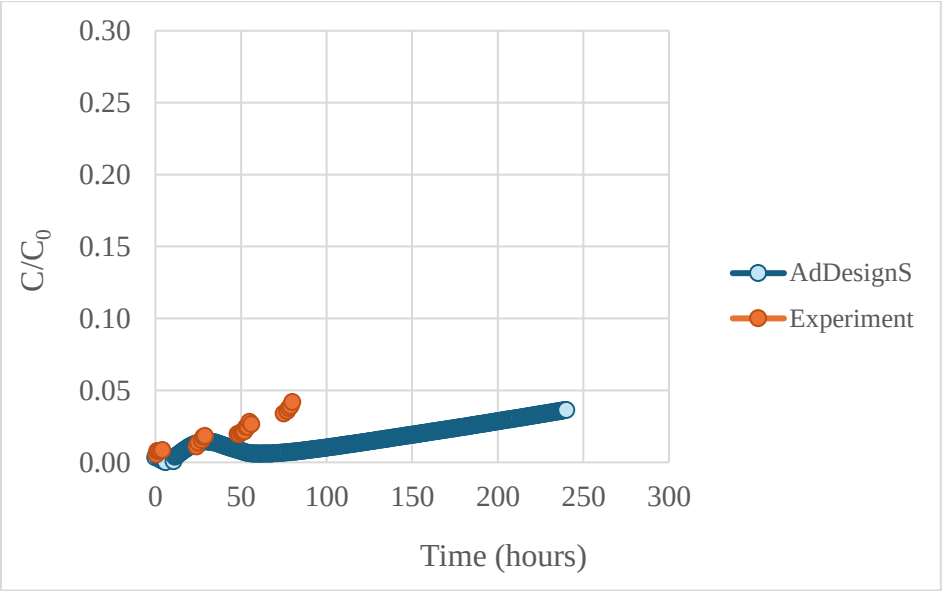


Figure 5.52. Comparison of experimental and AdDesignS-predicted breakthrough curves in the case of cyprodinil onto ground GAC in an RSSCT (C_0 = 1000 µg/L).

The breakthrough curves and model predictions provide insights into the adsorption behavior of cyprodinil and carbofuran on ground GAC. Both the experimental results and model predictions indicate a very low concentration ratio (C/C_0), remaining below 0.2 even after 200 hours. This low concentration ratio suggests strong adsorption for both pesticides.

When comparing the C/C_0 ratios, cyprodinil demonstrates a lower C/C_0 ratio than carbofuran at the same time intervals in both the experimental and model results. This suggests that cyprodinil has a delayed breakthrough compared to carbofuran, which aligns with cyprodinil's higher K_f value. The relationship between the Freundlich isotherm constant (K_f) and breakthrough behavior in adsorption processes is well-documented in the scientific literature (Cantoni et al., 2021; Velten et al., 2011; Worch, 2021; Çeçen & Aktaş, 2011). There is an inverse relationship between K_f and the breakthrough time of substances in a GAC column. A higher K_f means that the adsorbate can move from the bulk fluid to the GAC surface more easily, leading to more efficient adsorption onto the GAC. As a result, the GAC bed adsorbs a greater amount of the substance, causing the bed to reach saturation sooner. This results in a shorter breakthrough time, as the substance starts to appear in the effluent earlier.

The AdDesignS predictions and experimental results for cyprodinil and carbofuran were also compared. The AdDesignS predictions, based on Freundlich isotherm parameters, showed good agreement with the experimental data for both pesticides. This validates the reliability of the Freundlich isotherm parameters obtained from monocomponent isotherm experiments and confirms

their applicability in predicting column performance. While the model and experimental curves for carbofuran exhibit strong similarity, a slight discrepancy is observed for cyprodinil. The experimental results initially align well with the model predictions; however, as time progresses, the model predicts a more delayed breakthrough compared to the experimental results. This difference could be attributed to real-word complexities such as adsorbent surface irregularities, external diffusion resistance, or kinetic limitations not fully accounted for by the model.

The AdDesignS model was also used to predict the complete breakthrough time and shape for those pesticides. This is achieved by adjusting the experiment duration and set points. The resulting breakthrough curves for those pesticides are shown in Figure 5.53. While it takes 20 days for carbofuran to reach breakthrough, cyprodinil requires nearly 50 days. This delay in cyprodinil is expected, as it has higher K_f value and lower 1/n value than carbofuran, indicating that GAC has a greater affinity and adsorption capacity for cyprodinil.

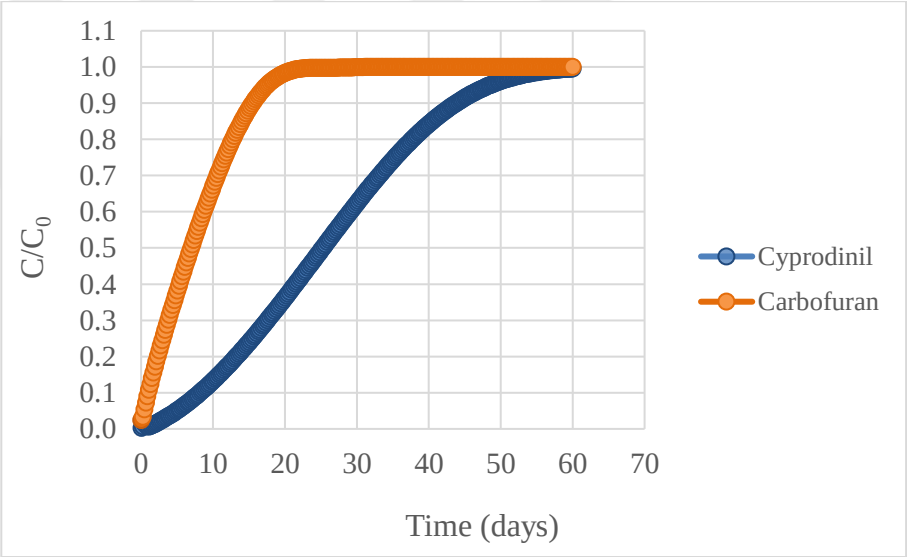


Figure 5.53. AdDesignS-predicted complete breakthrough curves for cyprodinil and carbofuran.

5.5.3. Adsorption of Background NOM onto Ground GAC in an RSSCT

The column was filled with ground GAC particles. A laboratory-prepared synthetic drinking water solution served as the source of NOM, with detailed composition specifications provided in Section 4.5. The experimental protocol involved maintaining continuous-flow through the column for a 24-hour period.

The breakthrough curve analysis revealed the temporal evolution of adsorbate concentrations in the effluent stream, with Figure 5.54 illustrating the normalized concentration ratios (C/C_0) of UV_{254}, UV_{280} and DOC parameters, where C and C_0 respectively, represent effluent and influent concentrations.

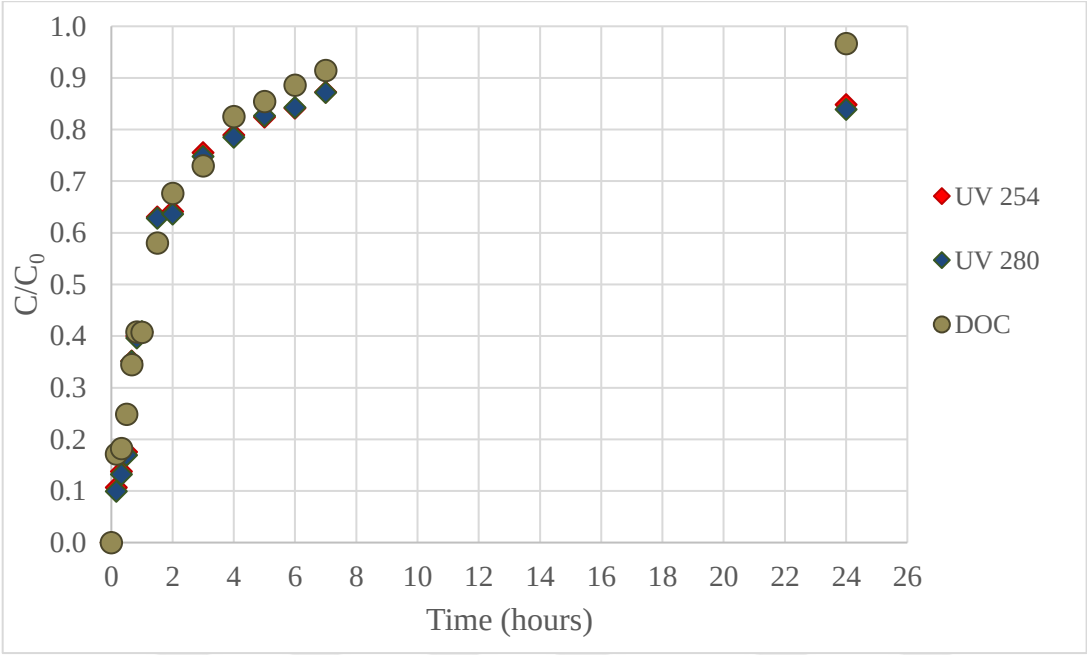


Figure 5.54. Experimental breakthrough curve of background NOM (in terms of absorbances and DOC) onto ground GAC in an RSSCT ($C_{0\text{-}DOC}$ = 3.5 mg DOC/L, $C_{0\text{-}254}$ = 0.105 cm^{-1}, $C_{0\text{-}280}$= 0.099 cm^{-1}).

Unlike the RSSCT done with ground GAC with pesticides, background NOM reached a breakthrough quickly for all measured parameters. There are several reasons for this faster breakthrough. First, the C_0 is greater in the background NOM experiment than in the pesticide experiments; it was 3.5 mg/L and 1 mg/L respectively. Higher influent concentration leads to quicker saturation of GAC pores and causes faster and steeper breakthrough curves (Worch, 2021).

The relationship between the molecular size of adsorbate, iodine number and methylene blue number for adsorbent are other factors that explain the observed difference in adsorption breakthrough. The Norit GAC has a high iodine number (1000 mg/g) whereas a low methylene blue number (22 mg/g) (as seen in Table 4.2). The high iodine number indicates an excellent micropore structure suitable for small molecules like pesticides, while the low methylene blue number suggests limited mesopore availability for larger molecules like humic acids (Zieliński et al., 2022). This is further supported by the significant difference in K_f values between pesticides (1764 and 1036 (mg DOC/g)(L/mg DOC)$^{1/n}$ for cyprodinil and carbofuran) and background NOM (11.34 (mg

DOC/g)(L/mg DOC)$^{1/n}$) (K_f for pesticides was also calculated in terms of dissolved organic carbon). These values clearly demonstrate the GAC's preferential adsorption capacity for smaller molecules over larger NOM compounds composed of humic acid substances, which explains the observed breakthrough patterns.

The data analysis revealed that it took approximately five hours (about 1500 BV) of continuous operation to reach an 85% breakthrough ($C/C_0 = 0.85$) for the overall background NOM, as measured by the DOC parameter. Similarly, absorbance measurements indicated that a slightly higher 90% breakthrough ($C/C_0 = 0.90$) was reached in about five hours (1500 BV) for the organic portion of background NOM that absorbs at 254 nm and 280 nm. Velten et al. (2011) also characterized different portions of NOM adsorption by GAC. Their findings similarly showed faster breakthroughs in terms of UV absorbances compared to the DOC parameter.

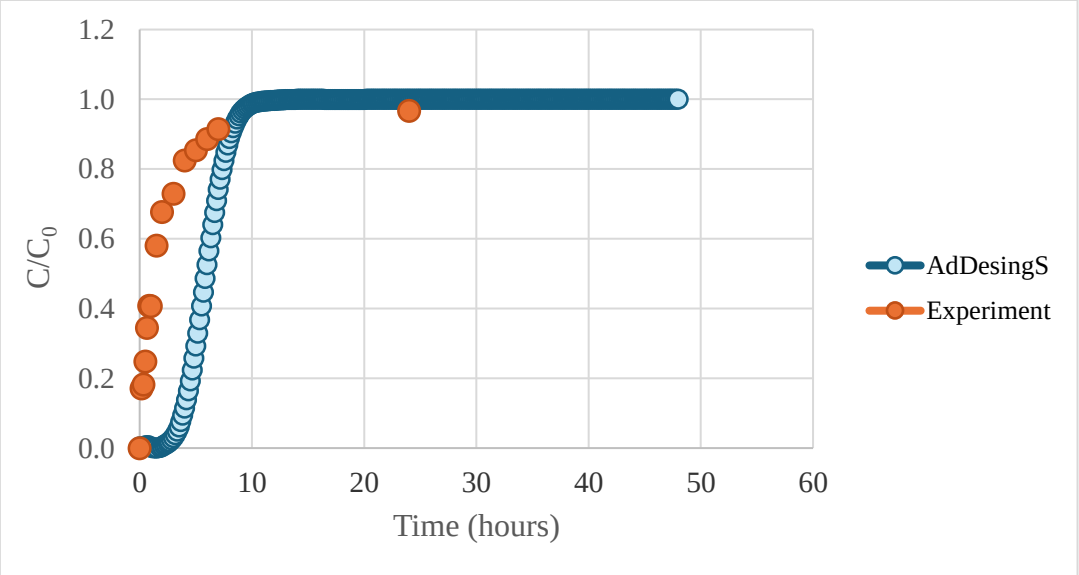


Figure 5.55. Comparison of experimental and AdDesignS-predicted breakthrough curves based on DOC measurements in the case of adsorption onto ground GAC in an RSSCT.

Figure 5.55 illustrates the adsorption breakthrough curve for background NOM, comparing experimental data (in terms of DOC measurements) with model predictions generated using AdDesignS. The model predictions employed the Freundlich isotherm parameters obtained from the adsorption isotherm experiment of background NOM onto ground GAC as explained in Section 5.2.2.4. . As shown in Table 5.11, background NOM has 1/n = 1.24 and K_f = 11.34 (mg DOC/g)(L/mg DOC)$^{1/n}$.

The simulated curve closely resembles the one obtained from experimental data. However, the experimental data follows a sigmoidal curve, increasing rapidly and reaching saturation. The model prediction shows a similar trend but a slightly delayed breakthrough. The experiment and model show a rapid increase in C/C_0, then reaching a plateau. During the transition phase, the model slightly underpredicts the experimental data, which can be attributed to the oversimplification of real conditions when transferring them to the model. The background NOM contains compounds with varying molecular weights and functional groups, whereas we introduce it to the model as a single molecule using the average molecular weight. While necessary for modeling purposes, this simplification may not fully capture the complex interactions and behaviors of diverse NOM compounds present.

5.5.4. Adsorption of Background NOM onto Non-Ground GAC in an RSSCT

In this experimental study, the rapid small-scale column was packed with non-ground (original) GAC (1 mm), and laboratory-prepared synthetic drinking water was continuously supplied to the column for 26 days. Grab samples were collected daily from the effluent stream and analyzed for UV_{254}, UV_{280} and DOC measurements.

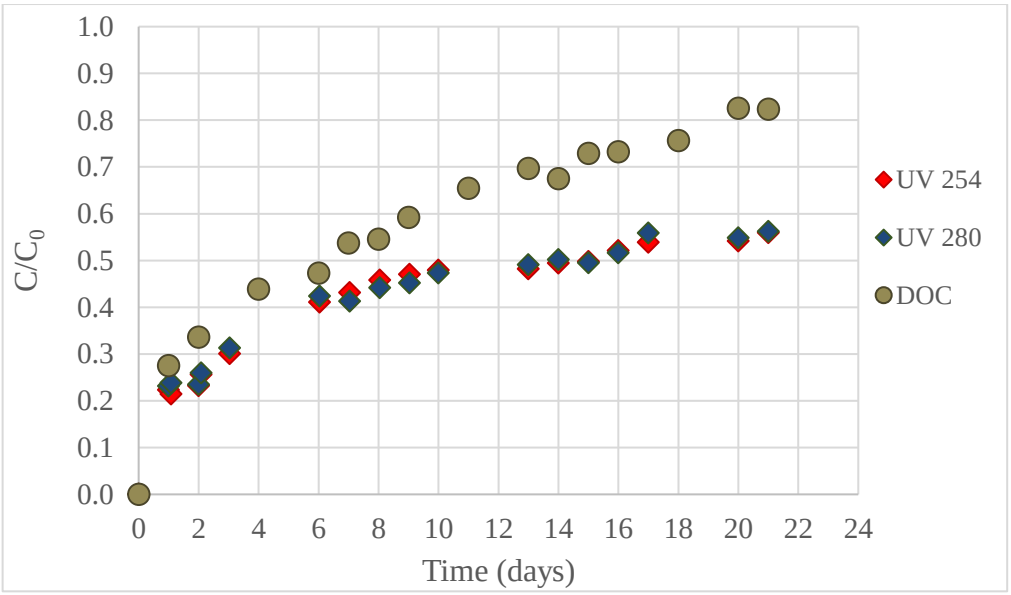


Figure 5.56. Experimental breakthrough curve of background NOM (in terms of absorbances and DOC) onto non-ground GAC in an RSSCT ($C_{0\text{-}DOC}$ = 3.5 mg DOC/L, $C_{0\text{-}254}$ = 0.105 cm^{-1}, $C_{0\text{-}280}$= 0.099 cm^{-1}).

Figure 5.56 displays the breakthrough curves. The data analysis revealed that it took approximately 216 hours (9 days or about 648 BV) of continuous operation to reach a 60% breakthrough ($C/C_0 = 0.7$) for the overall background NOM, as measured by the DOC parameter.

Similarly, absorbance measures indicated a similar duration of about 216 hours (9 days or 648 BV) was necessary to attain a 50% breakthrough ($C/C_0 = 0.5$) for the organic portion of background NOM that exhibit absorption at specific wavelengths, namely 254 nm and 280 nm. This suggests that, in terms of UV absorbance, the breakthrough was reached later.

According to Crittenden et al. (1986), there is an inverse relationship between 1/n and the breakthrough time in a GAC column. A lower 1/n indicates stronger adsorption affinity, meaning the adsorbate binds more effectively to the adsorbent. This stronger interaction delays the saturation of the GAC bed, leading to a longer breakthrough time as the substance takes longer to appear in the effluent. Conversely, a higher 1/n value suggests weaker adsorption, causing faster saturation of the GAC and an earlier breakthrough.

The adsorption of specific organic compounds, measured at 254 nm and 280 nm, exhibited similar characteristics at both wavelengths, aligning with previous batch isotherm experiments. Table 5.12 shows that the Freundlich isotherm constants (K_f and 1/n) for UV_{254} and UV_{280} are comparable, with K_f values of 25.84 and 30.21 $(1/g\ cm)(cm)^{1/n}$ and 1/n values of 1.39, 1.37, respectively. In comparison, the DOC measurements yielded a K_f value of 1.30 $(mg\ DOC/g)(L/mg\ DOC)^{1/n}$ and a slightly lower 1/n value of 1.27, further supporting the observed breakthrough behavior.

We compared the results of background NOM and non-ground GAC with our previous experiment using ground GAC. The two main differences between these experiments were the GAC size and the EBCT. The theoretical framework outlined in Section 4.9. , which relates to the RSSCT design, suggests that a 100-fold reduction in EBCT lead to a 10-fold reduction in GAC size. This relationship is mathematically expressed in Eq. 5.1. According to this equation, when we conducted the experiment with non-ground GAC (1mm), which size is 10 times greater than ground GAC (100 μm), the EBCT was set to 20 minutes compared to 0.02 minutes for ground GAC. This change should theoretically result in a 100-fold decrease in breakthrough time. Our experimental findings aligned closely with this theoretical prediction, demonstrating the validity of the RSSCT design principles.

$$Design\ Factor\ (DF) = 100 = \frac{EBCT_{SC}}{EBCT_{LC}} = \left[\frac{d_{p.SC}}{d_{p.LC}}\right]^2 = \left[\frac{t_{SC}}{t_{LC}}\right] \quad (5.1)$$

The experiment conducted in the previous section with background NOM and ground GAC showed that an 80% breakthrough of DOC occurred after approximately 4 hours. In contrast, the experiment using with non-ground GAC exhibited an 80% DOC breakthrough occurring significantly later, roughly 20 days (480 hours). This striking difference highlights the impact of GAC particle size and EBCT on adsorption performance. Reducing the GAC size by a factor of 10 and shortening the EBCT by a factor of 100 was expected to result in a 100-fold decrease in breakthrough time. Our measurements showed an approximately 120-fold decrease, which closely aligns with the theoretical prediction.

Additionally, the carbon usage rate (CUR) calculations were performed using the formula outlined in Table 2.1 and were compared between two experimental setups to reach 80% breakthrough in terms of DOC. In theory, this rate should remain constant across both conditions (Crittenden et al., 1991). The first experiment, using ground GAC, yielded a CUR of 434 mg/L while the second experiment, employing non-ground GAC, resulted in a CUR of 265 mg/L. Despite the numerical difference, these results can be interpreted as relatively consistent, considering the inherent variability in experimental conditions and measurement uncertainties. This similarity in CUR values suggests that the scaling principles applied in the RSSCT design effectively maintain the adsorption characteristics across different GAC particle sizes and contact times.

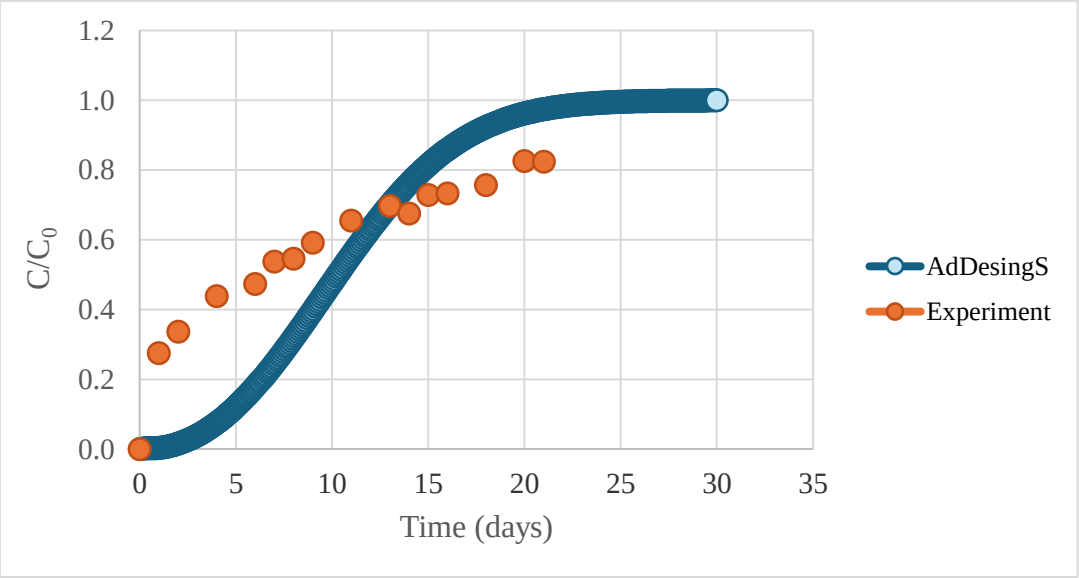


Figure 5.57. Breakthrough curves generated using AdDesign software and the experimental breakthrough curve measured in terms of DOC measurements onto non-ground GAC in an RSSCT.

Figure 5.57 compares adsorption breakthrough curves for background NOM (in terms of DOC) on non-ground GAC, showing both the experimental results and AdDesingS prediction. For the AdDesingS prediction, the Freundlich isotherm parameters from the adsorption isotherm experiment of background NOM onto non-ground GAC, as shown in Section 5.2.2.5. were used.

Both experimental and modeled curves reach a plateau indicating that the GAC has reached saturation and can no longer effectively adsorb background NOM. The timing of this plateau is relatively consistent between the two curves, supporting the validity of the model's prediction for total exhaustion.

The experimental breakthrough starting earlier than the model prediction suggests that the actual adsorption capacity of the GAC may be slightly lower than predicted. This observation aligns with the previously discussed underestimation (Section 5.5.3.), representing the background NOM as a single molecule in the model rather than accounting for its diverse molecular composition.

The model shows a slightly steeper breakthrough curve, meaning that once the breakthrough begins, the effluent concentration rises more rapidly than in experiments.

Overall, while there are some discrepancies between the experimental and predicted breakthrough curves, the AdDesignS provides a reasonable prediction of the GAC column performance for background NOM removal.

5.5.5. Adsorption of a Pesticides Mixture onto Ground GAC in an RSSCT

A solution containing a mixture of pesticides (200 μg of each) was continuously fed into the column packed with ground GAC over a 25-hour period. Effluent samples were obtained hourly and subsequently subjected to analysis. The results of this experiment are shown in Figure 5.58.

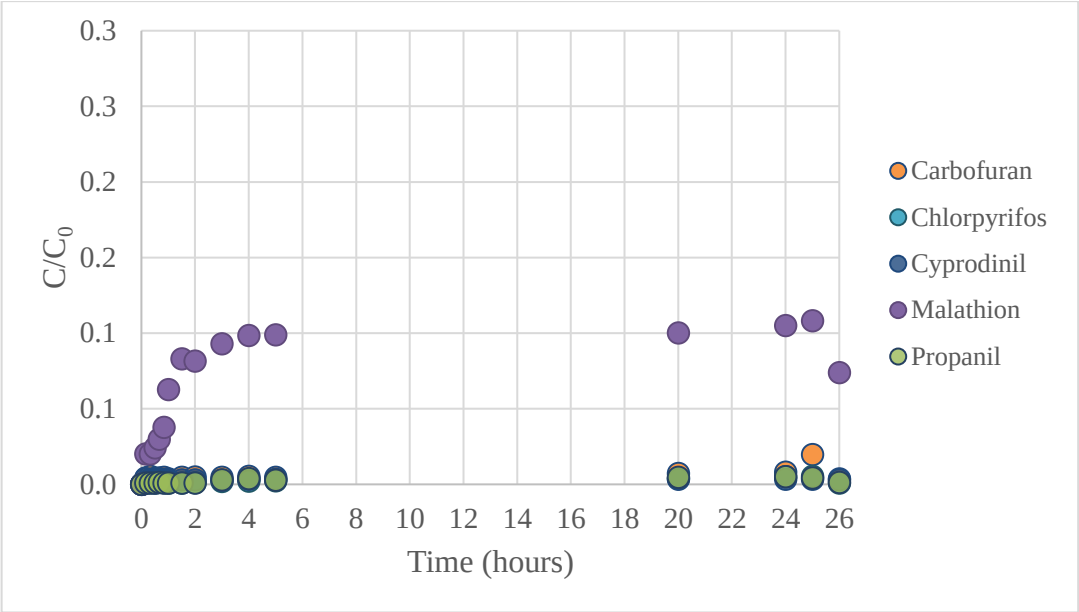


Figure 5.58. Experimental breakthrough curves in the case of a pesticide mixture onto ground GAC in an RSSCT (C_0 = 200 µg/L for each pesticide).

The concentration ratios (C/C_0) remained consistently low, staying below 0.2 for all pesticides. This indicates strong adsorption but makes distinguishing differences in adsorption behavior among the pesticides challenging.

However, malathion exhibited the fastest breakthrough among the pesticides, followed by carbofuran. This behavior aligns with the Freundlich isotherm parameters presented in Section 5.2.2.2. . As shown in Table 5.9, malathion and carbofuran have the lowest K_f values and highest 1/n values, indicating weaker adsorption onto GAC, and consequently, faster breakthrough times. In contrast, cyprodinil, chlorpyrifos, and propanil demonstrated delayed breakthroughs, consistent with their higher K_f values and lower 1/n values. These parameters suggest stronger adsorption affinities, which likely contribute to their prolonged retention on GAC.

Since a complete breakthrough was not observed during the experiment, the AdDesignS software was used to predict the breakthrough times of the pesticides. These predictions were based on the Freundlich isotherm parameters obtained from the isotherm experiment explained in Section 5.2.2.2. which analyzed pesticide adsorption in a mixture. Using the Freundlich parameters presented in Table 5.9, complete breakthrough curves were simulated and are shown in Figure 5.59. The simulation predicts that carbofuran reaches approximately 95% breakthrough within 1.2 days, malathion in 1.8 days, propanil in 3 days, cyprodinil in 5 days, and chlorpyrifos in 7 days.

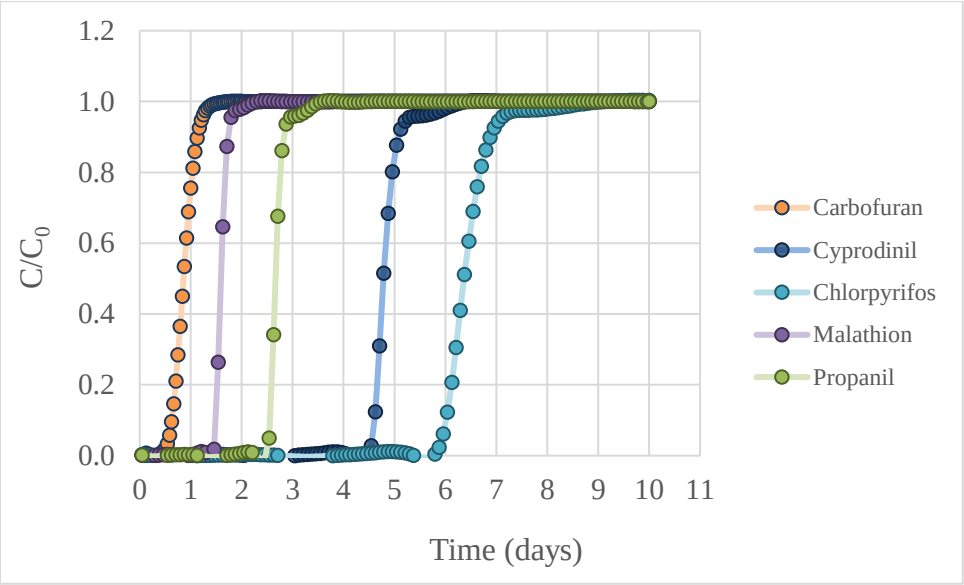


Figure 5.59. AdDesignS-predicted complete breakthrough curves for a pesticide mixture in the case of ground GAC.

When comparing the predicted breakthrough curves from AdDesignS with experimental results, a significant discrepancy was observed in the breakthrough time of carbofuran. The experimental data showed that carbofuran reached only 0.05% breakthrough at the 25th hour, whereas the model predicted an 80% breakthrough at the same time point. This suggests that while AdDesignS performs well in predicting breakthrough behavior in monocomponent systems (as seen in previous sections), its accuracy decreases in multicomponent systems. The software likely overestimates competitive adsorption effects, leading to a faster predicted breakthrough times. This observation highlights the critical role of experimental validation in adsorption studies, as the model alone may not fully capture the complexities of real systems. Therefore, experimental data remain essential for identifying discrepancies and ensuring that adsorption predictions align with actual application performance.

5.5.6. Adsorption of a Pesticides Mixture onto Non-Ground GAC in an RSSCT

A solution containing a mixture of pesticides (200 µg/L of each) was continuously fed into the column with non-ground GAC over a 12-day period. Grab samples were obtained on a daily basis and subsequently subjected to analysis.

The breakthrough curves for the pesticides are depicted in Figure 5.60. Analysis of the data indicates that malathion reached a 10% breakthrough ($C/C_0 = 0.1$) after approximately 290 hours of continuous operation, which is equivalent to about 12 days or 900 BV. In contrast, the breakthrough

of other pesticides was observed to be less than 4%. This is considered advantageous as it allows for extended use of carbon.

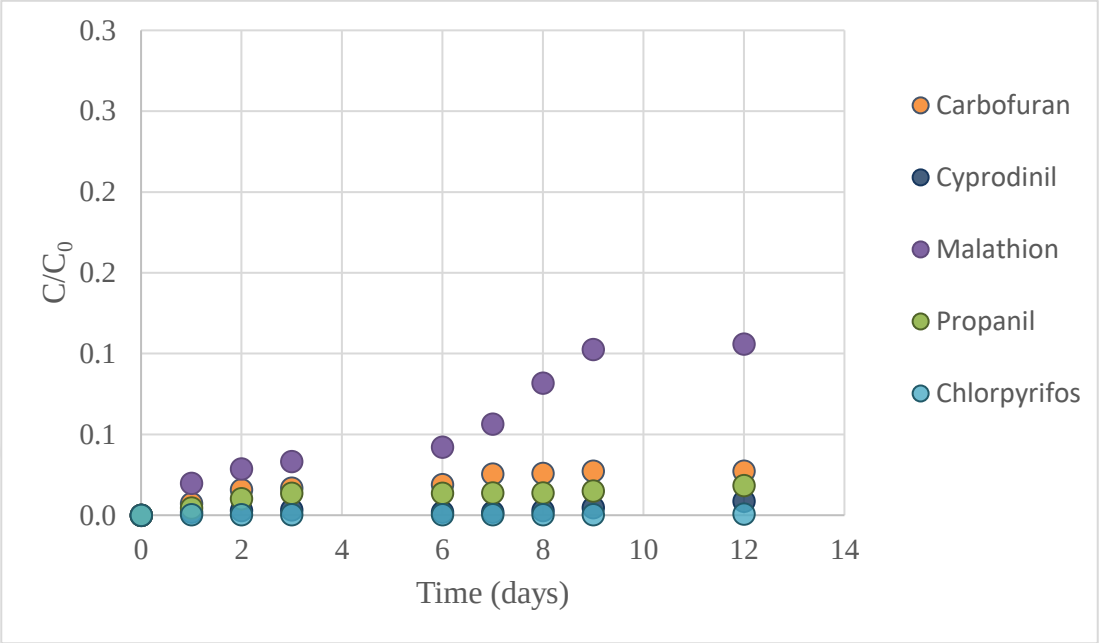


Figure 5.60. Experimental breakthrough curves in the case of a pesticide mixture onto non-ground GAC in an RSSCT (C_0 = 200 µg/L for each pesticide).

Malathion's a relatively faster breakthrough compared to the other pesticides, can be attributed to its Freundlich parameters - specifically, its lower K_f and higher 1/n values - as previously discussed in 5.2.2.3. . These characteristics allow malathion to reach its breakthrough point more quickly than the other pesticides, except for carbofuran. While carbofuran was expected to exhibit the fastest breakthrough due to having the lowest K_f and highest 1/n values, the observed trend deviated from this expectation. This discrepancy may stem from experimental uncertainties, particularly in the isotherm experiments or LC-MS/MS measurements, where reduced precision was noted at low malathion doses.

For the remaining pesticides, distinguishing their breakthrough times is challenging, as they are very close to each other. To address this, AdDesignS software was used to differentiate the breakthrough times and visualize the complete breakthrough curves for the studied pesticides. The predicted curves, shown in Figure 5.61, provide a clearer picture. According to the model-prediction, carbofuran reaches 95% breakthrough in 30 days, followed by malathion at 120 days, propanil at 150, cyprodinil at 360 and chlorpyrifos at 380 days.

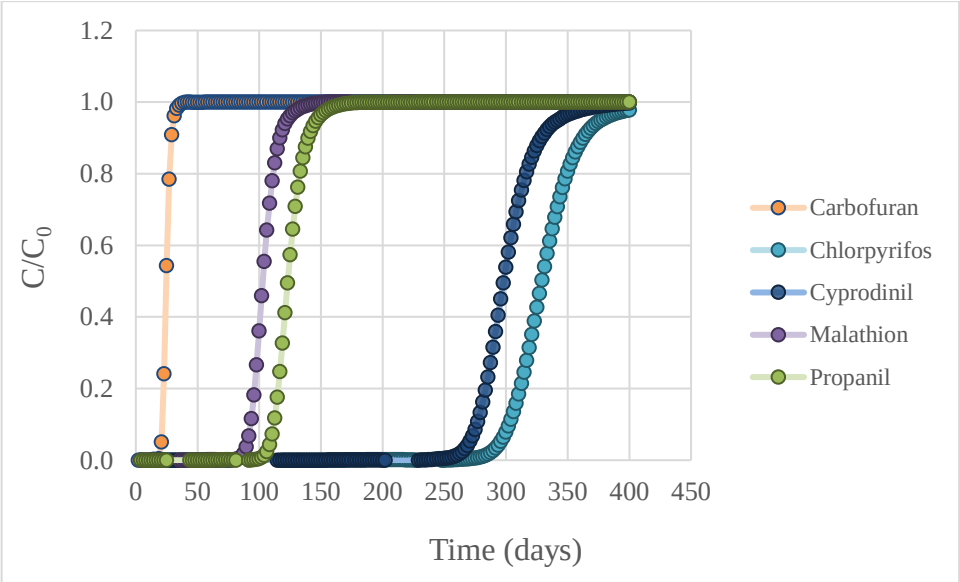


Figure 5.61. AdDesignS-predicted complete breakthrough curves for background NOM and pesticide mixture in the case of non-ground GAC.

Notably, while the trend is same as in the case of ground GAC (Figure 5.59), the breakthrough times observed in this part of the study are significantly longer than those reported in Section 5.5.5. where ground GAC was used. In the experiment with ground GAC, a 10% breakthrough of malathion occurred after just 3 hours, equivalent to approximately 900 BV. In contrast, when non-ground GAC was used, a 10% breakthrough of malathion was observed after 9 days, corresponding to approximately 650 BV. As explained in Section 5.5.4. the breakthrough time was expected to be 100 times higher in the ground GAC experiment. The results demonstrate that reducing the GAC particle size tenfold led to a breakthrough time reduction very close to the expected 100-fold decrease, reaching 72-fold.

Additionally, the carbon usage rate (CUR) for malathion was compared between the two experimental setups. The experiment with ground GAC yielded a CUR of 504 mg/L, while the non-ground GAC experiment resulted in a CUR of 638 mg/L. Despite the numerical differences, these results are relatively comparable, suggesting that both setups maintain similar adsorption efficiency in terms of carbon consumption. This consistency in CUR values further validates the scalability of the experimental design through constant diffusivity rapid small-scale columns (CD-RSSCT) application and confirms that both GAC configurations are effective for pesticide removal. This finding aligns with previous studies in the literature that have demonstrated CD-RSSCT's reliability in accurately representing micropollutant removal behavior by GAC (Cantoni et al., 2021; Crittenden et al., 1991; Hopkins & Knappe, 2024)

5.5.7. Simultaneous Adsorption of a Pesticides Mixture and Background NOM onto Ground GAC in an RSSCT

In this experimental investigation, the rapid small-scale column was packed with ground granular activated carbon (GAC, 100-125 μm). A solution containing a mixture of pesticides (200 μg/L of each) and synthetic drinking water containing NOM at a concentration of 3.5 mg DOC/L was continuously fed into the column over a 25-hour period. The breakthrough curves for the pesticides and NOM are depicted in Figure 5.62.

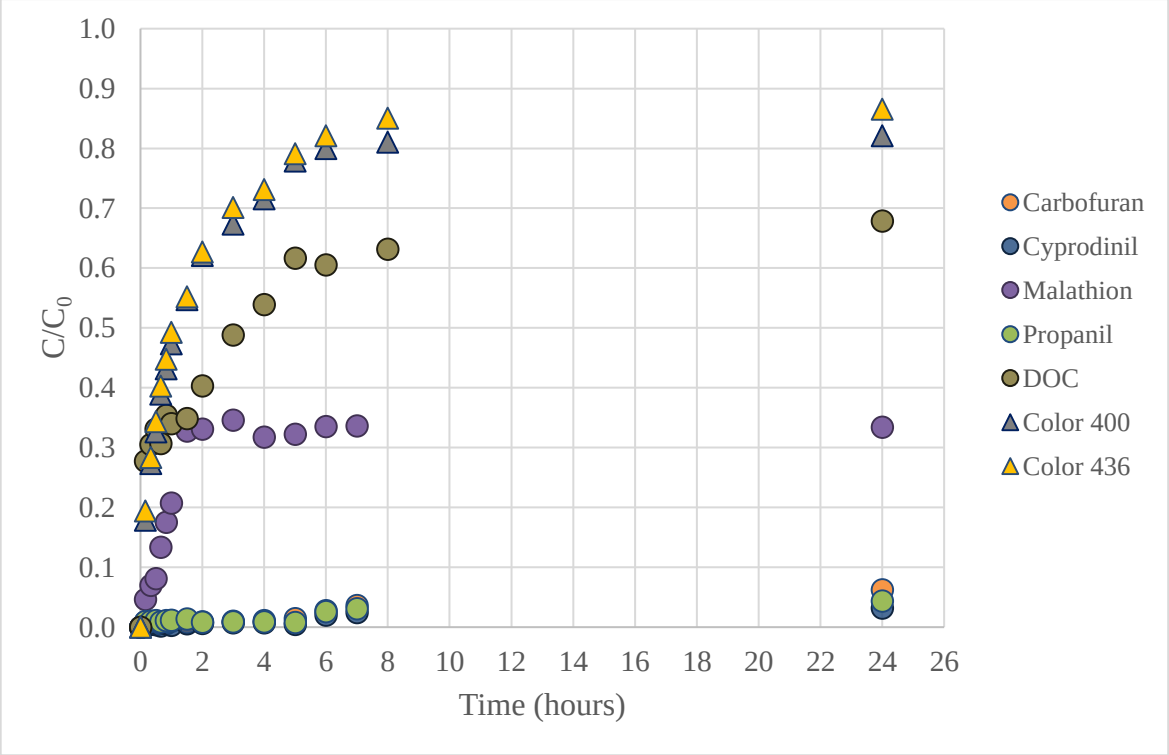


Figure 5.62. Experimental breakthrough curves in the case of simultaneous adsorption of a pesticide mixture and background NOM (in terms of absorbances and DOC) onto ground GAC in an RSSCT.

A comparison of the results presented in this section with those from the previous section reveals that pesticides exhibited earlier breakthroughs in the presence of background NOM. This finding indicates that NOM negatively affects the adsorption of pesticides as indicated in the literature (Kennedy & Summers, 2015).

The presence of NOM influences GAC adsorption capacity through several key mechanisms:

- Pore blockage: NOM can physically obstruct or clog GAC pores, limiting access to adsorption sites and reducing overall efficiency (De Ridder et al., 2011; Gayle Newcombe et al., 1997),
- Competitive adsorption: NOM and micropollutants, particularly smaller NOM fractions, directly compete for available adsorption sites, reducing the capacity for micropollutant removal (Reinert, 2013).
- Complex formation: NOM can interact with GAC, modifying its surface properties and potentially reducing its affinity for specific pollutants (Speth, 1991).

These findings underscore the significant role of NOM in adsorption dynamics and highlight the necessity of considering its impact when designing GAC-based treatment systems.

To evaluate the complete breakthrough behavior of pesticide in the presence of background NOM, AdDesignS software was used, and the results are presented in Figure 5.63. The breakthrough trend among pesticides was the same as the model predictions from the previous sections. However, significant discrepancies were observed between the software predictions and experimental data. The software predicted much earlier breakthrough times for pesticides compared to the experimental results while simultaneously overestimating the breakthrough times for background NOM.

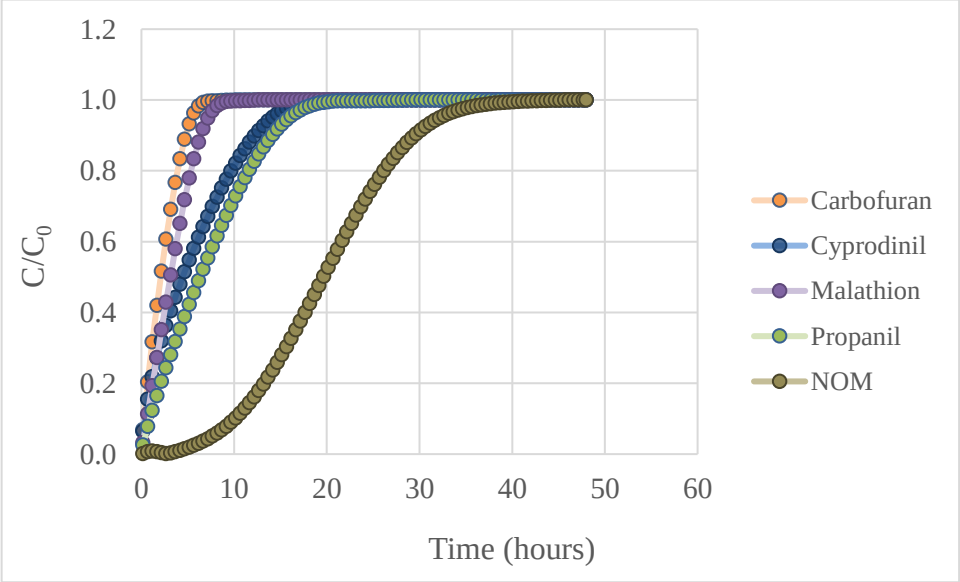


Figure 5.63. AdDesignS-predicted complete breakthrough curves for background NOM and pesticides in the case of ground-GAC.

As discussed in Section 5.5.5. these findings further highlight the limitations of AdDesingS software in accurately modeling multi-adsorbate systems. The presence of background NOM and multiple competing pesticides creates a complex adsorption environment that the software struggles to predict with precision. This discrepancy underscores the need for experimental validation when applying predictive models to real-world water treatment scenarios.

5.5.8. Simultaneous Adsorption of Background NOM and a Pesticide Mixture onto Ground GAC Surrounded with Biofilm in an RSSCT

In this experimental investigation, a rapid small-scale column was packed with ground biological activated carbon (BAC) particles. The BAC was created by combining ground GAC with biomass obtained from the SCFB reactor. This mixture was continuously aerated and fed (glucose and inorganic) bacteria twice a week for one month to promote the development of biofilm layers on the ground GAC particles.

After the one-month incubation period, the GAC particles, now likely to be covered with a biofilm layer and referred to as BAC, were taken from the Erlenmeyer flask. The particles were then thoroughly rinsed three times with ultrapure water to remove any loose biomass and any remaining substances from the feed. Finally, the column was prepared and packed with this material. After the column was ready, a solution containing a mixture of pesticides (200 µg/L of each) and synthetic drinking water containing NOM at a concentration of 3.5 mg DOC/L was continuously fed into the column over a 10-hour period. At the end of the 10^{th} hour, the experiment had to be terminated due to a decrease in flow. The breakthrough curves of pesticides and NOM are depicted in Figure 5.64 and Figure 5.65, respectively.

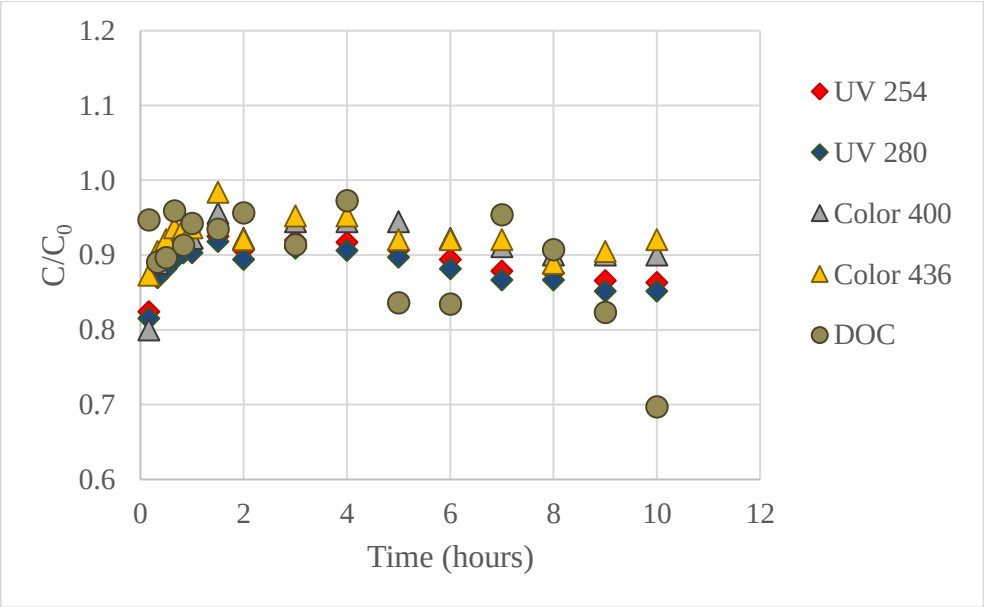


Figure 5.64. Experimental breakthrough curves of background NOM (in terms of absorbances and DOC) in the case of ground BAC in an RSSCT.

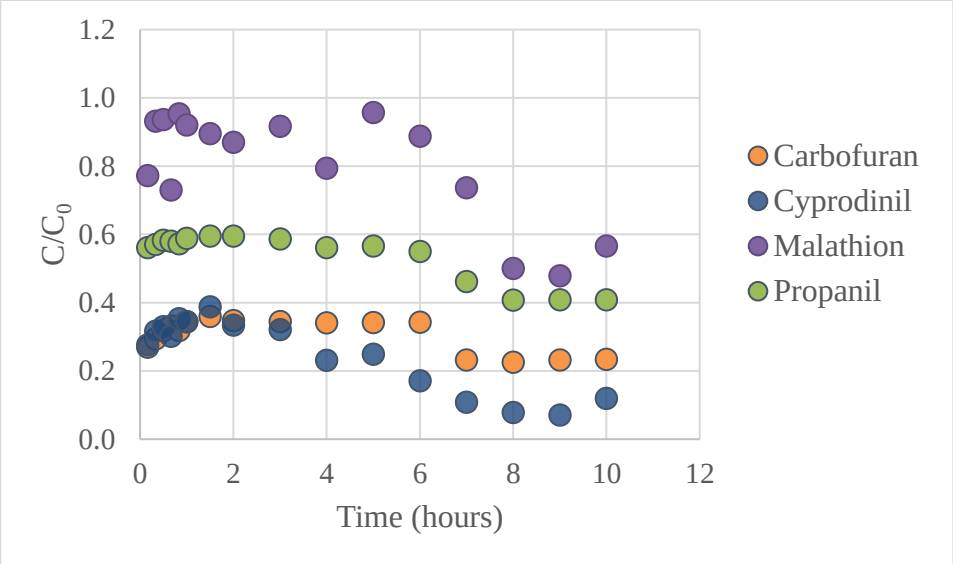


Figure 5.65. Experimental breakthrough curves of pesticides in case of ground BAC in an RSSCT (C_0 = 200 µg/L for each pesticide).

In the effluent the initially the C/C_0 ratios for both background NOM and pesticides were higher in the experiment with BAC compared to the experiment conducted with ground GAC without biofilm (as explained in the previous Section 5.5.7.). When GAC exhibits biological activity, its adsorption effectiveness is reduced, leading to a more rapid breakthrough. This outcome is expected due to the preloading of GAC pores with bacteria before to sustain microbial growth. This way the adsorption onto GAC may be reduced, leading to a more rapid breakthrough.

The presence of a biofilm may introduce diffusion limitations and increase competition for adsorption sites among background NOM, pesticides and attracted biomass, reducing removal efficiency. This phenomenon has been recorded in the literature (Rattier et al., 2012). Additionally, several studies have reported a decline in the adsorption capacity of GAC when biofilm formation occurs (Corwin & Summers, 2011; Rattier et al., 2012; Yu et al., 2009).

Despite these challenges, after some time the BAC column still achieved a reduction in pesticide concentrations in the effluent, demonstrating that biological activity can contribute to overall pesticide removal, even if adsorption efficiency is lower than in non-biological GAC systems.

Interestingly, the C/C_0 ratio decreased over time, suggesting that the adsorption performance of BAC improved as the experiment progressed. This phenomenon may be attributed to the higher affinity of pesticides and NOM for GAC compared to the preloaded materials occupying the pores. As time passes, weakly adsorbed organic matter initially occupying adsorption sites could have been displaced by stronger-binding compounds, allowing for increased pesticide retention. This behavior highlights the dynamic nature of adsorption in BAC systems and suggests that, despite its limitations, BAC can still exhibit effective pesticide removal over extended periods. However, further experimentation is necessary to fully understand and optimize its performance in such applications.

6. CONCLUSIONS

This study provides a comprehensive, data-driven analysis of pesticide adsorption and biodegradation, emphasizing the key factors influencing these processes, including adsorption kinetics, competitive effects, microbial degradation pathways, and their environmental impacts. The findings highlight the necessity of understanding these mechanisms to optimize pesticide removal through adsorption-based treatment strategies.

Kinetic adsorption experiments conducted on GAC revealed that the pseudo-second order (PSO) model best described pesticide adsorption, indicating that the adsorption rate is primarily controlled by the availability of surface sites on GAC. Additionally, the impact of GAC particle size was assessed, showing that finer GAC particles (100-125 μm) reached equilibrium significantly faster (24 hours) compared to non-ground GAC (1mm), which required 120 to 174 hours.

Batch isotherm experiments conducted under various conditions - including single pesticides and pesticide mixture systems, with and without background NOM – show that the Freundlich model provided a relatively better fit in most cases. Competitive adsorption was observed in multicomponent systems, where the presence of NOM or multiple pesticides reduced the adsorption capacities of individual compounds.

Biodegradation experiments, carried out using bacterial biomass cultivated from the Ömerli reservoir in a semi-continuously fed batch reactor (SCFB), confirmed the biodegradation of all pesticides along with background NOM. Among the tested compounds, propanil exhibited the highest biodegradation rate, with a high biodegradation rate constant (k_{biol} = 3.786 g_{MLVSS}^{-1}. d^{-1}).

To further assess pesticide adsorption under realistic conditions, a series of rapid small-scale column tests (RSSCTs) were performed. These tests examined the influence of factors such as GAC particle size, EBCT, and background NOM on adsorption performance. Results indicated that the constant diffusibility (CD) scaling approach in RSSCTs effectively preserved adsorption characteristics, with breakthrough times aligning with expected ratios when scaling from ground to non-ground GAC. Pesticides such as malathion and carbofuran exhibited faster breakthrough times due to their weaker adsorption affinities, while cyprodinil, chlorpyrifos, and propanil showed stronger adsorption with delayed breakthroughs. The presence of background NOM negatively affected adsorption performance.

Additionally, adsorption modeling using the AdDesignS software provided reliable predictions for adsorption behavior in monocomponent systems. However, its effectiveness is diminished when applied to multisolute systems. This limitation suggests that further optimization of the model's input parameters is needed to improve its ability to predict competitive behavior.

Overall, while batch isotherm experiments and AdDesignS modeling offered valuable insights into the adsorption behavior, experimental validation in continuous-flow systems remains essential for accurately assessing real-world adsorption dynamics. This study enhances the understanding of pesticide removal processes and provides guidance for optimizing GAC-based treatment systems in drinking water treatment applications.

7. FUTURE WORKS AND RECOMMENDATIONS

Based on the findings of this research, several key areas warrant further investigation and development:

1. Investigation of pH Effects: Conduct comprehensive studies on how pH variations affect the adsorption of pesticides and NOM by GAC. This research would help optimize treatment conditions and improve removal efficiency across different pH ranges.

2. Long-term Performance Studies: Extended studies on the long-term performance of GAC under various operational conditions, including multiple regeneration cycles, would provide valuable insights for practical applications.

3. Scale-up Studies: Pilot-scale studies can validate the laboratory findings and assess the feasibility of implementation in full-scale water treatment plants. These studies may include cost-benefit analyses and operational optimization studies.

4. Advanced Modeling and Simulation: Develop comprehensive mathematical models to predict pesticide behavior in multicomponent systems. These models would include both adsorption kinetics, competitive effects, and biodegradation processes, helping to optimize treatment design and operation.

5. Investigation of Pesticide Biodegradation Pathways and Metabolites: Further research is needed to identify and characterize the transformation products and metabolites formed during pesticide biodegradation. Understanding these pathways would help assess the potential environmental impacts of degradation products and optimize treatment strategies.

6. Advanced Bacterial Studies: Further research should focus on isolating and identifying specific bacterial strains responsible for pesticide degradation. This could lead to the development of more efficient biological treatment systems. Additionally, investigating the synergistic relationships between different bacterial communities, if there are any, could enhance biodegradation efficiency.

7. Alternative Treatment Technologies: Explore the integration of complementary treatment technologies, such as advanced oxidation processes or membrane filtration, with GAC adsorption and biodegradation to achieve more effective pesticide removal.

The conclusions drawn from this research provide insights into pesticide treatment processes, particularly regarding adsorption kinetics, competitive effects, and biodegradation. The recommendations for future work outline critical areas that require further investigation to enhance our understanding and improve treatment effectiveness.

These suggested research directions aim to bridge current knowledge gaps while advancing practical applications in water treatment facilities. By pursuing these recommendations, researchers and practitioners can work toward developing more efficient, sustainable, and economically viable solutions for pesticide removal from water sources.

REFERENCES

Aljerf, L., & AlMasri, N. (2018). Persistence and bioaccumulation of persistent organic pollutants (pops) in the soil and aquatic ecosystems: syrian frontiers in ecology and environment. *Sustainability in Environment*, *3*(4), 358. doi: 10.22158/SE.V3N4P358

Ando, N., Matsui, Y., Matsushita, T., & Ohno, K. (2011). Direct observation of solid-phase adsorbate concentration profile in powdered activated carbon particle to elucidate mechanism of high adsorption capacity on super-powdered activated carbon. *Water Research*, *45*(2), 761–767. doi: 10.1016/J.WATRES.2010.08.050

Arman, N. Z., Salmiati, S., Aris, A., Salim, M. R., Nazifa, T. H., Muhamad, M. S., & Marpongahtun, M. (2021). A Review on emerging pollutants in the water environment: existences, health effects and treatment processes. *Water*, *13*(22). doi: 10.3390/W13223258

Attia, A. A., Girgis, B. S., & Khedr, S. A. (2003). Capacity of activated carbon derived from pistachio shells by H3PO4 in the removal of dyes and phenolics. *Journal of Chemical Technology & Biotechnology*, *78*(6), 611–619. doi: 10.1002/JCTB.743

Ayranci, E., & Hoda, N. (2004). Adsorption of bentazon and propanil from aqueous solutions at the high area activated carbon-cloth. *Chemosphere*, *57*(8), 755–762. doi: 10.1016/j.chemosphere.2004.08.042

Ayranci, E., & Hoda, N. (2005). Adsorption kinetics and isotherms of pesticides onto activated carbon-cloth. *Chemosphere*, *60*(11), 1600–1607. doi: 10.1016/J.CHEMOSPHERE.2005.02.040

Ballard, B. D., & MacKay, A. A. (2005). Estimating the removal of anthropogenic organic chemicals from raw drinking water by coagulation flocculation. *Journal of Environmental Engineering*, *131*(1), 108–118. doi: 10.1061/(ASCE)0733-9372(2005)131:1(108)

Başpinar, H., Durmuşoğlu, E., & Mennan Yıldırım, E. (2010). Türkiye'de tarım ilaçları üretimi ve kullanımı. *Turkey Agricultural Engineering VII Technical Congress 15*.

Beaumelle, L., Tison, L., Eisenhauer, N., Hines, J., Malladi, S., Pelosi, C., … Phillips, H. R. P. (2023). Pesticide effects on soil fauna communities—A meta-analysis. *Journal of Applied Ecology*, *60*(7), 1239–1253. doi: 10.1111/1365-2664.14437

Beck, C. B. (1973). Physicochemical processes for water quality control, Walter J. Weber, Jr. (with eight contributors), Interscience, New York (1972). 640 pages. *AIChE Journal*, *19*(2), 413–413. doi: 10.1002/AIC.690190245

Bedia, J., Tasi´c, T. T., Milankovi´cmilankovi´c, V., Unterweger, C., Fürst, C., Breitenbach, S., … Lazarevi´clazarevi´c-Pašti, T. (2024). Highly porous cellulose-based carbon fibers as effective adsorbents for chlorpyrifos removal: Insights and applications. *C 2024, Vol. 10, Page 58*, *10*(3), 58. doi: 10.3390/C10030058

Bernal, V., Erto, A., Giraldo, L., & Moreno-Piraján, J. C. (2017). Effect of solution ph on the adsorption of paracetamol on chemically modified activated carbons. *Molecules : A Journal of Synthetic Chemistry and Natural Product Chemistry*, *22*(7), 1032. doi: 10.3390/MOLECULES22071032

Björk, J., Hanke, F., Palma, C. A., Samori, P., Cecchini, M., & Persson, M. (2010). Adsorption of aromatic and anti-aromatic systems on graphene through π-π Stacking. *Journal of Physical Chemistry Letters*, *1*(23), 3407–3412. doi: 10.1021/JZ101360K/SUPPL_FILE/JZ101360K_SI_001.PDF

Blachnio, M., Derylo-Marczewska, A., & Seczkowska, M. (2020). Influence of Pesticide Properties on Adsorption Capacity and Rate on Activated Carbon from Aqueous Solution. *Sorption in 2020s*. doi: 10.5772/INTECHOPEN.88726

Boethling, R. S., & Costanza, J. (2010). Domain of EPI suite biotransformation models. *SAR and QSAR in Environmental Research*, *21*(5–6), 415–443. doi: 10.1080/1062936X.2010.501816

Borrull, J., Colom, A., Fabregas, J., Borrull, F., & Pocurull, E. (2021). Presence, behaviour and removal of selected organic micropollutants through drinking water treatment. *Chemosphere*, *276*, 130023. doi: 10.1016/J.CHEMOSPHERE.2021.130023

Cantoni, B., Delli Compagni, R., Turolla, A., Epifani, I., & Antonelli, M. (2020). A statistical assessment of micropollutants occurrence, time trend, fate and human health risk using left-censored water quality data. *Chemosphere*, *257*, 127095. doi: 10.1016/J.CHEMOSPHERE.2020.127095

Cantoni, B., Turolla, A., Wellmitz, J., Ruhl, A. S., & Antonelli, M. (2021). Perfluoroalkyl substances (PFAS) adsorption in drinking water by granular activated carbon: Influence of activated carbon and PFAS characteristics. *Science of The Total Environment*, *795*, 148821. doi: 10.1016/J.SCITOTENV.2021.148821

Capel, P. D., Larson, S. J., & Winterstein, T. A. (2001). The behaviour of 39 pesticides in surface waters as a function of scale. *Hydrological Processes*, *15*(7), 1251–1269. doi: 10.1002/HYP.212

Caspi, R., Billington, R., Ferrer, L., Foerster, H., Fulcher, C. A., Keseler, I. M., … Karp, P. D. (2016). The MetaCyc database of metabolic pathways and enzymes and the BioCyc collection of pathway/genome databases. *Nucleic Acids Research*, *44*(D1), D471–D480. doi: 10.1093/NAR/GKV1164

Caspi, R., Billington, R., Keseler, I. M., Kothari, A., Krummenacker, M., Midford, P. E., … Karp, P. D. (2020). The MetaCyc database of metabolic pathways and enzymes - a 2019 update. *Nucleic Acids Research*, *48*(D1), D445–D453. doi: 10.1093/NAR/GKZ862

Çeçen, F., & Gül, G. (2021). Biodegradation of five pharmaceuticals: estimation by predictive models and comparison with activated sludge data. *International Journal of Environmental Science and Technology*, *18*(2), 327–340. doi: 10.1007/S13762-020-02820-Y/TABLES/5

Çeçen, Ferhan. (2024). Activated Carbon. *Kirk-Othmer Encyclopedia of Chemical Technology*, 1–32. doi: 10.1002/0471238961.0103200902011105.A01.PUB4

Çeçen, Ferhan, & Aktaş, Ö. (2011). Activated carbon for water and wastewater treatment: integration of adsorption and biological treatment. *Activated Carbon for Water and Wastewater Treatment: Integration of Adsorption and Biological Treatment*. doi: 10.1002/9783527639441

Çeçen, Ferhan, & Tezel, U. (2017). Hazardous pollutants in biological treatment systems: fundamentals and a guide to experimental research. *Water Intelligence Online*, *16*, 9781780407715. doi: 10.2166/9781780407715

Celso Gonçalves, A., Zimmermann, J., Schwantes, D., Tarley, C. R. T., Conradi Junior, E., Henrique Dias de Oliveira, V., … Ziemer, G. L. (2022). Renewable eco-friendly activated biochar from tobacco: kinetic, equilibrium and thermodynamics studies for chlorpyrifos removal. *Separation Science and Technology*, *57*(2), 159–179. doi: 10.1080/01496395.2021.1890776

Chemical pollution. (2024). Retrieved July 25, 2024, from https://www.theworldcounts.com/challenges/planet-earth/state-of-the-planet/chemical-pollution

Chen, S., Liu, C., Peng, C., Liu, H., Hu, M., & Zhong, G. (2012). Biodegradation of chlorpyrifos and its hydrolysis product 3,5,6-trichloro-2-pyridinol by a new fungal strain cladosporium cladosporioides Hu-01. *PLOS ONE*, *7*(10), e47205. doi: 10.1371/JOURNAL.PONE.0047205

Chen, Z., & Schäffer, A. (2016). The fate of the herbicide propanil in plants of the littoral zone of the Three Gorges Reservoir (TGR), China. *Journal of Environmental Sciences*, *48*, 24–33. doi: 10.1016/J.JES.2016.01.026

Chowdhury, Z. K. (2013). *Activated carbon : solutions for improving water quality*.

Christian, T., Schneider, R. J., Färber, H. A., Skutlarek, D., Meyer, M. T., & Goldbach, H. E. (2003). Determination of antibiotic residues in manure, soil, and surface waters. *Acta Hydrochimica et Hydrobiologica*, *31*(1), 36–44. doi: 10.1002/AHEH.200390014

Corwin, C. J., & Summers, R. S. (2011). Adsorption and desorption of trace organic contaminants from granular activated carbon adsorbers after intermittent loading and throughout backwash cycles. *Water Research*, *45*(2), 417–426. doi: 10.1016/J.WATRES.2010.08.039

Crapart, C., Andersen, T., Hessen, D. O., Valiente, N., & Vogt, R. D. (2021). Factors governing biodegradability of dissolved natural organic matter in lake water. *Water (Switzerland)*, *13*(16), 2210. doi: 10.3390/W13162210/S1

Crittenden, J. C., Hutzler, N. J., Geyer, D. G., Oravitz, J. L., Friedman, G., Crittenden, J. C., … Friedman, G. (1986). Transport of organic compounds with saturated groundwater flow: Model development and parameter sensitivity. *WRR*, *22*(3), 271–284. doi: 10.1029/WR022I003P00271

Crittenden, J. C., Reddy, P. S., Arora, H., Trynoski, J., Hand, D. W., Perram, D. L., & Summers, R. S. (1991). Predicting GAC performance with rapid small-scale column tests. *Journal - American Water Works Association*, *83*(1), 77–87. doi: 10.1002/J.1551-8833.1991.TB07088.X

Crittenden, J. C., Trussell, R. R., Hand, D. W., Howe, K. J., & Tchobanoglous, G. (2012). MWH's Water Treatment: Principles and Design: Third Edition. *MWH's Water Treatment: Principles and Design: Third Edition*. doi: 10.1002/9781118131473

Dabrowski, J. M., Peall, S. K. C., Van Niekerk, A., Reinecke, A. J., Day, J. A., & Schulz, R. (2002). Predicting runoff-induced pesticide input in agricultural sub-catchment surface waters: linking catchment variables and contamination. *Water Research*, *36*(20), 4975–4984. doi: 10.1016/S0043-1354(02)00234-8

Daneshvar, N., Aber, S., Khani, A., & Khataee, A. R. (2007). Study of imidaclopride removal from aqueous solution by adsorption onto granular activated carbon using an on-line spectrophotometric analysis system. *Journal of Hazardous Materials*, *144*(1–2), 47–51. doi: 10.1016/J.JHAZMAT.2006.09.081

De Ridder, D. J., Verliefde, A. R. D., Heijman, S. G. J., Verberk, J. Q. J. C., Rietveld, L. C., Van Der Aa, L. T. J., … Van Dijk, J. C. (2011). Influence of natural organic matter on equilibrium adsorption of neutral and charged pharmaceuticals onto activated carbon. *Water Science and Technology*, *63*(3), 416–423. doi: 10.2166/WST.2011.237

Dorota H. (2018). *The Possibility of Using UV Absorbance Measurements to Interpret the Results of Organic Matter Removal in the Biofiltration Process*.

Doulia, D., Leodopoulos, C., Gimouhopoulos, K., & Rigas, F. (2009). Adsorption of humic acid on acid-activated Greek bentonite. *Journal of Colloid and Interface Science*, *340*(2), 131–141. doi: 10.1016/J.JCIS.2009.07.028

Dubey, K. K., & Fulekar, M. H. (2012). Chlorpyrifos bioremediation in Pennisetum rhizosphere by a novel potential degrader Stenotrophomonas maltophilia MHF ENV20. *World Journal of Microbiology & Biotechnology*, *28*(4), 1715–1725. doi: 10.1007/S11274-011-0982-1

Ecobichon, D. J. (2001). Pesticide use in developing countries. *Toxicology*, *160*(1–3), 27–33. doi: 10.1016/S0300-483X(00)00452-2

EPA Federal Facilities Restoration, U., & Office, R. (2014). *Technical Fact Sheet – 1,2,3-Trichloropropane (TCP).*

Ettish, M. N., El-Sayyad, G. S., Elsayed, M. A., & Abuzalat, O. (2021). Preparation and characterization of new adsorbent from Cinnamon waste by physical activation for removal of Chlorpyrifos. *Environmental Challenges*, *5*, 100208. doi: 10.1016/J.ENVC.2021.100208

Farré, M. la, Pérez, S., Kantiani, L., & Barceló, D. (2008). Fate and toxicity of emerging pollutants, their metabolites and transformation products in the aquatic environment. *TrAC Trends in Analytical Chemistry*, *27*(11), 991–1007. doi: 10.1016/J.TRAC.2008.09.010

Faur, C., Métivier-Pignon, H., & Le Cloirec, P. (2005). Multicomponent adsorption of pesticides onto activated carbon fibers. *Adsorption*, *11*(5–6), 479–490. doi: 10.1007/S10450-005-5607-2

Fenner, K., Canonica, S., Wackett, L. P., & Elsner, M. (2013). Evaluating pesticide degradation in the environment: blind spots and emerging opportunities. *Science (New York, N.Y.)*, *341*(6147), 752–758. doi: 10.1126/SCIENCE.1236281

Freundlich isotherms - ECETOC. (2024). Technical Report 123: Freundlich isotherms. Retrieved September 7, 2024, from https://www.ecetoc.org/technical-report-123/measured-partitioning-property-data/adsorption-desorption-distribution-kd-and-organic-carbon-water-partition-koc-coefficients/freundlich-isotherms/

Galindo-Miranda, J. M., Guízar-González, C., Becerril-Bravo, E. J., Moeller-Chávez, G., León-Becerril, E., & Vallejo-Rodríguez, R. (2019). Occurrence of emerging contaminants in environmental surface waters and their analytical methodology – a review. *Water Supply*, *19*(7), 1871–1884. doi: 10.2166/WS.2019.087

Gao, J., Ellis, L. B. M., & Wackett, L. P. (2010). The University of Minnesota Biocatalysis/Biodegradation Database: improving public access. *Nucleic Acids Research*, *38*(Database issue). doi: 10.1093/NAR/GKP771

Gibert, Y., Sargis, R. M., & Nadal, A. (2019). Editorial: Endocrine disrupters and metabolism. *Frontiers in Endocrinology*, *10*, 506686. doi: 10.3389/FENDO.2019.00859/BIBTEX

Golovko, O., de Brito Anton, L., Cascone, C., Ahrens, L., Lavonen, E., & Köhler, S. J. (2020). sorption characteristics and removal efficiency of organic micropollutants in drinking water using granular activated carbon (GAC) in Pilot-Scale and Full-Scale Tests. *Water*, *12*(7), 2053. doi: 10.3390/w12072053

Guarnotta, V., Amodei, R., Frasca, F., Aversa, A., & Giordano, C. (2022). Impact of chemical endocrine disruptors and hormone modulators on the endocrine system. *International Journal of Molecular Sciences 2022, Vol. 23, Page 5710*, *23*(10), 5710. doi: 10.3390/IJMS23105710

Guo, W., Ngo, H. H., & Li, J. (2012). A mini-review on membrane fouling. *Bioresource Technology*, *122*, 27–34. doi: 10.1016/J.BIORTECH.2012.04.089

Guyton, K. Z., Loomis, D., Grosse, Y., El Ghissassi, F., Benbrahim-Tallaa, L., Guha, N., … Zeise, L. (2015). Carcinogenicity of tetrachlorvinphos, parathion, malathion, diazinon, and glyphosate. *The Lancet. Oncology*, *16*(5), 490–491. doi: 10.1016/S1470-2045(15)70134-8

Habila, M. A., ALOthman, Z. A., Al-Tamrah, S. A., Ghafar, A. A., & Soylak, M. (2015). Activated carbon from waste as an efficient adsorbent for malathion for detection and removal purposes. *Journal of Industrial and Engineering Chemistry*, *32*, 336–344. doi: 10.1016/J.JIEC.2015.09.009

Halsey, G. (1948). Physical adsorption on non-uniform surfaces. *The Journal of Chemical Physics*, *16*(10), 931–937. doi: 10.1063/1.1746689

Hamed, M. B., Burchacka, E., Angus, L., Marchand, A., De Geyter, J., Loos, M. S., … Economou, A. (2021). Effective small molecule antibacterials from a novel anti-protein secretion screen. *Microorganisms 2021, Vol. 9, Page 592*, *9*(3), 592. doi: 10.3390/MICROORGANISMS9030592

Hassler, J. W. (1963). *Activated carbon*. New York: Chemical Pub. Co.

Hopkins, Z. R., & Knappe, D. R. U. (2024). Predicting per- and polyfluoroalkyl substances removal in pilot-scale granular activated carbon adsorbers from rapid small-scale column tests. *AWWA Water Science*, *6*(2), e1369. doi: 10.1002/AWS2.1369

İSKİ. (2024). Retrieved August 23, 2024, from https://iski.istanbul/kurumsal/iski-tesisleri/icme-suyu-aritma-tesisleri/oemerli-icme-suyu-aritma-tesisleri/

Ibrahim, M., Nawaz, M. H., Rout, P. R., Lim, J. W., Mainali, B., & Shahid, M. K. (2023). Advances in produced water treatment technologies: an in-depth exploration with an emphasis on membrane-based systems and future perspectives. *Water 2023, Vol. 15, Page 2980*, *15*(16), 2980. doi: 10.3390/W15162980

Ike, I. A., Karanfil, T., Cho, J., & Hur, J. (2019). Oxidation byproducts from the degradation of dissolved organic matter by advanced oxidation processes – A critical review. *Water Research*, *164*, 114929. doi: 10.1016/J.WATRES.2019.114929

Iriarte-Velasco, U., Álvarez-Uriarte, J. I., Chimeno-Alaníc, N., & González-Velasco, J. R. (2008). Natural organic matter adsorption onto granular activated carbons: Implications in the molecular weight and disinfection byproducts formation. *Industrial and Engineering Chemistry Research*, *47*(20), 7868–7876. doi: 10.1021/IE800912Y

Islam, S. M. A., Math, R. K., Cho, K. M., Lim, W. J., Hong, S. Y., Kim, J. M., … Yun, H. D. (2010). Organophosphorus hydrolase (OpdB) of Lactobacillus brevis WCP902 from kimchi is able to degrade organophosphorus pesticides. *Journal of Agricultural and Food Chemistry*, *58*(9), 5380–5386. doi: 10.1021/JF903878E

Jatoi, A. S., Hashmi, Z., Adriyani, R., Yuniarto, A., Mazari, S. A., Akhter, F., & Mubarak, N. M. (2021). Recent trends and future challenges of pesticide removal techniques – A comprehensive review. *Journal of Environmental Chemical Engineering*, *9*(4), 105571. doi: 10.1016/J.JECE.2021.105571

Jin, P., Jin, X., Wang, X., Feng, Y., Wang, X. C., Jin, P., … Wang, X. C. (2013). Biological activated carbon treatment process for advanced water and wastewater treatment. *Biomass Now - Cultivation and Utilization*. doi: 10.5772/52021

Jocić, A., Breitenbach, S., Pašti, I. A., Unterweger, C., Fürst, C., & Lazarević-Pašti, T. (2022). Viscose-derived activated carbons as adsorbents for malathion, dimethoate, and chlorpyrifos-screening, trends, and analysis. *Environmental Science and Pollution Research International*, *29*(23), 35138–35149. doi: 10.1007/S11356-022-18721-1

Jusoh, A., Hartini, W. J. H., Ali, N., & Endut, A. (2011). Study on the removal of pesticide in agricultural run off by granular activated carbon. *Bioresource Technology*, *102*(9), 5312–5318. doi: 10.1016/J.BIORTECH.2010.12.074

Kanawi, E., Van Scoy, A. R., Budd, R., & Tjeerdema, R. S. (2016). Environmental fate and ecotoxicology of propanil: a review. *Toxicological & Environmental Chemistry*, *98*(7), 689–704. doi: 10.1080/02772248.2015.1133816

Katagi, T. (2010). Bioconcentration, bioaccumulation, and metabolism of pesticides in aquatic organisms. *Reviews of Environmental Contamination and Toxicology*, *204*, 1–132. doi: 10.1007/978-1-4419-1440-8_1

Kaur, H., Bansiwal, A., Hippargi, G., & Pophali, G. R. (2018). Effect of hydrophobicity of pharmaceuticals and personal care products for adsorption on activated carbon: Adsorption isotherms, kinetics and mechanism. *Environmental Science and Pollution Research International*, *25*(21), 20473–20485. doi: 10.1007/S11356-017-0054-7

Kennedy, A. M., Reinert, A. M., Knappe, D. R. U., Ferrer, I., & Summers, R. S. (2015). Full- and pilot-scale GAC adsorption of organic micropollutants. *Water Research*, *68*, 238–248. doi: 10.1016/J.WATRES.2014.10.010

Kennedy, A. M., & Summers, R. S. (2015). Effect of DOM size on organic micropollutant adsorption by GAC. *Environmental Science and Technology*, *49*(11), 6617–6624. doi: 10.1021/ACS.EST.5B00411/SUPPL_FILE/ES5B00411_SI_001.PDF

Kilduff, J. E., & Karanfil, T. (2002). Trichloroethylene adsorption by activated carbon preloaded with humic substances: effects of solution chemistry. *Water Research*, *36*(7), 1685–1698. doi: 10.1016/S0043-1354(01)00381-5

Kim, I. S., Ryu, J. Y., Hur, H. G., Gu, M. B., Kim, S. D., & Shim, J. H. (2004). Sphingomonas sp. strain SB5 degrades carbofuran to a new metabolite by hydrolysis at the furanyl ring. *Journal of Agricultural and Food Chemistry*, *52*(8), 2309–2314. doi: 10.1021/JF035502L

Knauf-Beiter, G., Dahmen, H., Heye, U., & Staub, T. (1995). Activity of cyprodinol: Optimal treatment timing and site of action. *Plant Disease*, *79*(11), 1098–1103. doi: 10.1094/PD-79-1098

Koresh, J. (1982). Study of molecular sieve carbons: The Langmuir modelin ultramicroporous adsorbents. *Journal of Colloid and Interface Science*, *88*(2), 398–406. doi: 10.1016/0021-9797(82)90268-5

Korshin, G., Chow, C. W. K., Fabris, R., & Drikas, M. (2009). Absorbance spectroscopy-based examination of effects of coagulation on the reactivity of fractions of natural organic matter with varying apparent molecular weights. *Water Research*, *43*(6), 1541–1548. doi: 10.1016/J.WATRES.2008.12.041

Koyama, Y., Fasaee, M. A. K., Berglund, E. Z., & Knappe, D. R. U. (2024). Machine learning models to predict early breakthrough of recalcitrant organic micropollutants in granular activated carbon adsorbers. *Environmental Science & Technology*. doi: 10.1021/ACS.EST.4C01316

Kremer, R. J., Kremer, R. J., & Keaster, A. J. (1992). Characterization and growth response of bacteria in soil following application of carbofuran. *Journal of Environmental Science and Health, Part B*, *27*(2), 139–154. doi: 10.1080/03601239209372771

Kumar, P., Singh, H., Kapur, M., & Mondal, M. K. (2014). Comparative study of malathion removal from aqueous solution by agricultural and commercial adsorbents. *Journal of Water Process Engineering*, *3*(C), 67–73. doi: 10.1016/J.JWPE.2014.05.010

Kumari, K., Singh, R. P., & Saxena, S. K. (1988). Adsorption thermodynamics of carbofuran on fly ash. *Colloids and Surfaces*, *33*(C), 55–61. doi: 10.1016/0166-6622(88)80048-9

Lee, C. L., Chin, K. L., H'ng, P. S., Hafizuddin, M. S., & Khoo, P. S. (2023). Activation temperature and particle size of palm kernel shell vs. the surface properties of activated carbon. *BioResources, 18*(1), 1714–1730. doi: 10.15376/BIORES.18.1.1714-1730

Levine, B. B., Madireddi, K., Lazarova, V., Stenstrom, M. K., & Suffet, I. H. (2000). Treatment of trace organic compounds by ozone–biological activated carbon for wastewater reuse: the lake Arrowhead pilot plant. *Water Environment Research, 72*(4), 388–396. doi: 10.2175/106143000X137914

Lewis, K. A., Tzilivakis, J., Warner, D. J., & Green, A. (2016). An international database for pesticide risk assessments and management. *Human and Ecological Risk Assessment: An International Journal, 22*(4), 1050–1064. doi: 10.1080/10807039.2015.1133242

Li, L., Quinlivan, P. A., & Knappe, D. R. U. (2002). Effects of activated carbon surface chemistry and pore structure on the adsorption of organic contaminants from aqueous solution. *Carbon, 40*(12), 2085–2100. doi: 10.1016/S0008-6223(02)00069-6

Li, Q., Snoeyink, V. L., Mariñas, B. J., & Campos, C. (2003). Pore blockage effect of NOM on atrazine adsorption kinetics of PAC: the roles of PAC pore size distribution and NOM molecular weight. *Water Research, 37*(20), 4863–4872. doi: 10.1016/J.WATRES.2003.08.018

Li, X., He, J., & Li, S. (2007). Isolation of a chlorpyrifos-degrading bacterium, Sphingomonas sp. strain Dsp-2, and cloning of the mpd gene. *Research in Microbiology, 158*(2), 143–149. doi: 10.1016/J.RESMIC.2006.11.007

Liang, C. H., Chiang, P. C., & Chang, E. E. (2007). Modeling the behaviors of adsorption and biodegradation in biological activated carbon filters. *Water Research, 41*(15), 3241–3250. doi: 10.1016/J.WATRES.2007.05.024

Liu, Y. (2008). New insights into pseudo-second-order kinetic equation for adsorption. *Colloids and Surfaces A: Physicochemical and Engineering Aspects, 320*(1–3), 275–278. doi: 10.1016/J.COLSURFA.2008.01.032

Lu, P., Li, Q., Liu, H., Feng, Z., Yan, X., Hong, Q., & Li, S. (2013). Biodegradation of chlorpyrifos and 3,5,6-trichloro-2-pyridinol by Cupriavidus sp. DT-1. *Bioresource Technology*, *127*, 337–342. doi: 10.1016/J.BIORTECH.2012.09.116

Luo, Y., Guo, W., Ngo, H. H., Nghiem, L. D., Hai, F. I., Zhang, J., … Wang, X. C. (2014). A review on the occurrence of micropollutants in the aquatic environment and their fate and removal during wastewater treatment. *Science of The Total Environment*, *473–474*, 619–641. doi: 10.1016/J.SCITOTENV.2013.12.065

Lyu, J., Yang, L., Zhang, L., Ye, B., & Wang, L. (2020). Antibiotics in soil and water in China–a systematic review and source analysis. *Environmental Pollution*, *266*, 115147. doi: 10.1016/J.ENVPOL.2020.115147

Mailler, R., Gasperi, J., Coquet, Y., Derome, C., Buleté, A., Vulliet, E., … Rocher, V. (2016). Removal of emerging micropollutants from wastewater by activated carbon adsorption: Experimental study of different activated carbons and factors influencing the adsorption of micropollutants in wastewater. *Journal of Environmental Chemical Engineering*, *4*(1), 1102–1109. doi: 10.1016/J.JECE.2016.01.018

Mansour, F., Al-Hindi, M., Yahfoufi, R., Ayoub, G. M., & Ahmad, M. N. (2017). The use of activated carbon for the removal of pharmaceuticals from aqueous solutions: a review. *Reviews in Environmental Science and Bio/Technology 2017 17:1*, *17*(1), 109–145. doi: 10.1007/S11157-017-9456-8

Matsui, Y., Knappe, D. R. U., & Takagi, R. (2002). Pesticide adsorption by granular activated carbon adsorbers. 1. effect of natural organic matter preloading on removal rates and model simplification. *Environmental Science and Technology*, *36*(15), 3426–3431. doi: 10.1021/ES0113652

Matsui, Y., Nakao, S., Sakamoto, A., Taniguchi, T., Pan, L., Matsushita, T., & Shirasaki, N. (2015). Adsorption capacities of activated carbons for geosmin and 2-methylisoborneol vary with activated carbon particle size: Effects of adsorbent and adsorbate characteristics. *Water Research*, *85*, 95–102. doi: 10.1016/J.WATRES.2015.08.017

McKinlay, R., Plant, J. A., Bell, J. N. B., & Voulvoulis, N. (2008). Endocrine disrupting pesticides: Implications for risk assessment. *Environment International*, *34*(2), 168–183. doi: 10.1016/J.ENVINT.2007.07.013

Meinel, F., Ruhl, A. S., Sperlich, A., Zietzschmann, F., & Jekel, M. (2015). Pilot-scale investigation of micropollutant removal with granular and powdered activated carbon. *Water, Air, and Soil Pollution*, *226*(1), 1–10. doi: 10.1007/S11270-014-2260-Y/METRICS

Memon, G., Bhanger, M. I., & Akhtar, M. (2007). The removal efficiency of chestnut shells for selected pesticides from aqueous solutions. *Journal of Colloid and Interface Science*, *315*(1), 33–40. doi: 10.1016/J.JCIS.2007.06.037

Merle, T., Knappe, D. R. U., Pronk, W., Vogler, B., Hollender, J., & Von Gunten, U. (2020). Assessment of the breakthrough of micropollutants in full-scale granular activated carbon adsorbers by rapid small-scale column tests and a novel pilot-scale sampling approach. *Environmental Science: Water Research & Technology*, *6*(10), 2742–2751. doi: 10.1039/D0EW00405G

Mertz, K., Gobin, F., Hand, D., Hokanson, D., & Crittenden, J. (1994). *Manual: Adsorption Design Software for Windows (ADdesignS)*.

MetaCyc carbofuran degradation II. (2024). Retrieved August 21, 2024, from https://metacyc.org/pathway?orgid=META&id=PWY-8287

MetaCyc chlorpyrifos degradation. (2024). Retrieved August 21, 2024, from https://metacyc.org/pathway?orgid=META&id=PWY-8065&detail-level=3

Miklos, D. B., Remy, C., Jekel, M., Linden, K. G., Drewes, J. E., & Hübner, U. (2018). Evaluation of advanced oxidation processes for water and wastewater treatment – A critical review. *Water Research*, *139*, 118–131. doi: 10.1016/J.WATRES.2018.03.042

Milanković, V., Tasić, T., Brković, S., Potkonjak, N., Unterweger, C., Pašti, I., & Lazarević-Pašti, T. (2024). The adsorption of chlorpyrifos and malathion under environmentally relevant conditions using biowaste carbon materials. *Journal of Hazardous Materials*, *480*, 135940. doi: 10.1016/J.JHAZMAT.2024.135940

Miller, D. G., Lee, C. M., & Rard, J. A. (2007). Ternary isothermal diffusion coefficients of NaCl-MgCl2-H 2O at 25°C. 7. seawater composition. *Journal of Solution Chemistry*, *36*(11–12), 1559–1567. doi: 10.1007/S10953-007-9207-5/METRICS

Mishra, S., Zhang, W., Lin, Z., Pang, S., Huang, Y., Bhatt, P., & Chen, S. (2020). Carbofuran toxicity and its microbial degradation in contaminated environments. *Chemosphere*, *259*. doi: 10.1016/J.CHEMOSPHERE.2020.127419

Musthofa, A. M. H., Syafila, M., & Helmy, Q. (2023). Effect of activated carbon particle size on methylene blue adsorption process in textile wastewater. *Indonesian Journal of Chemistry*, *23*(2), 461–474. doi: 10.22146/IJC.79784

Nam, S. W., Choi, D. J., Kim, S. K., Her, N., & Zoh, K. D. (2014). Adsorption characteristics of selected hydrophilic and hydrophobic micropollutants in water using activated carbon. *Journal of Hazardous Materials*, *270*, 144–152. doi: 10.1016/J.JHAZMAT.2014.01.037

Nelson, M. I., Alqahtani, R. T., & Hai, F. I. (2018). Mathematical modelling of the removal of organic micropollutants in the activated sludge process: a linear biodegradation model. *ANZIAM Journal*, *60*, 191. doi: 10.21914/ANZIAMJ.V60I0.12206

Nemeth-Konda, L., Füleky, G., Morovjan, G., & Csokan, P. (2002). Sorption behaviour of acetochlor, atrazine, carbendazim, diazinon, imidacloprid and isoproturon on Hungarian agricultural soil. *Chemosphere*, *48*(5), 545–552. doi: 10.1016/S0045-6535(02)00106-6

Newcombe, G., & Drikas, M. (1997). Adsorption of NOM onto activated carbon: Electrostatic and non-electrostatic effects. *Carbon*, *35*(9), 1239–1250. doi: 10.1016/S0008-6223(97)00078-X

Newcombe, Gayle. (1994). Activated carbon and soluble humic substances: Adsorption, desorption, and surface charge effects. *Journal of Colloid and Interface Science*, *164*(2), 452–462. doi: 10.1006/JCIS.1994.1188

Newcombe, Gayle, Drikas, M., & Hayes, R. (1997). Influence of characterised natural organic material on activated carbon adsorption: II. Effect on pore volume distribution and adsorption of 2-methylisoborneol. *Water Research*, *31*(5), 1065–1073. doi: 10.1016/S0043-1354(96)00325-9

Nguyen, T. P. O., De Mot, R., & Springael, D. (2015). Draft genome sequence of the carbofuran-mineralizing Novosphingobium sp. strain KN65.2. *Genome Announcements*, *3*(4). doi: 10.1128/GENOMEA.00764-15

Ninkovic, M. B., Petrovic, R. D., & Lausevic, M. D. (2010). Removal of organochlorine pesticides from water using virgin and regenerated granular activated carbon. *Journal of the Serbian Chemical Society*, *75*(4), 565–573. Retrieved from https://doaj.org/article/97099b7e9fbb4d26ab320ae02f41d087

NORMAN Network, Aalizadeh, R., Alygizakis, N., Schymanski, E., Slobodnik, J., Fischer, S., & Cirka, L. (2022). *S0 | SUSDAT | Mer*

Ormad, M. P., Miguel, N., Claver, A., Matesanz, J. M., & Ovelleiro, J. L. (2008). Pesticides removal in the process of drinking water production. *Chemosphere*, *71*(1), 97–106. doi: 10.1016/J.CHEMOSPHERE.2007.10.006

Pan, L., Nishimura, Y., Takaesu, H., Matsui, Y., Matsushita, T., & Shirasaki, N. (2017). Effects of decreasing activated carbon particle diameter from 30 μm to 140 nm on equilibrium adsorption capacity. *Water Research*, *124*, 425–434. doi: 10.1016/J.WATRES.2017.07.075

Park, M. R., Lee, S., Han, T., Oh, B., & Shim, J. (2006). A new intermediate in the degradation of carbofuran by Sphingomonas sp. strain SB5. *Journal of Microbiology and Biotechnology*.

Pathak, V. M., Verma, V. K., Rawat, B. S., Kaur, B., Babu, N., Sharma, A., … Cunill, J. M. (2022). Current status of pesticide effects on environment, human health and it's eco-friendly management as bioremediation: A comprehensive review. *Frontiers in Microbiology*, *13*, 962619. doi: 10.3389/FMICB.2022.962619

Pavan, M., & Worth, A. P. (2008). Review of estimation models for biodegradation. *QSAR & Combinatorial Science*, *27*(1), 32–40. doi: 10.1002/QSAR.200710117

Peiris, R. H., Budman, H., Moresoli, C., & Legge, R. L. (2013). Fouling control and optimization of a drinking water membrane filtration process with real-time model parameter adaptation using

fluorescence and permeate flux measurements. *Journal of Process Control*, *23*(1), 70–77. doi: 10.1016/J.JPROCONT.2012.10.001

Pelekani, C., & Snoeyink, V. L. (1999). Competitive adsorption in natural water: role of activated carbon pore size. *Water Research*, *33*(5), 1209–1219. doi: 10.1016/S0043-1354(98)00329-7

Peng, X., Zhang, J. S., Li, Y. Y., Li, W., Xu, G. M., & Yan, Y. C. (2008). Biodegradation of insecticide carbofuran by Paracoccus sp. YM3. *Journal of Environmental Science and Health, Part B*, *43*(7), 588–594. doi: 10.1080/03601230802234492

Pesticide Production vs Time Graph. (2017). Retrieved August 14, 2024, from https://scalar.usc.edu/works/engl205-07h-fall-2017/media/pesticide-production-vs-time-graph

Pesticide use per hectare of cropland, 2021- Our World in Data. (2024). Retrieved August 14, 2024, from https://ourworldindata.org/grapher/pesticide-use-per-hectare-of-cropland

Pesticides - Our World in Data. (2024). Retrieved July 26, 2024, from https://ourworldindata.org/pesticides

Pesticide Sales - Statistics | Eurostat. (2024). Retrieved July 26, 2024, from https://ec.europa.eu/eurostat/databrowser/view/aei_fm_salpest09/default/table?lang=en

Peyton, D. P., Healy, M. G., Fleming, G. T. A., Grant, J., Wall, D., Morrison, L., … Fenton, O. (2016). Nutrient, metal and microbial loss in surface runoff following treated sludge and dairy cattle slurry application to an Irish grassland soil. *Science of The Total Environment*, *541*, 218–229. doi: 10.1016/J.SCITOTENV.2015.09.053

Poddar, M., Brijesh Nair, A. N., & Mahindrakar, A. B. (2013). A review on the use of papid small scale column test (RSSCT) on predicting adsorption of various contaminants. *IOSR Journal Of Environmental Science*, *3*(1), 77. Retrieved from www.Iosrjournals.Org

Predieri, B., Iughetti, L., Bernasconi, S., & Street, M. E. (2022). Endocrine disrupting chemicals' effects in children: what we know and what we need to learn? *International Journal of Molecular Sciences 2022, Vol. 23, Page 11899*, *23*(19), 11899. doi: 10.3390/IJMS231911899

Qiao, K., Hu, T., Jiang, Y., Huang, J., Hu, J., Gui, W., … Zhu, G. (2021). Crosstalk of cholinergic pathway on thyroid disrupting effects of the insecticide chlorpyrifos in zebrafish (Danio rerio). *Science of The Total Environment*, *757*, 143769. doi: 10.1016/J.SCITOTENV.2020.143769

Quinlivan, P. A., Li, L., & Knappe, D. R. U. (2005). Effects of activated carbon characteristics on the simultaneous adsorption of aqueous organic micropollutants and natural organic matter. *Water Research*, *39*(8), 1663–1673. doi: 10.1016/J.WATRES.2005.01.029

Quintelas, C., Silva, B., Figueiredo, H., & Tavares, T. (2010). Removal of organic compounds by a biofilm supported on GAC: Modelling of batch and column data. *Biodegradation*, *21*(3), 379–392. doi: 10.1007/S10532-009-9308-5/FIGURES/6

Rattier, M., Reungoat, J., Gernjak, W., Keller, J., & Joss, A. (2012). Investigating the role of adsorption and biodegradation in the removal of organic micropollutants during biological activated carbon filtration of treated wastewater. *Journal of Water Reuse and Desalination*, *2*(3), 127–139. doi: 10.2166/WRD.2012.012

Reinert, A. M. (2013). *Granular activated carbon adsorption of micropollutants from surface water: field-scale adsorber performance and scale-up of bench-scale data.* North Carolina State Univertsity, North Carolina.

Roberts, D. W., Aptula, A., Schultz, T. W., Shen, J., Api, A. M., Bhatia, S., & Kromidas, L. (2015). A practical guidance for Cramer class determination. *Regulatory Toxicology and Pharmacology : RTP*, *73*(3), 971–984. doi: 10.1016/J.YRTPH.2015.09.017

Rodriguez-Narvaez, O. M., Peralta-Hernandez, J. M., Goonetilleke, A., & Bandala, E. R. (2017). Treatment technologies for emerging contaminants in water: A review. *Chemical Engineering Journal*, *323*, 361–380. doi: 10.1016/J.CEJ.2017.04.106

Rogers, H. R. (1996). Sources, behaviour and fate of organic contaminants during sewage treatment and in sewage sludges. *Science of The Total Environment*, *185*(1–3), 3–26. doi: 10.1016/0048-9697(96)05039-5

Rudzinski, W., & Plazinski, W. (2006). Kinetics of solute adsorption at solid/solution interfaces: a theoretical development of the empirical pseudo-first and pseudo-second order kinetic rate equations, based on applying the statistical rate theory of interfacial transport. *Journal of Physical Chemistry B*, *110*(33), 16514–16525. doi: 10.1021/JP061779N

Saleh, T. A. (2022). Kinetic models and thermodynamics of adsorption processes: classification. *Interface Science and Technology*, *34*, 65–97. doi: 10.1016/B978-0-12-849876-7.00003-8

Salih, H. H., Patterson, C. L., & Sorial, G. A. (2013). Comparative study on the implication of three nanoparticles on the removal of trichloroethylene by adsorption - The pilot and rapid small-scale column tests. *Water, Air, and Soil Pollution*, *224*(2). doi: 10.1007/S11270-012-1402-3

Salman, J. M., Abd, F. M., & Muhammed, A. A. (2011). Adsorption of carbofuran insecticide from aqueous solution using commercial activated carbon. *Int. J. Chem. Sci*, *9*(2), 557–564. Retrieved from www.sadgurupublications.com

Salman, J. M., & Hameed, B. H. (2010). Adsorption of 2,4-dichlorophenoxyacetic acid and carbofuran pesticides onto granular activated carbon. *Desalination*, *256*(1–3), 129–135. doi: 10.1016/J.DESAL.2010.02.002

Sambo, S. P., Marais, S. S., Msagati, T. A. M., Mamba, B. B., & Nkambule, T. T. I. (2020). Quantification of biodegradable natural organic matter (NOM) fractions and its impact on bacterial regrowth in a South African Water Treatment Plant. *Journal of Water Process Engineering*, *36*, 101332. doi: 10.1016/J.JWPE.2020.101332

Sampaio, E. F. S., Guimarães, V., Soares, O. S. G. P., Pereira, M. F. R., Rodrigues, C. S. D., & Madeira, L. M. (2022). Degradation of toluene from gas streams by heterogeneous fenton oxidation in a slurry bubble reactor with activated carbon-based catalysts. *Nanomaterials*, *12*(19), 3274. doi: 10.3390/NANO12193274/S1

Sangkarak, S., Phetrak, A., Kittipongvises, S., Kitkaew, D., Phihusut, D., & Lohwacharin, J. (2020). Adsorptive performance of activated carbon reused from household drinking water filter for hexavalent chromium-contaminated water. *Journal of Environmental Management*, *272*, 111085. doi: 10.1016/J.JENVMAN.2020.111085

Saravanan, A., Senthil Kumar, P., Jeevanantham, S., Karishma, S., Tajsabreen, B., Yaashikaa, P. R., & Reshma, B. (2021). Effective water/wastewater treatment methodologies for toxic pollutants removal: Processes and applications towards sustainable development. *Chemosphere*, *280*, 130595. doi: 10.1016/J.CHEMOSPHERE.2021.130595

Scharf, R. G., Johnston, R. W., Semmens, M. J., & Hozalski, R. M. (2010). Comparison of batch sorption tests, pilot studies, and modeling for estimating GAC bed life. *Water Research*, *44*(3), 769–780. doi: 10.1016/J.WATRES.2009.10.018

Schwarzenbach, R. P., Escher, B. I., Fenner, K., Hofstetter, T. B., Johnson, C. A., Von Gunten, U., & Wehrli, B. (2006). The challenge of micropollutants in aquatic systems. *Science*, *313*(5790), 1072–1077. doi: 10.1126/SCIENCE.1127291/ASSET/BECD692E-1426-4455-9ADD-4B7779A57C7A/ASSETS/GRAPHIC/313_1072_F1.JPEG

Servais, P., Billen, G., & Bouillot, P. (1994). Biological colonization of granular activated carbon filters in drinking-water treatment. *Journal of Environmental Engineering*, *120*(4), 888–899. doi: 10.1061/(ASCE)0733-9372(1994)120:4(888)

Sharma, A., Kumar, V., Shahzad, B., Tanveer, M., Preet Singh Sidhu, G., Handa, N., … Kumar Thukral, A. (2019). *Worldwide pesticide usage and its impacts on ecosystem*. doi: 10.1007/s42452-019-1485-1

Sharma, A., Kumar, V., Shahzad, B., Tanveer, M., Sidhu, G. P. S., Handa, N., … Thukral, A. K. (2019). Worldwide pesticide usage and its impacts on ecosystem. *SN Applied Sciences*, *1*(11), 1–16. doi: 10.1007/S42452-019-1485-1/TABLES/4

Shimabuku, K. K., Paige, J. M., Luna-Aguero, M., & Summers, R. S. (2017). Simplified modeling of organic contaminant adsorption by activated carbon and biochar in the presence of dissolved organic

matter and other competing adsorbates. *Environmental Science & Technology*, *51*(17), 10031–10040. doi: 10.1021/ACS.EST.7B00758

Sishu, F. K., Tilahun, S. A., Schmitter, P., Assefa, G., & Steenhuis, T. S. (2022). Pesticide contamination of surface and groundwater in an ethiopian highlands' watershed. *Water (Switzerland)*, *14*(21), 3446. doi: 10.3390/W14213446/S1

Smith, E. J., Davison, W., & Hamilton-Taylor, J. (2002). Methods for preparing synthetic freshwaters. *Water Research*, *36*(5), 1286–1296. doi: 10.1016/S0043-1354(01)00341-4

Sophia A., C., & Lima, E. C. (2018). Removal of emerging contaminants from the environment by adsorption. *Ecotoxicology and Environmental Safety*, *150*, 1–17. doi: 10.1016/J.ECOENV.2017.12.026

Sperlich, A., Harder, M., Zietzschmann, F., & Gnirss, R. (2017). Fate of trace organic compounds in granular activated carbon (gac) adsorbers for drinking water treatment. *Water*, *9*(7), 479. doi: 10.3390/w9070479

Speth, T. F. (1991). Evaluating capacities of gac preloaded with natural water. *Journal of Environmental Engineering*, *117*(1), 66–79. doi: 10.1061/(ASCE)0733-9372(1991)117:1(66)

Speth, T. F., & Miltner, R. J. (1990). Technical note: Adsorption capacity of gac for synthetic organics. *Journal - American Water Works Association*, *82*(2), 72–75. doi: 10.1002/J.1551-8833.1990.TB06922.X

Steffen, W., Richardson, K., Rockström, J., Cornell, S. E., Fetzer, I., Bennett, E. M., … Sörlin, S. (2015). Planetary boundaries: Guiding human development on a changing planet. *Science*, *347*(6223). doi: 10.1126/science.1259855

Stehle, S., & Schulz, R. (2015). Agricultural insecticides threaten surface waters at the global scale. *Proceedings of the National Academy of Sciences of the United States of America*, *112*(18), 5750–5755. doi: 10.1073/PNAS.1500232112

Stevenson, F. (1994). Humus chemistry: genesis, composition, reactions. *Humus Chemistry*, *72*(4), 512. Retrieved from https://www.wiley.com/en-us/Humus+Chemistry%3A+Genesis%2C+Composition%2C+Reactions%2C+2nd+Edition-p-9780471594741

Tagg, A. S., Brandes, E., Fischer, F., Fischer, D., Brandt, J., & Labrenz, M. (2022). Agricultural application of microplastic-rich sewage sludge leads to further uncontrolled contamination. *Science of The Total Environment*, *806*, 150611. doi: 10.1016/J.SCITOTENV.2021.150611

Taigbenu, A., & Liggett, J. A. (1986). An integral solution for the diffusion-advection equation. *Water Resources Research*, *22*(8), 1237–1246. doi: 10.1029/WR022I008P01237

Takam, B., Tarkwa, J. B., Acayanka, E., Nzali, S., Chesseu, D. M., Kamgang, G. Y., & Laminsi, S. (2020). Insight into the removal process mechanism of pharmaceutical compounds and dyes on plasma-modified biomass: the key role of adsorbate specificity. *Environmental Science and Pollution Research*, *27*(16), 20500–20515. doi: 10.1007/S11356-020-08536-3/METRICS

Teodosiu, C., Gilca, A. F., Barjoveanu, G., & Fiore, S. (2018). Emerging pollutants removal through advanced drinking water treatment: A review on processes and environmental performances assessment. *Journal of Cleaner Production*, *197*, 1210–1221. doi: 10.1016/J.JCLEPRO.2018.06.247

Ternes, T., & Joss, A. (2006). Human pharmaceuticals, hormones and fragrances - the challenge of micropollutants in urban water management. *Water Intelligence Online*, *5*(0), 9781780402468–9781780402468. doi: 10.2166/9781780402468

Tijani, J. O., Fatoba, O. O., Babajide, O. O., & Petrik, L. F. (2015). Pharmaceuticals, endocrine disruptors, personal care products, nanomaterials and perfluorinated pollutants: a review. *Environmental Chemistry Letters 2015 14:1*, *14*(1), 27–49. doi: 10.1007/S10311-015-0537-Z

Tiryaki, O. (2016). Pesticide residue analyses and researches carried out in Turkey. *Erciyes University Journal of the Institute of Science and Technology, 31(1),* 72-82.

Toğay, V. A., Yavuz Türel, G., Aşcı Çelik, D., Özgöçmen, M., Evgen Tülüceoğlu, E., Şen, İ., & Ayvaz, Y. (2021). DNA damage effect of cyprodinil and thiacloprid in adult zebrafish gills. *Environmental*

Science and Pollution Research, *28*(12), 14482–14487. doi: 10.1007/S11356-020-11668-1/METRICS

Tomasek, P. H., & Karns, J. S. (1989). Cloning of a carbofuran hydrolase gene from Achromobacter sp. strain WM111 and its expression in gram-negative bacteria. *Journal of Bacteriology*, *171*(7), 4038–4044. doi: 10.1128/JB.171.7.4038-4044.1989

Tomaszewski, J. E., Werner, D., & Luthy, R. G. (2007). Activated carbon amendment as a treatment for residual DDT in sediment from a superfund site in San Francisco Bay, Richmond, California, USA. *Environmental Toxicology and Chemistry*, *26*(10), 2143–2150. doi: 10.1897/07-179R.1

Toosi, E. R., Clinton, P. W., Beare, M. H., & Norton, D. A. (2012). Biodegradation of soluble organic matter as affected by land-use and soil depth. *Soil Science Society of America Journal*, *76*(5), 1667–1677. doi: 10.2136/SSSAJ2011.0437

Tröger, R., Köhler, S. J., Franke, V., Bergstedt, O., & Wiberg, K. (2020). A case study of organic micropollutants in a major Swedish water source – Removal efficiency in seven drinking water treatment plants and influence of operational age of granulated active carbon filters. *Science of The Total Environment*, *706*, 135680. doi: 10.1016/J.SCITOTENV.2019.135680

Velinov, N., Mitrović, J., Kostić, M., Radović, M., Petrović, M., Bojić, D., & Bojić, A. (2019). Wood residue reuse for a synthesis of lignocellulosic biosorbent: characterization and application for simultaneous removal of copper (II), Reactive Blue 19 and cyprodinil from water. *Wood Science and Technology*, *53*(3), 619–647. doi: 10.1007/S00226-019-01093-0/TABLES/4

Velten, S., Knappe, D. R. U., Traber, J., Kaiser, H. P., von Gunten, U., Boller, M., & Meylan, S. (2011). Characterization of natural organic matter adsorption in granular activated carbon adsorbers. *Water Research*, *45*(13), 3951–3959. doi: 10.1016/J.WATRES.2011.04.047

Vig, N. J. (1988). Pesticides and politics: the life cycle of a public issue. By Christopher J. Bosso (Pittsburgh: University of Pittsburgh Press, 1987. xvi, 294p. *American Political Science Review*, *82*(3), 985–986. doi: 10.2307/1962513

Wang, Z., Walker, G. W., Muir, D. C. G., & Nagatani-Yoshida, K. (2020). Toward a global understanding of chemical pollution: a first comprehensive analysis of national and regional chemical inventories. *Environmental Science and Technology*, *54*(5), 2575–2584. doi: 10.1021/ACS.EST.9B06379/ASSET/IMAGES/LARGE/ES9B06379_0002.JPEG

Westerhoff, P. K., Benn, T. M., Chen, A. S. C., Wang, L., Cumming, L. J., & Columbus, B. (2008). *US EPA Assessing Arsenic Removal by Metal (Hydr)Oxide Adsorptive Media Using Rapid Small Scale Column Tests April 2008*.

WHO. (2017). Guidelines for drinking-water quality, 4th edition, incorporating the 1st addendum. Geneva: World Health Organization. Geneva, Switzerland. *World Health Organization*. Retrieved from https://www.who.int/publications/i/item/9789241549950

Worch, E. (2021). Adsorption technology in water treatment. *Adsorption Technology in Water Treatment*. doi: 10.1515/9783110715507/HTML

Wu, C. H., Kuo, C. Y., Lin, C. F., & Lo, S. L. (2002). Modeling competitive adsorption of molybdate, sulfate, selenate, and selenite using a Freundlich-type multi-component isotherm. *Chemosphere*, *47*(3), 283–292. doi: 10.1016/S0045-6535(01)00217-X

Xiao, X., Li, F., Huang, J., Sheng, G. D., & Qiu, Y. (2012). Reduced adsorption of propanil to black carbon: Effect of dissolved organic matter loading mode and molecule size. *Environmental Toxicology and Chemistry*, *31*(6), 1187–1193. doi: 10.1002/ETC.1800

Yadav, M., Shukla, A. K., Srivastva, N., Nath, S., Suresh, U. &, Dubey, K., … Dubey, S. K. (2016). Utilization of microbial community potential for removal of chlorpyrifos: a review. *Critical Reviews in Biotechnology*, *36*(4), 727–742. doi: 10.3109/07388551.2015.1015958

Yahia, M. S., Elzaref, A. S., Awad, M. B., Tony, A. M., & Elfeky, A. S. (2022). Efficient adsorption of chlorpyrifos onto modified activated carbon by gamma irradiation; A plausible adsorption mechanism. *Zeitschrift Fur Physikalische Chemie*, *236*(1), 1–25. doi: 10.1515/ZPCH-2020-1765/MACHINEREADABLECITATION/RIS

Yan, X., Jin, W., Wu, G., Jiang, W., Yang, Z., Ji, J., … Hong, Q. (2018). Hydrolase CehA and monooxygenase CfdC are responsible for carbofuran degradation in Sphingomonas sp. strain CDS-1. *Applied and Environmental Microbiology*, *84*(16). doi: 10.1128/AEM.00805-18

Yang, C. H. (1993). Statistical mechanical aspects of adsorption systems obeying the Temkin isotherm. *Journal of Physical Chemistry*, *97*(27), 7097–7101. doi: 10.1021/J100129A029/ASSET/J100129A029.FP.PNG_V03

Yang, C., Liu, N., Guo, X., & Qiao, C. (2006). Cloning of mpd gene from a chlorpyrifos-degrading bacterium and use of this strain in bioremediation of contaminated soil. *FEMS Microbiology Letters*, *265*(1), 118–125. doi: 10.1111/J.1574-6968.2006.00478.X

Yang, K., & Fox, J. T. (2018). Adsorption of humic acid by acid-modified granular activated carbon and powder activated carbon. *Journal of Environmental Engineering*, *144*(10), 04018104. doi: 10.1061/(ASCE)EE.1943-7870.0001390

Yang, Y., Ok, Y. S., Kim, K. H., Kwon, E. E., & Tsang, Y. F. (2017). Occurrences and removal of pharmaceuticals and personal care products (PPCPs) in drinking water and water/sewage treatment plants: A review. *Science of The Total Environment*, *596–597*, 303–320. doi: 10.1016/J.SCITOTENV.2017.04.102

Yapsaklı, Kozet. (2008). *Application of biological activated carbon (BAC) in drinking water treatment*. Retrieved from http://digitalarchive.boun.edu.tr/handle/123456789/19489

Yu, Z., Peldszus, S., & Huck, P. M. (2009). Adsorption of selected pharmaceuticals and an endocrine disrupting compound by granular activated carbon. 1. Adsorption capacity and kinetics. *Environmental Science and Technology*, *43*(5), 1467–1473. doi: 10.1021/ES801961Y/SUPPL_FILE/ES801961Y_SI_001.PDF

Yuan, J., Fox, F., Crowe, G., Mortazavian, S., Passeport, E., & Hofmann, R. (2022). Is in-service granular activated carbon biologically active? an evaluation of alternative experimental methods to distinguish adsorption and biodegradation in GAC. *Environmental Science and Technology*, *56*(22), 16125–16133. doi: 10.1021/ACS.EST.2C03639/SUPPL_FILE/ES2C03639_SI_001.PDF

Zahan, T., Rahman, M. M., Hashem, A., Bell, R. W., & Begum, M. (2017). Performance of pre- and post-emergence herbicides in strip tillage Non-puddled transplanted Aman rice. *Bangladesh Journal of Agricultural Research*, *42*(4), 631–646. doi: 10.3329/BJAR.V42I4.35791

Zhang, J., Sun, J. Q., Yuan, Q. Y., Li, C., Yan, X., Hong, Q., & Li, S. P. (2011). Characterization of the propanil biodegradation pathway in Sphingomonas sp. Y57 and cloning of the propanil hydrolase gene prpH. *Journal of Hazardous Materials*, *196*, 412–419. doi: 10.1016/J.JHAZMAT.2011.09.040

Zhao, C., Wang, Y., Zhao, R., & Jiang, J. (2022). Removal of bisphenol S from drinking water by adsorption using activated carbon and the mechanisms involved. *International Journal of Environmental Science and Technology*, *19*(6), 5289–5300. doi: 10.1007/S13762-021-03446-4/METRICS

Zhou, L., Zhou, Y., Tang, X., Zhang, Y., & Jeppesen, E. (2021). Biodegradable dissolved organic carbon shapes bacterial community structures and co-occurrence patterns in large eutrophic Lake Taihu. *Journal of Environmental Sciences*, *107*, 205–217. doi: 10.1016/J.JES.2021.02.011

Zieliński, B., Miądlicki, P., & Przepiórski, J. (2022). Development of activated carbon for removal of pesticides from water: case study. *Scientific Reports 2022 12:1*, *12*(1), 1–14. doi: 10.1038/s41598-022-25247-6

Zietzschmann, F., Stützer, C., & Jekel, M. (2016). Granular activated carbon adsorption of organic micro-pollutants in drinking water and treated wastewater – Aligning breakthrough curves and capacities. *Water Research*, *92*, 180–187. doi: 10.1016/j.watres.2016.01.056

APPENDIX A: EXPERIMENTS ON ADSORPTION KINETICS

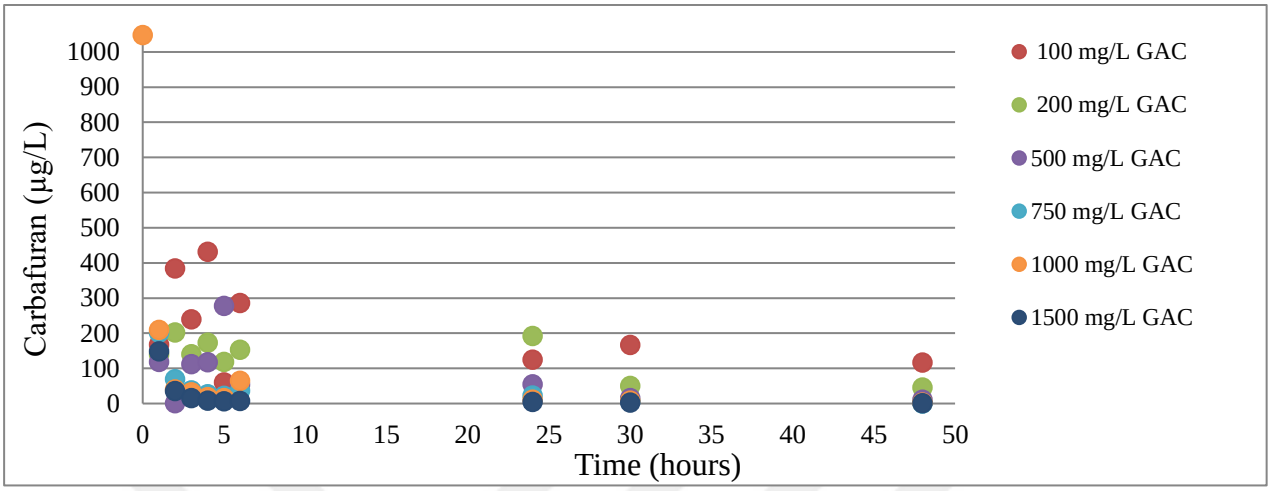


Figure A.1. Adsorption kinetics of carbofuran in pesticide mixture + ground GAC experiments.

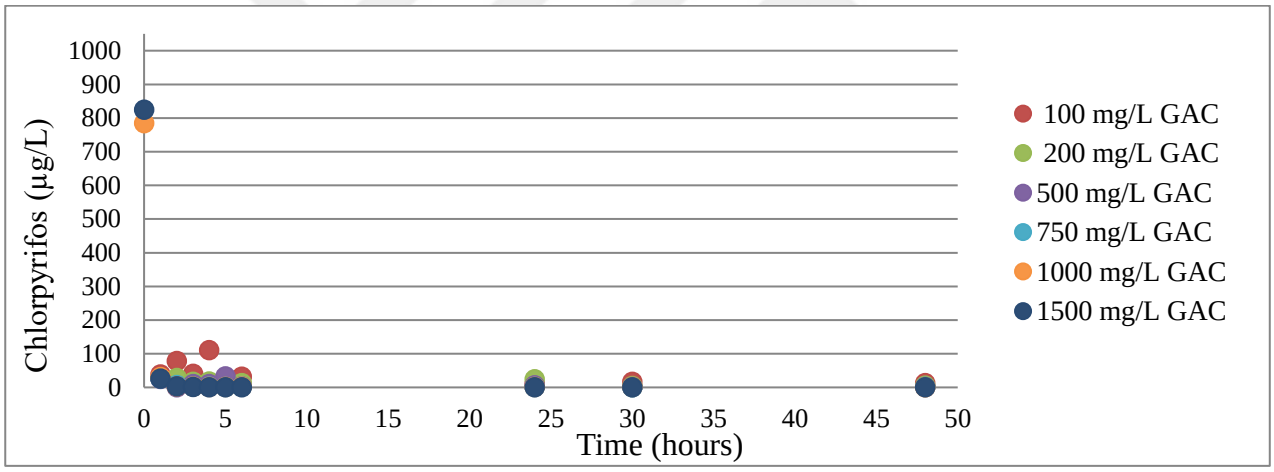


Figure A.2. Adsorption kinetics of chlorpyrifos in pesticide mixture + ground GAC experiments.

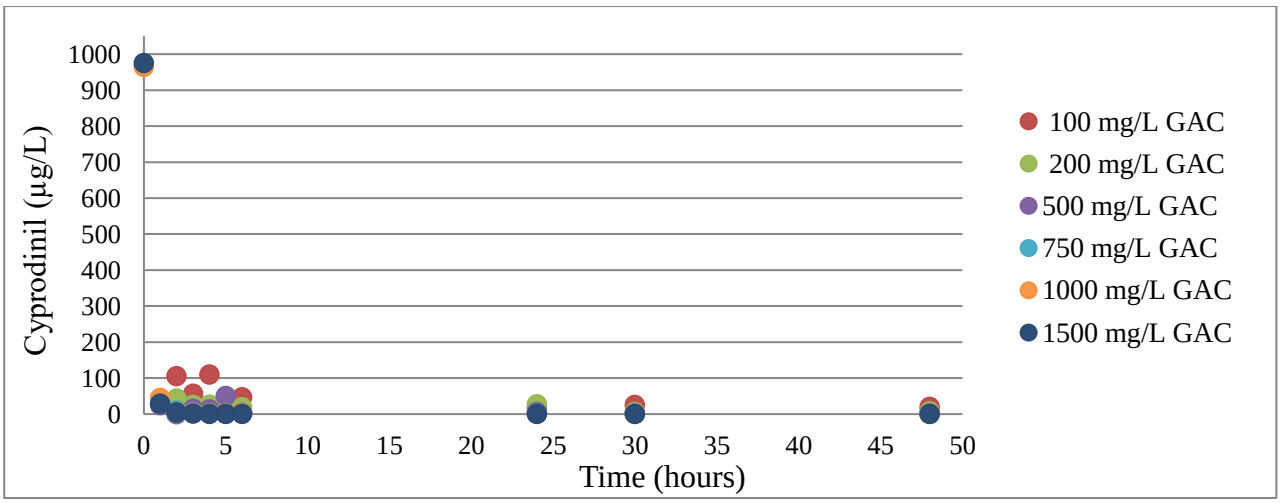


Figure A.3. Adsorption kinetics of cyprodinil in pesticide mixture + ground GAC experiments.

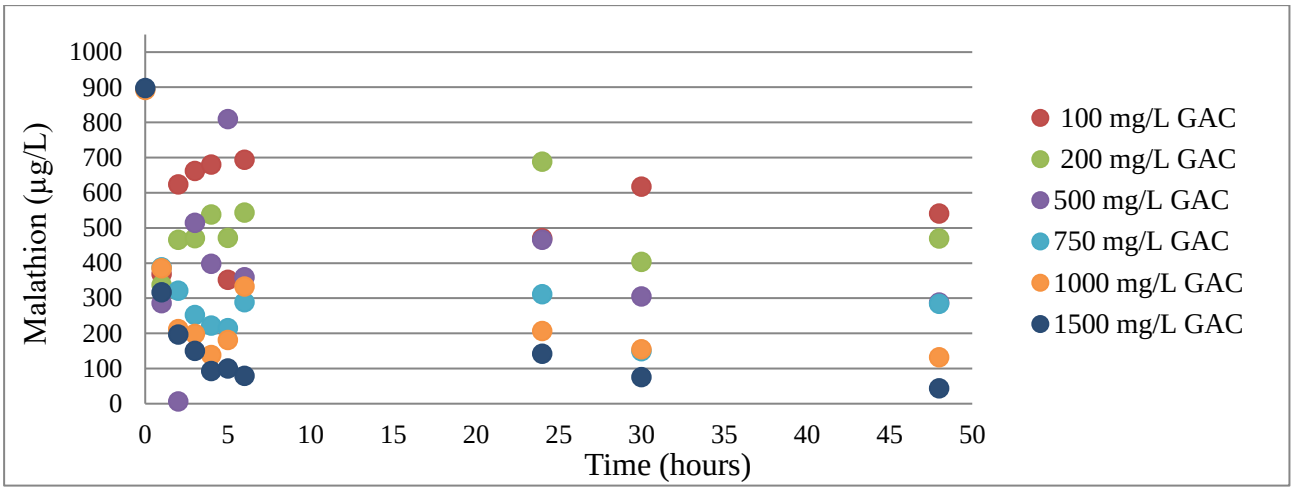


Figure A.4. Adsorption kinetics of malathion in pesticide mixture + ground GAC experiments.

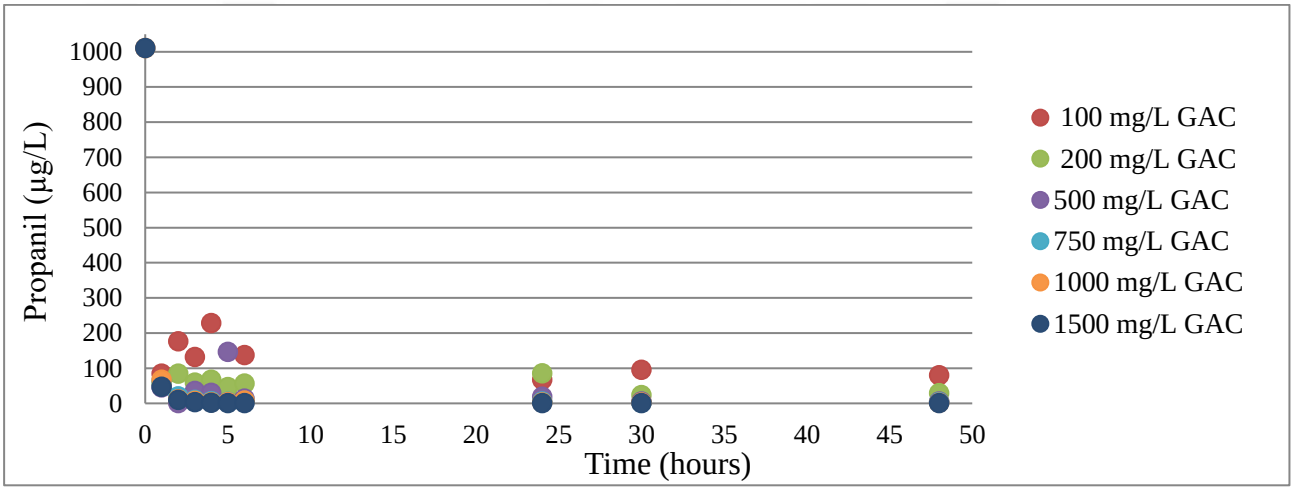


Figure A.5. Adsorption kinetics of propanil in pesticide mixture + ground GAC experiments.

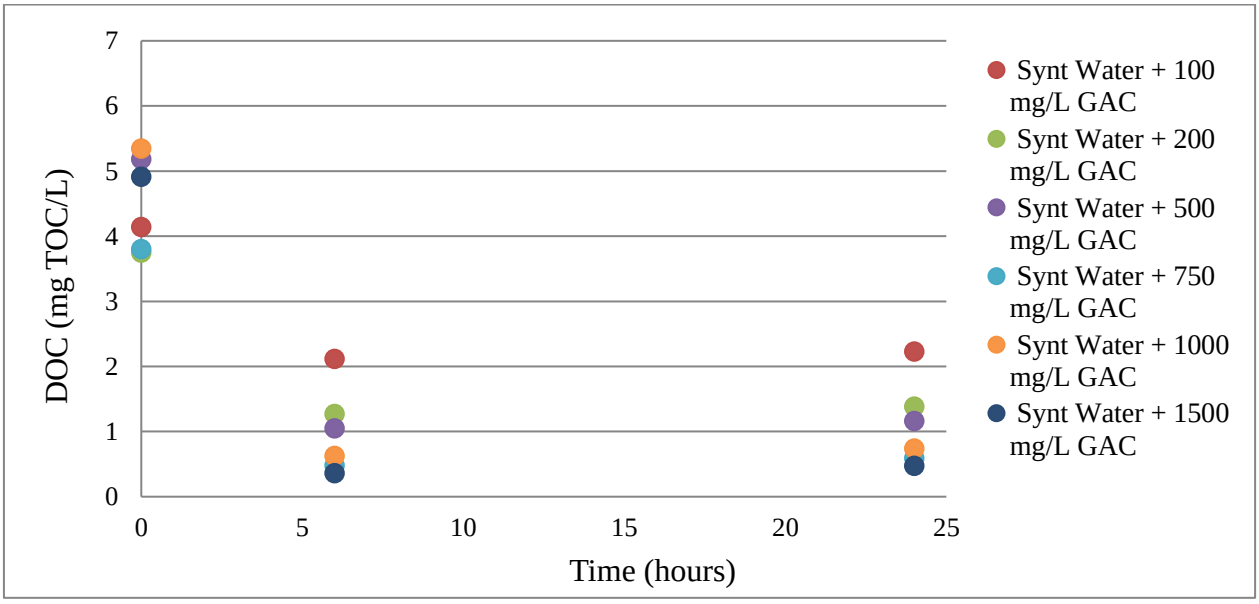


Figure A.6. Adsorption kinetics of DOC in background NOM + ground GAC experiments.

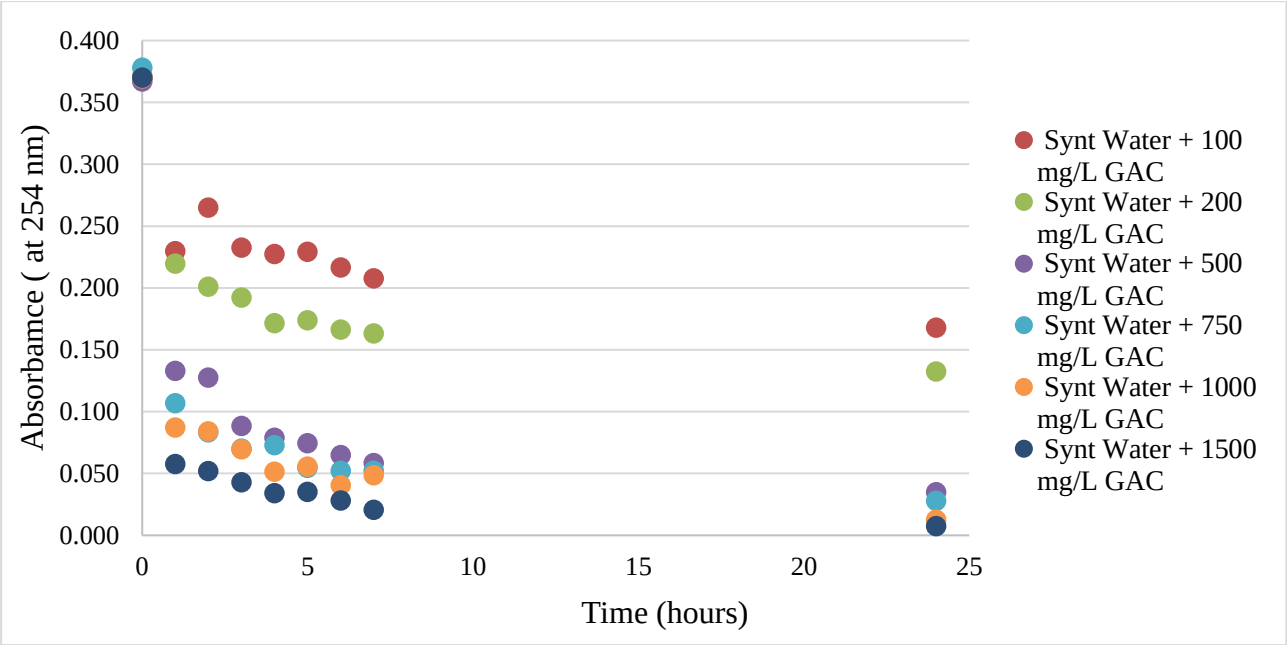


Figure A.7. Kinetics of organic substance removal: UV_{254} absorbance decay in background NOM + ground GAC experiments.

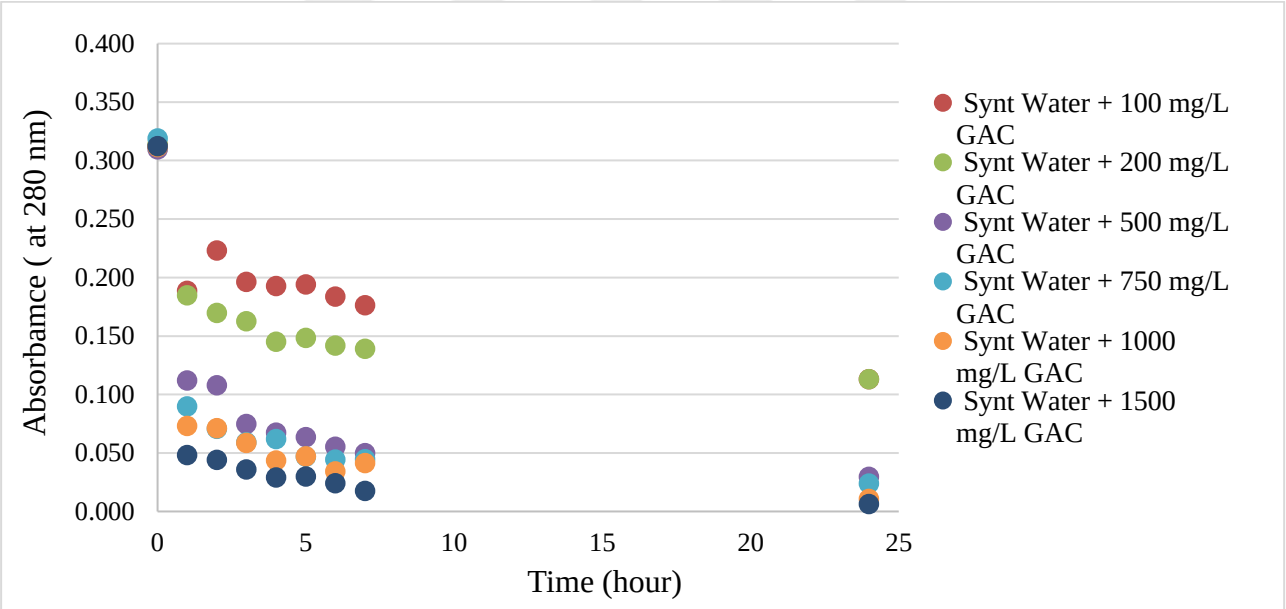


Figure A.8. Kinetics of organic substance removal: UV_{280} absorbance decay in background NOM + ground GAC experiments.

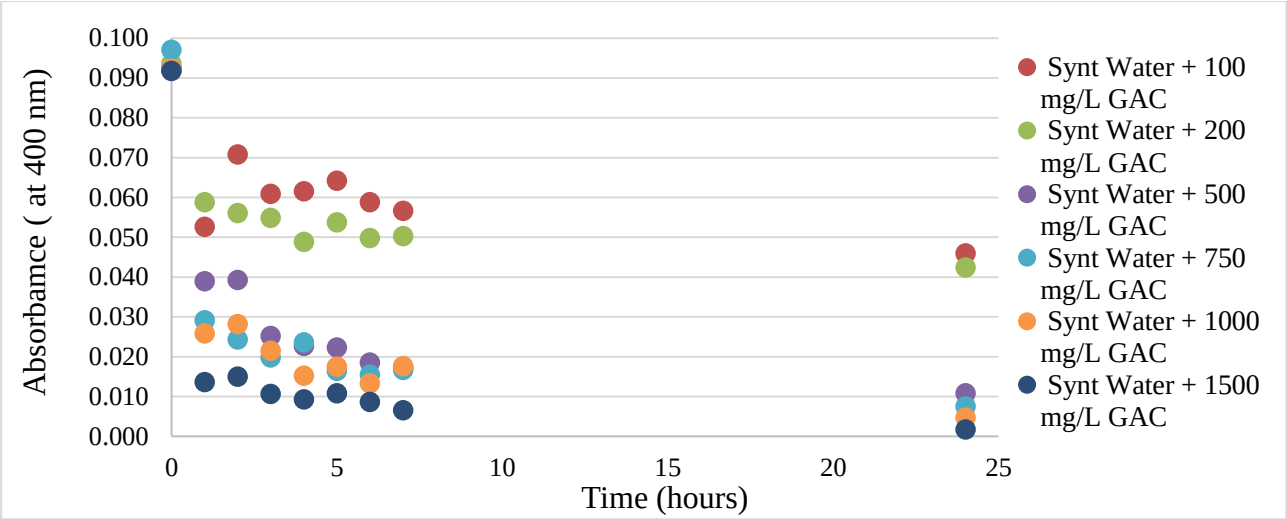


Figure A.9. Kinetics of organic substance removal: $Color_{400}$ absorbance decay in background NOM + ground GAC experiments.

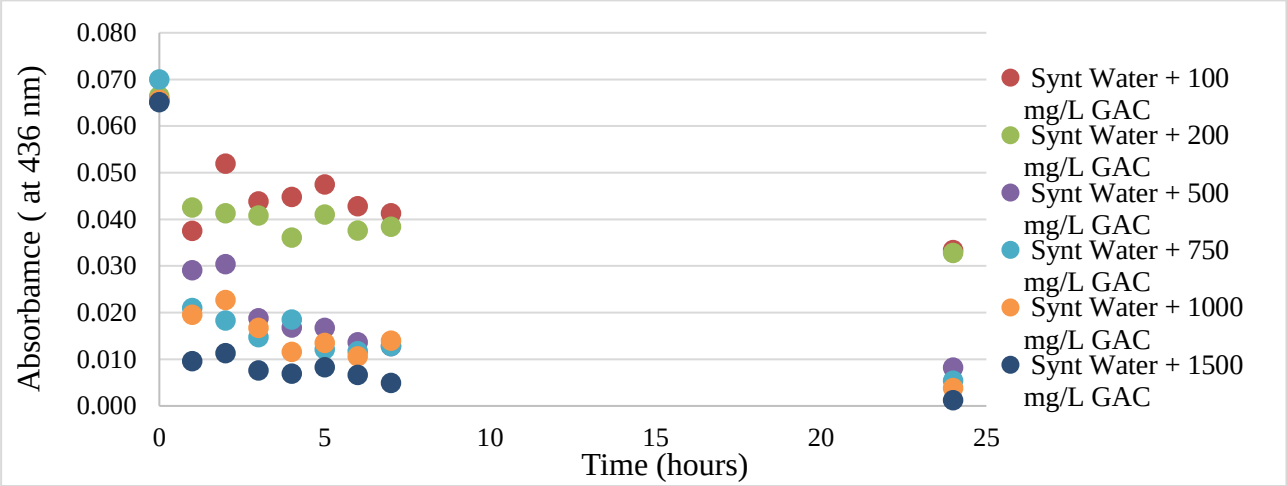


Figure A.10. Kinetics of organic substance removal: $Color_{436}$ absorbance decay in background NOM + ground GAC experiments.

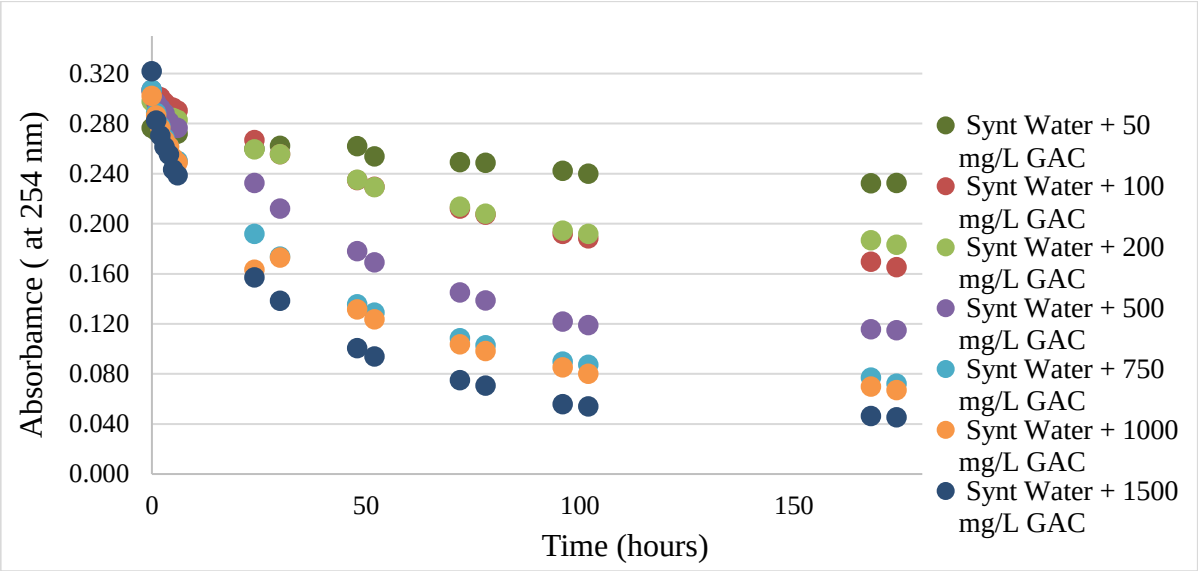


Figure A.11. Kinetics of organic substance removal: UV_{254} absorbance decay in background NOM + non-ground GAC experiments.

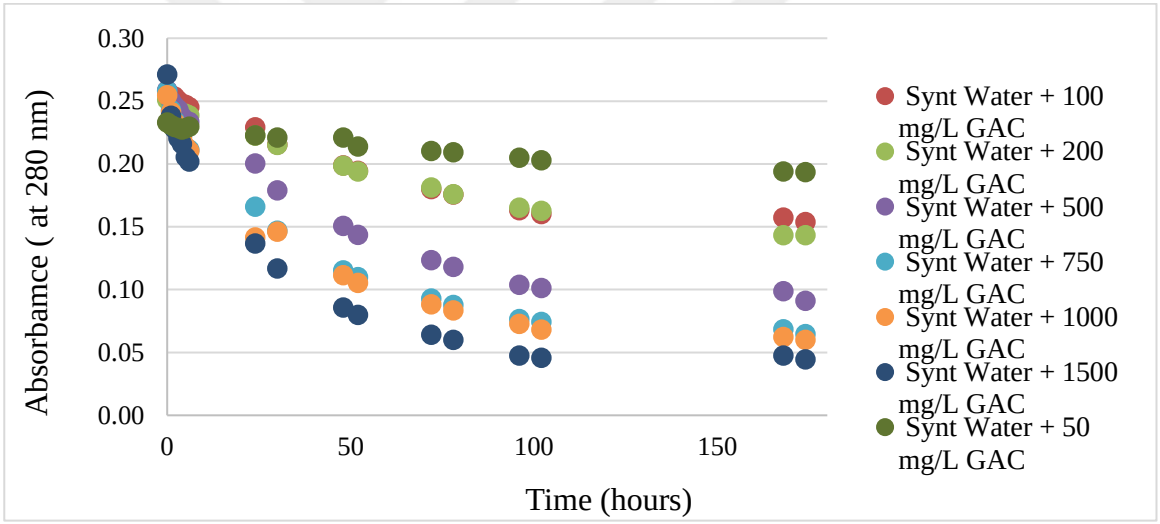


Figure A.12. Kinetics of organic substance removal: UV_{280} absorbance decay in background NOM + non-ground GAC experiments.

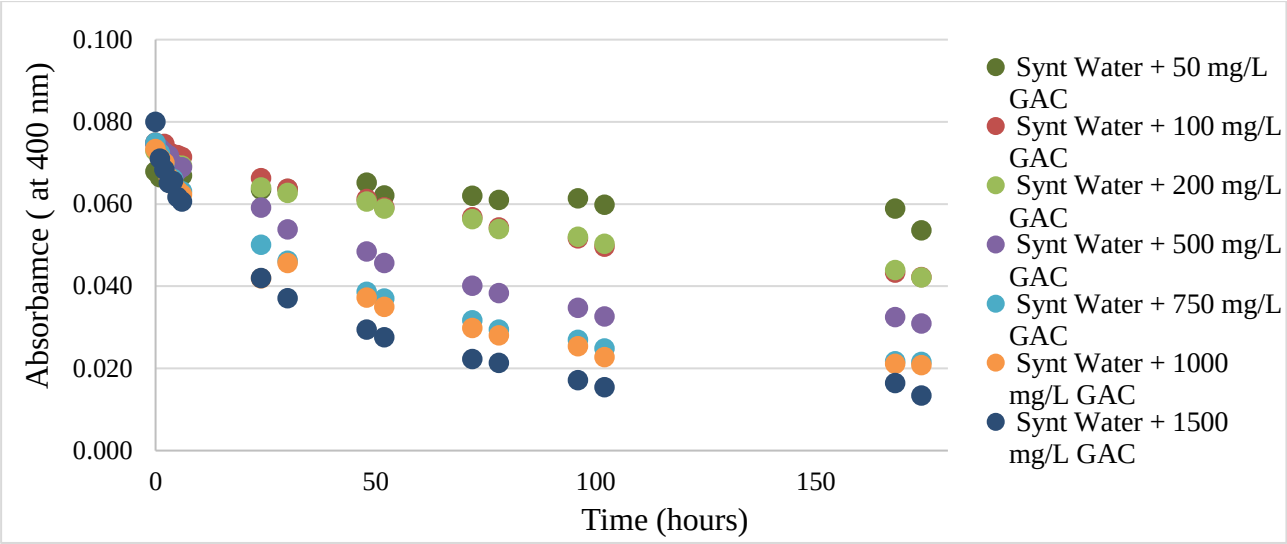


Figure A.13. Kinetics of organic substance removal: $Color_{400}$ absorbance decay in background NOM + non-ground GAC experiments.

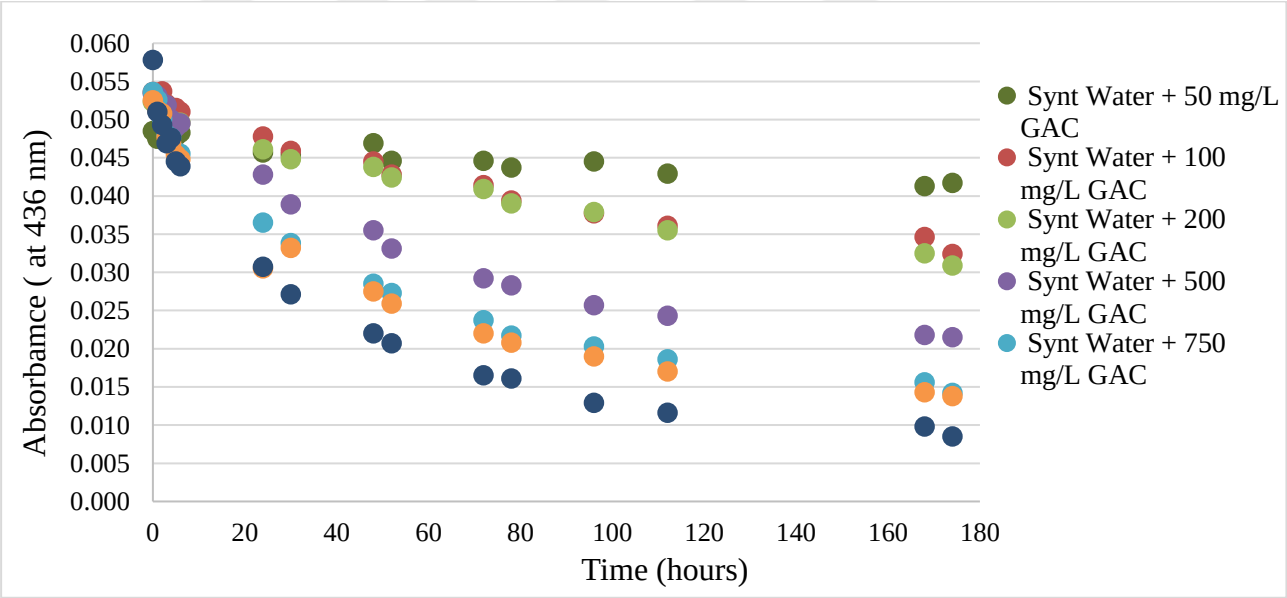


Figure A.14. Kinetics of organic substance removal: $Color_{436}$ absorbance decay in background NOM + non-ground GAC experiments.

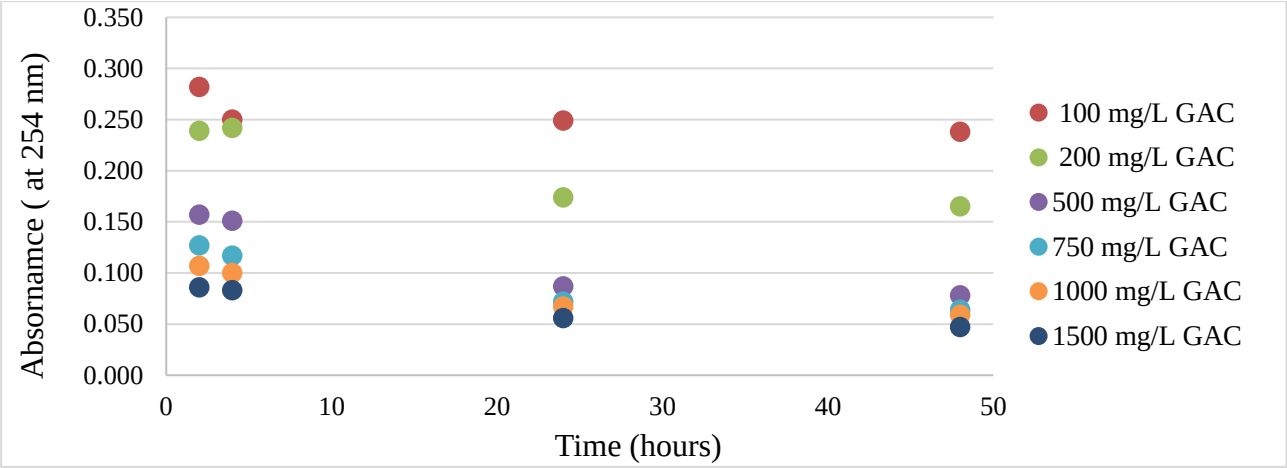


Figure A.15. Kinetics of organic substance removal: UV_{254} absorbance decay in background NOM + pesticide mixture + ground GAC experiments.

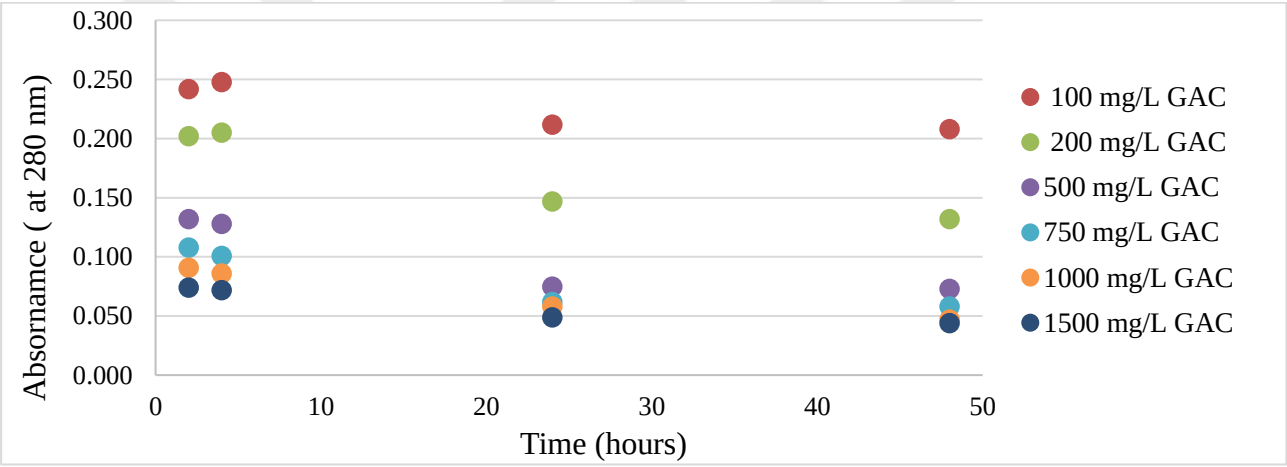


Figure A.16. Kinetics of organic substance removal: UV_{280} absorbance decay in background NOM + pesticide mixture + ground GAC experiments.

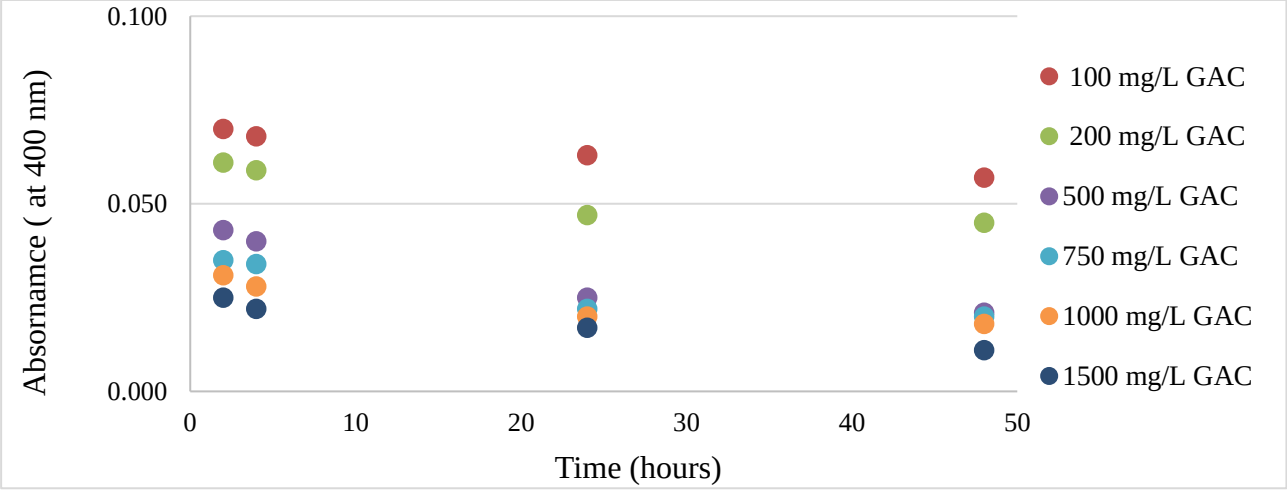


Figure A.17. Kinetics of organic substance removal: $Color_{400}$ absorbance decay in background NOM + pesticide mixture + ground GAC experiments.

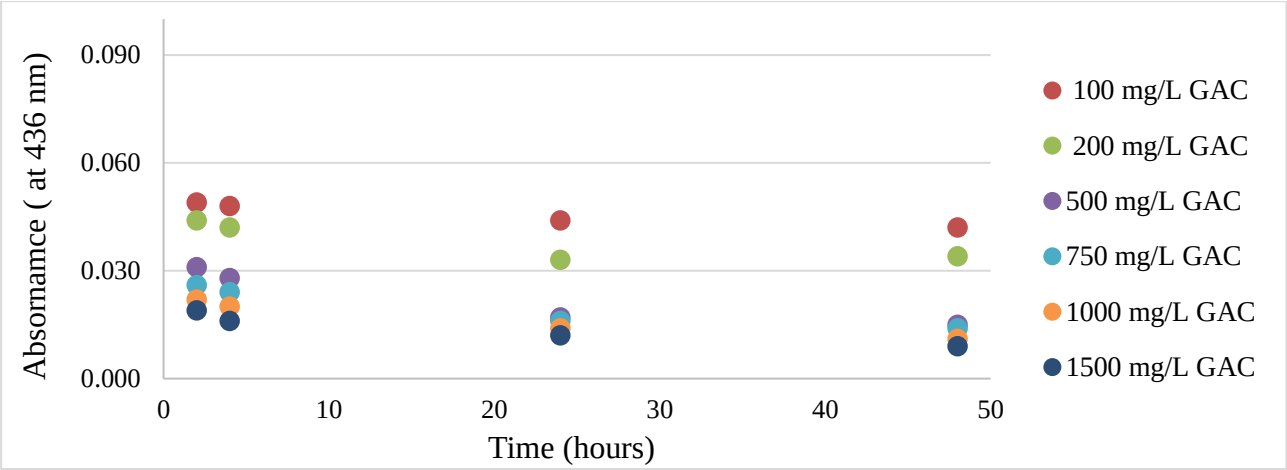


Figure A.18. Kinetics of organic substance removal: $Color_{436}$ absorbance decay in background NOM + pesticide mixture + ground GAC experiments.

APPENDIX B: OPERATIONAL RESULTS OF THE BIOLOGICAL REACTOR

Table B.1. Operational Results of the Biological Reactor – January 2023.

Run	**1**		**2**		**3**		**4**		**5**	
Date	2.01	5.01	9.01	12.01	16.01	19.01	24.01	27.01	30.01	01.02
pH	7.34	7.08	6.95	6.56	6.84	6.78	7.11	7.28	7.17	7.23
Temperature (℃)	22.4	22.6	23.1	23.2	22.8	22.4	23.2	23.0	23.2	23.2
DOC (mg/L)	95.5	7.0	48.0	6.7	38.3	4.3	60	4.7	53	3.8
DOC Removal (%)	92.7		86.0		88.8		92.2		92.8	
NH_4^+-N (mg/L)	2.38	12	2.16	0.77	1.52	0.56	3.6	0.05	1.75	0.02
NH_4^+-N Removal (%)	49.2		64.4		63.2		98.6		98.9	

Table B.2. Operational Results of the Biological Reactor – February 2023.

Run	**1**		**2**		**3**		**4**	
Date	6.02	10.02	13.02	17.02	20.02	23.02	28.02	02.03
pH	6.02	10.02	13.02	17.02	20.02	23.02	28.02	2.03
Temperature (℃)	7.27	7.18	6.85	6.27	6.34	6.49	6.96	7.05
DOC (mg/L)	23.5	23.2	22.8	23.1	23.4	23.2	22.2	22.1
DOC Removal (%)	92.8		87.8		90.9		87.5	
NH_4^+-N (mg/L)	1.15	0.03	1.30	0.08	2.00	0.03	1.05	0.06
NH_4^+-N Removal (%)	97.4		93.8		98.5		94.3	
MLSS (mg/L)	420		760		925		900	
MLVSS (mg/L)	240		675		815		805	
Run Period (day)	3.86		3.87		2.87		1.98	
F:M Ratio (mg DOC/mg MLVSS.day)	0.096		0.044		0.046		0.044	
S_0/X_0(mg DOC/mg MLVSS)	0.369		0.170		0.131		0.087	

Table B.3. Operational Results of the Biological Reactor – March 2023.

Run	**1**		**2**		**3**		**4**	
Date	6.03	9.03	13.03	17.03	20.03	23.03	27.03	30.03
pH	6.98	6.52	6.79	6.44	6.50	6.61	6.22	6.23
Temperature (°C)	22.4	22.6	23.1	23.2	23.4	23.1	23.4	23.46
DOC (mg/L)	94.0	9.6	98.8	9.7	72.0	7.9	59.6	9.0
DOC Removal (%)	89.8		90.2		88.9		84.8	
NH_4^+-N (mg/L)	1.85	0.07	1.35	0.07	0.70	0.06	1.75	0.04
NH_4^+-N Removal (%)	96.2		94.8		91.4		97.7	
MLSS (mg/L)	1040		940		1035		1075	
MLVSS (mg/L)	915		890		955		1195	
Run Period (day)	2.86		3.96		2.87		2.86	
F:M Ratio (mg DOC/mg MLVSS.day)	0.036		0.028		0.026		0.017	
S_0/X_0(mg DOC/mg MLVSS)	0.103		0.111		0.075		0.050	

Table B.4. Operational Results of the Biological Reactor – April 2023.

Run	**1**		**2**		**3**		**4**	
Date	3.04	7.04	10.04	14.04	17.04	20.04	24.04	28.04
pH	7.21	7.15	6.89	7.02	7.13	6.88	6.73	6.33
Temperature (°C)	22.9	23.1	23.4	22.8	22.4	22.6	22.8	23.4
DOC (mg/L)	85.0	9.7	101.2	11.1	96.4	10.4	80.2	14.7
DOC Removal (%)	88.6		89.0		89.2		81.9	
NH_4^+-N (mg/L)	2.20	0.03	2.45	0.02	2.85	0.05	1.05	0.03
NH_4^+-N Removal (%)	98.6		99.2		98.2		97.1	
MLSS (mg/L)	980		1305		1235		1240	
MLVSS (mg/L)	935		1105		1070		1195	
Run Period (day)	3.86		3.86		2.87		3.87	
F:M Ratio (mg DOC/mg MLVSS.day)	0.024		0.024		0.031		0.023	
S_0/X_0(mg DOC/mg MLVSS)	0.091		0.092		0.090		0.066	

Table B.5. Operational Results of the Biological Reactor – May 2023.

Run	**1**		**2**		**3**		**4**	
Date	2.05	5.05	8.05	12.05	16.05	18.05	22.05	25.05
pH	6.15	6.54	5.71	5.82	5.88	6.02	6.45	6.83
Temperature (°C)	23.8	23.4	24.2	24.4	24.3	23.8	23.7	23.4
DOC (mg/L)	86.6	10.6	87.6	9.0	46.9	6.5	110.8	8.5
DOC Removal (%)	87.7		89.7		86.1		92.3	
NH_4^+-N (mg/L)	1.65	0.03	1.65	0.03	0.50	0.12	1.95	0.05
NH_4^+-N Removal (%)	98.2		98.2		76.0		97.4	
MLSS (mg/L)	1220		1260		1250		1055	
MLVSS (mg/L)	1115		1220		1215		1005	
Run Period (day)	3.85		3.87		1.97		2.85	
F:M Ratio (mg DOC/mg MLVSS.day)	0.020		0.019		0.020		0.039	
S_0/X_0(mg DOC/mg MLVSS)	0.078		0.072		0.039		0.110	

Table B.6. Operational Results of the Biological Reactor – June 2023.

Run	**1**		**2**		**3**		**4**	
Date	30.05	2.06	5.06	9.06	12.06	16.06	23.06	26.06
pH	6.29	6.79	6.34	6.46	6.37	6.52	6.29	6.45
Temperature (°C)	24.3	24.4	25.4	25.8	26.1	26.3	26.1	26.4
DOC (mg/L)	85.9	8.9	110.2	8.2	112.6	12.0	123.1	11.8
DOC Removal (%)	89.6		92.5		89.3		90.4	
NH_4^+-N (mg/L)	1.65	0.08	2.40	0.05	1.15	0.16	1.95	0.14
NH_4^+-N Removal (%)	95.2		97.9		86.1		92.8	
MLSS (mg/L)	1285		1280		1290		1310	
MLVSS (mg/L)	1235		1170		1220		1285	
Run Period (day)	2.86		3.85		3.84		2.89	
F:M Ratio (mg DOC/mg MLVSS.day)	0.024		0.024		0.024		0.033	
S_0/X_0(mg DOC/mg MLVSS)	0.070		0.094		0.092		0.096	

Table B.7. Operational Results of the Biological Reactor – July 2023.

Run	**1**		**2**		**3**		**4**	
Date	04.07	7.07	10.07	14.07	17.07	20.07	26.07	30.07
pH	6.32	6.54	6.27	6.48	6.42	6.65	6.38	6.52
Temperature (°C)	26.4	27.2	26.6	26.7	27.3	27.4	27.5	27.4
DOC (mg/L)	167.0	23.0	98.8	20.0	96.5	20.4	101.4	19.5
DOC Removal (%)	86.2		79.6		78.8		80.7	
NH_4^+-N (mg/L)	2.95	0.24	2.15	0.13	1.80	0.24	2.30	0.1
NH_4^+-N Removal (%)	91.9		94.0		86.7		95.7	
MLSS (mg/L)	1315		1120		1160		1217	
MLVSS (mg/L)	1270		1060		1035		1087	
Run Period (day)	2.89		3.87		2.88		3.88	
F:M Ratio (mg DOC/mg MLVSS.day)	0.046		0.024		0.032		0.024	
S_0/X_0(mg DOC/mg MLVSS)	0.132		0.093		0.093		0.093	

Table B.8. Operational Results of the Biological Reactor – October 2023.

Run	**1**		**2**		**3**		**4**	
Date	02.10	5.10	09.10	12.10	16.10	19.10	23.10	26.10
pH	6.54	6.89	6.64	6.85	6.46	6.87	6.47	6.81
Temperature (°C)	25.3	22.5	25.7	26.2	25.4	23.8	26.4	22.9
DOC (mg/L)	117.6	11.4	106.5	23.4	98.7	20.5	101.8	19.9
DOC Removal (%)	86.2		79.6		78.8		80.4	
NH_4^+-N (mg/L)	1.45	0.03	1.90	0.05	1.60	0.06	2.15	0.04
NH_4^+-N Removal (%)	97.9		97.4		96.3		98.1	
MLSS (mg/L)	1470		1502		1347		1487	
MLVSS (mg/L)	1305		1462		1267		1316	
Run Period (day)	2.87		3.08		3.08		2.88	
F:M Ratio (mg DOC/mg MLVSS.day)	0.031		0.024		0.025		0.027	
S_0/X_0(mg DOC/mg MLVSS)	0.090		0.073		0.078		0.077	

Table B.9. Operational Results of the Biological Reactor – November 2023.

Run	**1**		**2**		**3**		**4**	
Date	30.10	2.11	06.11	10.11	13.11	16.11	20.11	23.11
pH	6.62	6.74	6.73	6.75	6.66	6.78	6.72	6.76
Temperature (°C)	23.8	22.7	22.9	21.9	20.5	23.2	22.8	22.7
DOC (mg/L)	119.6	15.6	92.1	17.9	112.0	13.7	139.1	18.2
DOC Removal (%)	86.9		80.5		87.7		86.9	
NH_4^+-N (mg/L)	3.55	0.05	1.35	0.03	2.15	0.02	2.70	0.02
NH_4^+-N Removal (%)	98.6		97.8		99.1		99.3	
MLSS (mg/L)	2105		1730		1880		1755	
MLVSS (mg/L)	1655		1692		1626		1680	
Run Period (day)	2.83		2.57		2.88		2.87	
F:M Ratio (mg DOC/mg MLVSS.day)	0.026		0.021		0.024		0.029	
S_0/X_0(mg DOC/mg MLVSS)	0.072		0.054		0.069		0.083	

Table B.10. Operational Results of the Biological Reactor – December 2023.

Run	**1**		**2**		**3**		**4**	
Date	4.12	7.12	11.12	14.12	18.12	21.12	25.12	28.12
pH	6.74	6.82	6.71	6.73	6.75	6.81	6.75	6.82
Temperature (°C)	22.3	22.8	21.2	22.9	23.1	22.8	23.2	23.7
DOC (mg/L)	134.7	21.6	106.5	12.2	105.9	9.4	92.8	13.1
DOC Removal (%)	84.0		81.6		91.1		85.9	
NH_4^+-N (mg/L)	2.00	0.05	1.65	0.04	3.10	0.02	1.50	0.02
NH_4^+-N Removal (%)	97.5		97.6		99.4		98.7	
MLSS (mg/L)	1980		2202		2135		2082	
MLVSS (mg/L)	1715		1892		1952		1917	
Run Period (day)	2.88		2.87		2.88		2.87	
F:M Ratio (mg DOC/mg MLVSS.day)	0.027		0.022		0.019		0.019	
S_0/X_0(mg DOC/mg MLVSS)	0.079		0.062		0.054		0.055	

Table B.11. Operational Results of the Biological Reactor – January 2024.

Run	**1**		**2**		**3**		**4**	
Date	8.01	11.01	15.01	18.01	22.01	25.01	29.01	01.02
pH	6.68	6.85	6.46	6.58	6.64	6.56	6.13	7.42
Temperature (℃)	22.5	22.5	20.7	20.8	17.4	19.7	18.4	20.8
DOC (mg/L)	116.6	21.4	94.5	17.7	95.3	16.1	138.9	20.6
DOC Removal (%)	81.6		81.2		83.1		85.2	
NH_4-N (mg/L)	2.40	0.06	1.86	0.04	2.80	0.04	2.60	0.18
NH_4-N Removal (%)	97.5		97.8		98.6		93.1	
MLSS (mg/L)	2197		2365		2525		2577	
MLVSS (mg/L)	2047		2286		2415		2435	
Run Period (day)	3.18		2.67		3.12		3.21	
F:M Ratio (mg DOC/mg MLVSS.day)	0.018		0.015		0.013		0.018	
S_0/X_0(mg DOC/mg MLVSS)	0.057		0.041		0.039		0.055	

Table B.12. Operational Results of the Biological Reactor – February 2024.

Run	**1**		**2**		**3**		**4**	
Date	5.02	8.02	12.02	15.02	19.02	22.02	26.02	01.03
pH	7.35	6.95	7.03	7.11	7.06	7.26	7.02	7.35
Temperature (℃)	18.6	22.9	22.7	22.6	18.0	19.9	21.3	
DOC (mg/L)	96.4	19.5	98.3	18.9	117.5	16.3	144.2	16.3
DOC Removal (%)	81.6		80.8		86.1		88.7	
NH_4-N (mg/L)	2.11	0.05	2.10	0.07	2.80	0.09	2.20	0.07
NH_4-N Removal (%)	97.6		96.7		96.8		96.8	
MLSS (mg/L)	2250		2762		3153		3026	
MLVSS (mg/L)	2367		2527		2927		2821	
Run Period (day)	3.18		2.67		3.12		3.21	
F:M Ratio (mg DOC/mg MLVSS.day)	0.015		0.014		0.013		0.017	
S_0/X_0(mg DOC/mg MLVSS)	0.045		0.039		0.040		0.051	

Table B.13. Operational Results of the Biological Reactor – March 2024.

Run	**1**		**2**		**3**		**4**	
Date	4.03	7.03	11.03	14.03	18.03	21.03	25.03	28.03
pH	6.82	6.58	6.62	7.56	7.24	7.38	7.43	7.05
Temperature (℃)	19.9	20.9	18.0	19.0	19.5	19.4	20.9	24.3
DOC (mg/L)	99.9	16.8	121.2	16.8	129.2	20.5	96.6	15.6
DOC Removal (%)	83.2		86.1		84.1		83.9	
NH_4-N (mg/L)	2.70	0.22	2.50	0.16	2.60	0.18	2.80	0.22
NH_4-N Removal (%)	91.9		93.6		93.1		92.1	
MLSS (mg/L)	2470		2685		2649		2847	
MLVSS (mg/L)	2267		2485		2487		2629	
Run Period (day)	3.02		2.98		3.01		2.96	
F:M Ratio (mg DOC/mg MLVSS.day)	0.015		0.016		0.017		0.012	
S_0/X_0(mg DOC/mg MLVSS)	0.044		0.049		0.052		0.037	

Table B.14. Operational Results of the Biological Reactor – April 2024.

Run	**1**		**2**		**3**		**4**	
Date	1.04	5.04	15.04	17.04	22.04	26.04	29.04	02.05
pH	7.11	6.90	6.61	6.81	6.93	6.72	6.59	6.72
Temperature (℃)	24.0	22.4	20.9	22.8	19.9	20.8	20.1	19.8
DOC (mg/L)	96.2	15.6	88.3	10.9	118.4	11.6	135.8	21.7
DOC Removal (%)	83.8		87.6		90.2		84.0	
NH_4-N (mg/L)	2.60	0.18	2.60	0.07	1.75	0.09	3.30	0.06
NH_4-N Removal (%)	93.1		97.3		94.9		98.2	
MLSS (mg/L)	2767		2930		2950		2997	
MLVSS (mg/L)	2567		2757		2440		2710	
Run Period (day)	3.92		4.03		3.87		4.02	
F:M Ratio (mg DOC/mg MLVSS.day)	0.010		0.008		0.013		0.012	
S_0/X_0(mg DOC/mg MLVSS)	0.037		0.032		0.049		0.050	

Table B.15. Operational Results of the Biological Reactor – June & September 2024.

Run	**1**		**2**		**3**		**4**	
Date	3.06	6.06	1.07	4.07	5.08	8.08	2.09	05.09
pH	6.89	6.92	6.82	6.84	6.86	6.82	6.84	6.87
Temperature (℃)	23.4	23.8	24.2	25.6	25.8	25.6	24.6	24.4
DOC (mg/L)	112.4	17.6	120.6	11.7	113.7	12.3	128.5	18.3
DOC Removal (%)	84.3		90.3		91.1		85.8	
NH_4-N (mg/L)	2.40	0.16	2.51	0.11	1.86	0.10	2.90	0.12
NH_4-N Removal (%)	93.3		95.6		94.6		95.9	
MLSS (mg/L)	2980		2977		2976		2964	
MLVSS (mg/L)	2587		2678		2645		2655	
Run Period (day)	3.98		3.89		3.87		3.78	
F:M Ratio (mg DOC/mg MLVSS.day)	0.011		0.012		0.013		0.013	
S_0/X_0(mg DOC/mg MLVSS)	0.043		0.045		0.052		0.048	

Table B.16. Operational Results of the Biological Reactor – October & January 2024-2025.

Run	**1**		**2**		**3**		**4**	
Date	7.10	10.10	4.11	7.11	2.12	5.12	6.01	10.01
pH	6.87	6.75	6.68	6.74	6.78	6.73	6.67	6.82
Temperature (℃)	24.2	24.1	22.3	22.7	20.9	20.3	21.1	20.8
DOC (mg/L)	108.7	15.5	117.4	12.0	126.4	11.7	109.4	10.5
DOC Removal (%)	85.7		89.8		90.7		90.4	
NH_4-N (mg/L)	2.30	0.15	2.40	0.12	2.66	0.11	2.67	0.13
NH_4-N Removal (%)	93.5		95.0		95.9		95.1	
MLSS (mg/L)	2966		2986		2996		2948	
MLVSS (mg/L)	2615		2627		2634		2648	
Run Period (day)	3.87		3.86		3.87		3.80	
F:M Ratio (mg DOC/mg MLVSS.day)	0.011		0.012		0.012		0.011	
S_0/X_0(mg DOC/mg MLVSS)	0.042		0.045		0.048		0.041	

APPENDIX C: RESULTS OF NOM BIODEGRADATION EXPERIMENTS

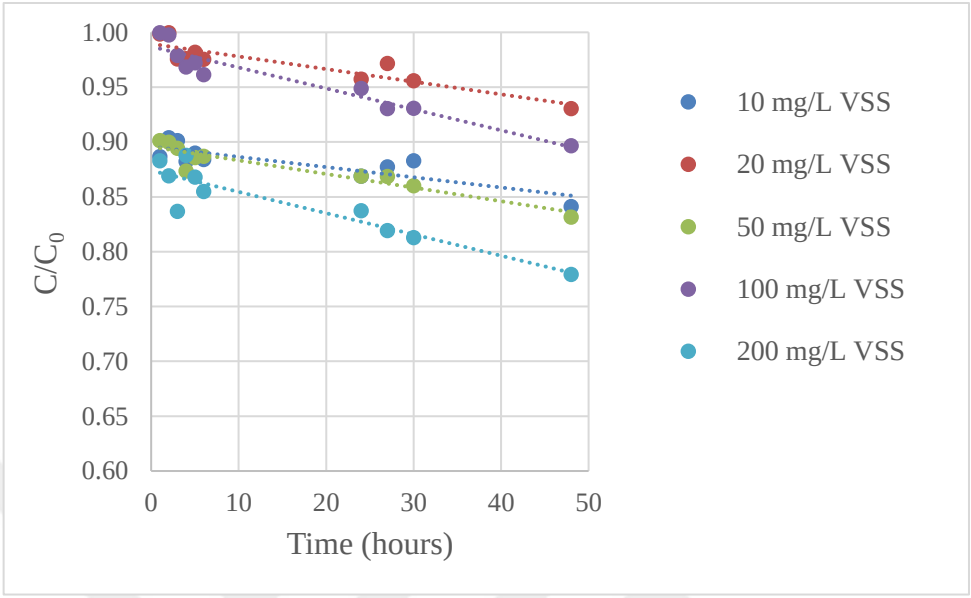


Figure C.1. Background NOM removal profile in a batch reactor: normalized UV_{254} absorbance measurements versus time.

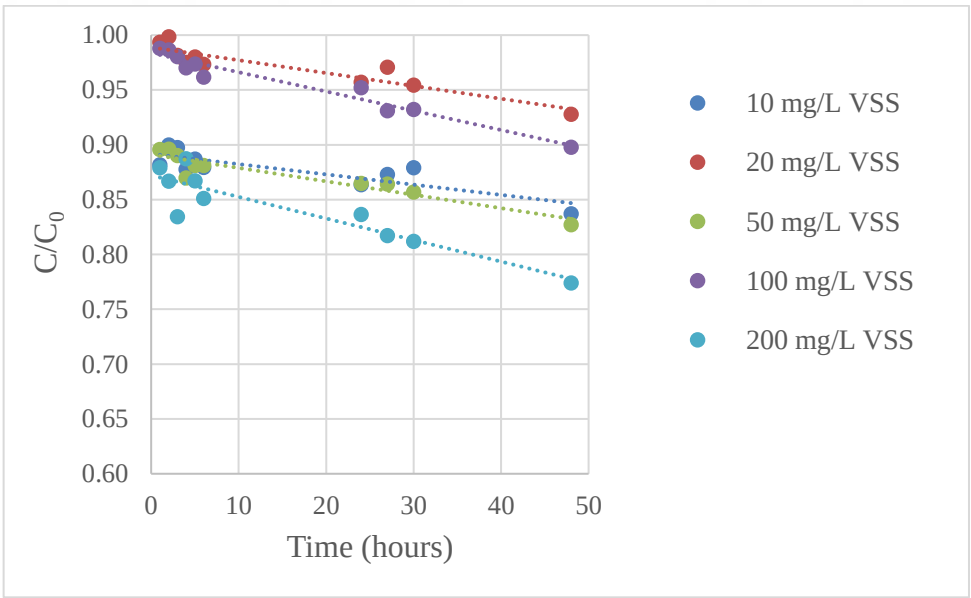


Figure C.2. Background NOM removal profile in a batch reactor: normalized UV_{280} absorbance measurements versus time.

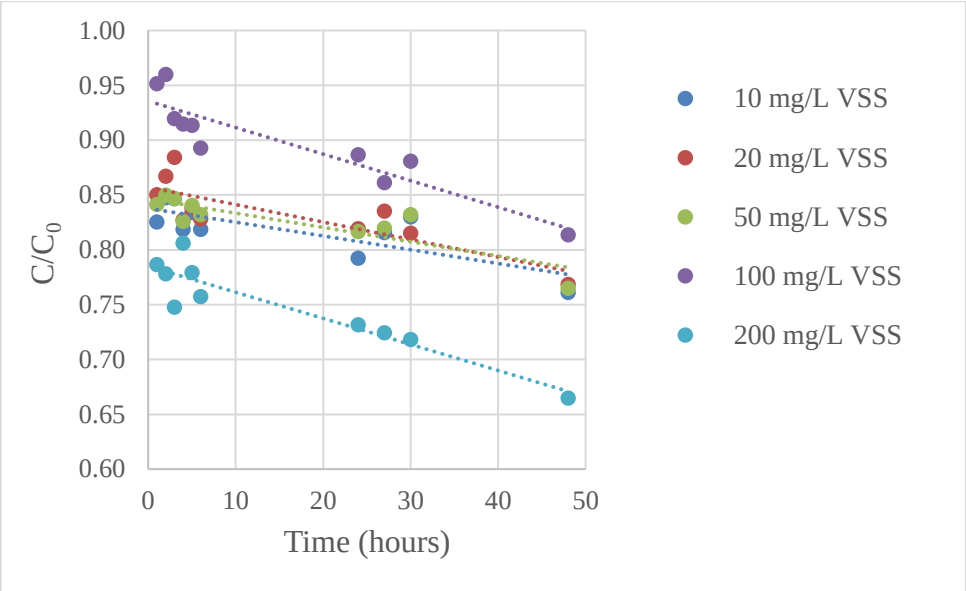


Figure C.3. Background NOM removal profile in a batch reactor: normalized $Color_{400}$ absorbance measurements versus time.

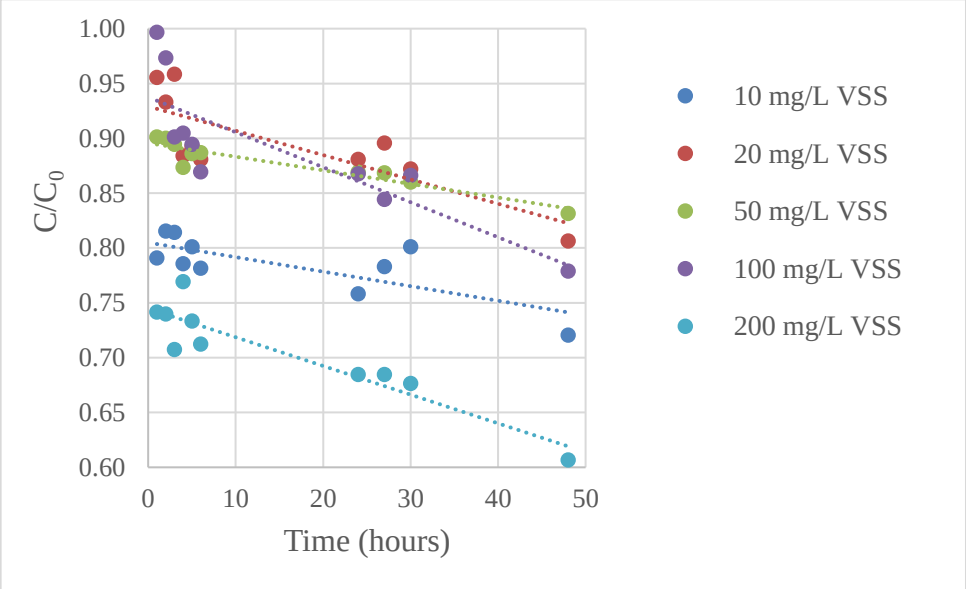


Figure C.4. Background NOM removal profile in a batch reactor: normalized $Color_{436}$ absorbance measurements versus time.